ADAPTING A BEAM-BASED ROTORDYNAMICS MODEL TO ACCEPT A GENERAL THREE-DIMENSIONAL FINITE-ELEMENT CASING MODEL

A Thesis

by

STEPHEN MATHEW JAMES

Submitted to the Office of Graduate Studies of
Texas A&M University
in partial fulfillment of the requirements for the degree of

MASTER OF SCIENCE

May 2010

Major Subject: Mechanical Engineering

ADAPTING A BEAM-BASED ROTORDYNAMICS MODEL TO ACCEPT A GENERAL THREE-DIMENSIONAL FINITE-ELEMENT CASING MODEL

A Thesis

by

STEPHEN MATHEW JAMES

Submitted to the Office of Graduate Studies of
Texas A&M University
in partial fulfillment of the requirements for the degree of

MASTER OF SCIENCE

Approved by:

Chair of Committee,	Dara W. Childs
Committee Members,	Luis A. San Andres
	S. Bart Childs
Head of Department,	Dennis L. O'Neal

May 2010

Major Subject: Mechanical Engineering

ABSTRACT

Adapting a Beam-Based Rotordynamics Model to Accept a
General Three-Dimensional Finite-Element Casing Model. (May 2010)
Stephen Mathew James, B.Tech., University of Kerala
Chair of Advisory Committee: Dr. Dara W. Childs

The subject of this thesis is an extension of a two-dimensional, axisymmetric, Timoshenko-beam finite-element rotordynamic code to include a three-dimensional non-axisymmetric solid-element casing model. Axisymmetric beams are sufficient to model rotors. Spring and damper forces provide the interface between the rotor and its casing and capture the dynamics of the full model. However, axisymmetric beams limit the modeling of real-case machine structures, where the casing is not axisymmetric.

Axisymmetric and non-axisymmetric 3D finite element casing structures are modeled. These structures are then reduced using a technique called substructuring. Modal equations are developed for axisymmetric and non-axisymmetric casing models. In a 3D non-axisymmetric model, structural dynamics modes can be modeled by lateral modes in two orthogonal planes. Modal information of the complex 3D casing structures are generated, and then incorporated into the 2D code after a series of pre-processing steps.

A reduction method called Component Mode Synthesis (CMS) is used to reduce the large dimensionality involved in calculation of rotordynamic coefficients. The results from the casing structures are merged with the rotor model to create a combined rotor-casing model. The analysis of the combined structure shows that there is a difference in the natural frequencies and unbalance response between the model that uses symmetrical casing and the one that uses non-axisymmetric casing.

XLTRC^2 is used as an example of a two-dimensional axisymmetric beam-element code. ANSYS is used as a code to build three-dimensional non-axisymmetric

solid-element casing models. The work done in this thesis opens the scope to incorporate complex non-axisymmetric casing models with XLTRC^2.

DEDICATION

This thesis is dedicated to all those who have taught me; who, over the years, have sacrificed their time, energy and effort so that I would excel. Without them, I would never be what I am today.

ACKNOWLEDGEMENTS

My foremost gratitude goes to God for everything He has given me. It is hard to escape the feeling that, underneath all the thesis proposals, drafts, reviews, and revisions, there was something of divine intervention that guided me in the right direction.

My heartfelt thanks go to my advisor, Dr. Dara Childs, for giving me the opportunity to work with him. I thank him for helping me immensely during my work. His patience, guidance and support encouraged me to work relentlessly towards an optimal solution in many critical areas of the project. I also thank Dr. Luis San Andres and Dr. Bart Childs for being on my committee and for their help and assistance. I am grateful to Dr. Steven Taliaferro who agreed to be a substitute for my thesis exam.

This thesis would have never taken off without the ideas brought forward by David Ransom at Southwest Research Institute™ (SwRI). I thank him for making several trips to College Station to help me develop the fundamental concepts. I have immense gratitude to the management at SwRI, in particular Dr. Klaus Brun and Dr. James Jeffrey Moore, who gave me the opportunity and resources to work on my thesis after I began my employment with them. I was fortunate to be put in the right projects at the right time, and this helped me gain crucial knowledge to quickly advance the software development behind my thesis.

Every major task has a set of unsung heroes who, at times, plug in the missing pieces in the puzzle. My appreciation goes to the dozens of ANSYS and VBA technical experts and user forums. While I may never know who all they are and they may never get to read this work, their role has been a vital element in this work.

I would like to thank Texas A&M University for giving me the opportunity to pursue my higher education at such a prestigious institution. I would also like to thank the generous sponsorship provided by the Turbo Research Consortium (TRC). I also thank the Department of Mechanical Engineering and the Office of Graduate Studies for providing me with scholarships.

During my time at Texas A&M University, I've experienced the rigors of student life just as the others. Having the best set of friends nullified the stress and gave me the much needed comic relief to get through the intense curriculum. I am indebted for the support they provided, in both my academic and extra-curricular activities.

The love and support of my parents, brothers and my extended family have been the foundation of my dreams and I'm extremely thankful to them for inspiring me to achieve them. Finally, and most importantly, a heartfelt thanks to my lovely wife Treasurin. Though I started this work without her, I am so glad that I could finish it with her. Having her in my life has made all of this worth it.

NOMENCLATURE

Units for physical quantities are marked by dimensional units of mass (M), length (L), time (T) and force (F).

$[A]$	– Eigenvector matrix of coupled rotor-casing model
$[a_c]$	– Matrix of eigenvectors of casing
$[A_c]$	– Component mode synthesis transformation matrix for casing
APDL	– ANSYS Parametric Design Language
$[a_r]$	– Matrix of eigenvectors of rotor
$[A_r]$	– Component mode synthesis transformation matrix for rotor
$[A_X]$	– Eigenvector matrix for $X-Z$ plane
$[A_Y]$	– Eigenvector matrix for $Y-Z$ plane
b1, *b2*, *b3*, *b4*	– Bearings used in component-mode-synthesis model
$[C]$	– System damping matrix in Guyan reduction model
$[C_{csc}]$	– Transformed casing damping matrix due to seal force on casing
$[C_{csr}]$	– Transformed casing damping matrix due to seal force on rotor
$c_{ij}\ ; i=1:m, j=1:n$	– Damping matrix element [FTL^{-1}]
$cj\ ; j=1:n$	– *j*th casing station
CMS	– Component Mode Synthesis
c_{rsc}	– Damping element entry in rotor due to seal force on casing [FTL^{-1}]
$[C_{rsc}]$	– Transformed rotor damping matrix due to seal force on casing
c_{rsr}	– Damping element entry in rotor due to seal force on rotor [FTL^{-1}]

$[C_{rsr}]$ – Transformed rotor damping matrix due to seal force on rotor

c_{si} $;i=1,2$ – Damping coefficient of *i*th seal [FTL^{-1}]

$\{F\}$ – System external forces matrix in Guyan reduction model

f_{bk} $;\mathrm{k}=1:p$ – Force acting at the *k*th bearing [F]

$\{F_{cB}\}$ – Transformed casing external forces matrix

f_{cj} $;j=1:n$ – Force acting at the *j*th station of casing [F]

f_{csi} – Force acting on casing due to *i*th seal [F]

FEA – Finite element analysis

FEM – Finite element methods

f_i $;i=1:m$ – *i*th force matrix element in Guyan reduction [F]

$\{F_{rB}\}$ – Transformed rotor external forces matrix

f_{ri} $;i=1:m$ – Force acting at the *i*th station of rotor [F]

f_{rsi} – Force acting on rotor due to *i*th seal [F]

f_x – Force along x-axis [F]

$\{F_X\}$ – $X-Z$ plane force matrix

f_y – Force along y-axis [F]

$\{F_Y\}$ – $Y-Z$ plane force matrix

$J_{i\beta yi}$ – Polar inertia coefficient of *i*th station about *i*th β_y direction [L^4]

$[K]$ – System stiffness matrix in Guyan reduction model

$[K_c]$ – Transformed casing stiffness matrix

k_{cicj} $;i=1:n,\ j=1:n$ – Stiffness matrix *i*,*j*-th entry of casing [FL^{-1}]

$[K_{csc}]$ – Transformed casing stiffness matrix due to seal force on casing

$[K_{csr}]$ – Transformed casing stiffness matrix due to seal force on rotor

k_{ij} $;i=1:m,\ j=1:n$ – Stiffness matrix element [FL^{-1}]

$[K_r]$ – Transformed rotor stiffness matrix

$k_{rirj}\ ; i = 1:m,\ j = 1:m$ – Stiffness matrix *i*,*j*-th entry of rotor [FL^{-1}]

k_{rsc} – Stiffness element entry in rotor due to seal force on casing [FL^{-1}]

$[K_{rsc}]$ – Transformed rotor stiffness matrix due to seal force on casing

k_{rsr} – Stiffness element entry in rotor due to seal force on rotor [FL^{-1}]

$[K_{rsr}]$ – Transformed rotor stiffness matrix due to seal force on rotor

$k_{si}\ ; i = 1,2$ – Stiffness coefficient of *i*th seal [FL^{-1}]

$[M]$ – System inertia matrix in Guyan reduction model

$[M_c]$ – Transformed casing inertia matrix

$m_{ci}\ ; j = 1:n$ – Inertia coefficient of *i*th station of casing [M]

$[M_{csc}]$ – Transformed casing inertia matrix due to seal force on casing

$[M_{csr}]$ – Transformed casing inertia matrix due to seal force on rotor

$m_i\ ; i = 1:m$ – *i*th inertia matrix element [M]

m_{iRxi} – Lateral inertia coefficient of *i*th station along *i*th R_x direction [M]

$m_{ri}\ ; i = 1:m$ – Inertia coefficient of *i*th station of rotor [M]

$[M_r]$ – Transformed rotor inertia matrix

m_{rsc} – Inertia element entry in rotor due to seal force on casing [M]

$[M_{rsc}]$ – Transformed rotor inertia matrix due to seal force on casing

m_{rsr} – Inertia element entry in rotor due to seal force on rotor [M]

$[M_{rsr}]$ – Transformed rotor inertia matrix due to seal force on rotor

$m_{si}\ ; i = 1,2$ – Inertia coefficient of *i*th seal [M]

$\hat{M}_y$ – Moment about y-axis [FL]

q_{cj} – *j*th casing modal coordinate

q_i – *i*th modal coordinate in coupled rotor-casing model

q_{iX} – *i*th modal coordinate in $X-Z$ plane

q_{iY} – *i*th modal coordinate in $Y-Z$ plane

q_{ri} – *i*th rotor modal coordinate

ri ;$i=1:m$ – *i*th rotor station

R_{xi} – *i*th displacement coordinate along x-axis

R_{yi} – *i*th displacement coordinate along y-axis

s1, s2 – Seals used in component mode synthesis model

$\{x\}$ – Matrix representing displacement terms

$\{X\}$ – $X-Z$ plane coordinate matrix

$\{\dot{x}\}$ – Matrix representing velocity terms

$\{\ddot{x}\}$ – Matrix representing acceleration terms

x_{cj} – Displacement term of the *j*th station of casing [L]

$\dot{x}_{cj}$ – Velocity term of the *j*th station of casing [LT^{-1}]

$\ddot{x}_{cj}$ – Acceleration term of the *j*th station of casing [LT^{-2}]

x_{ri} – Displacement term of the *i*th station of rotor [L]

$\dot{x}_{ri}$ – Velocity term of the *i*th station of rotor [LT^{-1}]

$\ddot{x}_{ri}$ – Acceleration term of the *i*th station of rotor [LT^{-2}]

$\{Y\}$ – $Y-Z$ plane coordinate matrix

β_{xi} – *i*th rotation coordinate about x-axis

β_{yi} – *i*th rotation coordinate about y-axis

λ_{cj} – Eigenvalue (natural frequency) of *j*th mode of casing

λ_{ri} – Eigenvalue of *i*th mode of rotor

ζ_{cj} – Modal damping coefficient for the *j*th mode of the casing

ζ_{ri} – Modal damping coefficient for the *i*th mode of the rotor

$[\Lambda]$ – Diagonal matrix of eigenvalues of coupled rotor-casing model

$[\Lambda_c]$ – Diagonal matrix of eigenvalues of casing

$[\Lambda_r]$ – Diagonal matrix of eigenvalues of rotor

$[\Lambda_X]$ – Diagonal matrix of eigenvalues in $X-Z$ plane

$[\Lambda_Y]$ – Diagonal matrix of eigenvalues in $Y-Z$ plane

B – Boundary coordinates in component mode synthesis model

I – Interior coordinates in component mode synthesis model

m – Master degree of freedom entry in Guyan reduction

s – Slave degree of freedom entry in Guyan reduction

TABLE OF CONTENTS

Page

Page

Page

LIST OF FIGURES

Page

Page

Page

Page

Page

Page

Page

LIST OF TABLES

Page

1 INTRODUCTION

1.1 XLTRC^2 Software

XLTRC^2[1] is a rotordynamic software suite characterized by the following features:

a. It is fast in building rotordynamic system models and running simulations.
b. It is accurate and has been benchmarked against other industry-standard suites and known analytical solutions.
c. It has a user-friendly interface.

XLTRC^2 uses Timoshenko–beam finite element models (FEM) that includes shear deflections. The Timoshenko–beam finite element model was developed with significant contributions by Nelson and McVaugh [1] and Nelson [2]. XLTRC^2 can model multiple nested shafts. Component mode synthesis (CMS) is used to reduce the dimensionality of the finite element beam model. The CMS method is explained later in section 2.2. XLTRC^2 can also accept a general pole-zero, reaction-force/displacement model for simulating foundation models.

In XLTRC^2, a rotor or casing structure can only be modeled using axisymmetric beams in a two dimensional system. Figure 1 shows a representative model of a rotor and casing. The axis of symmetry lies along the longitudinal axis. The spring and damper forces from bearings and seals provide the interface between the rotor and casing and capture the dynamics of the full model. Additional input such as added masses help to model impellers and liquid seals, for example.

The use of axisymmetric beams limit the modeling of real-case machine structures, e.g. volute pump casings, base plate assemblies, etc. where the casing structure is not axisymmetric. This *limitation* is in the context of a rotordynamics sense. Figure 2 shows an example of a compressor casing. The structure is non-symmetric

---

This thesis follows the style of Journal of Turbomachinery.

[1] XLTRC^2 is licensed by Texas Engineering Experiment Station and developed at the Turbomachinery Laboratory.

about at least one of the coordinate axes. Non-axisymmetric structures are common, but the availability of complete and convenient rotordynamic analysis tools for their analysis is limited.

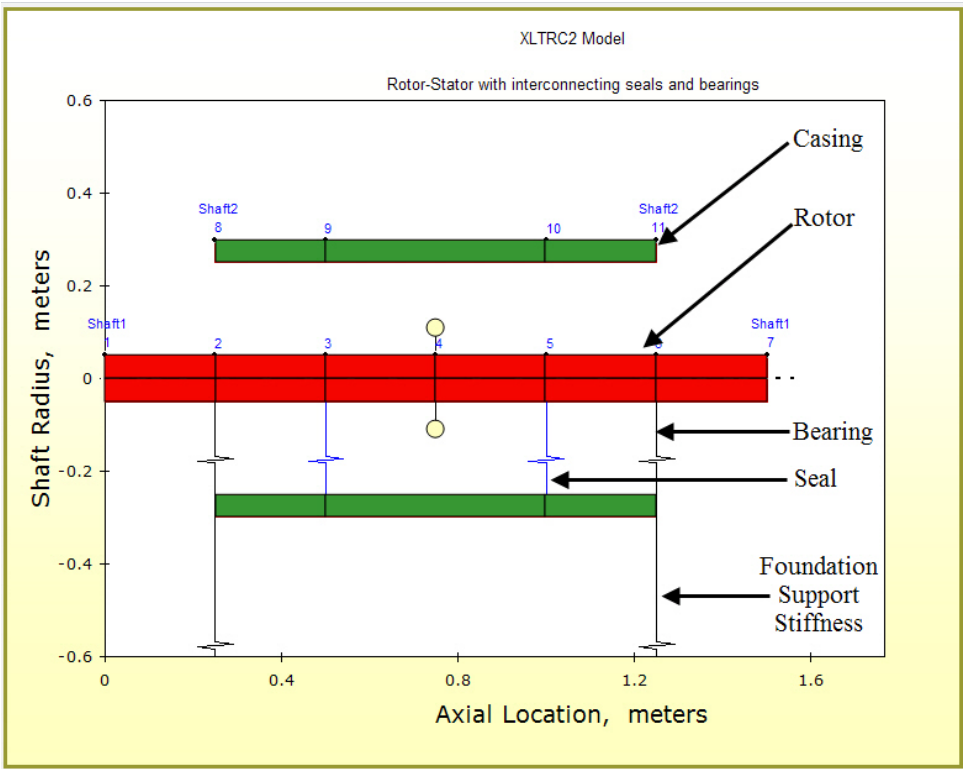

Figure 1 XLTRC^2 rotor-casing model with connecting bearings and seals [3]

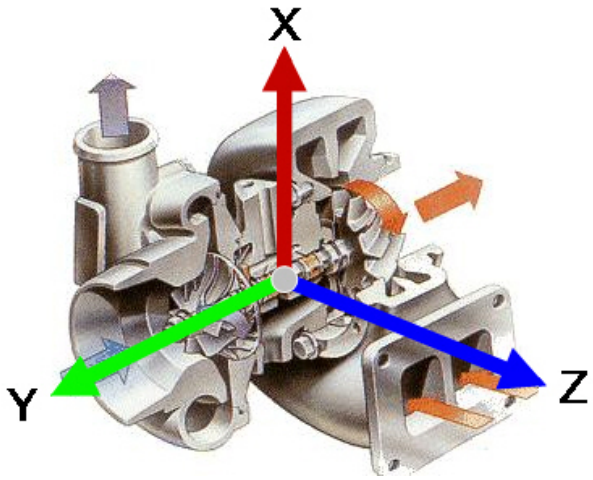

Figure 2 Compressor casing showing non-axisymmetric geometry [4]

1.2 XLTRC[2] vs. 3D Finite Element Analysis Tools

Modern finite element analysis (FEA) tools (e.g., ANSYS[2], MSC Nastran[3], Pro/Engineer[4], SolidWorks[5], etc.) use three dimensional (3D) elements to model the rotor, casing and foundation. Bearings and seals are modeled, with equivalent stiffness and damping coefficients, and then incorporated into the 3D finite element method (FEM) model. FEA tools do not have straightforward methods to incorporate speed dependent bearing and seal force coefficients. While able to analyze detailed models, they lack the spectrum of a complete rotordynamic analysis. XLTRC[2], on the other hand, can couple a rotor-casing or rotor-rotor model through connecting links at bearing and seal locations. General casing structures can also be incorporated by the use of point transfer functions. Physical coordinates are used to define the locations of nonlinear or linear connections with frequency-dependent coefficients, and this is achieved with component mode synthesis (CMS). Linear, frequency-independent connections are

[2] ANSYS is a trademark or registered trademark of ANSYS, Inc. or its subsidiaries located in the United States or other countries.
[3] MSC Nastran is a registered trademark of MSC.Software Corporation
[4] Pro/Engineer is a trademark of TriStar Computer Corporation
[5] SolidWorks is a trademark of Dassault Systemes S.A.

accounted for via modal stiffness, damping, and mass matrix entries. The following is a comparison of the features between XLTRC^2 and a general purpose finite element code:

a. XLTRC^2 is an easy application in terms of user friendliness and the learning time. 3D finite element codes are more complex as they incorporate a wide variety of parameters that are applicable to a range of disciplines. Selecting parameters specific to a rotordynamic analysis requires experience and a thorough understanding of the tool capabilities.
b. XLTRC^2 requires less time to create a model and uses a simple interface. Although 3D FEM codes use graphical interface and primitives (fundamental building blocks) for modeling, the resources required are more taxing than those for XLTRC^2.
c. XLTRC^2 uses only axisymmetric beam-element based modeling, and hence is limited to simple designs. Since 3D FEM codes employ a wide variety of elements (such as beams, shells, links, etc.) they can handle more complicated designs.
d. XLTRC^2 can model only two dimensional axisymmetric beam structures which are sufficient for rotors. Most other 3D FEM codes allow for full-fledged three dimensional analyses.

1.3 Research Objective

This research adapts the beam-element based XLTRC^2 rotordynamic model to accept a general three dimensional finite element casing model. This step combines the advantages of XLTRC^2 and a 3D finite element code.

1.4 Selection of Three Dimensional Finite Element Code

The choice of 3D finite element code is based on the following requirements:

a. A variety of element primitives must be available to model actual structures, because one element type cannot be accurately used to represent an entire model. For e.g., a beam element cannot accurately represent a component of the casing comprised of shell elements.

b. The code should be able to reduce the casing structure using component mode synthesis (CMS). This reduction technique, as described later in section 2.2, is used by XLTRC^2 and provides a compatible format without much restructuring to the existing XLTRC^2 code.
c. The modal information contained in the CMS reduced structure must be available for post processing. Most FEA codes use proprietary data–storage algorithms and databases. An algorithm, provided by the manufacturer of the FEA code, should exist to convert relevant portions of the proprietary database to open source format.
d. The finite element code should be widely used so that this feature can be readily employed among the XLTRC^2 user base.

Based on the above requirements, ANSYS is chosen as the favorable candidate over other codes such as MSC Nastran, Pro/Engineer, SolidWorks, etc. The analysis done in this thesis uses ANSYS Classic Release 11 (Service Pack 1) and ANSYS Workbench Release 11.

1.5 Previous Work

Previous analyses show that casings and foundation supports have a considerable effect on the critical speeds and response of a rotordynamic system.

Childs' [5] 1976 paper presents work done on a Dual-Rotor Jet Engine system that consists of two flexible rotors (low-speed and high-speed) and flexible casing structure (Figure 3). The procedure for a transient modal simulation model is described that includes the effect of bearing connections between the rotors and from the rotors to the housing[6] structure. The case structure is modeled as a collection of symmetrically connected rigid bodies.

A paper by Childs [6] in 1978 presents work on the Space Shuttle Main Engine (SSME) High-Pressure Fuel Turbopump (HPFTP) and High-Pressure Oxygen Turbopump (HPOTP). The model (Figure 4) uses exported modes from a general structural dynamic model of the housing. Modes are used that corresponded to zero

[6] The terms *stator*, *casing*, and *housing* are used interchangeably in this thesis.

reaction forces at the connection points. A schematic representation of the SSME HPFTP and HPOTP is shown in Figure 5. In an earlier research [7] in 1975, Childs shows that introducing stiffness asymmetry in the support structure predicts an improvement in turbopump stability. This is an example of how the supports influence the overall rotordynamic stability.

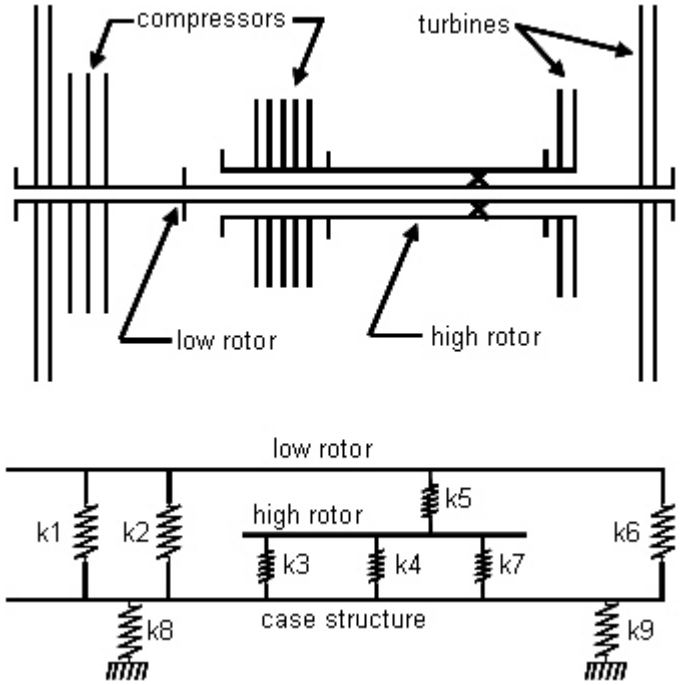

Figure 3 Dual-rotor/case system analyzed by Childs [5]

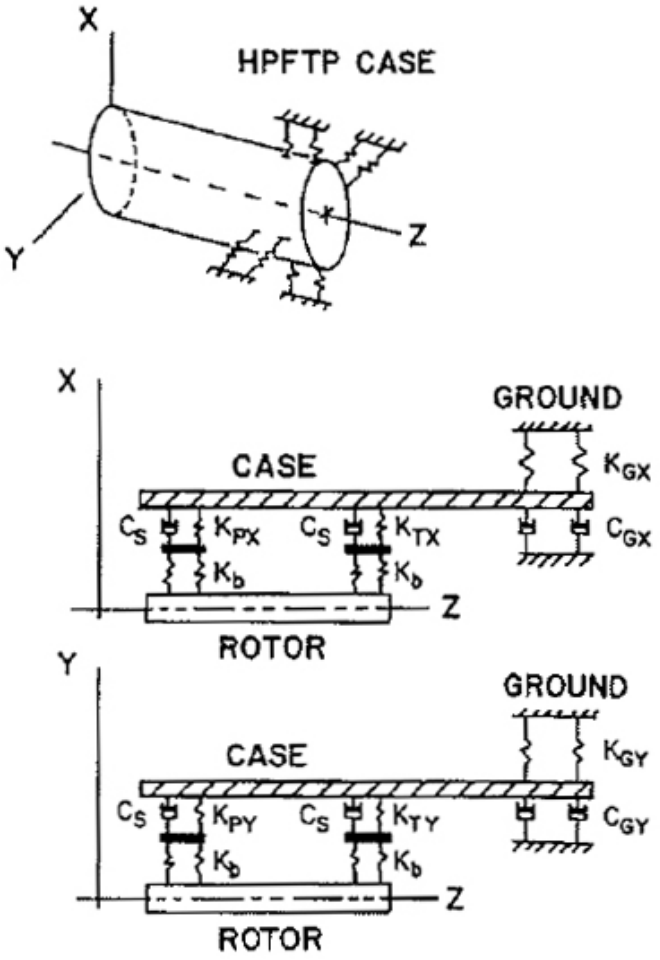

Figure 4 Structural dynamic model of the SSME HPFTP [6]

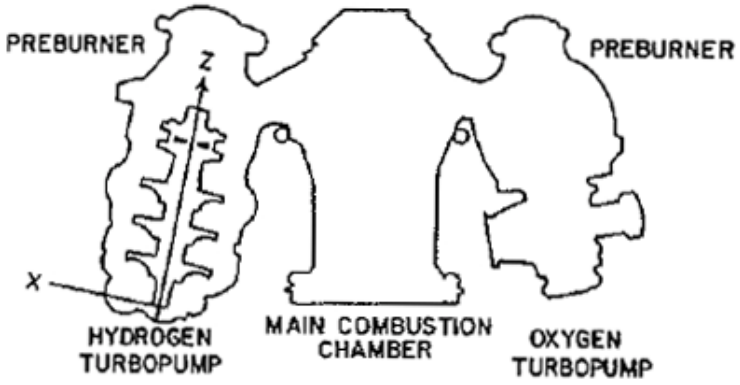

Figure 5 Schematic representation of the SSME HPFTP and HPOTP [6]

In 1978, Darlow, Smalley and Ogg [8] also presented work that involves casing effects on an axisymmetric vertical pump, represented by Figure 6. This pump comprises of three structural elements – the outermost level representing the pump casing, middle level representing the pump inner structure and the inner-most level, the pump rotor. The pump is cantilevered from above and supports a large impeller and volute casing. Semi-rigid connections are used between the top of the pump casing and the inner structure, and similarly between the top of the pump casing and ground. This pump presented an unusual rotordynamic situation in which the inner structure and the pump casing are separated at the bottom by close clearances, causing it to act as a squeeze-film damper. The work made use of two rotordynamic programs, CAD-26 [9] and CAD-27 [10], developed by J.W. Lund at Mechanical Technology Incorporated (MTI). In his 2003 paper, Memmott [11] cites the rotordynamic programs and states that the MTI programs uses the transfer matrix method.

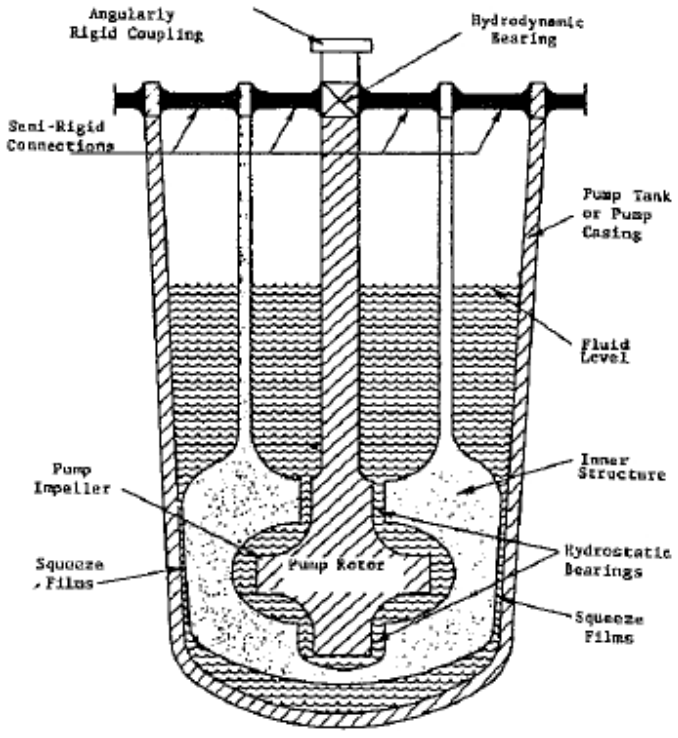

Figure 6 Schematic diagram of vertical pump analyzed by Darlow, et al [8]

In their 1985 paper, Bellamy, Jonson and Gaffney [12] present the capability of three dimensional analyses and their solutions. The paper mentions the use of large, three dimensional, non-axisymmetric detailed solid finite elements that replace the simpler beam type models. The demand on computation power was made possible by advancements in the development of digital computers. Three dimensional finite element based model predictions showed better correlation with static and dynamic analysis, when compared to the traditional single plane beam model. There was also a dramatic increase in the number of modes predicted by the three dimensional models.

Gerardin and Kill [13] in 1986 present a three dimensional approach for the dynamic analysis of a high by-pass aircraft engine and a cryogenic engine's turbopump rotor. For the aircraft engine analysis, the approach involves creating substructures out of the entire system, comprised of two rotors corresponding to the low and high pressure stages, the casing, and the aircraft pylon. The substructures are represented by superelements created by the component mode synthesis (CMS) method. The rotating parts, as shown in Figure 7 and Figure 8, are modeled with axisymmetric shell and solid elements. The fan blades are represented by quadrangular elements. Each rotor consists of two superelements. The casing, shown in Figure 9, and pylon are modeled by five superelements consisting of beam and shell elements.

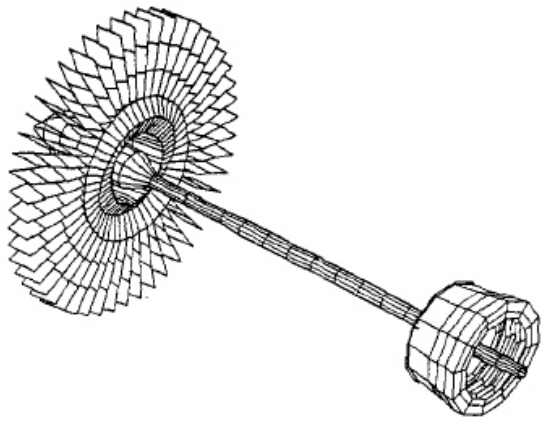

Figure 7 Superelement model of axisymmetric low pressure rotor comprising of shell and solid elements [13]

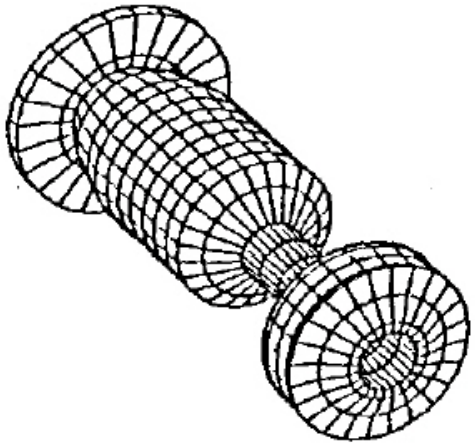

Figure 8 Superelement model of axisymmetric high pressure rotor comprising of shell and solid elements [13]

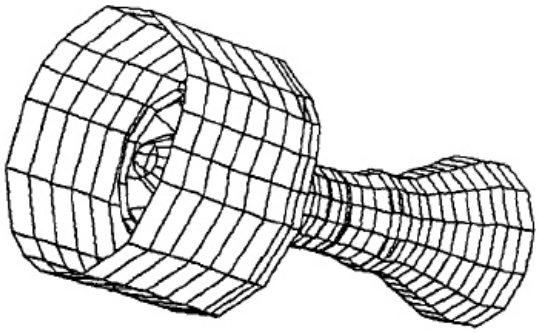

Figure 9 Superelement model of casing comprising of shell and solid elements [13]

For the turbopump rotor of the cryogenic engine, a beam-element approach is used to model the shaft, and CMS is used to reduce the size of the resulting system of equations from the finite element analysis. Gerardin and Kill used their substructure method to perform stability analysis, unbalanced response, and transient analysis. The same models were later extended [14] in 1990 to study maneuver loading of rotors.

Hylton and Burns' [15] 1994 paper use an axisymmetric finite element rotordynamic analysis routine for analysis of bearing loads in high speed turbofan engines that have encountered blade loss. Beam elements are used to model the engine

and supporting structure, and the beam elements coupled to the three dimensional finite element model of the complete structure. Mass elements are used to represent lumped masses. A combination of spring and damper elements are used to couple the rotating and stationary components. Figure 10 shows the finite element model used. The analysis involves calculation of damped and undamped critical speeds, steady state unbalance response and transient response. Although the term substructure is used in this paper, the reduction technique, if any, has not been specified.

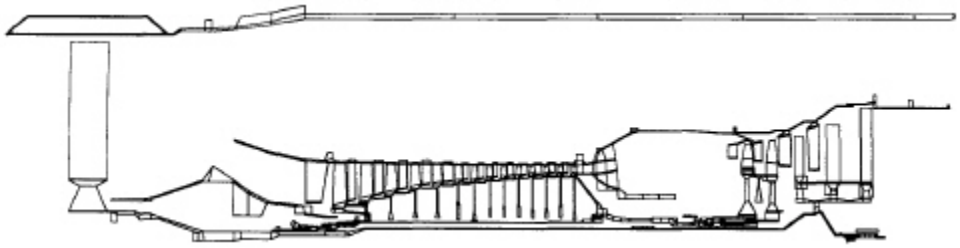

Figure 10 Finite element model of turbofan engine [15]

In 2002, Corbo, Stefanko and Leishar [16]document the rotordynamic analysis of a vertical pump. The rotordynamic model generation uses a *Two-Level Method.* The first level models the rotating pump shaft and the second level, the stationary pump column (casing). Each individual level is a complete rotordynamic model, and these levels are then linked at various locations to represent the vibration components that tie the two levels together. The *locations* refer to bearings, seals, coupling elements, etc. that allow complex dynamic interactions between the components to be accounted for. Two valid methods are used to analyze the system; first, use of a specialized rotordynamics code, and second a 3D finite element code. The authors emphasize that when the casing is modeled with a general-purpose FEM code, the fluid-structure-interactions between the casing and the rotor must be accounted for, a practice that is frequently ignored by pump manufacturers. The modeling procedure employs rotordynamics computer codes that can handle only axisymmetric elements. When non-axisymmetric slotted portions of the

pump casing are encountered, they are modeled as equivalent axisymmetric sections having the same area and area moment of inertia. The casing is modeled with beam elements, and the results are reported to be consistent with conventional beam theory.

Clark and Jurjevic [17] show improvements in finite element modeling in their 2007 paper. The casings are first represented with simplified rotor-bearing-support models. Beam elements represent the shaft while other predefined components model the flexible disk, coupling, bearing support, and gears. While the use of these components is useful to predict rotor critical speeds, rotor-structure interaction is not possible and cannot predict structural resonance. Standard rotordynamic tools include insufficient detail of casings with the supports modeled as single degree of freedom systems. This deficit causes limitations in determining the detailed response of the casings and foundations.

To overcome this drawback, a finite-element-based 3D geometry is used. The rotor is modeled with beam and pipe elements and validated with field data. For the casing, a procedure called *substructuring* is employed where the detailed non-axisymmetric casing model is represented as a compilation of super-elements. Each of these superelements is built starting from a FEM base comprising of solid elements. Modal analysis is carried out on each superelement, and then these superelements are built into an assembly. Figure 11 through Figure 13 show the process of building the assembly of superelements. The casing supports introduce non-axisymmetry into the system.

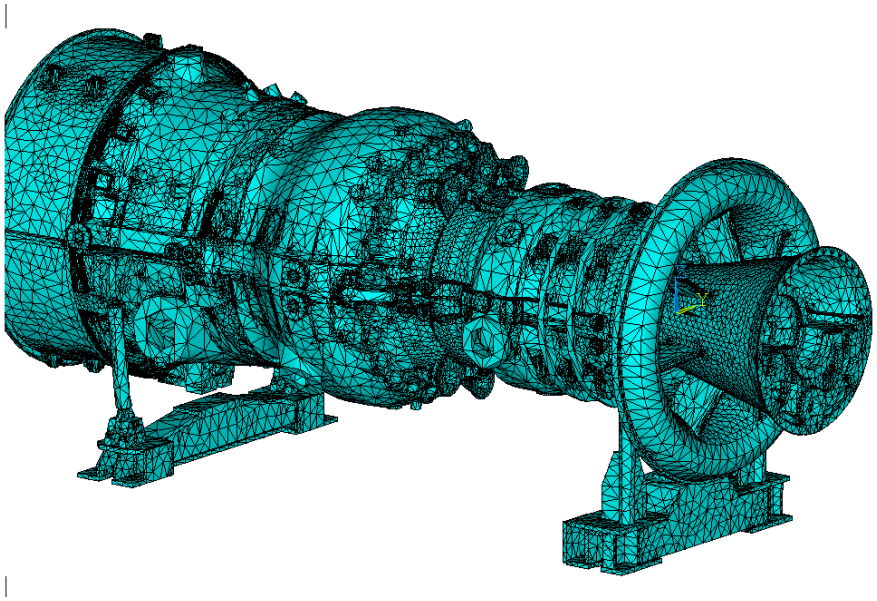

Figure 11 Detailed FEM model of gas turbine analyzed by Clark et al [17]

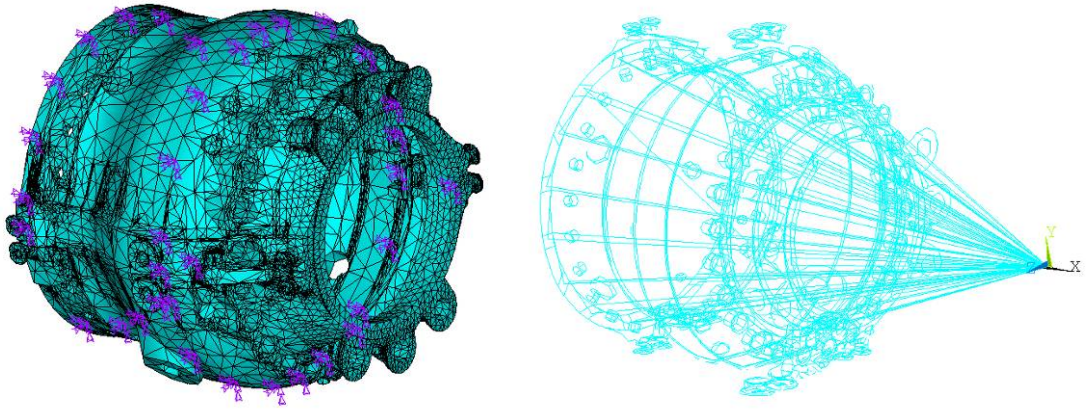

Figure 12 A section of the gas turbine and its corresponding superelement [17]

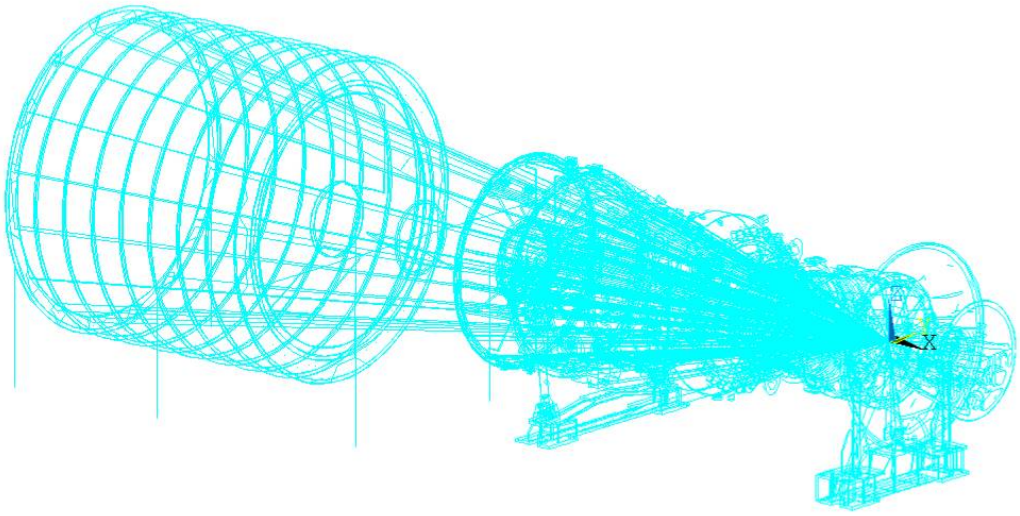

Figure 13 Assembly built out of the individual superelements [17]

The rotordynamics program used could carry out standard analyses as well as complex dynamic effects, such as rotor-structure coupling. The methodology reduced calculation time and provided capability for more detailed models.

1.6 Motivation

Moore, et al. [18] in 2006 present work that involves the rotordynamic analysis of a large industrial turbo-compressor. They demonstrate two approaches to capture the rotor-casing dynamics. The first involves the generation of a high-order polynomial in numerator-denominator transfer function format, which models the connection between the rotor and the ground at the bearings. This method is typically used in XLTRC^2 for modeling foundation supports and magnetic bearings. For the housing structure, a forced identification response is performed at each bearing in the vertical and horizontal directions. The resulting frequency response functions are used to derive the transfer functions and then incorporated into XLTRC^2. The rotor model is built in XLTRC^2, as seen in Figure 14.

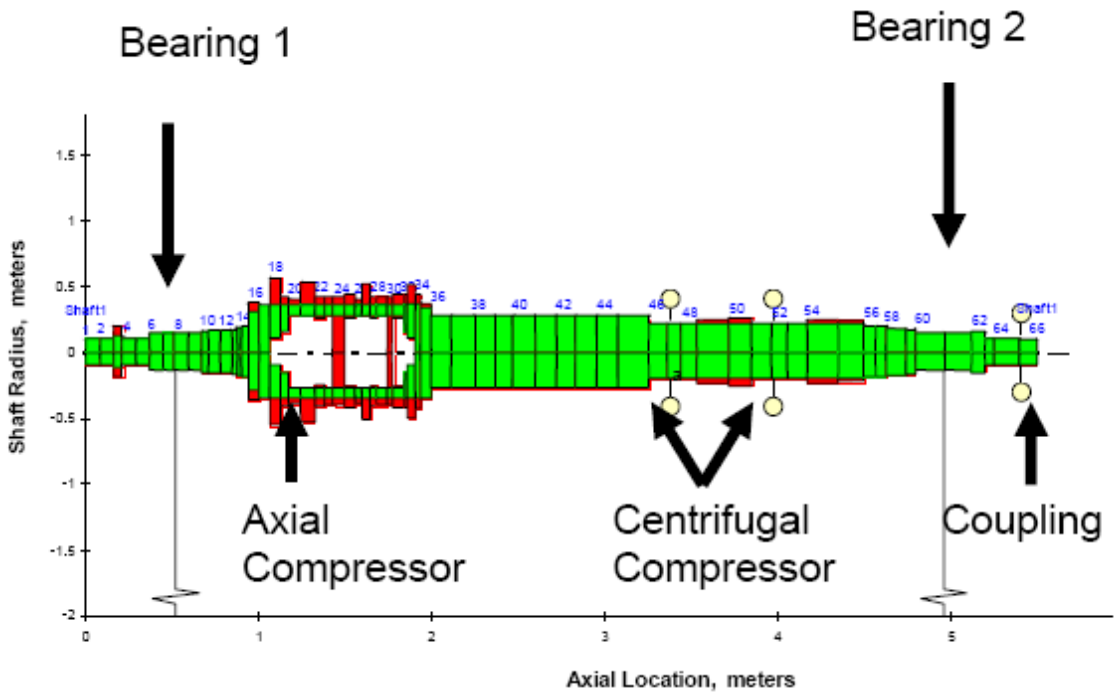

Figure 14 XLTRC^2 rotor model built by Moore et al [18]

While providing the rotordynamics code with the advantage that the analysis is computationally moderate, this approach is limited in that the motion of the separate bearings is uncoupled, which is not the case in real machines. A later personal discussion with one of the authors revealed that, even though not published in the paper, an analysis was done where the coupled effect of the bearings was studied. The results did not differ much from the uncoupled analysis. However the results were specific to this machine case, and other machines may require incorporating a coupled effect. Although this approach modeled the connections between the rotor and stator at the bearings, it erroneously left the connections at seals from rotor to ground, not rotor to housing.

The second approach used ANSYS to solve a fully coupled finite-element rotor and casing model. Figure 15 shows the original casing model built in ANSYS. The analysis eventually resulted in a refined model. Figure 16 shows the coupled rotor-casing model.

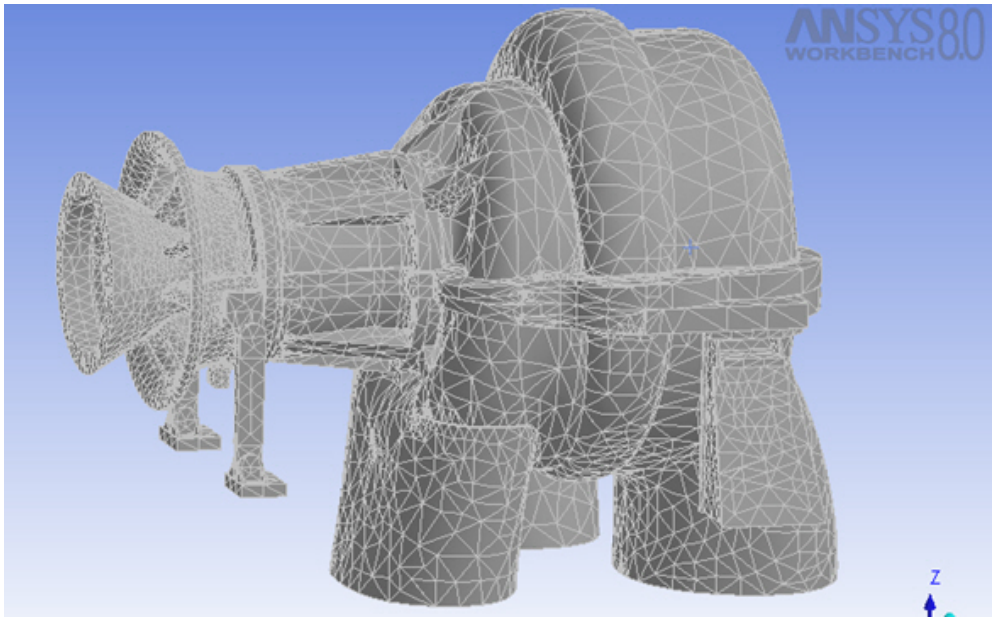

Figure 15 Casing geometry modeled in ANSYS [18]

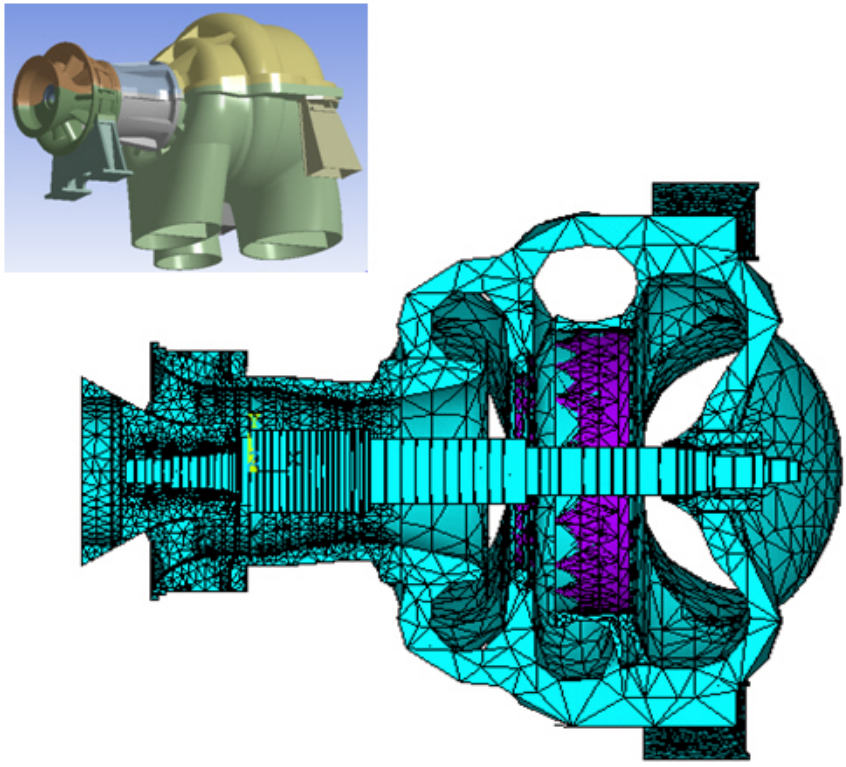

Figure 16 Sectional view of coupled rotor-casing. Inset view of entire model [18]

The FEM model, however, has two disadvantages in the scope of study. First, while ANSYS can model the bearings as a three-dimensional solid element, it does not have a direct functionality to include speed-dependent bearing coefficients. Second, capturing the interactions between the coupled rotor and casing model is computationally intense.

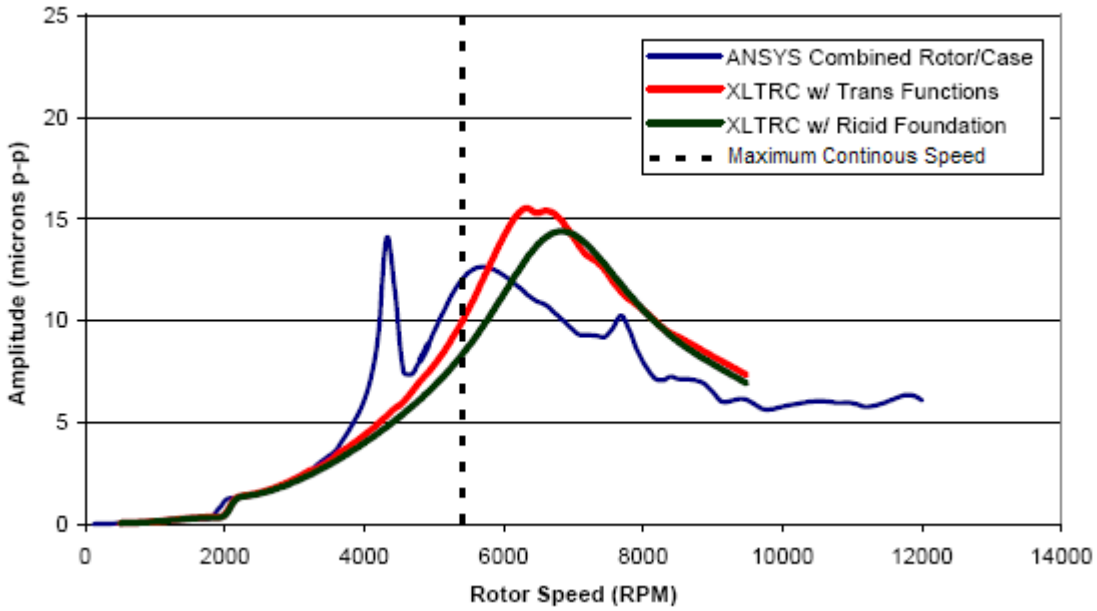

Figure 17 Unbalance response comparison between ANSYS and XLTRC^2 [18]

Figure 17 compares the vertical response at one of the bearings, between three cases – ANSYS combined rotor-casing model, XLTRC^2 rotor model that uses transfer functions, and XLTRC^2 rotor model supported on rigid foundations. Although the XLTRC^2 model with transfer functions reported the highest response amplitude, its behavior is similar to the combined rotor casing model.

The work by Moore et al. [18] stimulated this thesis, as it used the XLTRC^2 rotordynamic software suite. An alternate approach is used here with 3D FEM analysis of the casing to be done in ANSYS, and the resulting modal information incorporated

with XLTRC^2. This approach results in a combined reduced model that can be analyzed, and extends XLTRC^2 to account for three dimensional non-axisymmetric casing structures.

2 THEORY AND PRINCIPLES

2.1 Guyan Reduction

The Guyan Reduction [19] is a static reduction technique widely used to rewrite the equations of motion, representing a system such as a rotordynamic model, with a reduced number of degrees of freedom. The technique defines a set of interior coordinates in terms of boundary coordinates. By directly eliminating physical coordinates from a finite-element or lumped-parameter model, it reduces the dimensionality of the problem.

The degrees of freedom (DOFs) are categorized into master (retained) DOFs and slave (discarded) DOFs. The retained coordinates are generally selected so that they coincide with bearing locations, seal locations, unbalance locations, external-force locations, lumped masses, etc. Coordinates that are not of interest to the analysis, or are considered less important, are eliminated. Guyan suggested the reduction technique procedure so that coordinates, where no forces are applied, are eliminated. A general rotordynamic model can be represented by the following equation,

$$[M]\{\ddot{x}\}+[C]\{\dot{x}\}+[K]\{x\}=\{F\} \tag{1}$$

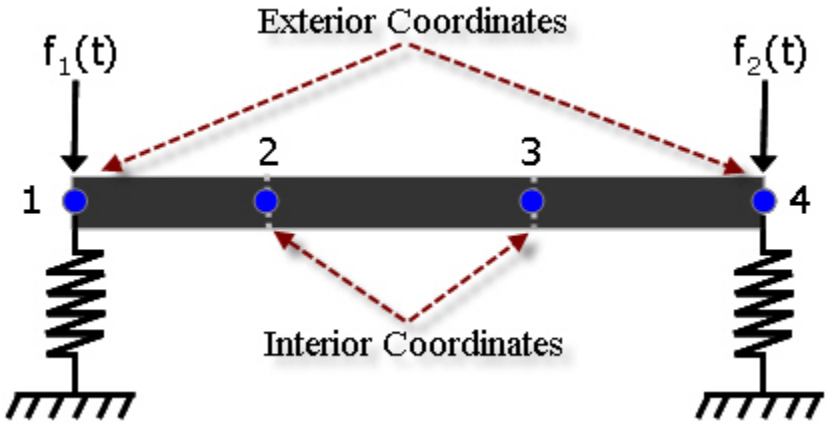

Figure 18 Simple rotor system to illustrate guyan reduction

Consider the basic equation form (without effects of damping) of a four-point mass system supported by springs at the outer ends, as shown in Figure 18. The physical model is defined by Eq.(2), and the **static** form of the equation given by Eq.(3).

$$\begin{bmatrix} m_1 & 0 & 0 & 0 \\ 0 & m_2 & 0 & 0 \\ 0 & 0 & m_3 & 0 \\ 0 & 0 & 0 & m_4 \end{bmatrix} \begin{Bmatrix} \ddot{x}_1 \\ \ddot{x}_2 \\ \ddot{x}_3 \\ \ddot{x}_4 \end{Bmatrix} + \begin{bmatrix} k_{11} & k_{12} & k_{13} & k_{14} \\ k_{21} & k_{22} & k_{23} & k_{24} \\ k_{31} & k_{32} & k_{33} & k_{34} \\ k_{41} & k_{42} & k_{43} & k_{44} \end{bmatrix} \begin{Bmatrix} x_1 \\ x_2 \\ x_3 \\ x_4 \end{Bmatrix} = \begin{Bmatrix} f_1 \\ 0 \\ 0 \\ f_4 \end{Bmatrix} \tag{2}$$

$$\begin{bmatrix} k_{11} & k_{12} & k_{13} & k_{14} \\ k_{21} & k_{22} & k_{23} & k_{24} \\ k_{31} & k_{32} & k_{33} & k_{34} \\ k_{41} & k_{42} & k_{43} & k_{44} \end{bmatrix} \begin{Bmatrix} x_1 \\ x_2 \\ x_3 \\ x_4 \end{Bmatrix} = \begin{Bmatrix} f_1 \\ 0 \\ 0 \\ f_4 \end{Bmatrix} \tag{3}$$

The bearing locations (stations 1 and 4) are selected to be the retained coordinates. Rearranging the model in terms of the boundary $(x_1,\ x_4)$ and interior $(x_2,\ x_3)$ coordinates,

$$\begin{bmatrix} k_{11} & k_{14} & k_{12} & k_{13} \\ k_{41} & k_{44} & k_{42} & k_{43} \\ k_{21} & k_{24} & k_{22} & k_{23} \\ k_{31} & k_{34} & k_{32} & k_{33} \end{bmatrix} \begin{Bmatrix} x_1 \\ x_4 \\ x_2 \\ x_3 \end{Bmatrix} = \begin{Bmatrix} f_1 \\ f_4 \\ 0 \\ 0 \end{Bmatrix} \tag{4}$$

The equation is now partitioned into two groups, representing master DOFs and slave DOFs. The master DOFs are represented by the subscript ‘m’ and slave by subscript ‘s’.

$$\begin{bmatrix} k_{mm} & k_{ms} \\ k_{sm} & k_{ss} \end{bmatrix} \begin{Bmatrix} x_m \\ x_s \end{Bmatrix} = \begin{Bmatrix} F_m \\ F_s \end{Bmatrix} \tag{5}$$

Expanding the above form leads to,

$$\begin{aligned} [k_{mm}]\{x_m\} + [k_{ms}]\{x_s\} &= \{F_m\} \\ [k_{sm}]\{x_m\} + [k_{ss}]\{x_s\} &= \{F_s\} \end{aligned} \tag{6}$$

In Guyan reduction, generally $\{F_s\} = 0$. The eliminated coordinates do not generally include external forces that need to be retained in the model. Eq.(6) becomes,

$$\begin{aligned}\left[k_{mm}\right]\left\{x_m\right\}+\left[k_{ms}\right]\left\{x_s\right\}&=\left\{F_m\right\}\\ \left[k_{sm}\right]\left\{x_m\right\}+\left[k_{ss}\right]\left\{x_s\right\}&=\left\{0\right\}\end{aligned} \tag{7}$$

Solving for the slave DOFs yields,

$$\left\{x_s\right\}=-\left[k_{ss}\right]^{-1}\left[k_{sm}\right]\left\{x_m\right\} \tag{8}$$

The transformation is then represented by,

$$\begin{Bmatrix}x_m\\ x_s\end{Bmatrix}=\begin{bmatrix}I\\ [B]\end{bmatrix}\left\{x_m\right\}=\left[B^*\right]\left\{x_m\right\} \tag{9}$$

Substituting Eq.(8) in (5) leads to the following expression that can be solved for the master DOFs.

$$\left[\left[k_{mm}\right]-\left[k_{ms}\right]\left[k_{ss}\right]^{-1}\left[k_{sm}\right]\right]\left\{x_m\right\}=\left\{F_m\right\} \tag{10}$$

Eq.(10) can be represented in general terms as,

$$\left[\hat{K}\right]\left\{\hat{x}\right\}=\left\{\hat{F}\right\} \tag{11}$$

where,

$$\left[\hat{K}\right]=\left[k_{mm}\right]-\left[k_{ms}\right]\left[k_{ss}\right]^{-1}\left[k_{sm}\right] \tag{12}$$

$$\left\{\hat{x}\right\}=\left\{x_m\right\} \tag{13}$$

$$\left\{\hat{F}\right\}=\left\{F_m\right\} \tag{14}$$

When considering the complete system Eq.(1), a similar expression can be obtained for the reduced mass and damping matrices. Since direct partitioning is not practical, owing to the time derivatives of displacement and their difficulty to implement, Guyan [19] illustrates a method by relating the structural energies of the system. This leads to the following reduced matrix forms for mass and damping matrices.

$$\left[\hat{M}\right] = \left[M_{mm}\right] - \left[K_{ms}\right]\left[K_{ss}\right]^{-1}\left[M_{sm}\right] - \left[M_{ms}\right]\left[K_{ss}\right]^{-1}\left[K_{sm}\right] + \left[K_{ms}\right]\left[K_{ss}\right]^{-1}\left[M_{ss}\right]\left[K_{ss}\right]^{-1}\left[K_{sm}\right] \tag{15}$$

$$\left[\hat{C}\right] = \left[C_{mm}\right] - \left[K_{ms}\right]\left[K_{ss}\right]^{-1}\left[C_{sm}\right] - \left[C_{ms}\right]\left[K_{ss}\right]^{-1}\left[K_{sm}\right] + \left[K_{ms}\right]\left[K_{ss}\right]^{-1}\left[C_{ss}\right]\left[K_{ss}\right]^{-1}\left[K_{sm}\right] \tag{16}$$

The final system equation, after transformations have been applied, can be represented by,

$$\left[\hat{M}\right]\left\{\ddot{x}_m\right\} + \left[\hat{C}\right]\left\{\dot{x}_m\right\} + \left[\hat{K}\right]\left\{x_m\right\} = \left\{F\right\} \tag{17}$$

$$\left\{x_s\right\} = \left[B\right]\left\{x_m\right\} \tag{18}$$

Guyan Reduction is based on the assumption that the dynamic content of the system can be defined by the retained coordinates, and that the dynamic deflected shapes are the same as the static. Since there is no modal reduction, an analyst will therefore have to have a good understanding of the system before selecting those coordinates to be retained. Ignoring critical coordinates may result in a system with results that are not accurate.

Note that none of the structural complexity is lost in the reduced stiffness matrix since all the elements make a contribution. The reduced mass matrix, however, contains both stiffness and mass elements. Rouch and Kao [20] present comparisons between a complete finite-element model of an industrial compressor on hydrodynamic bearings and its corresponding reduced models of various dimensions. The full model has 46 translation DOFs and 5 rotational DOFs. The smallest reduced model has only nine translational DOFs and zero rotational DOFs. Good correlation is demonstrated in results through the fourth calculated mode.

2.2 Component Mode Synthesis

In the analysis of rotordynamic systems, solving simultaneous equations for synchronous response or determining complex eigenvalues and eigenvectors involves large dimensionality of the underlying equations of motion. Dimensionality is common to structural-dynamics, but is intensified in rotor dynamics by reaction forces defined by nonsymmetrical stiffness, damping, and inertia matrices. These matrices can result in complex eigenvalues and eigenvectors. Component Mode Synthesis (CMS) is a method that allows reduction in the size of the overall system problem while retaining essential dynamic characteristics. CMS has been used extensively in structural analysis of buildings, frames, etc. The work of Nelson and Glasgow [21] first extended CMS for rotordynamics. Childs [22] presents a simple model to explain the component mode development.

This section illustrates CMS development to show its importance with respect to reduction of a simple rotordynamic system that consists of a rotor, casing, casing support springs, and interconnecting bearings and seals. Figure 19 shows the representative model. A lumped-parameter beam model is used to represent the rotor and the casing. To reduce the complexity of this model, only one degree of freedom is assumed at each station.

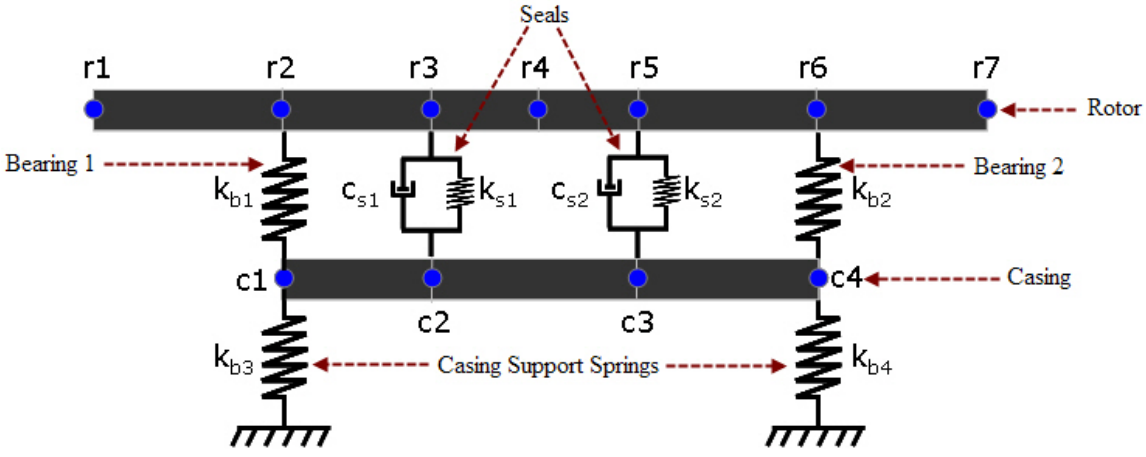

Figure 19 Rotor-casing model with bearings and seals

The rotor has 6 beams and 7 stations – *r1*, *r2*, *r3*, *r4*, *r5*, *r6*, and *r7*. The casing is made of 3 beams and has 4 stations – *c1*, *c2*, *c3*, and *c4*. The casing is connected to ground and supported by two housing support springs, *b3* and *b4*, at stations *c1* and *c4*. The rotor is supported by two bearings, *b1* and *b2* at stations *r2* and *r6*, and they provide the stiffness connection to the casing. Two interconnecting seals, *s1* and *s2*, are used between the rotor and the casing.

The development of CMS involves separating the coordinates into boundary coordinates and interior coordinates. This step is similar to Guyan Reduction where the degrees of freedom (DOFs) are categorized into master (retained) DOFs and slave (discarded) DOFs. However the advantage of CMS is that all the interior coordinates get absorbed into modal coordinates. This helps to retain all the dynamic content of the rotordynamic system. Usually, boundary coordinates are selected to coincide with frequency-dependent or nonlinear reaction locations.

Various forces act on the system. Bearing reaction forces occur at the bearing locations. In the above model, the bearing forces in the rotor acting at stations *r2*, *r6*, *c1*, and *c4* are represented by Eq.(19). For simplicity, the terms f_{r2}, f_{r6}, f_{c1}, and f_{c4} are expressed in terms of the bearing indices.

$$\begin{aligned} f_{r2} &= -f_{c1} = f_{b1} = N.L.\left(x_{r2}, x_{c1}, \dot{x}_{r2}, \dot{x}_{c1}\right) \\ f_{r6} &= -f_{c4} = f_{b2} = N.L.\left(x_{r6}, x_{c4}, \dot{x}_{r6}, \dot{x}_{c4}\right) \end{aligned} \tag{19}$$

The housing support springs forces are given by

$$\begin{aligned} f_{c1} &= f_{b3} = N.L.\left(x_{c1}, \dot{x}_{c1}\right) \\ f_{c4} &= f_{b4} = N.L.\left(x_{c4}, \dot{x}_{c4}\right) \end{aligned} \tag{20}$$

The seal forces act at stations *r3*, *c2*, *r5*, and *c3*. The rotor-model seal forces are given by,

$$\begin{aligned} f_{rs1} &= -m_{s1}\left(\ddot{x}_{r3} - \ddot{x}_{c2}\right) - c_{s1}\left(\dot{x}_{r3} - \dot{x}_{c2}\right) - k_{s1}\left(x_{r3} - x_{c2}\right) \\ f_{rs2} &= -m_{s2}\left(\ddot{x}_{r5} - \ddot{x}_{c3}\right) - c_{s2}\left(\dot{x}_{r5} - \dot{x}_{c3}\right) - k_{s2}\left(x_{r5} - x_{c3}\right) \end{aligned} \tag{21}$$

For the casing model, the seal forces have a change in sign and are represented by,

$$\begin{aligned} f_{cs1} &= m_{s1}\left(\ddot{x}_{r3} - \ddot{x}_{c2}\right) + c_{s1}\left(\dot{x}_{r3} - \dot{x}_{c2}\right) + k_{s1}\left(x_{r3} - x_{c2}\right) \\ f_{cs2} &= m_{s2}\left(\ddot{x}_{r5} - \ddot{x}_{c3}\right) + c_{s2}\left(\dot{x}_{r5} - \dot{x}_{c3}\right) + k_{s2}\left(x_{r5} - x_{c3}\right) \end{aligned} \tag{22}$$

In the first step of CMS, each shaft is assembled individually into its system matrices. For the system defined in this example, seals are the only source of damping. The initial physical model for the rotor is stated by Eq.(23). In practice, many of the stiffness coefficients are zero. The right-hand side of Eq.(23) represents the bearing reaction forces and the seal forces.

$$\begin{bmatrix} m_{r1} & 0 & 0 & 0 & 0 & 0 & 0 \\ 0 & m_{r2} & 0 & 0 & 0 & 0 & 0 \\ 0 & 0 & m_{r3} & 0 & 0 & 0 & 0 \\ 0 & 0 & 0 & m_{r4} & 0 & 0 & 0 \\ 0 & 0 & 0 & 0 & m_{r5} & 0 & 0 \\ 0 & 0 & 0 & 0 & 0 & m_{r6} & 0 \\ 0 & 0 & 0 & 0 & 0 & 0 & m_{r7} \end{bmatrix} \begin{Bmatrix} \ddot{x}_{r1} \\ \ddot{x}_{r2} \\ \ddot{x}_{r3} \\ \ddot{x}_{r4} \\ \ddot{x}_{r5} \\ \ddot{x}_{r6} \\ \ddot{x}_{r7} \end{Bmatrix}$$
$$+ \begin{bmatrix} k_{r1r1} & k_{r1r2} & k_{r1r3} & k_{r1r4} & k_{r1r5} & k_{r1r6} & k_{r1r7} \\ k_{r2r1} & k_{r2r2} & k_{r2r3} & k_{r2r4} & k_{r2r5} & k_{r2r6} & k_{r2r7} \\ k_{r3r1} & k_{r3r2} & k_{r3r3} & k_{r3r4} & k_{r3r5} & k_{r3r6} & k_{r3r7} \\ k_{r4r1} & k_{r4r2} & k_{r4r3} & k_{r4r4} & k_{r4r5} & k_{r4r6} & k_{r4r7} \\ k_{r5r1} & k_{r5r2} & k_{r5r3} & k_{r5r4} & k_{r5r5} & k_{r5r6} & k_{r5r7} \\ k_{r6r1} & k_{r6r2} & k_{r6r3} & k_{r6r4} & k_{r6r5} & k_{r6r6} & k_{r6r7} \\ k_{r7r1} & k_{r7r2} & k_{r7r3} & k_{r7r4} & k_{r7r5} & k_{r7r6} & k_{r7r7} \end{bmatrix} \begin{Bmatrix} x_{r1} \\ x_{r2} \\ x_{r3} \\ x_{r4} \\ x_{r5} \\ x_{r6} \\ x_{r7} \end{Bmatrix} = \begin{Bmatrix} 0 \\ f_{b1} \\ 0 \\ 0 \\ 0 \\ f_{b2} \\ 0 \end{Bmatrix} + \begin{Bmatrix} 0 \\ 0 \\ f_{rs1} \\ 0 \\ f_{rs2} \\ 0 \\ 0 \end{Bmatrix} \tag{23}$$

The companion equation that defines the physical model of the casing is given by Eq.(24).

$$\begin{bmatrix} m_{c1} & 0 & 0 & 0 \\ 0 & m_{c2} & 0 & 0 \\ 0 & 0 & m_{c3} & 0 \\ 0 & 0 & 0 & m_{c4} \end{bmatrix} \begin{Bmatrix} \ddot{x}_{c1} \\ \ddot{x}_{c2} \\ \ddot{x}_{c3} \\ \ddot{x}_{c4} \end{Bmatrix} + \begin{bmatrix} k_{c1c1} & k_{c1c2} & k_{c1c3} & k_{c1c4} \\ k_{c2c1} & k_{c2c2} & k_{c2c3} & k_{c2c4} \\ k_{c3c1} & k_{c3c2} & k_{c3c3} & k_{c3c4} \\ k_{c4c1} & k_{c4c2} & k_{c4c3} & k_{c4c4} \end{bmatrix} \begin{Bmatrix} x_{c1} \\ x_{c2} \\ x_{c3} \\ x_{c4} \end{Bmatrix} = \begin{Bmatrix} f_{b3} - f_{b1} \\ 0 \\ 0 \\ f_{b4} - f_{b2} \end{Bmatrix} + \begin{Bmatrix} 0 \\ f_{cs1} \\ f_{cs2} \\ 0 \end{Bmatrix} \tag{24}$$

The expansion of seal forces on the right-hand side of Eq.(23) in terms of Eq.(21) is shown in Eq.(25).

$$\begin{aligned} \begin{Bmatrix} 0 \\ 0 \\ f_{rs1} \\ 0 \\ f_{rs2} \\ 0 \\ 0 \end{Bmatrix} = & - \begin{bmatrix} 0 & 0 & 0 & 0 & 0 & 0 & 0 \\ 0 & 0 & 0 & 0 & 0 & 0 & 0 \\ 0 & 0 & m_{s1} & 0 & 0 & 0 & 0 \\ 0 & 0 & 0 & 0 & 0 & 0 & 0 \\ 0 & 0 & 0 & 0 & m_{s2} & 0 & 0 \\ 0 & 0 & 0 & 0 & 0 & 0 & 0 \\ 0 & 0 & 0 & 0 & 0 & 0 & 0 \end{bmatrix} \begin{Bmatrix} \ddot{x}_{r1} \\ \ddot{x}_{r2} \\ \ddot{x}_{r3} \\ \ddot{x}_{r4} \\ \ddot{x}_{r5} \\ \ddot{x}_{r6} \\ \ddot{x}_{r7} \end{Bmatrix} + \begin{bmatrix} 0 & 0 & 0 & 0 \\ 0 & 0 & 0 & 0 \\ 0 & m_{s1} & 0 & 0 \\ 0 & 0 & 0 & 0 \\ 0 & 0 & m_{s2} & 0 \\ 0 & 0 & 0 & 0 \\ 0 & 0 & 0 & 0 \end{bmatrix} \begin{Bmatrix} \ddot{x}_{c1} \\ \ddot{x}_{c2} \\ \ddot{x}_{c3} \\ \ddot{x}_{c4} \end{Bmatrix} \\ & - \begin{bmatrix} 0 & 0 & 0 & 0 & 0 & 0 & 0 \\ 0 & 0 & 0 & 0 & 0 & 0 & 0 \\ 0 & 0 & c_{s1} & 0 & 0 & 0 & 0 \\ 0 & 0 & 0 & 0 & 0 & 0 & 0 \\ 0 & 0 & 0 & 0 & c_{s2} & 0 & 0 \\ 0 & 0 & 0 & 0 & 0 & 0 & 0 \\ 0 & 0 & 0 & 0 & 0 & 0 & 0 \end{bmatrix} \begin{Bmatrix} \dot{x}_{r1} \\ \dot{x}_{r2} \\ \dot{x}_{r3} \\ \dot{x}_{r4} \\ \dot{x}_{r5} \\ \dot{x}_{r6} \\ \dot{x}_{r7} \end{Bmatrix} + \begin{bmatrix} 0 & 0 & 0 & 0 \\ 0 & 0 & 0 & 0 \\ 0 & c_{s1} & 0 & 0 \\ 0 & 0 & 0 & 0 \\ 0 & 0 & c_{s2} & 0 \\ 0 & 0 & 0 & 0 \\ 0 & 0 & 0 & 0 \end{bmatrix} \begin{Bmatrix} \dot{x}_{c1} \\ \dot{x}_{c2} \\ \dot{x}_{c3} \\ \dot{x}_{c4} \end{Bmatrix} \\ & - \begin{bmatrix} 0 & 0 & 0 & 0 & 0 & 0 & 0 \\ 0 & 0 & 0 & 0 & 0 & 0 & 0 \\ 0 & 0 & k_{s1} & 0 & 0 & 0 & 0 \\ 0 & 0 & 0 & 0 & 0 & 0 & 0 \\ 0 & 0 & 0 & 0 & k_{s2} & 0 & 0 \\ 0 & 0 & 0 & 0 & 0 & 0 & 0 \\ 0 & 0 & 0 & 0 & 0 & 0 & 0 \end{bmatrix} \begin{Bmatrix} x_{r1} \\ x_{r2} \\ x_{r3} \\ x_{r4} \\ x_{r5} \\ x_{r6} \\ x_{r7} \end{Bmatrix} + \begin{bmatrix} 0 & 0 & 0 & 0 \\ 0 & 0 & 0 & 0 \\ 0 & k_{s1} & 0 & 0 \\ 0 & 0 & 0 & 0 \\ 0 & 0 & k_{s2} & 0 \\ 0 & 0 & 0 & 0 \\ 0 & 0 & 0 & 0 \end{bmatrix} \begin{Bmatrix} x_{c1} \\ x_{c2} \\ x_{c3} \\ x_{c4} \end{Bmatrix} \end{aligned} \tag{25}$$

To simplify the development, the contribution of the seals to the inertia, damping, and stiffness terms will be accounted for after the transformation matrix is obtained. The rotor coordinates are now rearranged into boundary and interior coordinates as shown in Eq.(26). The coordinates which coincide with bearing locations $\left(x_{r2},\, x_{r6}\right)$ are selected as boundary coordinates.

$$\begin{bmatrix} m_{r2} & 0 & 0 & 0 & 0 & 0 & 0 \\ 0 & m_{r6} & 0 & 0 & 0 & 0 & 0 \\ 0 & 0 & m_{r1} & 0 & 0 & 0 & 0 \\ 0 & 0 & 0 & m_{r3} & 0 & 0 & 0 \\ 0 & 0 & 0 & 0 & m_{r4} & 0 & 0 \\ 0 & 0 & 0 & 0 & 0 & m_{r5} & 0 \\ 0 & 0 & 0 & 0 & 0 & 0 & m_{r7} \end{bmatrix} \begin{Bmatrix} \ddot{x}_{r2} \\ \ddot{x}_{r6} \\ \ddot{x}_{r1} \\ \ddot{x}_{r3} \\ \ddot{x}_{r4} \\ \ddot{x}_{r5} \\ \ddot{x}_{r7} \end{Bmatrix}$$

$$+ \begin{bmatrix} k_{r2r2} & k_{r2r6} & k_{r2r1} & k_{r2r3} & k_{r2r4} & k_{r2r5} & k_{r2r7} \\ k_{r6r2} & k_{r6r6} & k_{r6r1} & k_{r6r3} & k_{r6r4} & k_{r6r5} & k_{r6r7} \\ k_{r1r2} & k_{r1r6} & k_{r1r1} & k_{r1r3} & k_{r1r4} & k_{r1r5} & k_{r1r7} \\ k_{r3r2} & k_{r3r6} & k_{r3r1} & k_{r3r3} & k_{r3r4} & k_{r3r5} & k_{r3r7} \\ k_{r4r2} & k_{r4r6} & k_{r4r1} & k_{r4r3} & k_{r4r4} & k_{r4r5} & k_{r4r7} \\ k_{r5r2} & k_{r5r6} & k_{r5r1} & k_{r5r3} & k_{r5r4} & k_{r5r5} & k_{r5r7} \\ k_{r7r2} & k_{r7r6} & k_{r7r1} & k_{r7r3} & k_{r7r4} & k_{r7r5} & k_{r7r7} \end{bmatrix} \begin{Bmatrix} x_{r2} \\ x_{r6} \\ x_{r1} \\ x_{r3} \\ x_{r4} \\ x_{r5} \\ x_{r7} \end{Bmatrix} = \begin{Bmatrix} f_{b1} \\ f_{b2} \\ 0 \\ 0 \\ 0 \\ 0 \\ 0 \end{Bmatrix} + \begin{Bmatrix} 0 \\ 0 \\ 0 \\ f_{rs1} \\ 0 \\ f_{rs2} \\ 0 \end{Bmatrix} \tag{26}$$

The expansion of seal forces on the right-hand side of Eq.(24) in terms of Eq.(22) is shown in Eq.(27). As in the development of rotor equations, the contribution of the seals to the inertia, damping, and stiffness terms of the casing equation will be accounted for after the transformation matrix is obtained.

$$\begin{Bmatrix} 0 \\ f_{cs1} \\ f_{cs2} \\ 0 \end{Bmatrix} = -\begin{bmatrix} 0 & 0 & 0 & 0 \\ 0 & m_{s1} & 0 & 0 \\ 0 & 0 & m_{s2} & 0 \\ 0 & 0 & 0 & 0 \end{bmatrix} \begin{Bmatrix} \ddot{x}_{c1} \\ \ddot{x}_{c2} \\ \ddot{x}_{c3} \\ \ddot{x}_{c4} \end{Bmatrix} + \begin{bmatrix} 0 & 0 & 0 & 0 & 0 & 0 & 0 \\ 0 & 0 & m_{s1} & 0 & 0 & 0 & 0 \\ 0 & 0 & 0 & 0 & m_{s2} & 0 & 0 \\ 0 & 0 & 0 & 0 & 0 & 0 & 0 \end{bmatrix} \begin{Bmatrix} \ddot{x}_{r1} \\ \ddot{x}_{r2} \\ \ddot{x}_{r3} \\ \ddot{x}_{r4} \\ \ddot{x}_{r5} \\ \ddot{x}_{r6} \\ \ddot{x}_{r7} \end{Bmatrix}$$

$$- \begin{bmatrix} 0 & 0 & 0 & 0 \\ 0 & c_{s1} & 0 & 0 \\ 0 & 0 & c_{s2} & 0 \\ 0 & 0 & 0 & 0 \end{bmatrix} \begin{Bmatrix} \dot{x}_{c1} \\ \dot{x}_{c2} \\ \dot{x}_{c3} \\ \dot{x}_{c4} \end{Bmatrix} + \begin{bmatrix} 0 & 0 & 0 & 0 & 0 & 0 & 0 \\ 0 & 0 & c_{s1} & 0 & 0 & 0 & 0 \\ 0 & 0 & 0 & 0 & c_{s2} & 0 & 0 \\ 0 & 0 & 0 & 0 & 0 & 0 & 0 \end{bmatrix} \begin{Bmatrix} \dot{x}_{r1} \\ \dot{x}_{r2} \\ \dot{x}_{r3} \\ \dot{x}_{r4} \\ \dot{x}_{r5} \\ \dot{x}_{r6} \\ \dot{x}_{r7} \end{Bmatrix}$$

$$- \begin{bmatrix} 0 & 0 & 0 & 0 \\ 0 & k_{s1} & 0 & 0 \\ 0 & 0 & k_{s2} & 0 \\ 0 & 0 & 0 & 0 \end{bmatrix} \begin{Bmatrix} x_{c1} \\ x_{c2} \\ x_{c3} \\ x_{c4} \end{Bmatrix} + \begin{bmatrix} 0 & 0 & 0 & 0 & 0 & 0 & 0 \\ 0 & 0 & k_{s1} & 0 & 0 & 0 & 0 \\ 0 & 0 & 0 & 0 & k_{s2} & 0 & 0 \\ 0 & 0 & 0 & 0 & 0 & 0 & 0 \end{bmatrix} \begin{Bmatrix} x_{r1} \\ x_{r2} \\ x_{r3} \\ x_{r4} \\ x_{r5} \\ x_{r6} \\ x_{r7} \end{Bmatrix} \quad (27)$$

The casing equation rearranged into boundary $(x_{c1},\, x_{c4})$ and interior $(x_{c2},\, x_{c3})$ coordinates is shown in Eq.(26).

$$\begin{bmatrix} m_{c1} & 0 & 0 & 0 \\ 0 & m_{c4} & 0 & 0 \\ 0 & 0 & m_{c2} & 0 \\ 0 & 0 & 0 & m_{c3} \end{bmatrix} \begin{Bmatrix} \ddot{x}_{c1} \\ \ddot{x}_{c4} \\ \ddot{x}_{c2} \\ \ddot{x}_{c3} \end{Bmatrix} + \begin{bmatrix} k_{c1c1} & k_{c1c4} & k_{c1c2} & k_{c1c3} \\ k_{c4c1} & k_{c2c4} & k_{c4c2} & k_{c4c3} \\ k_{c2c1} & k_{c2c4} & k_{c2c2} & k_{c2c3} \\ k_{c3c1} & k_{c3c4} & k_{c3c2} & k_{c3c3} \end{bmatrix} \begin{Bmatrix} x_{c1} \\ x_{c4} \\ x_{c2} \\ x_{c3} \end{Bmatrix} = \begin{Bmatrix} f_{b3} - f_{b1} \\ f_{b4} - f_{b2} \\ 0 \\ 0 \end{Bmatrix} + \begin{Bmatrix} 0 \\ 0 \\ f_{cs1} \\ f_{cs2} \end{Bmatrix} \quad (28)$$

Static constraint modes for the rotor are now defined by producing a unit displacement of each boundary coordinate in turn, with all other boundary coordinates fixed and all interior coordinates unconstrained and unloaded. From Eq.(26) the first

static displacement vector is obtained by setting $x_{r2}=1$ and $x_{r6}=0$. When applied to Eq.(26), it leads to Eq.(31) via Eq.(29) and Eq.(30).

$$\begin{bmatrix} k_{r1r2} & k_{r1r6} & k_{r1r1} & k_{r1r3} & k_{r1r4} & k_{r1r5} & k_{r1r7} \\ k_{r3r2} & k_{r3r6} & k_{r3r1} & k_{r3r3} & k_{r3r4} & k_{r3r5} & k_{r3r7} \\ k_{r4r2} & k_{r4r6} & k_{r4r1} & k_{r4r3} & k_{r4r4} & k_{r4r5} & k_{r4r7} \\ k_{r5r2} & k_{r5r6} & k_{r5r1} & k_{r5r3} & k_{r5r4} & k_{r5r5} & k_{r5r7} \\ k_{r7r2} & k_{r7r6} & k_{r7r1} & k_{r7r3} & k_{r7r4} & k_{r7r5} & k_{r7r7} \end{bmatrix} \begin{Bmatrix} 1 \\ 0 \\ x_{r1} \\ x_{r3} \\ x_{r4} \\ x_{r5} \\ x_{r7} \end{Bmatrix} = \begin{Bmatrix} 0 \\ 0 \\ 0 \\ 0 \\ 0 \end{Bmatrix} \tag{29}$$

$$\Rightarrow \quad \begin{Bmatrix} k_{r1r2} \\ k_{r3r2} \\ k_{r4r2} \\ k_{r5r2} \\ k_{r7r2} \end{Bmatrix} + \begin{bmatrix} k_{r1r1} & k_{r1r3} & k_{r1r4} & k_{r1r5} & k_{r1r7} \\ k_{r3r1} & k_{r3r3} & k_{r3r4} & k_{r3r5} & k_{r3r7} \\ k_{r4r1} & k_{r4r3} & k_{r4r4} & k_{r4r5} & k_{r4r7} \\ k_{r5r1} & k_{r5r3} & k_{r5r4} & k_{r5r5} & k_{r5r7} \\ k_{r7r1} & k_{r7r3} & k_{r7r4} & k_{r7r5} & k_{r7r7} \end{bmatrix} \begin{Bmatrix} x_{r1} \\ x_{r3} \\ x_{r4} \\ x_{r5} \\ x_{r7} \end{Bmatrix} = \begin{Bmatrix} 0 \\ 0 \\ 0 \\ 0 \\ 0 \end{Bmatrix} \tag{30}$$

$$\Rightarrow \quad \begin{Bmatrix} x_{r1} \\ x_{r3} \\ x_{r4} \\ x_{r5} \\ x_{r7} \end{Bmatrix} = -\begin{bmatrix} k_{r1r1} & k_{r1r3} & k_{r1r4} & k_{r1r5} & k_{r1r7} \\ k_{r3r1} & k_{r3r3} & k_{r3r4} & k_{r3r5} & k_{r3r7} \\ k_{r4r1} & k_{r4r3} & k_{r4r4} & k_{r4r5} & k_{r4r7} \\ k_{r5r1} & k_{r5r3} & k_{r5r4} & k_{r5r5} & k_{r5r7} \\ k_{r7r1} & k_{r7r3} & k_{r7r4} & k_{r7r5} & k_{r7r7} \end{bmatrix}^{-1} \begin{Bmatrix} k_{r1r2} \\ k_{r3r2} \\ k_{r4r2} \\ k_{r5r2} \\ k_{r7r2} \end{Bmatrix} = \begin{Bmatrix} b_{r11} \\ b_{r13} \\ b_{r14} \\ b_{r15} \\ b_{r17} \end{Bmatrix} \tag{31}$$

By employing $x_{r2}=0$ and $x_{r6}=1$, the second static displacement vector is obtained

$$\begin{Bmatrix} x_{r1} \\ x_{r3} \\ x_{r4} \\ x_{r5} \\ x_{r7} \end{Bmatrix} = -\begin{bmatrix} k_{r1r1} & k_{r1r3} & k_{r1r4} & k_{r1r5} & k_{r1r7} \\ k_{r3r1} & k_{r3r3} & k_{r3r4} & k_{r3r5} & k_{r3r7} \\ k_{r4r1} & k_{r4r3} & k_{r4r4} & k_{r4r5} & k_{r4r7} \\ k_{r5r1} & k_{r5r3} & k_{r5r4} & k_{r5r5} & k_{r5r7} \\ k_{r7r1} & k_{r7r3} & k_{r7r4} & k_{r7r5} & k_{r7r7} \end{bmatrix}^{-1} \begin{Bmatrix} k_{r1r6} \\ k_{r3r6} \\ k_{r4r6} \\ k_{r5r6} \\ k_{r7r6} \end{Bmatrix} = \begin{Bmatrix} b_{r21} \\ b_{r23} \\ b_{r24} \\ b_{r25} \\ b_{r27} \end{Bmatrix} \tag{32}$$

The interior coordinates can now be expressed in terms of the boundary coordinates by the following transformation.

$$\begin{Bmatrix} x_{r1} \\ x_{r3} \\ x_{r4} \\ x_{r5} \\ x_{r7} \end{Bmatrix} = \begin{bmatrix} b_{r11} & b_{r21} \\ b_{r13} & b_{r23} \\ b_{r14} & b_{r24} \\ b_{r15} & b_{r25} \\ b_{r17} & b_{r27} \end{bmatrix} \begin{Bmatrix} x_{r2} \\ x_{r6} \end{Bmatrix} = [B_r] \begin{Bmatrix} x_{r2} \\ x_{r6} \end{Bmatrix} \tag{33}$$

Next, the constraint normal modes are obtained by setting the boundary coordinates to zero and solving free vibration problem for the interior coordinates as shown in Eq.(34).

$$\begin{bmatrix} m_{r1} & 0 & 0 & 0 & 0 \\ 0 & m_{r3} & 0 & 0 & 0 \\ 0 & 0 & m_{r4} & 0 & 0 \\ 0 & 0 & 0 & m_{r5} & 0 \\ 0 & 0 & 0 & 0 & m_{r7} \end{bmatrix} \begin{Bmatrix} \ddot{x}_{r1} \\ \ddot{x}_{r3} \\ \ddot{x}_{r4} \\ \ddot{x}_{r5} \\ \ddot{x}_{r7} \end{Bmatrix} + \begin{bmatrix} k_{r1r1} & k_{r1r3} & k_{r1r4} & k_{r1r5} & k_{r1r7} \\ k_{r3r1} & k_{r3r3} & k_{r3r4} & k_{r3r5} & k_{r3r7} \\ k_{r4r1} & k_{r4r3} & k_{r4r4} & k_{r4r5} & k_{r4r7} \\ k_{r5r1} & k_{r5r3} & k_{r5r4} & k_{r5r5} & k_{r5r7} \\ k_{r7r1} & k_{r7r3} & k_{r7r4} & k_{r7r5} & k_{r7r7} \end{bmatrix} \begin{Bmatrix} x_{r1} \\ x_{r3} \\ x_{r4} \\ x_{r5} \\ x_{r7} \end{Bmatrix} = \begin{Bmatrix} 0 \\ 0 \\ 0 \\ 0 \\ 0 \end{Bmatrix} \tag{34}$$

This yields the eigenvalue problem described by Eq.(35).

$$\left(-\lambda_{ri}^{\,2} \begin{bmatrix} m_{r1} & 0 & 0 & 0 & 0 \\ 0 & m_{r3} & 0 & 0 & 0 \\ 0 & 0 & m_{r4} & 0 & 0 \\ 0 & 0 & 0 & m_{r5} & 0 \\ 0 & 0 & 0 & 0 & m_{r7} \end{bmatrix} + \begin{bmatrix} k_{r1r1} & k_{r1r3} & k_{r1r4} & k_{r1r5} & k_{r1r7} \\ k_{r3r1} & k_{r3r3} & k_{r3r4} & k_{r3r5} & k_{r3r7} \\ k_{r4r1} & k_{r4r3} & k_{r4r4} & k_{r4r5} & k_{r4r7} \\ k_{r5r1} & k_{r5r3} & k_{r5r4} & k_{r5r5} & k_{r5r7} \\ k_{r7r1} & k_{r7r3} & k_{r7r4} & k_{r7r5} & k_{r7r7} \end{bmatrix} \right) \begin{Bmatrix} a_{ri1} \\ a_{ri3} \\ a_{ri4} \\ a_{ri5} \\ a_{ri7} \end{Bmatrix} = \begin{Bmatrix} 0 \\ 0 \\ 0 \\ 0 \\ 0 \end{Bmatrix} \tag{35}$$

A simplified representation of Eq.(35) is shown by Eq.(36)

$$\left\{ -\lambda_{ri}^{\,2} [m_{ri}] + [k_{rirj}] \right\} \{a_{rij}\} = \{0\} \tag{36}$$

The matrix of eigenvectors is given by,

$$[a_r] = \begin{bmatrix} a_{r11} & a_{r21} & a_{r31} & a_{r41} & a_{r51} \\ a_{r13} & a_{r23} & a_{r33} & a_{r43} & a_{r53} \\ a_{r14} & a_{r24} & a_{r35} & a_{r44} & a_{r54} \\ a_{r15} & a_{r25} & a_{r35} & a_{r45} & a_{r55} \\ a_{r17} & a_{r27} & a_{r37} & a_{r47} & a_{r57} \end{bmatrix} \tag{37}$$

and has been normalized to satisfy

$$[a_r]^T \begin{bmatrix} m_{r1} & 0 & 0 & 0 & 0 \\ 0 & m_{r3} & 0 & 0 & 0 \\ 0 & 0 & m_{r4} & 0 & 0 \\ 0 & 0 & 0 & m_{r5} & 0 \\ 0 & 0 & 0 & 0 & m_{r7} \end{bmatrix} [a_r] = [I] \tag{38}$$

$$[a_r]^T \begin{bmatrix} k_{r1r1} & k_{r1r3} & k_{r1r4} & k_{r1r5} & k_{r1r7} \\ k_{r3r1} & k_{r3r3} & k_{r3r4} & k_{r3r5} & k_{r3r7} \\ k_{r4r1} & k_{r4r3} & k_{r4r4} & k_{r4r5} & k_{r4r7} \\ k_{r5r1} & k_{r5r3} & k_{r5r4} & k_{r5r5} & k_{r5r7} \\ k_{r7r1} & k_{r7r3} & k_{r7r4} & k_{r7r5} & k_{r7r7} \end{bmatrix} [a_r] = \begin{bmatrix} \lambda_{r1}^2 & 0 & 0 & 0 & 0 \\ 0 & \lambda_{r2}^2 & 0 & 0 & 0 \\ 0 & 0 & \lambda_{r3}^2 & 0 & 0 \\ 0 & 0 & 0 & \lambda_{r4}^2 & 0 \\ 0 & 0 & 0 & 0 & \lambda_{r5}^2 \end{bmatrix} \Rightarrow [\Lambda_r] \tag{39}$$

A coordinate transformation can now be used to express the interior coordinates as the superposition of two types of displacement modes: Constrained normal modes, the displacement relative to the fixed component boundaries and constraint modes, the displacement produced by displacing boundary coordinates.

$$\begin{Bmatrix} x_{r1} \\ x_{r3} \\ x_{r4} \\ x_{r5} \\ x_{r7} \end{Bmatrix} = \begin{bmatrix} b_{1r1} & b_{2r1} \\ b_{1r3} & b_{2r3} \\ b_{1r4} & b_{2r4} \\ b_{1r5} & b_{2r5} \\ b_{1r7} & b_{2r7} \end{bmatrix} \begin{Bmatrix} x_{r2} \\ x_{r6} \end{Bmatrix} + \begin{bmatrix} a_{r11} & a_{r21} & a_{r31} & a_{r41} & a_{r51} \\ a_{r13} & a_{r23} & a_{r33} & a_{r43} & a_{r53} \\ a_{r14} & a_{r24} & a_{r35} & a_{r44} & a_{r54} \\ a_{r15} & a_{r25} & a_{r35} & a_{r45} & a_{r55} \\ a_{r17} & a_{r27} & a_{r37} & a_{r47} & a_{r57} \end{bmatrix} \begin{Bmatrix} q_{r1} \\ q_{r2} \\ q_{r3} \\ q_{r4} \\ q_{r5} \end{Bmatrix} \tag{40}$$

The complete transformation is given by Eq.(41), which shows that the boundary coordinates do not change.

$$\begin{Bmatrix} x_{r2} \\ x_{r6} \\ x_{r1} \\ x_{r3} \\ x_{r4} \\ x_{r5} \\ x_{r7} \end{Bmatrix} = \begin{bmatrix} 1 & 0 & 0 & 0 & 0 & 0 & 0 \\ 0 & 1 & 0 & 0 & 0 & 0 & 0 \\ b_{r11} & b_{r21} & a_{r11} & a_{r21} & a_{r31} & a_{r41} & a_{r51} \\ b_{r13} & b_{r23} & a_{r13} & a_{r23} & a_{r33} & a_{r43} & a_{r53} \\ b_{r14} & b_{r24} & a_{r14} & a_{r24} & a_{r34} & a_{r44} & a_{r54} \\ b_{r15} & b_{r25} & a_{r15} & a_{r25} & a_{r35} & a_{r45} & a_{r55} \\ b_{r17} & b_{r27} & a_{r17} & a_{r27} & a_{r37} & a_{r47} & a_{r57} \end{bmatrix} \begin{Bmatrix} x_{r2} \\ x_{r6} \\ q_{r1} \\ q_{r2} \\ q_{r3} \\ q_{r4} \\ q_{r5} \end{Bmatrix} \tag{41}$$

The transformation can be expressed as

$$\begin{Bmatrix} x_{r2} \\ x_{r6} \\ x_{r1} \\ x_{r3} \\ x_{r4} \\ x_{r5} \\ x_{r7} \end{Bmatrix} = [A_r] \begin{Bmatrix} x_{r2} \\ x_{r6} \\ q_{r1} \\ q_{r2} \\ q_{r3} \\ q_{r4} \\ q_{r5} \end{Bmatrix} = [A_r] \begin{Bmatrix} \{x_r\}_{2\times1} \\ \{q_r\}_{5\times1} \end{Bmatrix}_{7\times1} \tag{42}$$

where the transformation matrix $[A_r]$ is

$$[A_r] = \begin{bmatrix} [I]_{2\times2} & [0]_{2\times5} \\ [B_r]_{5\times2} & [a_r]_{5\times5} \end{bmatrix}_{7\times7} \tag{43}$$

In a similar methodology, a transformation matrix can be obtained for the casing coordinates as

$$\begin{Bmatrix} x_{c1} \\ x_{c4} \\ x_{c2} \\ x_{c3} \end{Bmatrix} = [A_c] \begin{Bmatrix} x_{c1} \\ x_{c4} \\ q_{c1} \\ q_{c2} \end{Bmatrix} = [A_c] \begin{Bmatrix} \{x_c\}_{2\times1} \\ \{q_c\}_{2\times1} \end{Bmatrix}_{4\times1} \tag{44}$$

where the transformation vector $[A_c]$ can be represented by,

$$[A_c] = \begin{bmatrix} [I]_{2\times2} & [0]_{2\times2} \\ [B_c]_{2\times2} & [a_c]_{2\times2} \end{bmatrix}_{4\times4} \tag{45}$$

The equation of the rotor system including the seal contributions, shown in Eq.(26), is expressed in simpler terms of boundary and interior coordinates by Eq.(46).

$$
\begin{aligned}
&\begin{bmatrix} [m_{rBB}]_{2\times2} & [m_{rBI}]_{2\times5} \\ [m_{rIB}]_{5\times2} & [m_{rII}]_{5\times5} \end{bmatrix}_{7\times7} \begin{Bmatrix} \{\ddot{x}_{rB}\}_{2\times1} \\ \{\ddot{x}_{rI}\}_{5\times1} \end{Bmatrix}_{7\times1} + \begin{bmatrix} [k_{rBB}]_{2\times2} & [k_{rBI}]_{2\times5} \\ [k_{rIB}]_{5\times2} & [k_{rII}]_{5\times5} \end{bmatrix}_{7\times7} \begin{Bmatrix} \{x_{rB}\}_{2\times1} \\ \{x_{rI}\}_{5\times1} \end{Bmatrix}_{7\times1} \\
&= \begin{Bmatrix} \{f_{rB}\}_{2\times1} \\ \{0\}_{5\times1} \end{Bmatrix}_{7\times1} \\
&- \begin{bmatrix} [m_{rsrBB}]_{2\times2} & [m_{rsrBI}]_{2\times5} \\ [m_{rsrIB}]_{5\times2} & [m_{rsrII}]_{5\times5} \end{bmatrix}_{7\times7} \begin{Bmatrix} \{\ddot{x}_{rB}\}_{2\times1} \\ \{\ddot{x}_{rI}\}_{5\times1} \end{Bmatrix}_{7\times1} + \begin{bmatrix} [m_{rscBB}]_{2\times2} & [m_{rscBI}]_{2\times2} \\ [m_{rscIB}]_{5\times2} & [m_{rscII}]_{5\times2} \end{bmatrix}_{7\times4} \begin{Bmatrix} \{\ddot{x}_{cB}\}_{2\times1} \\ \{\ddot{x}_{cI}\}_{2\times1} \end{Bmatrix}_{4\times1} \\
&- \begin{bmatrix} [c_{rsrBB}]_{2\times2} & [c_{rsrBI}]_{2\times5} \\ [c_{rsrIB}]_{5\times2} & [c_{rsrII}]_{5\times5} \end{bmatrix}_{7\times7} \begin{Bmatrix} \{\dot{x}_{rB}\}_{2\times1} \\ \{\dot{x}_{rI}\}_{5\times1} \end{Bmatrix}_{7\times1} + \begin{bmatrix} [c_{rscBB}]_{2\times2} & [c_{rscBI}]_{2\times2} \\ [c_{rscIB}]_{5\times2} & [c_{rscII}]_{5\times2} \end{bmatrix}_{7\times4} \begin{Bmatrix} \{\ddot{x}_{cB}\}_{2\times1} \\ \{\ddot{x}_{cI}\}_{2\times1} \end{Bmatrix}_{4\times1} \\
&- \begin{bmatrix} [k_{rsrBB}]_{2\times2} & [k_{rsrBI}]_{2\times5} \\ [k_{rsrIB}]_{5\times2} & [k_{rsrII}]_{5\times5} \end{bmatrix}_{7\times7} \begin{Bmatrix} \{x_{rB}\}_{2\times1} \\ \{x_{rI}\}_{5\times1} \end{Bmatrix}_{7\times1} + \begin{bmatrix} [k_{rscBB}]_{2\times2} & [k_{rscBI}]_{2\times2} \\ [k_{rscIB}]_{5\times2} & [k_{rscII}]_{5\times2} \end{bmatrix}_{7\times4} \begin{Bmatrix} \{\ddot{x}_{cB}\}_{2\times1} \\ \{\ddot{x}_{cI}\}_{2\times1} \end{Bmatrix}_{4\times1}
\end{aligned}
\tag{46}
$$

where

$$
\begin{bmatrix} [m_{rBB}]_{2\times2} & [m_{rBI}]_{2\times5} \\ [m_{rIB}]_{5\times2} & [m_{rII}]_{5\times5} \end{bmatrix}_{7\times7} = \begin{bmatrix} \begin{bmatrix} m_{r2} & 0 \\ 0 & m_{r6} \end{bmatrix}_{2\times2} & \begin{bmatrix} 0 & 0 & 0 & 0 & 0 \\ 0 & 0 & 0 & 0 & 0 \end{bmatrix}_{2\times5} \\ \begin{bmatrix} 0 & 0 \\ 0 & 0 \\ 0 & 0 \\ 0 & 0 \\ 0 & 0 \end{bmatrix}_{5\times2} & \begin{bmatrix} m_{r1} & 0 & 0 & 0 & 0 \\ 0 & m_{r3} & 0 & 0 & 0 \\ 0 & 0 & m_{r4} & 0 & 0 \\ 0 & 0 & 0 & m_{r5} & 0 \\ 0 & 0 & 0 & 0 & m_{r7} \end{bmatrix}_{5\times5} \end{bmatrix}_{7\times7}
$$

$$\begin{bmatrix} [k_{rBB}]_{2\times2} & [k_{rBI}]_{2\times5} \\ [k_{rIB}]_{5\times2} & [k_{rII}]_{5\times5} \end{bmatrix}_{7\times7} = \begin{bmatrix} \begin{bmatrix} k_{r2r2} & k_{r2r6} \\ k_{r6r2} & k_{r6r6} \end{bmatrix}_{2\times2} & \begin{bmatrix} k_{r2r1} & k_{r2r3} & k_{r2r4} & k_{r2r5} & k_{r2r7} \\ k_{r6r1} & k_{r6r3} & k_{r6r4} & k_{r6r5} & k_{r6r7} \end{bmatrix}_{2\times5} \\ \begin{bmatrix} k_{r1r2} & k_{r1r6} \\ k_{r3r2} & k_{r3r6} \\ k_{r4r2} & k_{r4r6} \\ k_{r5r2} & k_{r5r6} \\ k_{r7r2} & k_{r7r6} \end{bmatrix}_{5\times2} & \begin{bmatrix} k_{r1r1} & k_{r1r3} & k_{r1r4} & k_{r1r5} & k_{r1r7} \\ k_{r3r1} & k_{r3r3} & k_{r3r4} & k_{r3r5} & k_{r3r7} \\ k_{r4r1} & k_{r4r3} & k_{r4r4} & k_{r4r5} & k_{r4r7} \\ k_{r5r1} & k_{r5r3} & k_{r5r4} & k_{r5r5} & k_{r5r7} \\ k_{r7r1} & k_{r7r3} & k_{r7r4} & k_{r7r5} & k_{r7r7} \end{bmatrix}_{5\times5} \end{bmatrix}_{7\times7}$$

$$\begin{Bmatrix} \{f_{rB}\}_{2\times1} \\ \{0\}_{5\times1} \end{Bmatrix}_{7\times1} = \begin{Bmatrix} \begin{Bmatrix} f_{b1} \\ f_{b2} \end{Bmatrix}_{2\times1} \\ \begin{Bmatrix} 0 \\ 0 \\ 0 \\ 0 \\ 0 \end{Bmatrix}_{5\times1} \end{Bmatrix}_{7\times1} \qquad \begin{Bmatrix} \{x_{rB}\}_{2\times1} \\ \{x_{rI}\}_{5\times1} \end{Bmatrix}_{7\times1} = \begin{Bmatrix} \begin{Bmatrix} x_{r2} \\ x_{r6} \end{Bmatrix}_{2\times1} \\ \begin{Bmatrix} x_{r1} \\ x_{r3} \\ x_{r4} \\ x_{r5} \\ x_{r7} \end{Bmatrix}_{5\times1} \end{Bmatrix}_{7\times1}$$

$$\begin{bmatrix} [m_{rsrBB}]_{2\times2} & [m_{rsrBI}]_{2\times5} \\ [m_{rsrIB}]_{5\times2} & [m_{rsrII}]_{5\times5} \end{bmatrix}_{7\times7} = \begin{bmatrix} \begin{bmatrix} 0 & 0 \\ 0 & 0 \end{bmatrix}_{2\times2} & \begin{bmatrix} 0 & 0 & 0 & 0 & 0 \\ 0 & 0 & 0 & 0 & 0 \end{bmatrix}_{2\times5} \\ \begin{bmatrix} 0 & 0 \\ 0 & 0 \\ 0 & 0 \\ 0 & 0 \\ 0 & 0 \end{bmatrix}_{5\times2} & \begin{bmatrix} 0 & 0 & 0 & 0 & 0 \\ 0 & m_{s1} & 0 & 0 & 0 \\ 0 & 0 & 0 & 0 & 0 \\ 0 & 0 & 0 & m_{s2} & 0 \\ 0 & 0 & 0 & 0 & 0 \end{bmatrix}_{5\times5} \end{bmatrix}_{7\times7}$$

$$\begin{bmatrix} [m_{rscBB}]_{2\times2} & [m_{rscBI}]_{2\times2} \\ [m_{rscIB}]_{5\times2} & [m_{rscII}]_{5\times2} \end{bmatrix}_{7\times4} = \begin{bmatrix} \begin{bmatrix} 0 & 0 \\ 0 & 0 \end{bmatrix}_{2\times2} & \begin{bmatrix} 0 & 0 \\ 0 & 0 \end{bmatrix}_{2\times2} \\ \begin{bmatrix} 0 & 0 \\ 0 & 0 \\ 0 & 0 \\ 0 & 0 \\ 0 & 0 \end{bmatrix}_{5\times2} & \begin{bmatrix} 0 & 0 \\ m_{s1} & 0 \\ 0 & 0 \\ 0 & m_{s2} \\ 0 & 0 \end{bmatrix}_{5\times2} \end{bmatrix}_{7\times4}$$

$$\begin{bmatrix} [c_{rsrBB}]_{2\times2} & [c_{rsrBI}]_{2\times5} \\ [c_{rsrIB}]_{5\times2} & [c_{rsrII}]_{5\times5} \end{bmatrix}_{7\times7} = \begin{bmatrix} \begin{bmatrix} 0 & 0 \\ 0 & 0 \end{bmatrix}_{2\times2} & \begin{bmatrix} 0 & 0 & 0 & 0 & 0 \\ 0 & 0 & 0 & 0 & 0 \end{bmatrix}_{2\times5} \\ \begin{bmatrix} 0 & 0 \\ 0 & 0 \\ 0 & 0 \\ 0 & 0 \\ 0 & 0 \end{bmatrix}_{5\times2} & \begin{bmatrix} 0 & 0 & 0 & 0 & 0 \\ 0 & c_{s1} & 0 & 0 & 0 \\ 0 & 0 & 0 & 0 & 0 \\ 0 & 0 & 0 & c_{s2} & 0 \\ 0 & 0 & 0 & 0 & 0 \end{bmatrix}_{5\times5} \end{bmatrix}_{7\times7}$$

$$\begin{bmatrix} [c_{rscBB}]_{2\times2} & [c_{rscBI}]_{2\times2} \\ [c_{rscIB}]_{5\times2} & [c_{rscII}]_{5\times2} \end{bmatrix}_{7\times4} = \begin{bmatrix} \begin{bmatrix} 0 & 0 \\ 0 & 0 \end{bmatrix}_{2\times2} & \begin{bmatrix} 0 & 0 \\ 0 & 0 \end{bmatrix}_{2\times2} \\ \begin{bmatrix} 0 & 0 \\ 0 & 0 \\ 0 & 0 \\ 0 & 0 \\ 0 & 0 \end{bmatrix}_{5\times2} & \begin{bmatrix} 0 & 0 \\ c_{s1} & 0 \\ 0 & 0 \\ 0 & c_{s2} \\ 0 & 0 \end{bmatrix}_{5\times2} \end{bmatrix}_{7\times4}$$

$$\begin{bmatrix} [k_{rsrBB}]_{2\times2} & [k_{rsrBI}]_{2\times5} \\ [k_{rsrIB}]_{5\times2} & [k_{rsrII}]_{5\times5} \end{bmatrix}_{7\times7} = \begin{bmatrix} \begin{bmatrix} 0 & 0 \\ 0 & 0 \end{bmatrix}_{2\times2} & \begin{bmatrix} 0 & 0 & 0 & 0 & 0 \\ 0 & 0 & 0 & 0 & 0 \end{bmatrix}_{2\times5} \\ \begin{bmatrix} 0 & 0 \\ 0 & 0 \\ 0 & 0 \\ 0 & 0 \\ 0 & 0 \end{bmatrix}_{5\times2} & \begin{bmatrix} 0 & 0 & 0 & 0 & 0 \\ 0 & k_{s1} & 0 & 0 & 0 \\ 0 & 0 & 0 & 0 & 0 \\ 0 & 0 & 0 & k_{s2} & 0 \\ 0 & 0 & 0 & 0 & 0 \end{bmatrix}_{5\times5} \end{bmatrix}_{7\times7}$$

$$\begin{bmatrix} [k_{rscBB}]_{2\times2} & [k_{rscBI}]_{2\times2} \\ [k_{rscIB}]_{5\times2} & [k_{rscII}]_{5\times2} \end{bmatrix}_{7\times4} = \begin{bmatrix} \begin{bmatrix} 0 & 0 \\ 0 & 0 \end{bmatrix}_{2\times2} & \begin{bmatrix} 0 & 0 \\ 0 & 0 \end{bmatrix}_{2\times2} \\ \begin{bmatrix} 0 & 0 \\ 0 & 0 \\ 0 & 0 \\ 0 & 0 \\ 0 & 0 \end{bmatrix}_{5\times2} & \begin{bmatrix} 0 & 0 \\ k_{s1} & 0 \\ 0 & 0 \\ 0 & k_{s2} \\ 0 & 0 \end{bmatrix}_{5\times2} \end{bmatrix}_{7\times4}$$

The transformations obtained in Eq.(42) and Eq.(44) are applied to Eq.(46), and the equation is pre-multiplied by $[A_r]^T$, as shown in Eq.(47).

$$
\begin{aligned}
&[A_r]^T\begin{bmatrix}[m_{rBB}] & [m_{rBI}]\\ [m_{rIB}] & [m_{rII}]\end{bmatrix}[A_r]\begin{Bmatrix}\{\ddot{x}_{rB}\}\\ \{\ddot{q}_r\}\end{Bmatrix}+[A_r]^T\begin{bmatrix}[k_{rBB}] & [k_{rBI}]\\ [k_{rIB}] & [k_{rII}]\end{bmatrix}[A_r]\begin{Bmatrix}\{x_{rB}\}\\ \{q_r\}\end{Bmatrix}\\
&=[A_r]^T\begin{Bmatrix}\{f_{rB}\}\\ \{0\}\end{Bmatrix}\\
&-[A_r]^T\begin{bmatrix}[m_{rsrBB}] & [m_{rsrBI}]\\ [m_{rsrIB}] & [m_{rsrII}]\end{bmatrix}[A_r]\begin{Bmatrix}\{\ddot{x}_{rB}\}\\ \{\ddot{q}_r\}\end{Bmatrix}+[A_r]^T\begin{bmatrix}[m_{rscBB}] & [m_{rscBI}]\\ [m_{rscIB}] & [m_{rscII}]\end{bmatrix}[A_c]\begin{Bmatrix}\{\ddot{x}_{cB}\}\\ \{\ddot{q}_c\}\end{Bmatrix}\\
&-[A_r]^T\begin{bmatrix}[c_{rsrBB}] & [c_{rsrBI}]\\ [c_{rsrIB}] & [c_{rsrII}]\end{bmatrix}[A_r]\begin{Bmatrix}\{\dot{x}_{rB}\}\\ \{\dot{q}_r\}\end{Bmatrix}+[A_r]^T\begin{bmatrix}[c_{rscBB}] & [c_{rscBI}]\\ [c_{rscIB}] & [c_{rscII}]\end{bmatrix}[A_c]\begin{Bmatrix}\{\dot{x}_{cB}\}\\ \{\dot{q}_c\}\end{Bmatrix}\\
&-[A_r]^T\begin{bmatrix}[k_{rsrBB}] & [k_{rsrBI}]\\ [k_{rsrIB}] & [k_{rsrII}]\end{bmatrix}[A_r]\begin{Bmatrix}\{x_{rB}\}\\ \{q_r\}\end{Bmatrix}+[A_r]^T\begin{bmatrix}[k_{rscBB}] & [k_{rscBI}]\\ [k_{rscIB}] & [k_{rscII}]\end{bmatrix}[A_c]\begin{Bmatrix}\{x_{cB}\}\\ \{q_c\}\end{Bmatrix}
\end{aligned}
\tag{47}
$$

After the transformations are applied, the rotor system equation is expressed in terms of physical and modal coordinates by Eq.(48).

$$
\begin{aligned}
&\begin{bmatrix}[M_{r11}]_{2\times2} & [M_{r12}]_{2\times5}\\ [M_{r21}]_{5\times2} & [I]_{5\times5}\end{bmatrix}_{7\times7}\begin{Bmatrix}\{\ddot{x}_{rB}\}_{2\times1}\\ \{\ddot{q}_r\}_{5\times1}\end{Bmatrix}_{7\times1}+\begin{bmatrix}[K_{r11}]_{2\times2} & [K_{r12}]_{2\times5}\\ [K_{r21}]_{5\times2} & [\Lambda_r]_{5\times5}\end{bmatrix}_{7\times7}\begin{Bmatrix}\{x_{rB}\}_{2\times1}\\ \{q_r\}_{5\times1}\end{Bmatrix}_{7\times1}\\
&=\begin{Bmatrix}\{F_{rB}\}_{2\times1}\\ \{0\}_{5\times1}\end{Bmatrix}_{7\times1}\\
&-\begin{bmatrix}[M_{rsr11}]_{2\times2} & [M_{rsr12}]_{2\times5}\\ [M_{rsr21}]_{5\times2} & [M_{rsr22}]_{5\times5}\end{bmatrix}_{7\times7}\begin{Bmatrix}\{\ddot{x}_{rB}\}_{2\times1}\\ \{\ddot{q}_r\}_{5\times1}\end{Bmatrix}_{7\times1}+\begin{bmatrix}[M_{rsc11}]_{2\times2} & [M_{rsc12}]_{2\times2}\\ [M_{rsc21}]_{5\times2} & [M_{rsc22}]_{5\times2}\end{bmatrix}_{7\times4}\begin{Bmatrix}\{\ddot{x}_{cB}\}_{2\times1}\\ \{\ddot{q}_c\}_{2\times1}\end{Bmatrix}_{4\times1}\\
&-\begin{bmatrix}[C_{rsr11}]_{2\times2} & [C_{rsr12}]_{2\times5}\\ [C_{rsr21}]_{5\times2} & [C_{rsr22}]_{5\times5}\end{bmatrix}_{7\times7}\begin{Bmatrix}\{\dot{x}_{rB}\}_{2\times1}\\ \{\dot{q}_r\}_{5\times1}\end{Bmatrix}_{7\times1}+\begin{bmatrix}[C_{rsc11}]_{2\times2} & [C_{rsc12}]_{2\times2}\\ [C_{rsc21}]_{5\times2} & [C_{rsc22}]_{5\times2}\end{bmatrix}_{7\times4}\begin{Bmatrix}\{\dot{x}_{cB}\}_{2\times1}\\ \{\dot{q}_c\}_{2\times1}\end{Bmatrix}_{4\times1}\\
&-\begin{bmatrix}[K_{rsr11}]_{2\times2} & [K_{rsr12}]_{2\times5}\\ [K_{rsr21}]_{5\times2} & [K_{rsr22}]_{5\times5}\end{bmatrix}_{7\times7}\begin{Bmatrix}\{x_{rB}\}_{2\times1}\\ \{q_r\}_{5\times1}\end{Bmatrix}_{7\times1}+\begin{bmatrix}[K_{rsc11}]_{2\times2} & [K_{rsc12}]_{2\times2}\\ [K_{rsc21}]_{5\times2} & [K_{rsc22}]_{5\times2}\end{bmatrix}_{7\times4}\begin{Bmatrix}\{x_{cB}\}_{2\times1}\\ \{q_c\}_{2\times1}\end{Bmatrix}_{4\times1}
\end{aligned}
\tag{48}
$$

Similarly, transformations are applied to the casing system equations to express them in terms of physical and modal coordinates as shown by Eq.(49).

$$
\begin{bmatrix} [M_{c11}]_{2\times2} & [M_{c12}]_{2\times2} \\ [M_{c21}]_{2\times2} & [I]_{2\times2} \end{bmatrix}_{4\times4} \begin{Bmatrix} \{\ddot{x}_{cB}\}_{2\times1} \\ \{\ddot{q}_c\}_{2\times1} \end{Bmatrix}_{4\times1} + \begin{bmatrix} [K_{c11}]_{2\times2} & [K_{c12}]_{2\times2} \\ [K_{c21}]_{2\times2} & [\Lambda_c]_{2\times2} \end{bmatrix}_{4\times4} \begin{Bmatrix} \{x_{cB}\}_{2\times1} \\ \{q_c\}_{2\times1} \end{Bmatrix}_{4\times1}
$$

$$
= \begin{Bmatrix} \{F_{cB}\}_{2\times1} \\ \{0\}_{2\times1} \end{Bmatrix}_{4\times1}
$$

$$
- \begin{bmatrix} [M_{csc11}]_{2\times2} & [M_{csc12}]_{2\times2} \\ [M_{csc21}]_{2\times2} & [M_{csc22}]_{2\times2} \end{bmatrix}_{4\times4} \begin{Bmatrix} \{\ddot{x}_{cB}\}_{2\times1} \\ \{\ddot{q}_c\}_{2\times1} \end{Bmatrix}_{4\times1} + \begin{bmatrix} [M_{csr11}]_{2\times2} & [M_{csr12}]_{2\times5} \\ [M_{csr21}]_{2\times2} & [M_{csr22}]_{2\times5} \end{bmatrix}_{4\times7} \begin{Bmatrix} \{\ddot{x}_{rB}\}_{2\times1} \\ \{\ddot{q}_r\}_{5\times1} \end{Bmatrix}_{7\times1}
$$

$$
- \begin{bmatrix} [C_{csc11}]_{2\times2} & [C_{csc12}]_{2\times2} \\ [C_{csc21}]_{2\times2} & [C_{csc22}]_{2\times2} \end{bmatrix}_{4\times4} \begin{Bmatrix} \{\dot{x}_{cB}\}_{2\times1} \\ \{\dot{q}_c\}_{2\times1} \end{Bmatrix}_{4\times1} + \begin{bmatrix} [C_{csr11}]_{2\times2} & [C_{csr12}]_{2\times5} \\ [C_{csr21}]_{5\times2} & [C_{csr22}]_{2\times5} \end{bmatrix}_{4\times7} \begin{Bmatrix} \{\dot{x}_{rB}\}_{2\times1} \\ \{\dot{q}_r\}_{5\times1} \end{Bmatrix}_{7\times1}
$$

$$
- \begin{bmatrix} [K_{csc11}]_{2\times2} & [K_{csc12}]_{2\times2} \\ [K_{csc21}]_{2\times2} & [K_{csc22}]_{2\times2} \end{bmatrix}_{4\times4} \begin{Bmatrix} \{x_{cB}\}_{2\times1} \\ \{q_c\}_{2\times1} \end{Bmatrix}_{4\times1} + \begin{bmatrix} [K_{csr11}]_{2\times2} & [K_{csr12}]_{2\times5} \\ [K_{csr21}]_{5\times2} & [K_{csr22}]_{2\times5} \end{bmatrix}_{4\times7} \begin{Bmatrix} \{x_{rB}\}_{2\times1} \\ \{q_r\}_{5\times1} \end{Bmatrix}_{7\times1} \tag{49}
$$

The rotor and casing equations, (Eq.(48) and Eq.(49)), can be combined into a single model as shown in Eq.(50).

$$
\begin{bmatrix} [M_{r11}] & [M_{r12}] & 0 & 0 \\ [M_{r21}] & [I] & 0 & 0 \\ 0 & 0 & [M_{c11}] & [M_{c12}] \\ 0 & 0 & [M_{c21}] & [I] \end{bmatrix} \begin{Bmatrix} \{\ddot{x}_{rB}\} \\ \{\ddot{q}_r\} \\ \{\ddot{x}_{cB}\} \\ \{\ddot{q}_c\} \end{Bmatrix} + \begin{bmatrix} [K_{r11}] & [K_{r12}] & 0 & 0 \\ [K_{r21}] & [\Lambda_r] & 0 & 0 \\ 0 & 0 & [K_{c11}] & [K_{c12}] \\ 0 & 0 & [K_{c21}] & [\Lambda_c] \end{bmatrix} \begin{Bmatrix} \{x_{rB}\} \\ \{q_r\} \\ \{x_{cB}\} \\ \{q_c\} \end{Bmatrix}
$$

$$
= \begin{Bmatrix} \{F_{rB}\} \\ \{0\} \\ \{F_{cB}\} \\ \{0\} \end{Bmatrix} - \begin{bmatrix} [M_{rsr11}] & [M_{rsr12}] & -[M_{rsc11}] & -[M_{rsc12}] \\ [M_{rsr21}] & [M_{rsr22}] & -[M_{rsc21}] & -[M_{rsc22}] \\ -[M_{csr11}] & -[M_{csr12}] & [M_{csc11}] & [M_{csc12}] \\ -[M_{csr21}] & -[M_{csr22}] & [M_{csc21}] & [M_{csc22}] \end{bmatrix} \begin{Bmatrix} \{\ddot{x}_{rB}\} \\ \{\ddot{q}_r\} \\ \{\ddot{x}_{cB}\} \\ \{\ddot{q}_c\} \end{Bmatrix}
$$

$$
- \begin{bmatrix} [C_{rsr11}] & [C_{rsr12}] & -[C_{rsc11}] & -[C_{rsc12}] \\ [C_{rsr21}] & [C_{rsr22}] & -[C_{rsc21}] & -[C_{rsc22}] \\ -[C_{csr11}] & -[C_{csr12}] & [C_{csc11}] & [C_{csc12}] \\ -[C_{csr21}] & -[C_{csr22}] & [C_{csc21}] & [C_{csc22}] \end{bmatrix} \begin{Bmatrix} \{\dot{x}_{rB}\} \\ \{\dot{q}_r\} \\ \{\dot{x}_{cB}\} \\ \{\dot{q}_c\} \end{Bmatrix}
$$

$$
- \begin{bmatrix} [K_{rsr11}] & [K_{rsr12}] & -[K_{rsc11}] & -[K_{rsc12}] \\ [K_{rsr21}] & [K_{rsr22}] & -[K_{rsc21}] & -[K_{rsc22}] \\ -[K_{csr11}] & -[K_{csr12}] & [K_{csc11}] & [K_{csc12}] \\ -[K_{csr21}] & -[K_{csr22}] & [K_{csc21}] & [K_{csc22}] \end{bmatrix} \begin{Bmatrix} \{x_{rB}\} \\ \{q_r\} \\ \{x_{cB}\} \\ \{q_c\} \end{Bmatrix} \tag{50}
$$

The system equation can also be ordered first by physical coordinates and then by modal coordinates. Combining the inertia, damping and stiffness matrices and arranging them by physical and modal coordinates leads to Eq.(51).

$$\begin{Bmatrix} \begin{bmatrix} [M_{r11}] & 0 & [M_{r12}] & 0 \\ [M_{r21}] & 0 & [I] & 0 \\ 0 & [M_{c11}] & 0 & [M_{c12}] \\ 0 & [M_{c21}] & 0 & [I] \end{bmatrix} + \begin{bmatrix} [M_{rsr11}] & -[M_{rsc11}] & [M_{rsr12}] & -[M_{rsc12}] \\ [M_{rsr21}] & -[M_{rsc21}] & [M_{rsr22}] & -[M_{rsc22}] \\ -[M_{csr11}] & [M_{csc11}] & -[M_{csr12}] & [M_{csc12}] \\ -[M_{csr21}] & [M_{csc21}] & -[M_{csr22}] & [M_{csc22}] \end{bmatrix} \end{Bmatrix} \begin{Bmatrix} \{\ddot{x}_{rB}\} \\ \{\ddot{x}_{cB}\} \\ \{\ddot{q}_r\} \\ \{\ddot{q}_c\} \end{Bmatrix}$$

$$+ \begin{Bmatrix} \begin{bmatrix} [C_{rsr11}] & -[C_{rsc11}] & [C_{rsr12}] & -[C_{rsc12}] \\ [C_{rsr21}] & -[C_{rsc21}] & [C_{rsr22}] & -[C_{rsc22}] \\ -[C_{csr11}] & [C_{csc11}] & -[C_{csr12}] & [C_{csc12}] \\ -[C_{csr21}] & [C_{csc21}] & -[C_{csr22}] & [C_{csc22}] \end{bmatrix} \end{Bmatrix} \begin{Bmatrix} \{\dot{x}_{rB}\} \\ \{\dot{x}_{cB}\} \\ \{\dot{q}_r\} \\ \{\dot{q}_c\} \end{Bmatrix}$$

$$+ \begin{Bmatrix} \begin{bmatrix} [K_{r11}] & 0 & [K_{r12}] & 0 \\ [K_{r21}] & 0 & [\Lambda_r] & 0 \\ 0 & [K_{c11}] & 0 & [K_{c12}] \\ 0 & [K_{c21}] & 0 & [\Lambda_c] \end{bmatrix} + \begin{bmatrix} [K_{rsr11}] & -[K_{rsc11}] & [K_{rsr12}] & -[K_{rsc12}] \\ [K_{rsr21}] & -[K_{rsc21}] & [K_{rsr22}] & -[K_{rsc22}] \\ -[K_{csr11}] & [K_{csc11}] & -[K_{csr12}] & [K_{csc12}] \\ -[K_{csr21}] & [K_{csc21}] & -[K_{csr22}] & [K_{csc22}] \end{bmatrix} \end{Bmatrix} \begin{Bmatrix} \{x_{rB}\} \\ \{x_{cB}\} \\ \{q_r\} \\ \{q_c\} \end{Bmatrix} = \begin{Bmatrix} \{F_{rB}\} \\ \{F_{cB}\} \\ \{0\} \\ \{0\} \end{Bmatrix} \tag{51}$$

If internal viscous damping is present, modal damping factors can be introduced as shown in Eq.(52). Here ζ_{ri} and λ_{ri} represent the modal damping coefficient and natural frequency for the *i*th mode of the rotor. Similarly, ζ_{cj} and λ_{cj} represent modal damping coefficient and natural frequency for the *j*th mode of the casing.

$$\begin{bmatrix} [0] & [0] & [0] & & [0] & \\ [0] & [0] & [0] & & [0] & \\ & & \begin{bmatrix} \ddots & 0 & 0 \\ 0 & 2\zeta_{ri}\lambda_{ri} & 0 \\ 0 & 0 & \ddots \end{bmatrix} & & & \\ [0] & [0] & & & [0] & \\ & & & \begin{bmatrix} \ddots & 0 & 0 \\ 0 & 2\zeta_{cj}\lambda_{cj} & 0 \\ 0 & 0 & \ddots \end{bmatrix} & & \\ [0] & [0] & [0] & & & \end{bmatrix} \tag{52}$$

Combining Eq.(51) and Eq.(52) finally leads to

$$\left\{\begin{bmatrix} [M_{r11}] & 0 & [M_{r12}] & 0 \\ [M_{r21}] & 0 & [I] & 0 \\ 0 & [M_{c11}] & 0 & [M_{c12}] \\ 0 & [M_{c21}] & 0 & [I] \end{bmatrix} + \begin{bmatrix} [M_{rsr11}] & -[M_{rsc11}] & [M_{rsr12}] & -[M_{rsc12}] \\ [M_{rsr21}] & -[M_{rsc21}] & [M_{rsr22}] & -[M_{rsc22}] \\ -[M_{csr11}] & [M_{csc11}] & -[M_{csr12}] & [M_{csc12}] \\ -[M_{csr21}] & [M_{csc21}] & -[M_{csr22}] & [M_{csc22}] \end{bmatrix}\right\}\begin{Bmatrix} \{\ddot{x}_{rB}\} \\ \{\ddot{x}_{cB}\} \\ \{\ddot{q}_r\} \\ \{\ddot{q}_c\} \end{Bmatrix}$$

$$+\left\{\begin{bmatrix} [0] & [0] & [0] & [0] \\ [0] & [0] & [0] & [0] \\ [0] & [0] & \begin{bmatrix} \ddots & 0 & 0 \\ 0 & 2\zeta_{ri}\lambda_{ri} & 0 \\ 0 & 0 & \ddots \end{bmatrix} & [0] \\ [0] & [0] & [0] & \begin{bmatrix} \ddots & 0 & 0 \\ 0 & 2\zeta_{cj}\lambda_{cj} & 0 \\ 0 & 0 & \ddots \end{bmatrix} \end{bmatrix} + \begin{bmatrix} [C_{rsr11}] & -[C_{rsc11}] & [C_{rsr12}] & -[C_{rsc12}] \\ [C_{rsr21}] & -[C_{rsc21}] & [C_{rsr22}] & -[C_{rsc22}] \\ -[C_{csr11}] & [C_{csc11}] & -[C_{csr12}] & [C_{csc12}] \\ -[C_{csr21}] & [C_{csc21}] & -[C_{csr22}] & [C_{csc22}] \end{bmatrix}\right\}\begin{Bmatrix} \{\dot{x}_{rB}\} \\ \{\dot{x}_{cB}\} \\ \{\dot{q}_r\} \\ \{\dot{q}_c\} \end{Bmatrix}$$

$$+\left\{\begin{bmatrix} [K_{r11}] & 0 & [K_{r12}] & 0 \\ [K_{r21}] & 0 & [\Lambda_r] & 0 \\ 0 & [K_{c11}] & 0 & [K_{c12}] \\ 0 & [K_{c21}] & 0 & [\Lambda_c] \end{bmatrix} + \begin{bmatrix} [K_{rsr11}] & -[K_{rsc11}] & [K_{rsr12}] & -[K_{rsc12}] \\ [K_{rsr21}] & -[K_{rsc21}] & [K_{rsr22}] & -[K_{rsc22}] \\ -[K_{csr11}] & [K_{csc11}] & -[K_{csr12}] & [K_{csc12}] \\ -[K_{csr21}] & [K_{csc21}] & -[K_{csr22}] & [K_{csc22}] \end{bmatrix}\right\}\begin{Bmatrix} \{x_{rB}\} \\ \{x_{cB}\} \\ \{q_r\} \\ \{q_c\} \end{Bmatrix} = \begin{Bmatrix} \{F_{rB}\} \\ \{F_{cB}\} \\ \{0\} \\ \{0\} \end{Bmatrix} \tag{53}$$

Eq.(53) represents a simple single-plane model and can be extended to represent a full scale model that includes finite element models, gyroscopic effects, cross-coupled stiffness, and multi-plane solutions. As seen in the development leading to Eq.(53), CMS is independent of the nature of the supports at the boundary coordinates. Hence the CMS method can be extended for analysis of nonlinear supports.

In the CMS approach, truncating the number of constrained normal modes determines the number of degrees of freedom to be retained for the entire system. Though truncation criteria depend on the application, usually modes are retained whose natural frequencies are moderately above the running speed of the rotor. For the CMS development shown in this section, all modes are retained. The highest frequency modes can be truncated with little effect on the important lower modes. CMS can therefore allow a significant reduction in the size of the overall problem while retaining the essential dynamic characteristics of the lower modes.

2.3 Substructuring

Substructuring is the process of packing a group of components or groups of finite elements into one single element, called the superelement[7]. Substructuring uses Guyan reduction to reduce the model. This technique helps to reduce the time required in solving systems that have a large number of equations. The work done by Clark and Jurjevic [17], described earlier in section 1.5, shows extensive use of substructuring. A substructure can comprise a single superelement or a collection of superelements.

The process of creating a superelement using substructuring consists of the following steps:

- **Create the base model** – Here the model that needs to be substructured is created using elements types, element real constants, material properties, and the model geometry. When ANSYS is used, certain element types have restrictions for use with a substructure analysis. Figure 20 shows an example of a simple model constructed with solid elements.
- **Identify retained coordinates** – Retained coordinates are nodes designated as master degrees of freedom that define the interface between the superelement and other elements (or superelements). The dynamic characteristics of the system are then defined by these retained coordinates. Nodes representing retained coordinates are selected in such a way that they can be used later for applying constraints and forces, or at locations where output values are desired, such as nodal displacement, stress, etc. Figure 22 shows nodes that are selected as retained coordinates from the full scale node set shown in Figure 21.
- **Reduce the model** – Using the specified retained coordinates the entire model is now reduced. Reduction can be done using a Guyan reduction or component mode synthesis. The reduced model will be treated as a single superelement, as shown in Figure 23, and this reduced model can be used in further analysis.

[7] Superelement is described in detail in section 2.6.9

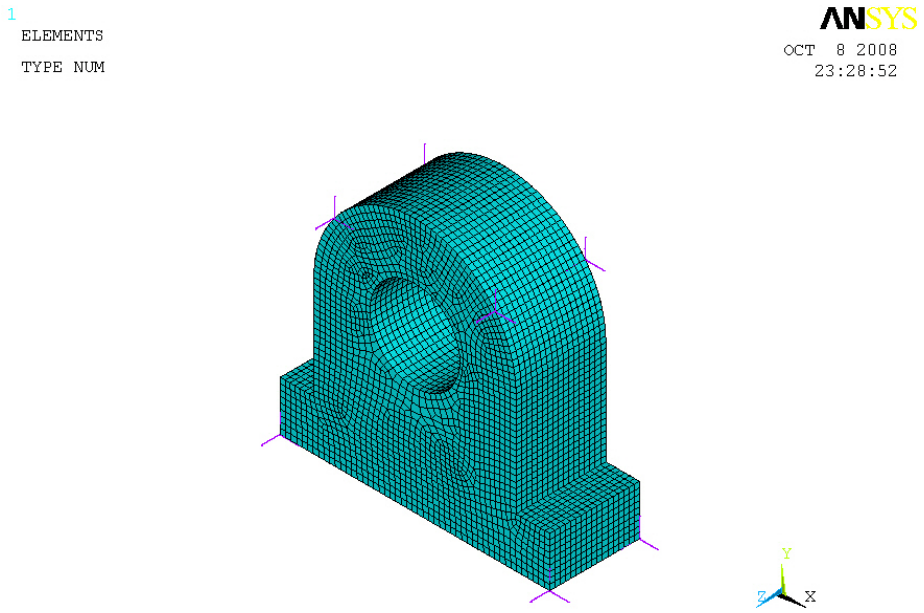

Figure 20 Example of a full scale model built with finite elements

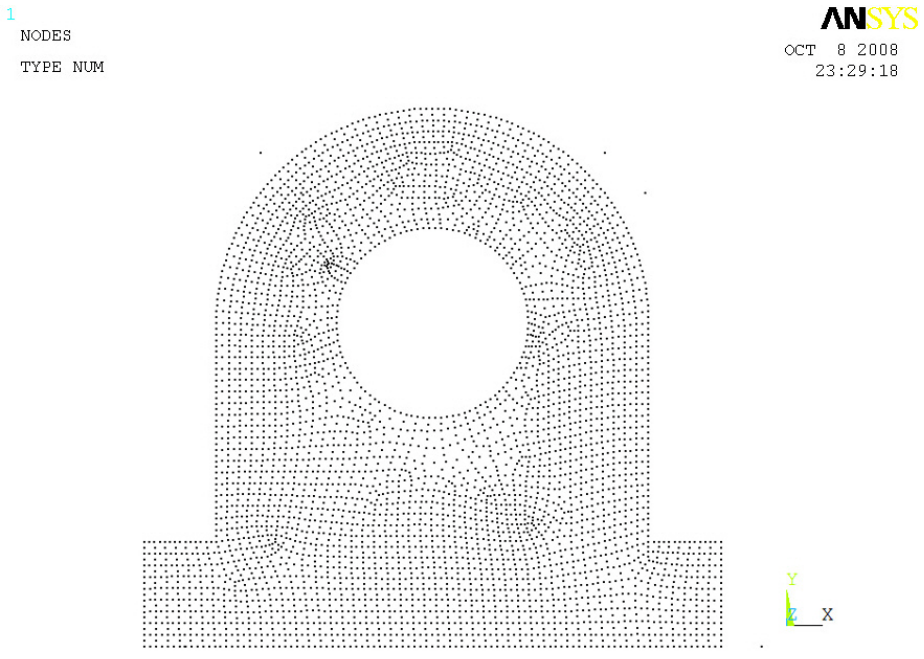

Figure 21 Front view of the complete node set in full scale model

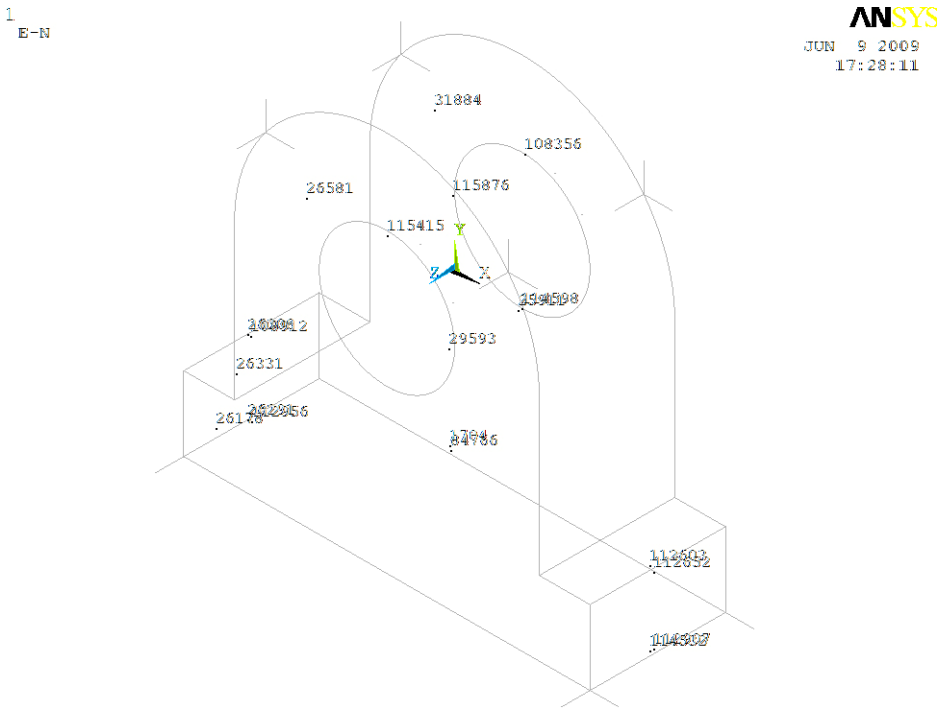

Figure 22 Nodes selected to represent retained coordinates

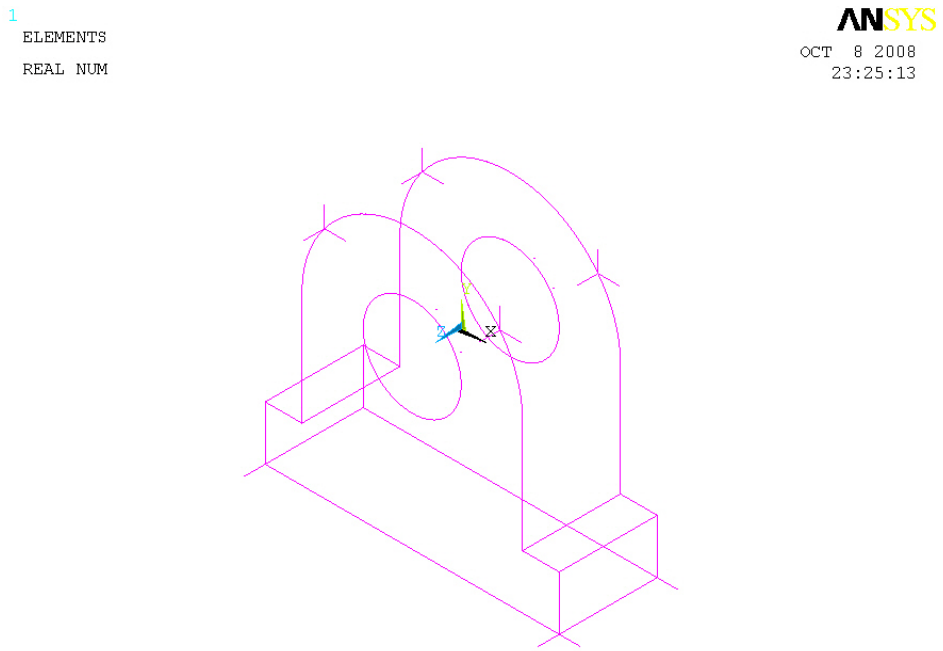

Figure 23 Superelement representation of reduced model

ANSYS includes the ANSYS Parametric Design Language (APDL) [28] that can be used to programmatically transform the coordinate system. In ANSYS, substructuring is done using the SUBSTR analysis option [29]. Figure 24 shows an APDL code snippet with the algorithm that can be used to perform substructuring.

```
! **GENERATION PASS**
! Enter the solution processor
/SOLU
! Specify the substructure analysis type
ANTYPE, SUBSTR
! Set substructure options
SEOPT, model, 2, 1, 0, resolve
! Specify solver and perform solution
EQSLV, SPARSE
SOLVE
! Create substructure file listing
SELIST, brgpdstl, 0

FINISH


! **USE PASS**
! Enter the preprocessor
/PREP7
! Define superelement and reduced model as a superelement
ET, 3000, MATRIX50
! Create material type and real constant set
TYPE, 3000
REAL, 3000
! Load the CMS reduced substructure file
SE,model, , , 0.1

FINISH
```

Figure 24 APDL code to perform substructure reduction

2.4 Modal Equations for Axisymmetric and Non-Axisymmetric Case Models

In a 3D non-axisymmetric model, structural dynamics modes can be shown by lateral modes in two orthogonal planes. This section shows the development of modal equations for axisymmetric and non-axisymmetric structural models. A simple lumped-parameter model will be used to represent a casing, as shown in Figure 25.

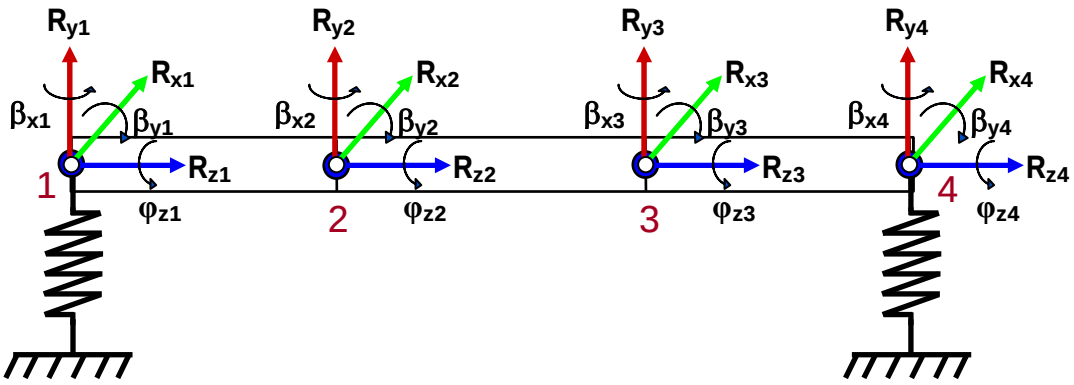

Figure 25 Lumped-parameter representation of a casing model

The casing is made of 3 beams and has 4 stations. It is connected to ground and supported by two housing support springs. Each station has six degrees of freedom – three translational motions along the *x*, *y*, and *z* axes and three rotations about the *x*, *y*, and *z* axes. The vector representing the degrees of freedom at a station is shown by Eq.(54). The second expression is simplified to eliminate the *z*-axis dependency.

$$\begin{aligned} &\left\{R_x \quad \beta_y \quad R_y \quad \beta_x \quad R_z \quad \varphi_z\right\}^T \\ &\left\{R_x \quad \beta_y \quad R_y \quad \beta_x\right\}^T \end{aligned} \tag{54}$$

Housing support reaction forces and moments, that occur at the support station 1 and 4, are given by Eq.(55).

$$\begin{aligned} f_1 &= N.L.\left(R_{x1}, \dot{R}_{x1}, R_{y1}, \dot{R}_{y1}\right) \;\; ; \;\; \hat{M}_1 = N.L.\left(\beta_{y1}, \dot{\beta}_{y1}, \beta_{x1}, \dot{\beta}_{x1}\right) \\ f_4 &= N.L.\left(R_{x4}, \dot{R}_{x4}, R_{y4}, \dot{R}_{y4}\right) \;\; ; \;\; \hat{M}_4 = N.L.\left(\beta_{y4}, \dot{\beta}_{y4}, \beta_{x4}, \dot{\beta}_{x4}\right) \end{aligned} \tag{55}$$

First, modal equations are developed for the uncoupled casing model. Separate uncoupled modal differential equations are developed for each plane. The initial physical model for the casing in the $X-Z$ plane is

$$\begin{bmatrix} m_{1R_{x1}} & 0 & 0 & 0 & 0 & 0 & 0 & 0 \\ 0 & J_{1\beta_{y1}} & 0 & 0 & 0 & 0 & 0 & 0 \\ 0 & 0 & m_{2R_{x2}} & 0 & 0 & 0 & 0 & 0 \\ 0 & 0 & 0 & J_{2\beta_{y2}} & 0 & 0 & 0 & 0 \\ 0 & 0 & 0 & 0 & m_{3R_{x3}} & 0 & 0 & 0 \\ 0 & 0 & 0 & 0 & 0 & J_{3\beta_{y3}} & 0 & 0 \\ 0 & 0 & 0 & 0 & 0 & 0 & m_{4R_{x4}} & 0 \\ 0 & 0 & 0 & 0 & 0 & 0 & 0 & J_{4\beta_{y4}} \end{bmatrix}_{8x8} \begin{Bmatrix} \ddot{R}_{x1} \\ \ddot{\beta}_{y1} \\ \ddot{R}_{x2} \\ \ddot{\beta}_{y2} \\ \ddot{R}_{x3} \\ \ddot{\beta}_{y3} \\ \ddot{R}_{x4} \\ \ddot{\beta}_{y4} \end{Bmatrix}_{8x1}$$

$$+ \begin{bmatrix} k_{R_{x1}R_{x1}} & k_{R_{x1}\beta_{y1}} & k_{R_{x1}R_{x2}} & k_{R_{x1}\beta_{y2}} & k_{R_{x1}R_{x3}} & k_{R_{x1}\beta_{y3}} & k_{R_{x1}R_{x4}} & k_{R_{x1}\beta_{y4}} \\ k_{\beta_{y1}R_{x1}} & k_{\beta_{y1}\beta_{y1}} & k_{\beta_{y1}R_{x2}} & k_{\beta_{y1}\beta_{y2}} & k_{\beta_{y1}R_{x3}} & k_{\beta_{y1}\beta_{y3}} & k_{\beta_{y1}R_{x4}} & k_{\beta_{y1}\beta_{y4}} \\ k_{R_{x2}R_{x1}} & k_{R_{x2}\beta_{y1}} & k_{R_{x2}R_{x2}} & k_{R_{x2}\beta_{y2}} & k_{R_{x2}R_{x3}} & k_{R_{x2}\beta_{y3}} & k_{R_{x2}R_{x4}} & k_{R_{x2}\beta_{y4}} \\ k_{\beta_{y2}R_{x1}} & k_{\beta_{y2}\beta_{y1}} & k_{\beta_{y2}R_{x2}} & k_{\beta_{y2}\beta_{y2}} & k_{\beta_{y2}R_{x3}} & k_{\beta_{y2}\beta_{y3}} & k_{\beta_{y2}R_{x4}} & k_{\beta_{y2}\beta_{y4}} \\ k_{R_{x3}R_{x1}} & k_{R_{x3}\beta_{y1}} & k_{R_{x3}R_{x2}} & k_{R_{x3}\beta_{y2}} & k_{R_{x3}R_{x3}} & k_{R_{x3}\beta_{y3}} & k_{R_{x3}R_{x4}} & k_{R_{x3}\beta_{y4}} \\ k_{\beta_{y3}R_{x1}} & k_{\beta_{y3}\beta_{y1}} & k_{\beta_{y3}R_{x2}} & k_{\beta_{y3}\beta_{y2}} & k_{\beta_{y3}R_{x3}} & k_{\beta_{y3}\beta_{y3}} & k_{\beta_{y3}R_{x4}} & k_{\beta_{y3}\beta_{y4}} \\ k_{R_{x4}R_{x1}} & k_{R_{x4}\beta_{y1}} & k_{R_{x4}R_{x2}} & k_{R_{x4}\beta_{y2}} & k_{R_{x4}R_{x3}} & k_{R_{x4}\beta_{y3}} & k_{R_{x4}R_{x4}} & k_{R_{x4}\beta_{y4}} \\ k_{\beta_{y4}R_{x1}} & k_{\beta_{y4}\beta_{y1}} & k_{\beta_{y4}R_{x2}} & k_{\beta_{y4}\beta_{y2}} & k_{\beta_{y4}R_{x3}} & k_{\beta_{y4}\beta_{y3}} & k_{\beta_{y4}R_{x4}} & k_{\beta_{y4}\beta_{y4}} \end{bmatrix}_{8x8} \begin{Bmatrix} R_{x1} \\ \beta_{y1} \\ R_{x2} \\ \beta_{y2} \\ R_{x3} \\ \beta_{y3} \\ R_{x4} \\ \beta_{y4} \end{Bmatrix}_{8x1} = \begin{Bmatrix} f_{x1} \\ \hat{M}_{y1} \\ 0 \\ 0 \\ 0 \\ 0 \\ f_{x4} \\ \hat{M}_{y4} \end{Bmatrix}_{8x1} \quad (56)$$

For simplicity, the coordinates, forces, and moments are stated by Eq.(57). Each term in the simplified coordinate will include both displacement and rotation. Similarly, each term in the simplified force expression will include both lateral force and moment.

$$\begin{aligned} \{X\} &= \{R_x \quad \beta_y\}^T \quad ; \quad \{F_X\} = \{f_x \quad \hat{M}_y\}^T \\ \{Y\} &= \{R_y \quad \beta_x\}^T \quad ; \quad \{F_Y\} = \{f_y \quad \hat{M}_x\}^T \end{aligned} \quad (57)$$

The simplified terms defined in Eq.(57) are applied to Eq.(56) to result in

$$\begin{bmatrix} M_{1X} & 0 & 0 & 0 \\ 0 & M_{2X} & 0 & 0 \\ 0 & 0 & M_{3X} & 0 \\ 0 & 0 & 0 & M_{4X} \end{bmatrix}_{8x8} \begin{Bmatrix} \ddot{X}_1 \\ \ddot{X}_2 \\ \ddot{X}_3 \\ \ddot{X}_4 \end{Bmatrix}_{8x1} + \begin{bmatrix} K_{1X1X} & K_{1X2X} & K_{1X3X} & K_{1X4X} \\ K_{2x1X} & K_{2X2X} & K_{2X3X} & K_{2X4X} \\ K_{3X1X} & K_{3X2X} & K_{3X3X} & K_{3X4X} \\ K_{4X1X} & K_{4X2X} & K_{4X3X} & K_{4X4X} \end{bmatrix}_{8x8} \begin{Bmatrix} X_1 \\ X_2 \\ X_3 \\ X_4 \end{Bmatrix}_{8x1} = \begin{Bmatrix} F_{1X} \\ 0 \\ 0 \\ F_{4X} \end{Bmatrix}_{8x1} \tag{58}$$

Eq.(58) is rearranged into boundary and interior coordinates. The bearing locations are selected as the boundary coordinates to obtain

$$\begin{bmatrix} M_{1X} & 0 & 0 & 0 \\ 0 & M_{4X} & 0 & 0 \\ 0 & 0 & M_{2X} & 0 \\ 0 & 0 & 0 & M_{3X} \end{bmatrix}_{8x8} \begin{Bmatrix} \ddot{X}_1 \\ \ddot{X}_4 \\ \ddot{X}_2 \\ \ddot{X}_3 \end{Bmatrix}_{8x1} + \begin{bmatrix} K_{1X1X} & K_{1X4X} & K_{1X2X} & K_{1X3X} \\ K_{4X1X} & K_{4X4X} & K_{4X2X} & K_{4X3X} \\ K_{2X1X} & K_{2X4X} & K_{2X2X} & K_{2X3X} \\ K_{3X1X} & K_{3X4X} & K_{3X2X} & K_{3X3X} \end{bmatrix}_{8x8} \begin{Bmatrix} X_1 \\ X_4 \\ X_2 \\ X_3 \end{Bmatrix}_{8x1} = \begin{Bmatrix} F_{1X} \\ F_{4X} \\ 0 \\ 0 \end{Bmatrix}_{8x1} \tag{59}$$

CMS is performed on the model. A transformation vector $[A_X]$ is developed to express the interior coordinates as the superposition of two types of displacement modes – *constrained normal modes*, the displacement relative to the fixed component boundaries and *constraint modes*, the displacement produced by displacing boundary coordinates. The complete transformation is given by Eq.(60). The boundary coordinates do not change while interior coordinates are changed by the transformation.

$$\begin{Bmatrix} X_1 \\ X_4 \\ X_2 \\ X_3 \end{Bmatrix}_{8x1} = [A_X]_{8x8} \begin{Bmatrix} X_1 \\ X_4 \\ (q_X)_i \end{Bmatrix}_{8x1} \tag{60}$$

Applying the transformation $[A_X]$ to Eq.(59), pre-multiplying by $[A_X]^T$, and simplifying the expression, results in

$$\begin{bmatrix} \bar{M}_{1X1X} & \bar{M}_{1X2X} \\ \bar{M}_{2X1X} & I \end{bmatrix}_{8x8} \begin{Bmatrix} \ddot{X}_1 \\ \ddot{X}_4 \\ (\ddot{q}_X)_i \end{Bmatrix}_{8x1} + \begin{bmatrix} \bar{K}_{1X1X} & \bar{K}_{1X2X} \\ \bar{K}_{2X1X} & \Lambda_X \end{bmatrix}_{8x8} \begin{Bmatrix} X_1 \\ X_4 \\ (q_X)_i \end{Bmatrix}_{8x1} = [A_X]^T_{8x8} \begin{Bmatrix} F_{1X} \\ F_{4X} \\ 0 \\ 0 \end{Bmatrix}_{8x1} \tag{61}$$

In a similar manner, the modal differential equation for the $Y-Z$ plane is

$$\begin{bmatrix} \bar{M}_{1Y1Y} & \bar{M}_{1Y2Y} \\ \bar{M}_{2Y1Y} & I \end{bmatrix}_{8x8} \begin{Bmatrix} \ddot{Y}_1 \\ \ddot{Y}_4 \\ (\ddot{q}_Y)_i \end{Bmatrix}_{8x1} + \begin{bmatrix} \bar{K}_{1Y1Y} & \bar{K}_{1Y2Y} \\ \bar{K}_{2Y1Y} & \Lambda_Y \end{bmatrix}_{8x8} \begin{Bmatrix} Y_1 \\ Y_4 \\ (q_Y)_i \end{Bmatrix}_{8x1} = [A_Y]^T_{8x8} \begin{Bmatrix} F_{1Y} \\ F_{4Y} \\ 0 \\ 0 \end{Bmatrix}_{8x1} \quad (62)$$

As seen from Eq.(61) and Eq.(62), the $X-Z$ plane has one set of equations and eigenvectors. The $Y-Z$ plane has a comparable set of equations and eigen data for axisymmetric structures. In the CMS development, different number of modes can be retained in $X-Z$ and $Y-Z$ planes. If the same m stations are used in both planes, $[A_X]$ will be a $2m\times(4+j)$ matrix where m indicates the number of casing stations (each with two DOF), and j denotes the modes retained in the $X-Z$ plane. Likewise, $[A_Y]$ will be a $2m\times(4+k)$ matrix where k denotes modes retained in the $Y-Z$ plane.

The initial physical model for the casing in the coupled non-axisymmetric model is given by one set of equations, as shown in Eq.(63).

$$\begin{bmatrix} M_{1X} & 0 & 0 & 0 & 0 & 0 & 0 & 0 \\ 0 & M_{2X} & 0 & 0 & 0 & 0 & 0 & 0 \\ 0 & 0 & M_{3X} & 0 & 0 & 0 & 0 & 0 \\ 0 & 0 & 0 & M_{4X} & 0 & 0 & 0 & 0 \\ 0 & 0 & 0 & 0 & M_{1Y} & 0 & 0 & 0 \\ 0 & 0 & 0 & 0 & 0 & M_{2Y} & 0 & 0 \\ 0 & 0 & 0 & 0 & 0 & 0 & M_{3Y} & 0 \\ 0 & 0 & 0 & 0 & 0 & 0 & 0 & M_{4Y} \end{bmatrix} \begin{Bmatrix} \ddot{X}_1 \\ \ddot{X}_2 \\ \ddot{X}_3 \\ \ddot{X}_4 \\ \ddot{Y}_1 \\ \ddot{Y}_2 \\ \ddot{Y}_3 \\ \ddot{Y}_4 \end{Bmatrix}$$

$$+ \begin{bmatrix} K_{1X1X} & K_{1X2X} & K_{1X3X} & K_{1X4X} & K_{1X1Y} & K_{1X2Y} & K_{1X3Y} & K_{1X4Y} \\ K_{2x1X} & K_{2X2X} & K_{2X3X} & K_{2X4X} & K_{2X1Y} & K_{2X2Y} & K_{2X3Y} & K_{2X4Y} \\ K_{3X1X} & K_{3X2X} & K_{3X3X} & K_{3X4X} & K_{3X1Y} & K_{3X2Y} & K_{3X3Y} & K_{3X4Y} \\ K_{4X1X} & K_{4X2X} & K_{4X3X} & K_{4X4X} & K_{4X1Y} & K_{4X2Y} & K_{4X3Y} & K_{4X4Y} \\ K_{1Y1X} & K_{1Y2X} & K_{1Y3X} & K_{1Y4X} & K_{1Y1Y} & K_{1Y2Y} & K_{1Y3Y} & K_{1Y4Y} \\ K_{2Y1X} & K_{2Y2X} & K_{2Y3X} & K_{2Y4X} & K_{2Y1Y} & K_{2Y2Y} & K_{2Y3Y} & K_{2Y4Y} \\ K_{3Y1X} & K_{3Y2X} & K_{3Y3X} & K_{3Y4X} & K_{3Y1Y} & K_{3Y2Y} & K_{3Y3Y} & K_{3Y4Y} \\ K_{4Y1X} & K_{4Y2X} & K_{4Y3X} & K_{4Y4X} & K_{4Y1Y} & K_{4Y2Y} & K_{4Y3Y} & K_{4Y4Y} \end{bmatrix} \begin{Bmatrix} X_1 \\ X_2 \\ X_3 \\ X_4 \\ Y_1 \\ Y_2 \\ Y_3 \\ Y_4 \end{Bmatrix} = \begin{Bmatrix} F_{1X} \\ 0 \\ 0 \\ F_{4X} \\ F_{1Y} \\ 0 \\ 0 \\ F_{4Y} \end{Bmatrix} \quad (63)$$

Eq. (63) is rearranged into boundary and interior coordinates.

$$\begin{bmatrix} M_{1X} & 0 & 0 & 0 & 0 & 0 & 0 & 0 \\ 0 & M_{1Y} & 0 & 0 & 0 & 0 & 0 & 0 \\ 0 & 0 & M_{4X} & 0 & 0 & 0 & 0 & 0 \\ 0 & 0 & 0 & M_{4Y} & 0 & 0 & 0 & 0 \\ 0 & 0 & 0 & 0 & M_{2X} & 0 & 0 & 0 \\ 0 & 0 & 0 & 0 & 0 & M_{2Y} & 0 & 0 \\ 0 & 0 & 0 & 0 & 0 & 0 & M_{3X} & 0 \\ 0 & 0 & 0 & 0 & 0 & 0 & 0 & M_{3Y} \end{bmatrix} \begin{Bmatrix} \ddot{X}_1 \\ \ddot{Y}_1 \\ \ddot{X}_4 \\ \ddot{Y}_4 \\ \ddot{X}_2 \\ \ddot{Y}_2 \\ \ddot{X}_3 \\ \ddot{Y}_3 \end{Bmatrix}$$

$$+ \begin{bmatrix} K_{1X1X} & K_{1X1Y} & K_{1X4X} & K_{1X4Y} & K_{1X2X} & K_{1X2Y} & K_{1X3X} & K_{1X3Y} \\ K_{1Y1X} & K_{1Y1Y} & K_{1Y4X} & K_{1Y4Y} & K_{1Y2X} & K_{1Y2Y} & K_{1Y3X} & K_{1Y3Y} \\ K_{4X1X} & K_{4X1Y} & K_{4X4X} & K_{4X4Y} & K_{4X2X} & K_{4X2Y} & K_{4X3X} & K_{4X3Y} \\ K_{4Y1X} & K_{4Y1Y} & K_{4Y4X} & K_{4Y4Y} & K_{4Y2X} & K_{4Y2Y} & K_{4Y3X} & K_{4Y3Y} \\ K_{2X1X} & K_{2X1Y} & K_{2X4X} & K_{2X4Y} & K_{2X2X} & K_{2X2Y} & K_{2X3X} & K_{2X3Y} \\ K_{2Y1X} & K_{2Y1Y} & K_{2Y4X} & K_{2Y4Y} & K_{2Y2X} & K_{2Y2Y} & K_{2Y3X} & K_{2Y3Y} \\ K_{3X1X} & K_{3X1Y} & K_{3X4X} & K_{3X4Y} & K_{3X2X} & K_{3X2Y} & K_{3X3X} & K_{3X3Y} \\ K_{3Y1X} & K_{3Y1Y} & K_{3Y4X} & K_{3Y4Y} & K_{3Y2X} & K_{3Y2Y} & K_{3Y3X} & K_{3Y3Y} \end{bmatrix} \begin{Bmatrix} X_1 \\ Y_1 \\ X_4 \\ Y_4 \\ X_2 \\ Y_2 \\ X_3 \\ Y_3 \end{Bmatrix} = \begin{Bmatrix} F_{1X} \\ F_{1Y} \\ F_{4X} \\ F_{4Y} \\ 0 \\ 0 \\ 0 \\ 0 \end{Bmatrix} \quad (64)$$

A transformation vector $[A]$ is used to express the interior coordinates in terms of the boundary coordinates as shown in Eq.(65).

$$\begin{Bmatrix} X_1 \\ Y_1 \\ X_4 \\ Y_4 \\ X_2 \\ Y_2 \\ X_3 \\ Y_3 \end{Bmatrix} = [A] \begin{Bmatrix} X_1 \\ Y_1 \\ X_4 \\ Y_4 \\ (q)_i \end{Bmatrix} \quad (65)$$

Applying the transformation vector $[A]$ to Eq.(64), pre-multiplying by $[A]^T$, and simplifying the expression, results in

$$\begin{bmatrix} \bar{M}_{11} & \bar{M}_{12} \\ \bar{M}_{21} & I \end{bmatrix} \begin{Bmatrix} \ddot{X}_1 \\ \ddot{Y}_1 \\ \ddot{X}_4 \\ \ddot{Y}_4 \\ (\ddot{q})_i \end{Bmatrix} + \begin{bmatrix} \bar{K}_{11} & \bar{K}_{12} \\ \bar{K}_{21} & \Lambda \end{bmatrix} \begin{Bmatrix} X_1 \\ Y_1 \\ X_4 \\ Y_4 \\ (q)_i \end{Bmatrix} = [A]^T \begin{Bmatrix} F_{1X} \\ F_{1Y} \\ F_{4X} \\ F_{4Y} \\ 0 \\ 0 \\ 0 \\ 0 \end{Bmatrix} \tag{66}$$

Eq.(66) represents the casing CMS model. The eigenvector $[A]$ defines motion in both orthogonal planes. If m stations are used in both planes, $[A]$ will be a $4m \times (4 + j)$ matrix where m indicates the number of casing stations (each with four DOF), and j denotes the modes retained. Eq.(66) can be extended to represent a full scale model that includes finite elements, structural damping, and seal forces.

2.5 Coordinate Transformation

Coordinate transformation is the process by which one coordinate system is converted to another, to describe the same space. A direction-cosine matrix is used to relate components of the same vector in two different coordinate systems. The direction-cosine matrix relates the components in two coordinate systems and is defined as a real square matrix whose transpose is its inverse and whose determinant is 1. If $[A]$ is a direction-cosine matrix, then

$$\begin{aligned} &[A]^T [A] = [I] = [A]^T [A] \\ &|A| = 1 \end{aligned} \tag{67}$$

Numerous references exist about the process of coordinate transformation. Childs [23] explains the process for coordinate transformation in a Two-Coordinate system. Consider a vector U in a $X - Y$ coordinate system. If the coordinate system $X - Y$ is rotated through an angle α in the counter-clockwise direction to get the $X' - Y'$ system, the transformation can be defined as the following

$$\begin{Bmatrix} U_{X'} \\ U_{Y'} \end{Bmatrix} = \begin{bmatrix} \cos\alpha & \sin\alpha \\ -\sin\alpha & \cos\alpha \end{bmatrix} \begin{Bmatrix} U_X \\ U_Y \end{Bmatrix} \tag{68}$$

$$\text{or} \quad \{U'\} = [A]\{U\}$$

where $[A]$ is called the direction-cosine matrix.

The above result can be extended to a Three-Coordinate system. Three ordered angles that are used to transform one coordinate system to another are referred to as *Euler angles*. Figure 26 shows the Euler angles α, β and γ used to rotate the coordinate system from XYZ to $X'Y'Z'$. In generating three sets of rotation, when transforming from one coordinate system to another, there are several choices in which no two adjacent rotation indices are the same. These various sets are called Euler angle sequences.

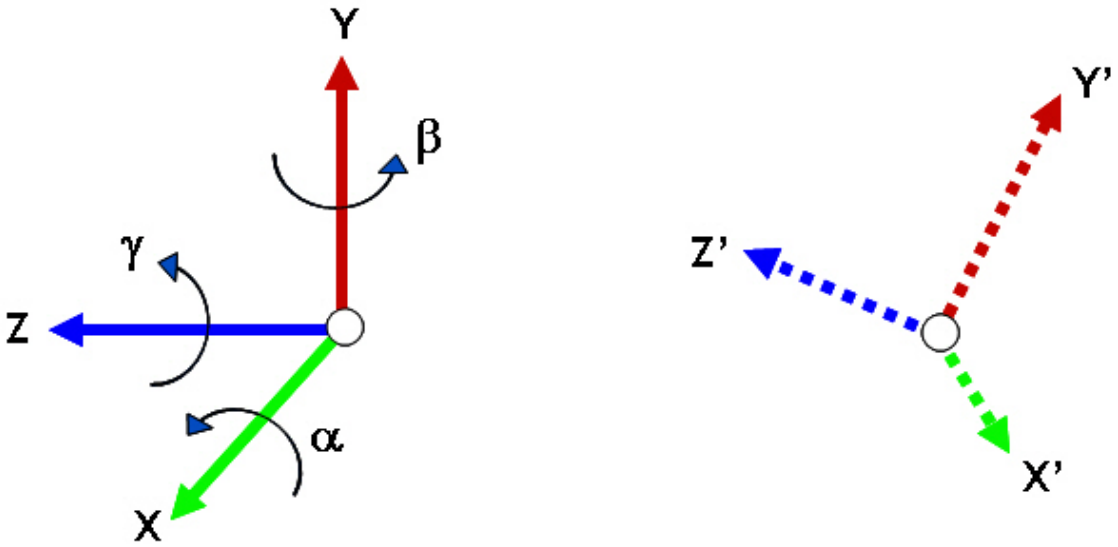

Figure 26 Euler angles used for transformation from XYZ coordinate system to X'Y'Z' coordinate system

Baruh [24] describes some of the historically important sequences, such as 3-2-3 also known as NASA Standard Aerospace, 3-2-1 also known as NASA Standard Airplane, etc.

The transformation matrices used in Figure 26 can be expressed as the following

$$[A_1]=\begin{bmatrix}1 & 0 & 0\\ 0 & \cos\alpha & -\sin\alpha\\ 0 & \sin\alpha & \cos\alpha\end{bmatrix}$$
$$[A_2]=\begin{bmatrix}\cos\beta & 0 & -\sin\beta\\ 0 & 1 & 0\\ \sin\beta & 0 & \cos\beta\end{bmatrix} \tag{69}$$
$$[A_3]=\begin{bmatrix}\cos\gamma & -\sin\gamma & 0\\ \sin\gamma & \cos\gamma & 0\\ 0 & 0 & 1\end{bmatrix}$$

The coordinate transformation 3-2-1 can then be defined by

$$\begin{Bmatrix}X'\\ Y'\\ Z'\end{Bmatrix}=[A_1][A_2][A_3]\begin{Bmatrix}X\\ Y\\ Z\end{Bmatrix} \tag{70}$$

2.6 Element Types

The following section illustrates the various element types that have been utilized for the work present. Note that the objective of this thesis, as mentioned in section 1.3, is not limited to these elements and can include any predefined or user-defined element type.

2.6.1 3D Beam Element (BEAM4)

The beam element BEAM4 represents a 3D elastic Timoshenko beam that has tension, compression and torsion capabilities. The element is represented by two nodes and each node has six degrees of freedom – three translational motions along the nodal *x*, *y*, and *z* axes and three rotations about the nodal *x*, *y*, and *z* axes. This element is used to model the rotor elements and has a spin component that can be used to include gyroscopic effects. While BEAM4 is an ANSYS defined 3D beam element, it can also be used to replicate the 2D beam element used in XLTRC^2. As seen in 0, this element is used to replicate the XLTRC^2 model in ANSYS for verification purpose.

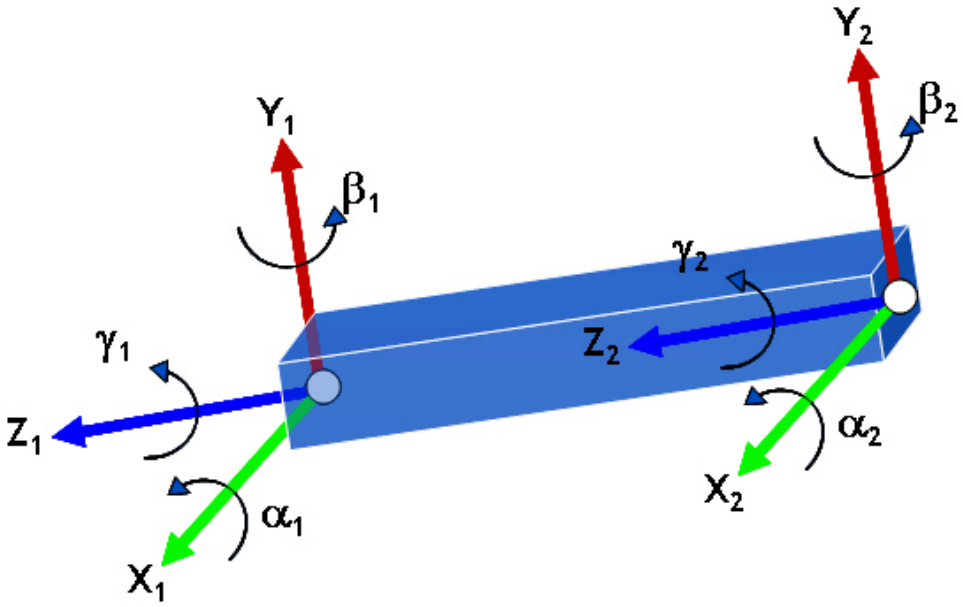

Figure 27 Beam element

The BEAM4 element, shown in Figure 27, is described by real parameter constants such as cross-sectional area, area moment of inertia, thickness, torsional moment of inertia, initial strain, shear deflection and rotational frequency (for gyroscopic effects). The BEAM4 element cannot have zero length or area. For the work done in this thesis, the element has been used to represent circular beam (including hollow beams) although the element can be used for any cross-sectional shape for which moment of inertia can be calculated. This beam element can also be used to represent a tapered beam.

2.6.2 Structural Mass Element (MASS21)

Mass element MASS21, shown in Figure 28, represents a single node element that has concentrated mass components along the *x*, *y*, and *z* coordinate directions and moments of inertia about the element coordinate axes. The element properties can be used as a 3D or 2D mass element. This element can input masses and moments of inertia as real constants or as volumes and density. MATRIX27 element (section 2.6.8) can be used in place of MASS21 if components along non-principal axis need to be specified.

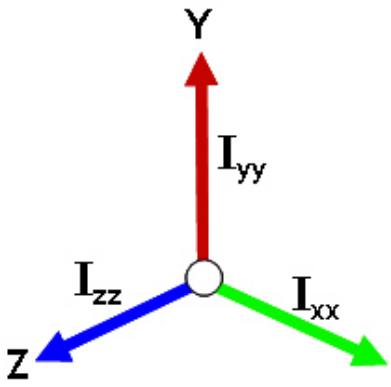

Figure 28 Mass element

2.6.3 Multipoint Constraint Element (MPC184)

The multipoint constraint element MPC184 is used to impose kinematic constraints between nodes. Rigid link, rigid beam, and spherical joints are examples of constraints. Internal constraint equations are generated for the kinematic constraints which lead to the elimination of degrees of freedom of a dependent node in the system equations. Although MPC184 represents a general class of multipoint constraint elements, its application in rotordynamic comes in the form of either rigid links or rigid beams. Rigid links are identified by two nodes and three translational DOF at each node, while rigid beams are associated with two nodes and six DOF at each node – three translational and three rotational.

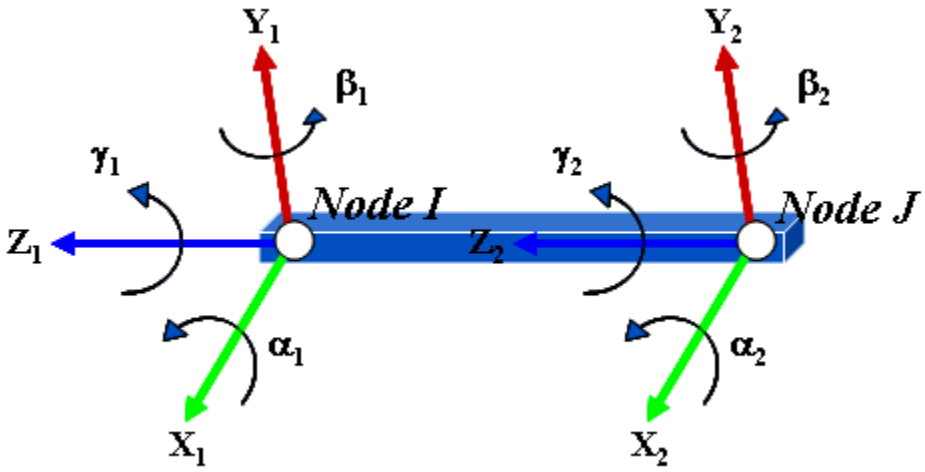

Figure 29 Rigid beam used as constraint element between Node I and Node J

Figure 29 shows a constraint element used as a rigid beam when all six degrees of freedom have constraint equations defined. The element simplifies to a rigid link when the rotational degrees of freedom - α, β and γ - are suppressed.

2.6.4 3D Structural Solid Element (SOLID45)

The 3D structural solid element is widely used for 3D modeling of casing structures. This element is defined by eight nodes, one at each of the vertex of the element. Each node has three degrees of freedom defined in the nodal *x*, *y*, and *z* directions. Figure 30 shows a representative example of this element type. It can also be used to replicate prism-shaped and tetrahedron-shaped elements by duplicating appropriate nodes. In Figure 30, a prism element is formed by duplicating nodes 7-8 and 3-4. A tetrahedron is formed by duplicating nodes 5-6-7-8 and 3-4.

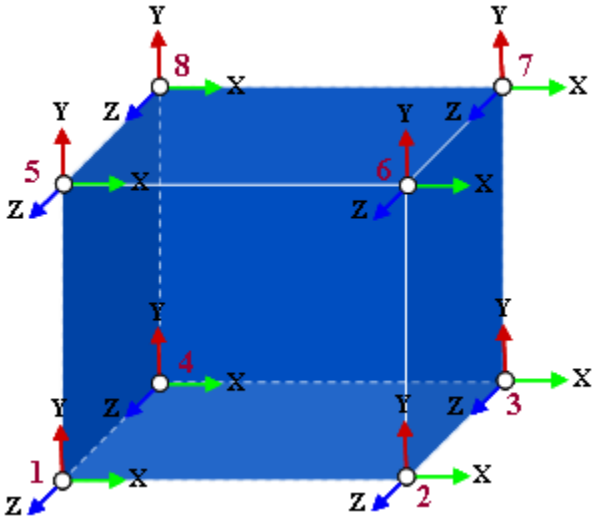

Figure 30 3D solid structural element defined by 8 nodes

2.6.5 3D 20–Node Structural Solid (SOLID186)

The SOLID186 element is used to model 3D structural solids. It is defined by 20 nodes, one at each vertex of the element as well as midway along each edge. Each node has three translational degrees of freedom along the nodal *x*, *y*, and *z* directions. SOLID186 is useful for modeling irregular meshes and is generally selected by ANSYS while importing solids designed by general CAD/CAM systems. Functional capabilities

of this element include stress stiffening, large deflections, large strains, elasticity, and plasticity. Variations of the element can be used to enable tetrahedral, pyramid, and prism elements, as seen in Figure 31. With the capability of having layers, this element can be also used to model thick shells or solids.

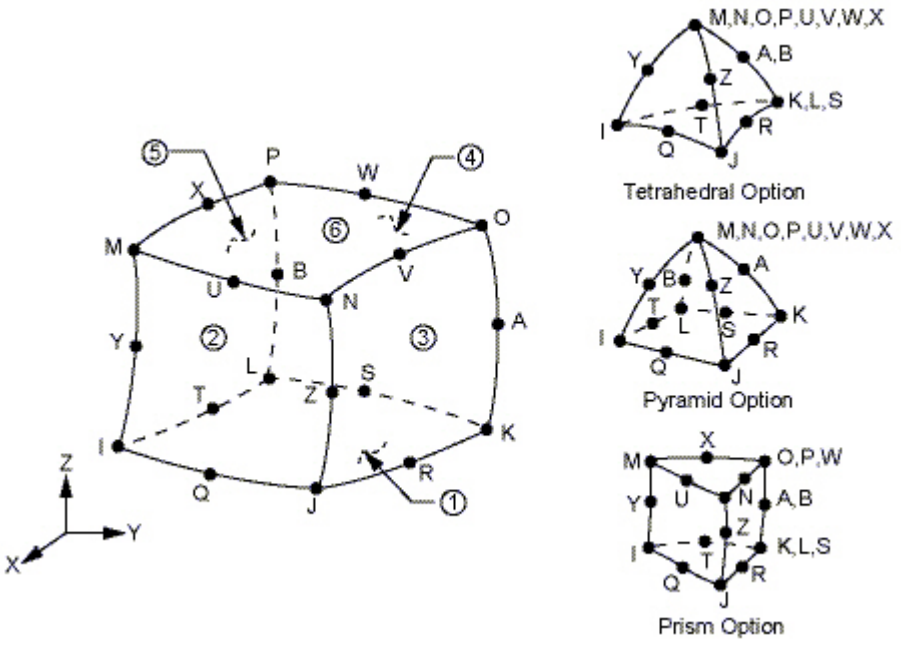

Figure 31 SOLID186 element used to represent structural solids and shells [25]

2.6.6 3D 10–Node Tetrahedral Structural Solid (SOLID187)

SOLID187 solid element is similar to SOLID186 in terms of the functional capabilities. The element has 10 nodes with each node having three degrees of freedom along the nodal *x*, *y*, and *z* directions. This element resembles SOLID186 tetrahedral option, as seen in Figure 31.

2.6.7 Spring–Damper Element (COMBI214)

The spring-damper element COMBI214 is used to model a 2D general spring or damper element that can input direct and general non-symmetric stiffness and damping matrix coefficients. The element is represented by two nodes with each node having up to two degrees of freedom. Figure 32 is representative of the element used along *x* and *y* coordinates, however options can be set to change them to any 2D coordinate system. The stiffness coefficients use the unit of Force/Length, and the damping coefficients are expressed in Force*Time/Length unit. The stiffness and/or damping matrices can be input as real constants or as speed dependent entries. Note that the current ANSYS simulation cannot automatically calculate speed dependent coefficients. Hence they have to be calculated separately for each speed and then included in the analysis.

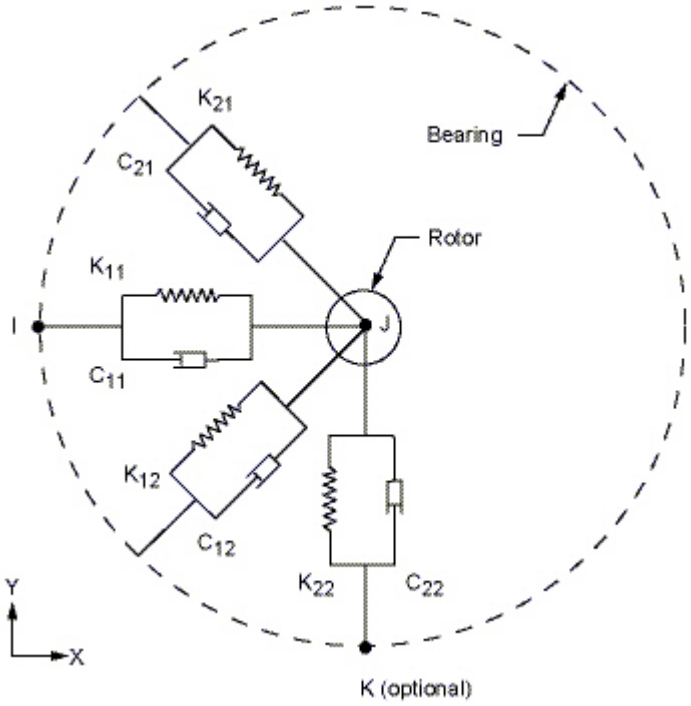

Figure 32 COMBI214 element representing a 2D spring-damper element along X and Y coordinates [25]

Although useful in many analysis types, COMBI214 has two main disadvantages. COMBI214 can represent only tension-compression and cannot be used for bending or torsion. Additionally this element has no mass entries and hence cannot be used to represent seals that have inertia contributions.

2.6.8 Stiffness, Damping, or Mass Matrix Element (MATRIX27)

The MATRIX27 spring-damper-mass element overcomes the shortcomings of the COMBI214 element. The COMBI214 element is easier to set up but is less general than the MATRIX27 element. This element has two nodes with six degrees of freedom at each node – three translational motions along the nodal *x*, *y*, and *z* axes and three rotations about the nodal *x*, *y*, and *z* axes. Figure 33 shows a representation of the MATRIX27 element.

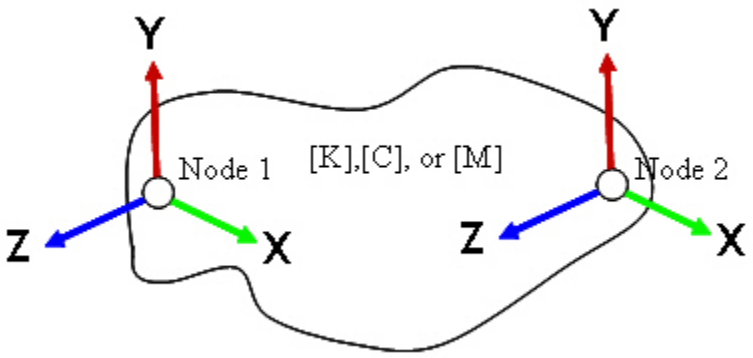

Figure 33 MATRIX27 element representing a general stiffness, damping or mass element

All matrices generated by this element are of size 12 by 12 with the degrees of freedom ordered by translation and rotation DOFs for 1st node followed by those for the 2nd node. This element can be used to represent both symmetrical as well as nonsymmetrical formulations. When used for an analysis, the stiffness, damping and mass elements are represented by individual MATRIX27 elements by the use of

appropriate options. Stiffness values are expressed in units of Force/Length or Force*Length/Radian, damping values in units of Force*Time/Length or Force*Length*Time/Radian, and mass constants in units of Force*Time^2/Length or Force*Time^2*Length/Radian.

2.6.9 Superelement (MATRIX50)

The use of superelements or substructures has been referenced a number of times in the earlier section [1.5] on previous work. MATRIX50 is the element that is used to group a number of previously assembled elements into a single element. As shown in Figure 34, the element does not have a physical geometry and is simply a mathematical matrix representation of a structure where the number of nodes and degrees of freedom are determined by the individual elements that make up the superelement. Superelements can, in turn, contain other superelements.

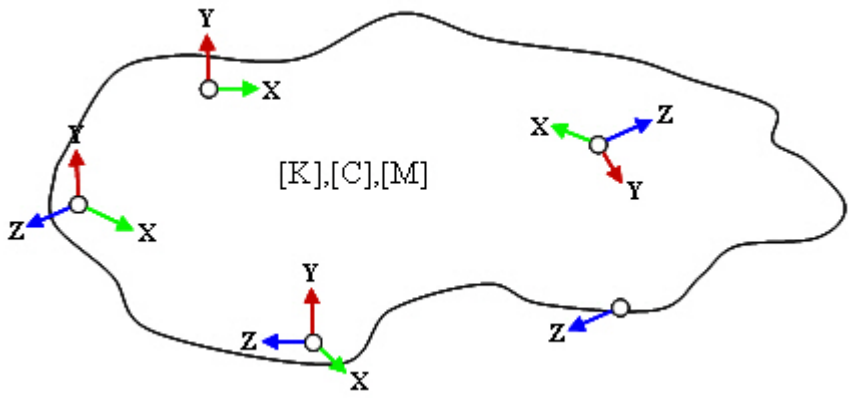

Figure 34 Superelement representation

This element type has tremendous application in analysis where the large dimensionality of the problem is of concern. Nodes which are of interest, such as master degrees of freedom, constraint locations, etc., are selected in individual assemblies. Reduction methods such as the Guyan reduction or component mode synthesis are then

used to reduce individual elements in such a way that required dynamic content is retained. The superelement is then constructed with these individual elements.

Figure 35, taken from the work done by Clark and Jurjevic [17], shows individual assemblies of a gas turbine. Each assembly was reduced and converted into a superelement, as the one shown in Figure 36. Individual superelements are combined into one final superelement, as shown in Figure 37.

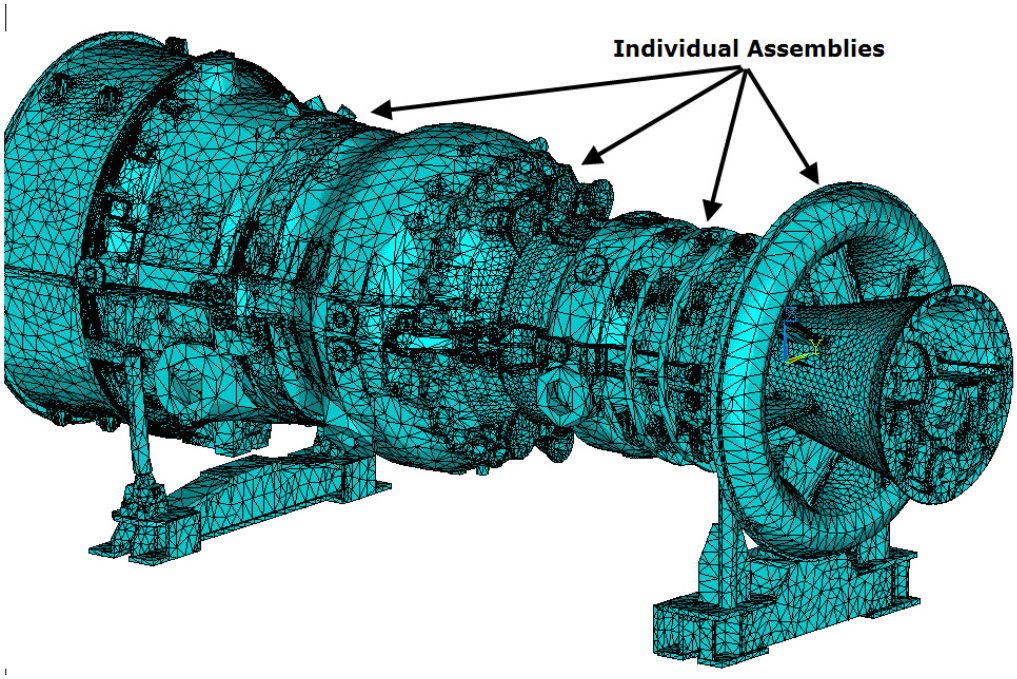

Figure 35 Individual assemblies in the work done by Clark and Jurjevic [17]

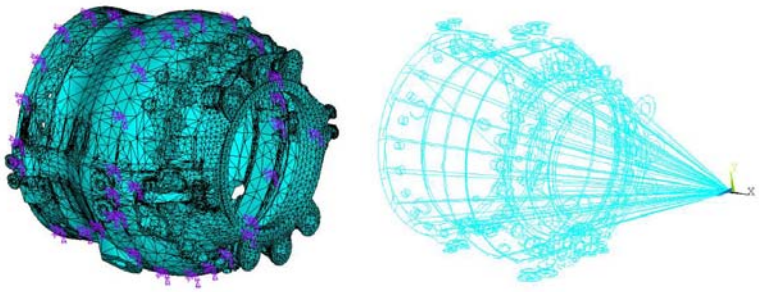

Figure 36 Superelement of one of the component assemblies [17]

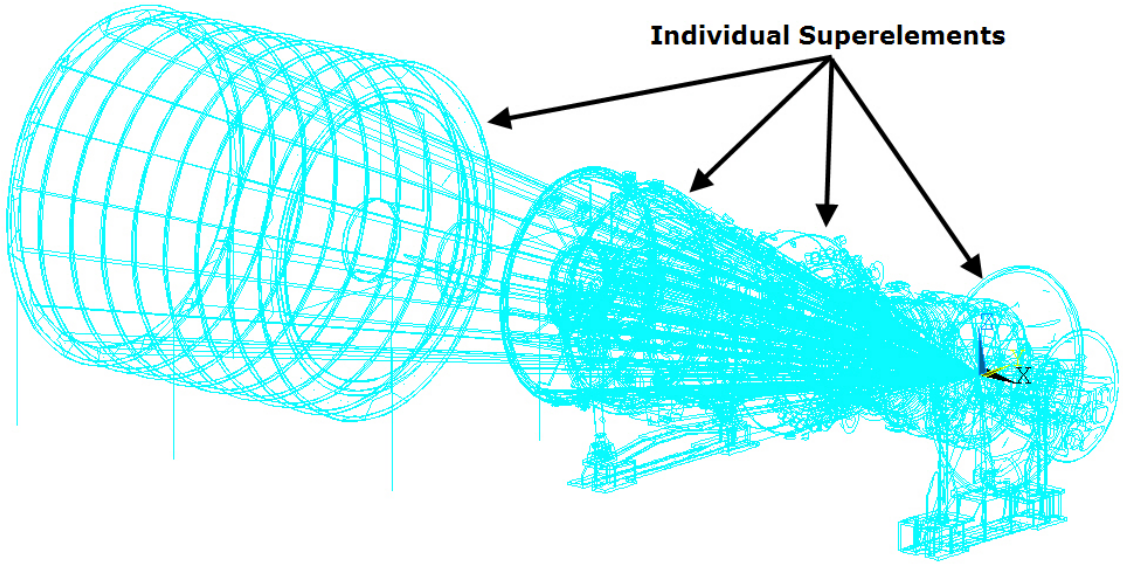

Figure 37 Individual superelements constructed into one superelement [17]

2.7 Preprocessing Steps

This section describes the concepts and steps involved making the ANSYS structural data compatible with XLTRC^2 system.

2.7.1 Axis Alignment Between ANSYS And XLTRC^2

A common practice seen in the industry is that a machine, comprised of many sub-components, may be designed by a number of individuals. While adopting common standards are desirable, feasibility plays a big role in their adherence. One such standard is the coordinate system. A casing and rotor, for example, may be designed by two individuals who may not have adopted the same base coordinate systems. When combining both the components, units and coordinate systems must be matched so that the data being read in is interpreted correctly.

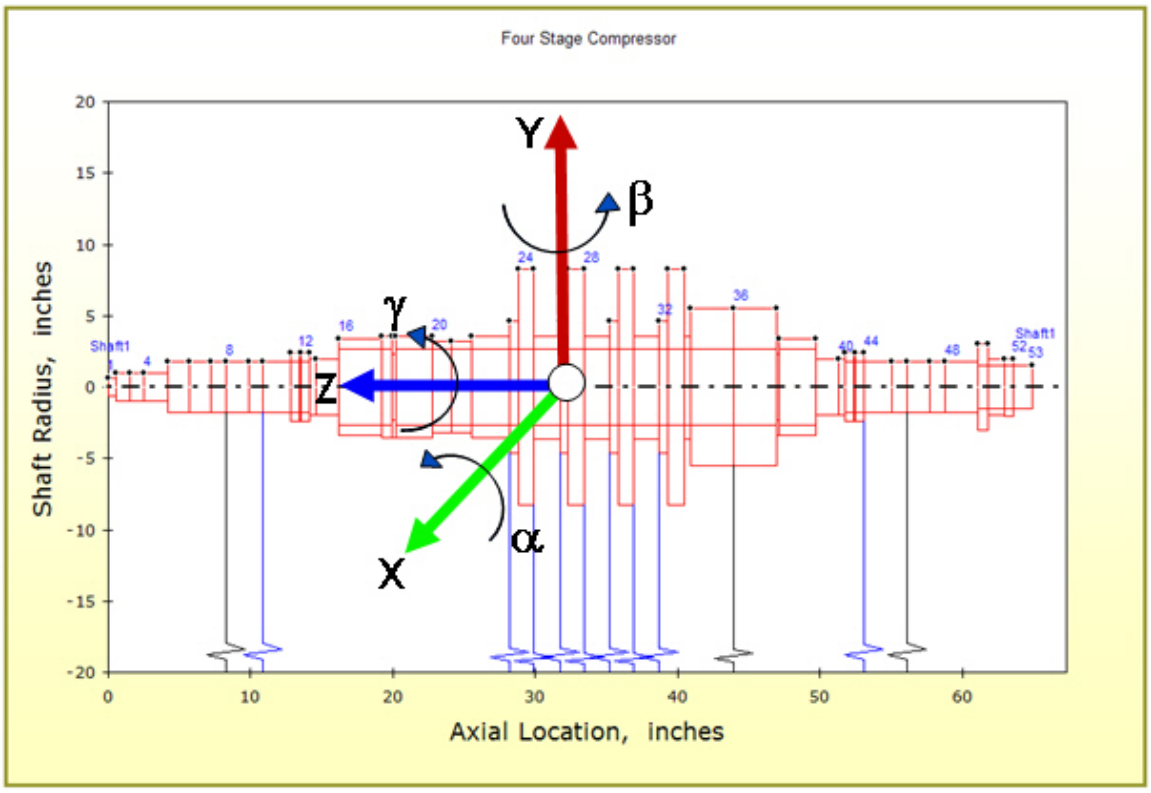

Figure 38 Coordinate system used in XLTRC^2 [3]

Figure 38 shows an example XLTRC^2 model with the coordinate system used, in which the *Z*-coordinate represents the axial direction. Note that the *X*-coordinate is normal to the plane of the paper and coming out of it. The coordinates in XLTRC^2 system is fixed and are not transformed. The *Z*-coordinate always represents the axial direction.

Figure 39 shows a representative casing and rotor[8] model built with ANSYS. In this model, the *X*-coordinate was used for the axial direction. The coordinate systems in Figure 38 and Figure 39 clearly do not match, and hence one of them has to be reoriented in space.

[8] Appearance of the rotor as a series of cube–shaped elements is explained in section 2.8

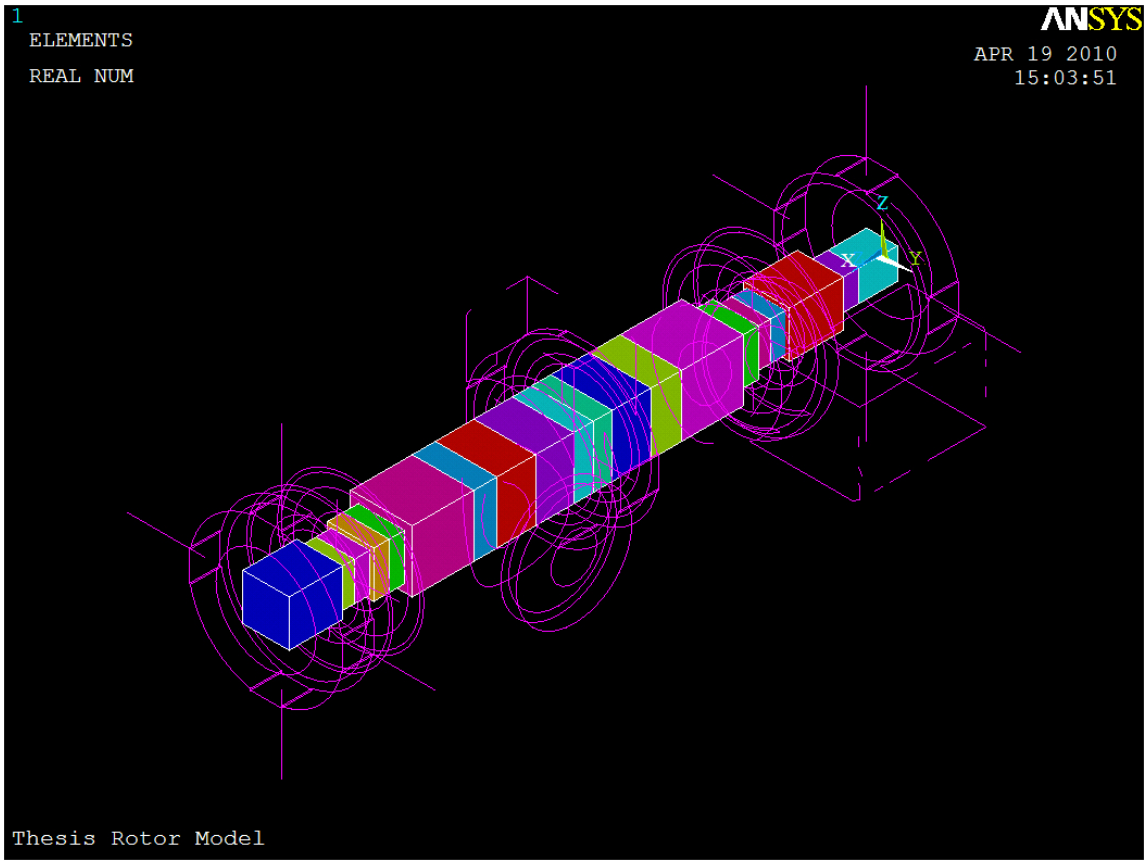

Figure 39 Representative ANSYS model

The transformation follows the principle as described in section 2.5. The Euler angles γ, β and α represent the angle by which the *z*, *y*, and *x* coordinates in the original coordinate system need to be rotated. Suppose the transformation followed the 3-1-2 order, the transformation matrices are defined by

$$[A_1]=\begin{bmatrix}\cos\beta & 0 & -\sin\beta\\ 0 & 1 & 0\\ \sin\beta & 0 & \cos\beta\end{bmatrix}\quad [A_2]=\begin{bmatrix}1 & 0 & 0\\ 0 & \cos\alpha & -\sin\alpha\\ 0 & \sin\alpha & \cos\alpha\end{bmatrix}\quad [A_3]=\begin{bmatrix}\cos\gamma & -\sin\gamma & 0\\ \sin\gamma & \cos\gamma & 0\\ 0 & 0 & 1\end{bmatrix} \quad (71)$$

The coordinate transformation 3-2-1 can then be defined

$$\begin{Bmatrix} X' \\ Y' \\ Z' \end{Bmatrix} = [A_1][A_2][A_3] \begin{Bmatrix} X \\ Y \\ Z \end{Bmatrix} \tag{72}$$

Where $X-Y-Z$ and $X'-Y'-Z'$ represent the coordinate systems of ANSYS and XLTRC^2, respectively. A graphical representation of the coordinate transformation is shown in Figure 40.

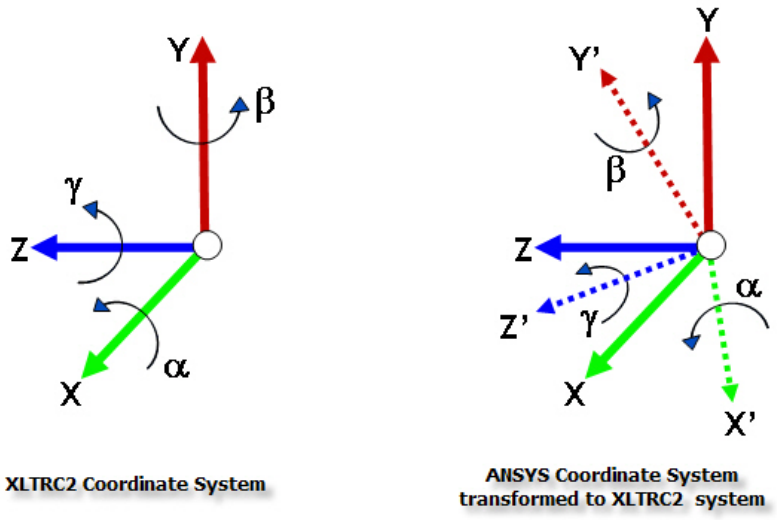

Figure 40 Transformation from ANSYS coordinate system to that of XLTRC^2

Since ANSYS provides better computational capability in terms of the size of the transformation matrix, it should be used to perform nodal coordinate transformation. ANSYS includes the ANSYS Parametric Design Language (APDL) that can be used to programmatically transform the coordinate system. Figure 41 shows an APDL code snippet that can be used to perform the nodal rotation.

```
! **COORDINATE ROTATION**
!select all defined master DOF
nsel, s, m, , all
!define local coordinate system with spin about X
clocal, 100, 0, xlocal, ylocal, zlocal, thxy, thyz, thzx
!switch to the local coordinate system
csys, 100
!rotate all selected nodes
nrotat, all
```

Figure 41 APDL code to perform nodal rotation

First, the master degrees of freedom (MDOFs) are selected using the *nsel* command. The MDOFs comprises of all nodes that the user selects for transformation. A local coordinate system is defined with the *clocal* command, and one is created such that it aligns with the XLTRC^2 coordinate system. *xlocal*, *ylocal*, and *zlocal* are the location of the origin of the new coordinate system. The last three parameters of the clocal command (thxy, thyz, and thzx) are the transformation angles and represent first rotation about local *Z* (positive *X* toward *Y*), second rotation about local *X* (positive *Y* toward *Z*), and third rotation about local *Y* (positive *Z* toward *X*).

The entire transformation can be done with one *clocal* command. Once the coordinate system has been switched to the created local coordinate system, using the *csys* command, the selected nodes are rotated with the *nrotat* command. For the example shown in Figure 39, the *clocal* command would have to be used with $thzx = -90$ to align the ANSYS coordinate system with that of XLTRC^2.

2.7.2 Coordinate Elimination of Casing Model using ANSYS

A 3D beam element model uses six degrees of freedom at each node to represent the translational and rotational motion about each coordinate. The degrees of freedom about the X, Y, and Z coordinates are shown in Figure 42, Figure 43, and Figure 44, respectively. XLTRC^2, being a 2D beam element analysis tool, limits the degrees of freedom to four at each node. In the construction of the XLTRC^2 beam model, a Guyan

reduction is used to eliminate the axial translation and rotation coordinates in ANSYS. This section illustrates the reasoning behind eliminating the axial casing coordinate from the analysis. Note that this coordinate elimination holds irrespective of whether the casing has been modeled with beam, shell, and/or solid elements.

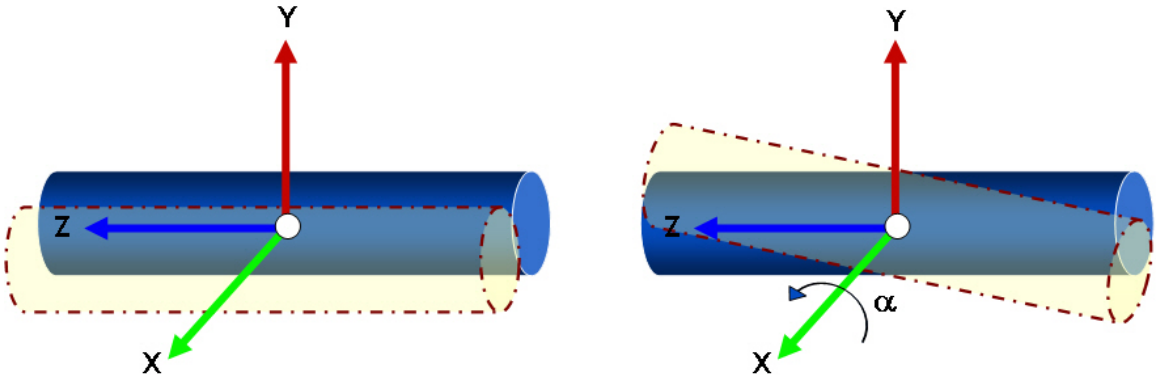

Figure 42 Translational and rotational motion (pitch) about the X-coordinate

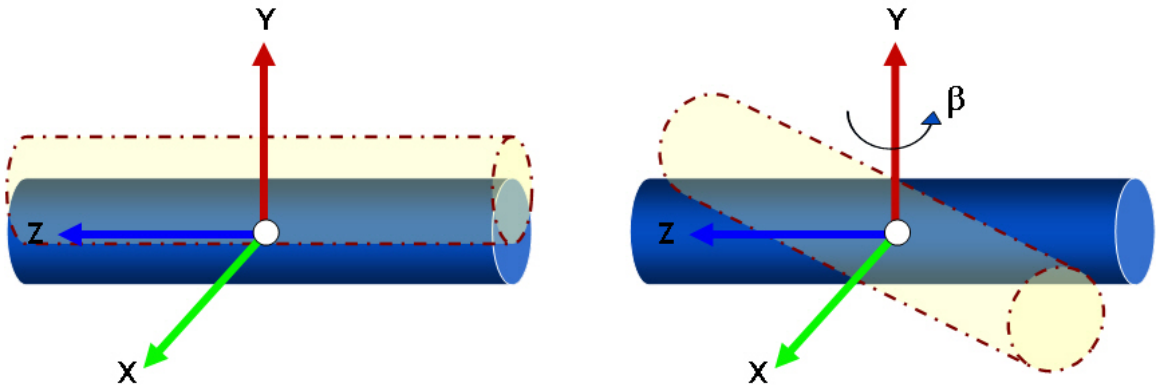

Figure 43 Translational and rotational motion (yaw) about the Y-coordinate

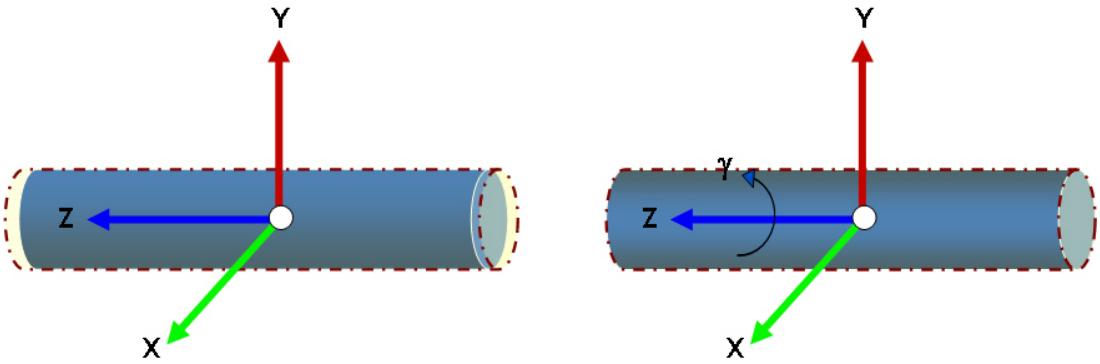

Figure 44 Translational and rotational motion (roll) about the Z-coordinate

This assumption of eliminating the axial coordinate is based on generalized rotordynamics cases. If significant axial forces exist in the system, the motion along the *Z*-coordinate should be considered. One such example is where the casing modes can be connected to axial rotor motion through a balance piston or thrust bearing. However, in this thesis axial displacements are ignored for simplicity.

With the *Z* coordinate eliminated, a two dimensional system defined by the *X* and *Y* coordinates results. The orthogonal *X*-*Z* and *Y*-*Z* planes are retained for analysis, as shown in Figure 45.

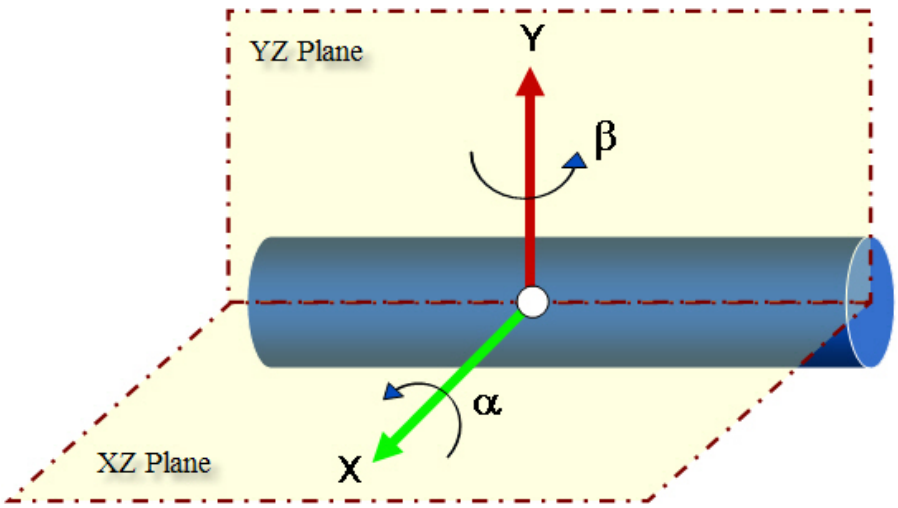

Figure 45 Retained analysis planes lie in the XZ and YZ planes

2.7.3 Node Matching Between Rotor and Casing Nodes

Once the models have been aligned to a common coordinate system and the number of degrees of freedom has been matched, the nodes between the rotor and the casing must be coupled correctly. Coupling does not mean physically connecting them. It is a mathematical representation of the link between nodes. The analysis tool uses this to formulate the system matrices in terms of stiffness, damping and inertia terms as well as to calculate relative displacements, mode shapes, etc. Examples of points where nodes are matched are bearing locations on casing and rotor, seal locations on casing and rotor, and points which are constrained in relative motion.

A model built in XLTRC^2 will consist of one or more shafts which are in turn made up of a number of beam elements. Each element is geometrically defined by its length, inner diameter and outer diameter. The left and right ends of an element stand for the left and right stations (also called nodes), respectively. Stations are used by XLTRC^2 to represent the location of bearings, seals, impellers, etc.

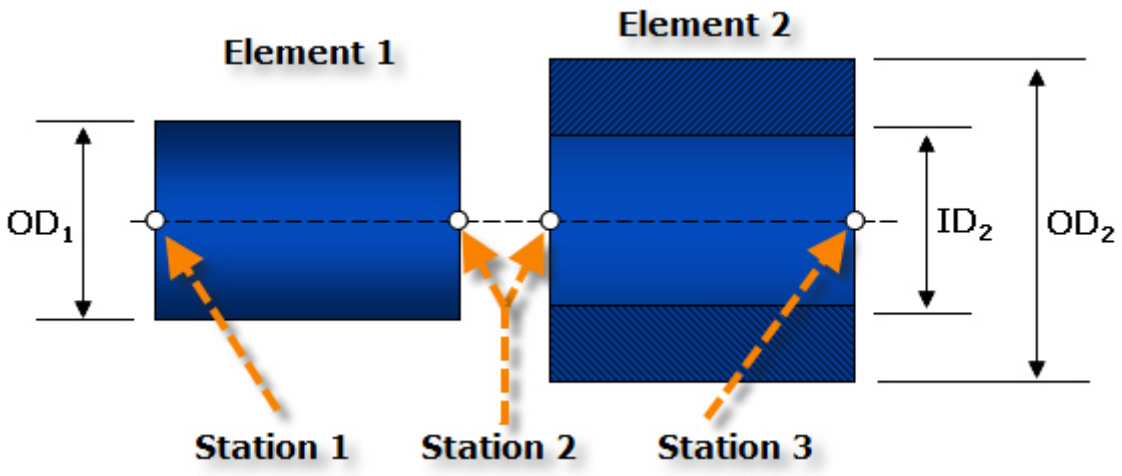

Figure 46 Representation of elements and stations (nodes) in XLTRC^2

In XLTRC^2 the nodes are represented by successive station numbers. Numbering starts with element 1 and continues until all elements have been accounted for. The number of stations in a beam is always one more than its number of elements. Two consecutive elements share a node. For example, as seen in Figure 46, the right station of element 1 is the same node as the left station of element 2. XLTRC^2 builds the elements such that the nodes coincide with the geometric center of the beam. XLTRC^2 can also section an element into sub-elements (along the axial direction) and layers (along the radial direction); however, that does not affect node numbering.

In constructing a casing structure in ANSYS, the primary difference is that 3D solid elements may be used. If auto meshing is used, the program decides on the element type. Depending on the nature of the elements used, the number of nodes and their spatial locations can vary. The example from section 2.3 is used for representation. Figure 47 shows the solid model of a representative bearing pedestal A finite element mesh is first created as shown in Figure 48.

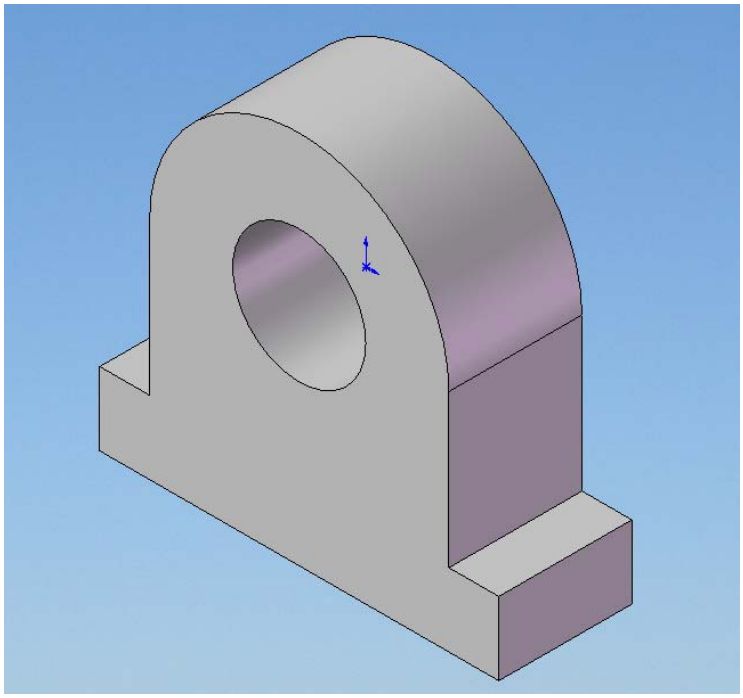

Figure 47 Solid model of a bearing pedestal

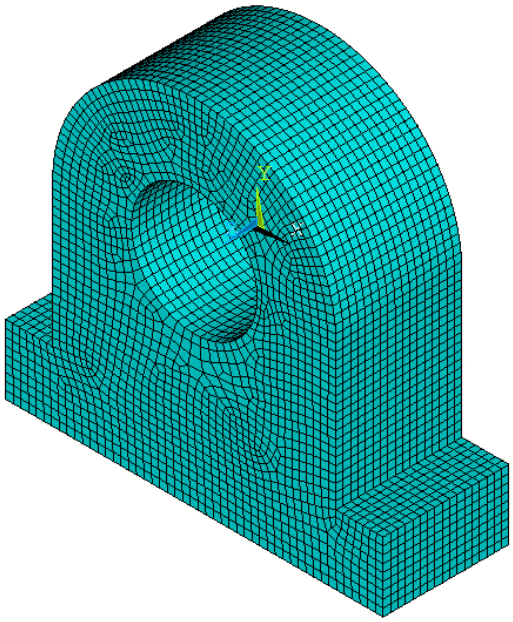

Figure 48 Finite element mesh of bearing pedestal

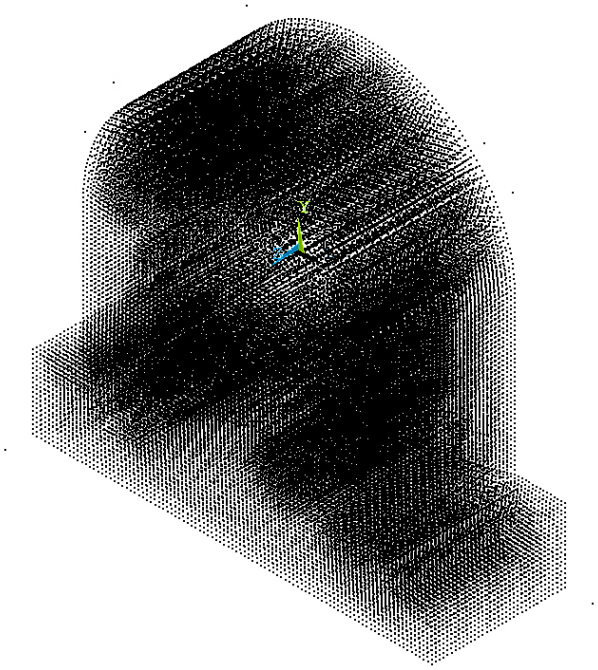

Figure 49 Nodes created using high density mesh (Note that the appearance of nodes as a dense cluster is not due to low image quality, but due to the high level refinement of the finite element mesh used)

Figure 49 shows the nodes created in the meshing process. High density meshing that is used results in the large number of nodes. Within the limits of computational capability, it is advisable to use as high a mesh density as possible. This helps in the process of having a choice of nodes at desired locations.

The nodes created in Figure 49 are driven by equations that associate their relative displacements, forces, etc. Change in parameter for one node also influences the others. In XLTRC^2 a bearing location on the rotor will be represented by a single node, so that node must be matched with the appropriate node(s) in the bearing pedestal mesh. One node-matching method is to attach all the nodes on the inner surface of the pedestal with the rotor bearing node. However, this is computationally intense since it increases the number of equations in the system matrix. It is also time consuming for an analyst to select all nodes. A good approximation can be used by selecting only those nodes that occur in the axial plane coinciding with the bearing location in the XLTRC^2 rotor. This approximation is standard practice. Figure 50 shows the nodes selected at the midsection plane of the bearing pedestal. The view from the front plane is shown in Figure 51.

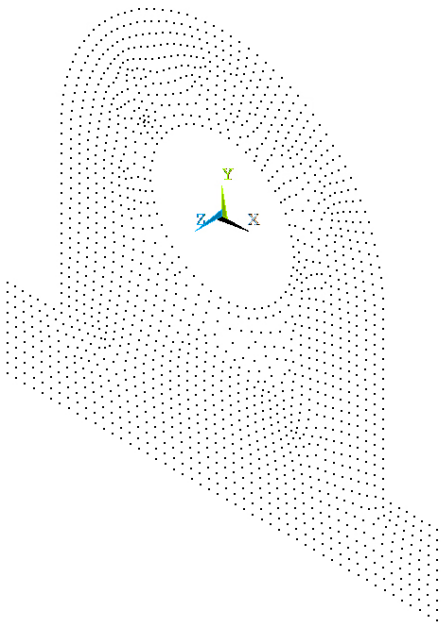

Figure 50 Nodes in the geometric center plane of the bearing pedestal

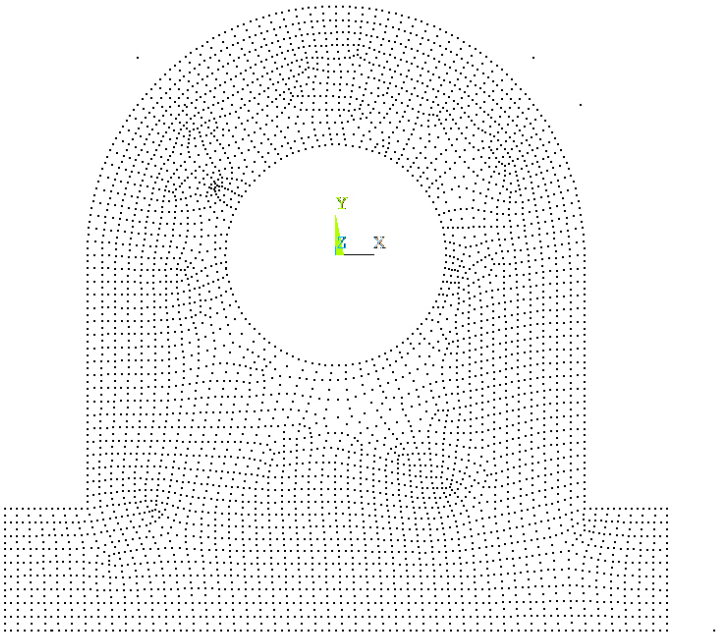

Figure 51 Center nodes seen from the front plane

Figure 52 illustrates the process of matching the nodes on the rotor and casing models. As seen earlier in section 2.7.2, the planes of interest are the orthogonal *X*-*Z* and *Y*-*Z* planes. The nodes that coincide with these planes in the interior surface of the bearing, shown in the figure by red dots, are selected. A new node, shown in the figure by the green dot, is created at the geometric center location of the pedestal by using the coordinates of the four selected nodes. Finally the selected bearing nodes are connected to the center node using MPC184 rigid beam type constraint elements. The behavior of the newly created node will now follow those selected on the bearing inner surface due to the imposed translational and/or rotational constraints. The advantage of this process is easily explained. Using all the initial nodes shown in Figure 49 would increase the complexity and time required for finding a solution. By creating a single center node at the bearing-center location, dynamic content is retained. Also a single node makes it easier to use a bearing or damper element to connect the rotor to the casing.

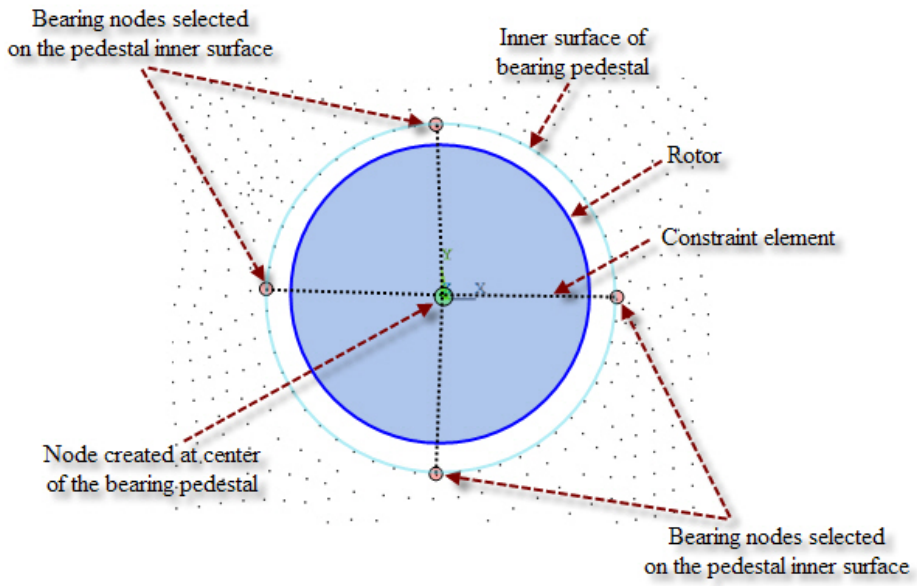

Figure 52 Close up view of the bearing pedestal center to illustrating the selection of matching nodes

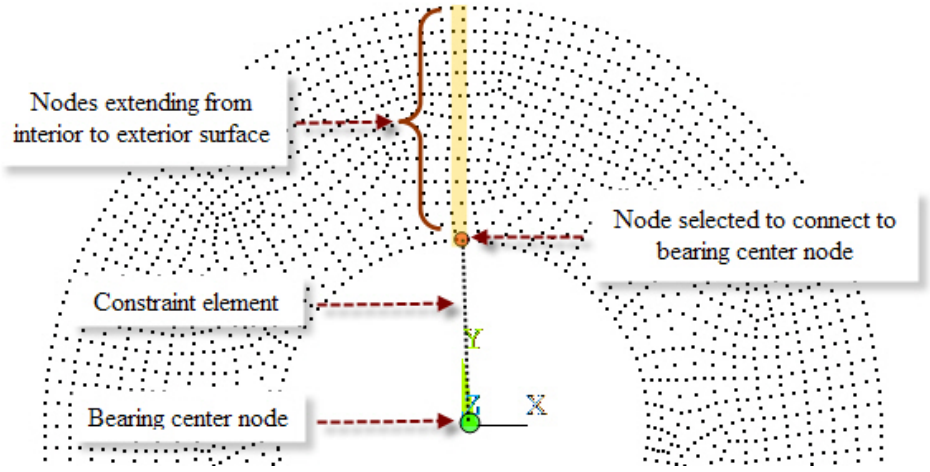

Figure 53 Pedestal showing nodes extending from interior to exterior surface

The above approximation also generalizes the node matching process for cases where the casing is modeled with shell elements versus cases where the casing is modeled with general 3D elements. When using the latter, as in the representative model

used here, a number of nodes extend from the interior to the exterior surface (Figure 53). The node on the interior surface is selected and it will respond to the dynamic behavior of the other nodes around it. This holds good for rotordynamic applications.

2.8 Graphical Representation

The center-node creation in the above section may lead to the question – How do the newly created node and the bearing node in the XLTRC^2 model relate if they are at the same location in the coordinate system? The answer is that this is only a visual representation. The earlier section 2.2 on CMS formulation shows that when bearings and seals are used, their stiffness, damping and inertia contributions go into the appropriate locations in the system matrices. To the ANSYS and XLTRC^2 codes, only this mathematical representation is of concern. The graphical display is only to aid an analyst to visually perceive the relative placements of the casing and rotor. Hence although both nodes visually take up the same location, the codes can mathematically distinguish between the radial locations.

The appearance of the rotor as a series of cube-shaped elements, in Figure 39, is also because of the above mentioned reason – *visual representation*. The rotor model is built in ANSYS Classic and APDL by using 3D BEAM4 beam elements. Although the beam appears to have a square cross-section, the geometric, material, element and mesh information are the same as a beam represented as a cylinder with circular cross-section.

A verification test is conducted to ensure that the results obtained from the various tools agree with each other. A solid cylindrical model is tested using XLTRC^2, ANSYS Classic with APDL and ANSYS Workbench. XLTRC^2 and ANSYS Classic used beam elements, whereas ANSYS Workbench employed solid elements. The results showed excellent agreement with each other. 0 shows the details of the verification test.

2.9 API Unbalance Specification

This section describes the specifications in American Petroleum Institute (API) Standard paragraphs 617 [26] and API Standard paragraphs 684 [27] for including effects of unbalance on the system, and will be used later in this thesis for calculation of unbalance response. The influencing factors for unbalance magnitude are the weight of the rotor and the maximum continuous operating speed, as shown in Eq.(73).

$$\begin{aligned} U &= 6350 \times \frac{W}{N} \quad [\text{SI Units}] \\ &= 4 \times \frac{W}{N} \quad [\text{US Customary Units}] \end{aligned} \tag{73}$$

$U \rightarrow$ Unbalance magnitude in g-mm (oz.-in.)

$W \rightarrow$ Static load in kg (SI units) or lbs (US units)

$N \rightarrow$ Maximum continous operating speed (RPM)

In the analyses of rotating machinery, the actual distribution of the calculated unbalance along the length and circumference of the rotor is more or less random. However, for analysis they are usually placed at locations where they tend to impose a maximum undesirable affect on a particular mode, i.e. create maximum response. An example is shown in Figure 54 that represents a rotor supported between bearings. In this case, an unbalance applied to the rotor mid-span typically tends to excite the first bending mode. When proportional unbalance amounts are applied to quarter and three-quarter span locations they are likely to excite the second bending mode.

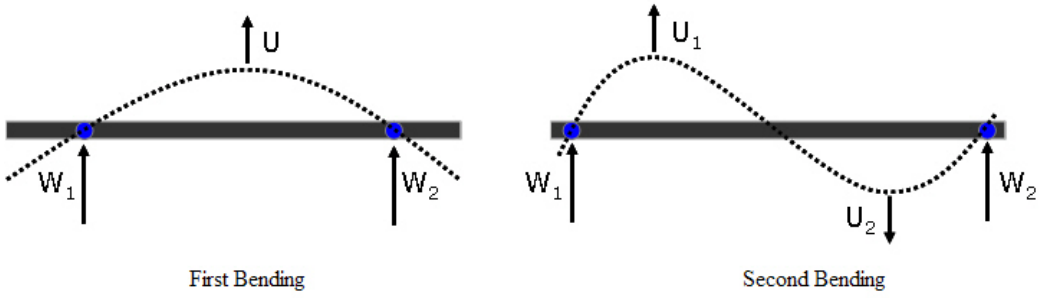

Figure 54 Typical first and second bending mode shape for a rotor

3 PROCEDURE

This section describes the steps involved in creating the various rotordynamic models used for analyses in this thesis. SI units are used for all models, and English unit equivalents, where necessary, have been mentioned. A straight-through compressor design is used as the representative model. Note that these models do not represent any proprietary data. Various validation steps are performed to ensure model reliability. These steps compare initial results obtained from XLTRC^2 with ANSYS and thus ensure that both the tools are benchmarked against one another.

The procedure begins by building the casing models. This research seeks to examine the difference between using an axisymmetric and non-axisymmetric casing structure in XLTRC^2. The axisymmetric casing model is built in both XLTRC^2 and ANSYS, shown in sections 3.1.1 and 3.1.2 respectively. This step provides a benchmark for the current approach to modeling casing structures. A solid-element non-axisymmetric casing model is then built, described in section 3.1.3, and the reduced model incorporated with XLTRC^2 for analysis. The required pre-processing steps are performed to convert the ANSYS casing data into a compatible format with XLTRC^2. These steps were described in detail in section 2.7.

The XLTRC^2 rotor model is built next, and is described in section 3.2. The rotor is modeled with beam elements and has stations to provide interface for the bearings and seal. The rotor has also been modeled with added inertias to represent lumped masses. Bearings and seals that are used to connect the rotor to the casing structure are then defined in section 3.3 and 3.4, respectively.

Once individual rotordynamic components are created, they are assembled into the final coupled rotor-casing model. The axisymmetric and non-axisymmetric casing models, built out of solid elements in ANSYS, are reduced and incorporated with XLTRC^2.

3.1 Casing Models

Simple casing models are developed based on representative straight-through compressor designs. To validate the difference between using axisymmetric and non-axisymmetric models, separate casing models are developed. The casing models described in this section will be used hereafter. Steel is used as the material for all casing models. The material properties are taken from the standard XLTRC^2 template and have the following properties,

Density (ρ)	=	7833.412 kg/m^3	(Specific weight = 0.283 lb/in^3)
Elastic Modulus (E)	=	206.842E+9 N/m^2	(30.0E+6 lbf/in^2)
Shear Modulus (G)	=	82.737E+9 N/m^2	(12.0E+6 lbf/in^2)

3.1.1 Axisymmetric XLTRC^2 Beam Element Casing Model

The first casing model is developed in XLTRC^2 as an axisymmetric beam element model to validate the current analysis technique used in XLTRC^2. It provides benchmark results to make sure that procedures used for incorporating casing data are working correctly.

A verification test for bending mode frequencies is conducted between a beam-element based XLTRC^2 beam model and its corresponding solid-element based ANSYS model, documented in 0, and showed excellent agreement in the reported frequencies. However, note that it is necessary to divide the XLTRC^2 model into a sufficiently large number of beam elements. The reason is that the number of critical speeds is dependent on the number of elements in the model. The smaller the number of beam elements in the finite element model, the larger will be the margin in the eigen solution when compared to a finite element model based on solid elements, which typically has a larger number of elements. When using fewer elements, certain roots may be missed. The length-to-diameter aspect ratio is not relevant to finite element models, and usually a single element will work for most constant-diameter sections. Two cases of the axisymmetric XLTRC^2 beam-element casing models with different mesh densities are

constructed to cross-check the accuracy of the ANSYS solid element casing model. The validation test is documented in APPENDIX B.

Based on this test the following XLTRC^2 model is used for the casing. The casing is made of 160 beam elements of varying lengths and diameters to fit the geometry of the encasing rotor. Figure 55 shows the model. The element properties are described in Table 1. Note that not all the elements are shown due to space restrictions, and the gaps denoted by the ellipses indicate elements of the same geometric properties. For example, elements 32 through 39 have the same geometric properties as elements 31 and 40. The summary of the complete casing is described in Table 2 and shows a total length of 4.00 meters (157.48 inches) and a mass of 9010.11 kg; weight of 19863.9 lb.

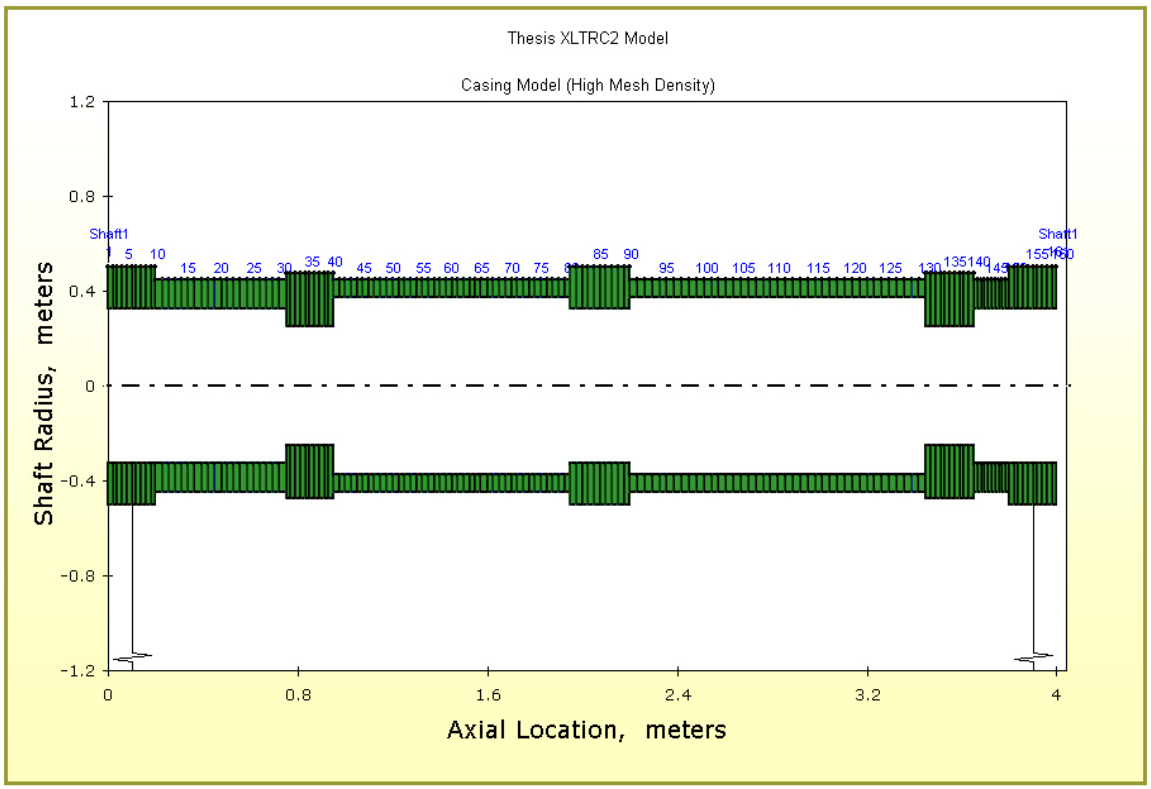

Figure 55 Geometric plot of XLTRC^2 axisymmetric casing model

Table 1 Element properties of XLTRC^2 axisymmetric casing model

Casing Model Data Entry						
Shaft #	Element #	Length (m)	Left		Right	
			OD(m)	ID(m)	OD(m)	ID(m)
1	1	0.0200	1.000	0.650	1.000	0.650
…	…	…	…	…	…	…
1	10	0.0200	1.000	0.650	1.000	0.650
1	11	0.0275	0.900	0.650	0.900	0.650
…	…	…	…	…	…	…
1	30	0.0275	0.900	0.650	0.900	0.650
1	31	0.0200	0.950	0.500	0.950	0.500
…	…	…	…	…	…	…
1	40	0.0200	0.950	0.500	0.950	0.500
1	41	0.0250	0.900	0.750	0.900	0.750
…	…	…	…	…	…	…
1	80	0.0250	0.900	0.750	0.900	0.750
1	81	0.0250	1.000	0.650	1.000	0.650
…	…	…	…	…	…	…
1	90	0.0250	1.000	0.650	1.000	0.650
1	91	0.3125	0.900	0.750	0.900	0.750
…	…	…	…	…	…	…
1	130	0.3125	0.900	0.750	0.900	0.750
1	131	0.0200	0.950	0.500	0.950	0.500
…	…	…	…	…	…	…
1	140	0.0200	0.950	0.500	0.950	0.500
1	141	0.0150	0.900	0.650	0.900	0.650
…	…	…	…	…	…	…
1	150	0.0150	0.900	0.650	0.900	0.650
1	151	0.0200	1.000	0.650	1.000	0.650
…	…	…	…	…	…	…
1	160	0.0200	1.000	0.650	1.000	0.650

Table 2 Summary of the complete XLTRC^2 casing model

1st STN #	Nth STN #	Total Length (m)	Total Mass (Kg)	C.G. location (m)	Total It at C.G. (Kg-m²)	Total Ip about C.G. (Kg-m²)
1	161	4.00	9010.11	1.971	15154.81908	1486.87

3.1.2 Axisymmetric ANSYS Solid Element Casing Model

The second casing model is built in ANSYS as an axisymmetric solid element model. Geometric properties are the same as in the XLTRC^2 model. Due to familiarity with the software, SolidWorks is used for solid modeling. Figure 56 and Figure 57 shows the geometric features. The model is then imported into ANSYS, shown by Figure 58. The finite element meshed model is shown in Figure 59.

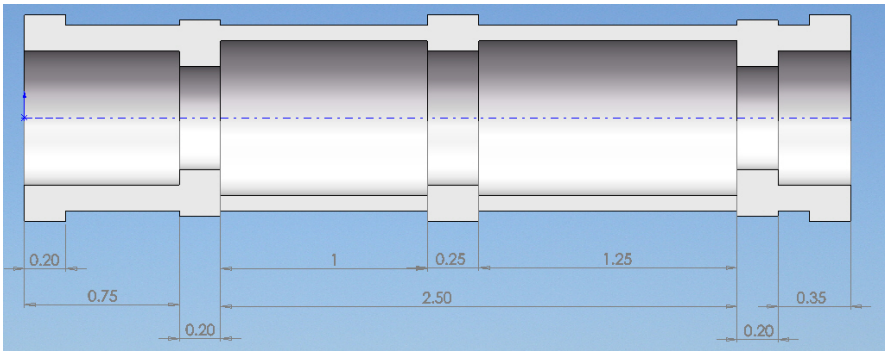

Figure 56 Side view of SolidWorks casing model showing section lengths

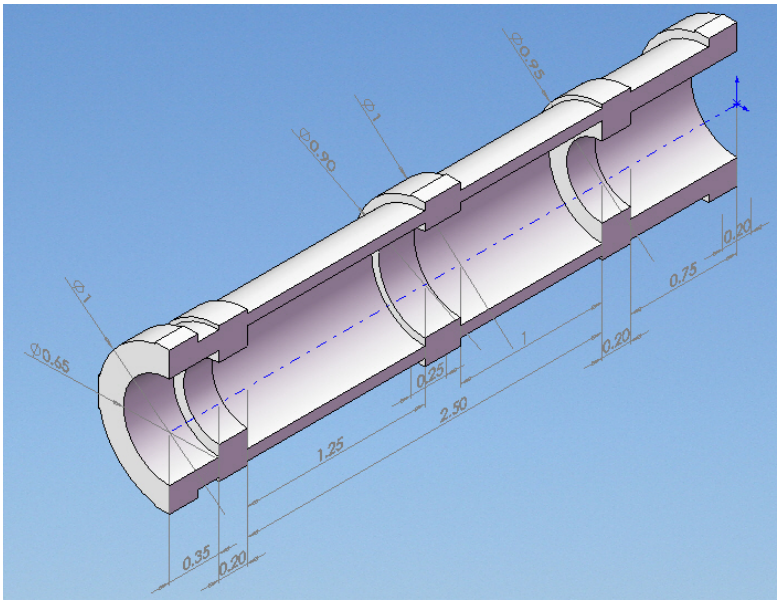

Figure 57 Isometric view of SolidWorks model showing section diameters

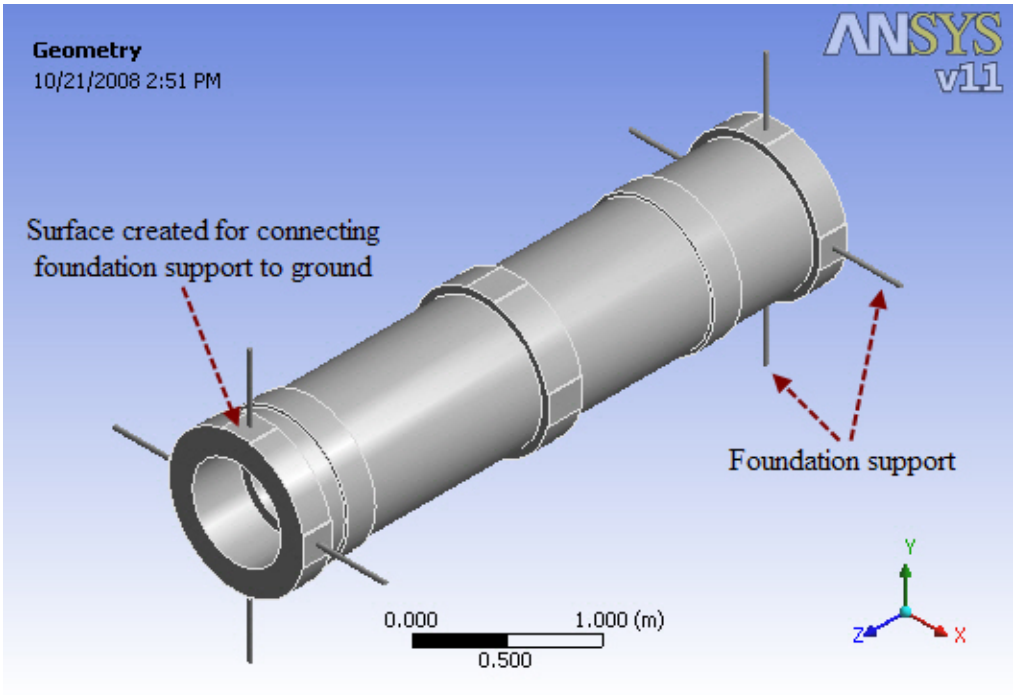

Figure 58 Solid model of ANSYS axisymmetric casing

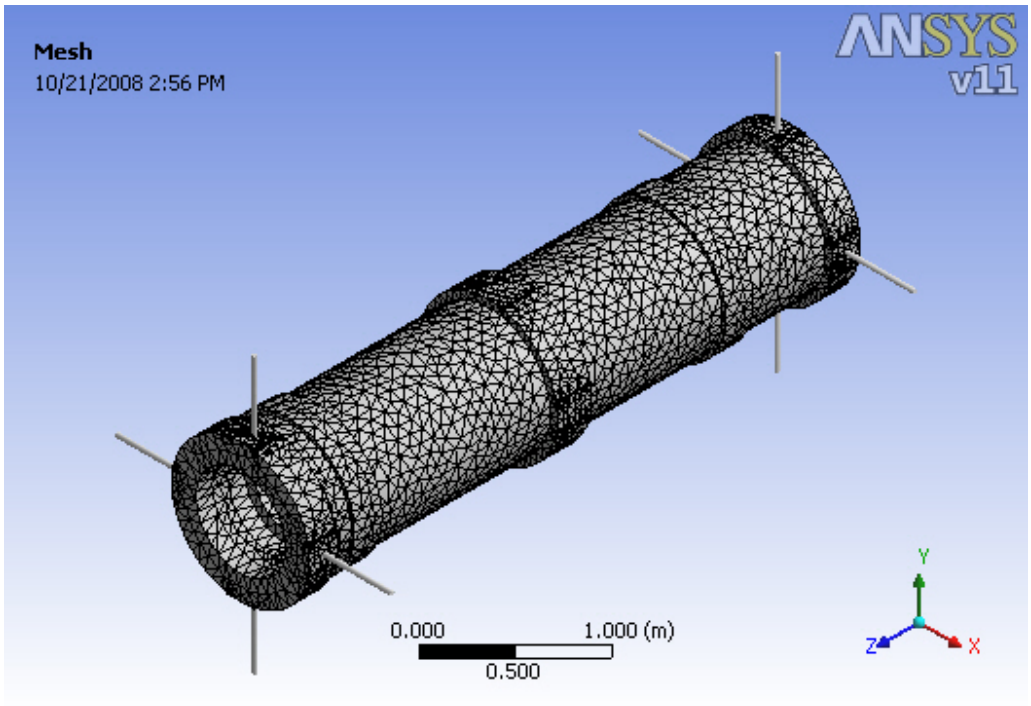

Figure 59 Finite element model of ANSYS axisymmetric casing

Bounding Box	
Length X	1. m
Length Y	1. m
Length Z	4. m
Properties	
Volume	1.152 m³
Mass	9023.8 kg
Centroid X	2.5539e-005 m
Centroid Y	5.1093e-011 m
Centroid Z	1.971 m
Moment of Inertia Ip1	15127 kg·m²
Moment of Inertia Ip2	15127 kg·m²
Moment of Inertia Ip3	1473.2 kg·m²
Statistics	
Nodes	36723
Elements	19225

Figure 60 Summary of ANSYS axisymmetric casing model

The finite element mesh consists of 19,225 elements and 36,723 corresponding nodes. Figure 60 shows summary parameter data for the ANSYS axisymmetric casing model. These values agree well with the XLTRC^2 casing model summary shown in Table 2. Note that the slight difference in mass and inertia properties is due to the additional surfaces created in the ANSYS model that provide the interface to connect foundation supports to ground, as shown in Figure 58. This method to have body to ground connections is chosen for convenience, and does not make a big influence as the parameters vary in value by only 0.1%. APPENDIX C shows a comparison of the Free-Free modes of casing models with and without the additional surfaces. The results show negligible change when the additional surfaces are used.

3.1.3 Non–Axisymmetric ANSYS Solid Element Casing Model

The third casing model is built in ANSYS as a non-axisymmetric solid element model. This model is identical to the axisymmetric ANSYS model except with the addition of two flanges and a module representing instrumentation and lubrication box,

as shown in Figure 61. The non-symmetrical elements are only placed to induce non-symmetry so the geometric coordinates are not important.

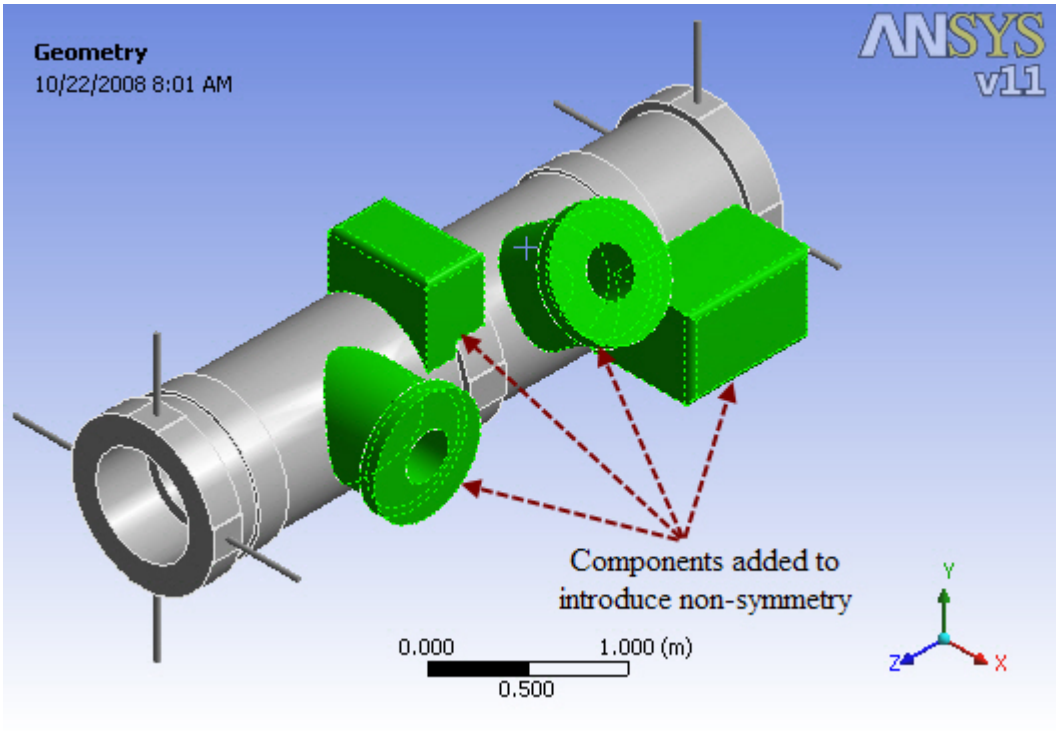

Figure 61 Solid model of ANSYS non-axisymmetric casing

Figure 62 shows a summary of the ANSYS non-axisymmetric casing model. The FEM mesh consists of 20,753 elements and 39,391 corresponding nodes. The effect of non-symmetry is evident in the change in location of the center of gravity and values of inertia when comparing them with the values of the axisymmetric model in Figure 60.

Bounding Box	
Length X	1.4523 m
Length Y	1.3234 m
Length Z	4. m
Properties	
Volume	1.738 m³
Mass	13614 kg
Centroid X	0.1836 m
Centroid Y	5.0731e-002 m
Centroid Z	1.808 m
Moment of Inertia Ip1	19825 kg·m²
Moment of Inertia Ip2	20454 kg·m²
Moment of Inertia Ip3	3132. kg·m²
Statistics	
Nodes	39391
Elements	20753

Figure 62 Summary of ANSYS non-axisymmetric casing model

3.2 Rotor Model

A rotor model is developed based on representative straight-through compressor models. Note that this model does not represent any proprietary rotor data. The rotor model described will be used for the remaining of the analyses to be performed.

The rotor is constructed of 21 beam elements of varying lengths and diameters. Steel is used as the material for the rotor. The material properties are taken from the standard XLTRC^2 template and have the following properties,

Density (ρ) = 7833.412 kg/m^3 (Specific weight = 0.283 lb/in^3)

Elastic Modulus (E) = 206.842E+9 N/m^2 (30.0E+6 lbf/in^2)

Shear Modulus (G) = 82.737E+9 N/m^2 (12.0E+6 lbf/in^2)

Table 3 describes the shaft properties of the rotor model. To reduce the complexity of the analysis, the use of sub-elements and layers is not employed. The rotor is a solid shaft, i.e. inner diameter = 0 m. To simulate the effect of impellers, lumped masses are added to various stations in the model, as shown in Table 4. Summaries for each element in the rotor model, comprising the length, center of gravity, mass,

transverse moment of inertia, and polar moment of inertia, is stated in Table 5. The summary of the complete rotor is described in Table 6 and shows a total length of 4.00 meters (157.48 inches) and a mass of 6370.05 kg (weight of 14043.50 lb). Figure 63 shows a graphical representation of the rotor.

APDL is used to create the rotor model in ANSYS. The source code has been included in APPENDIX E.

Table 3 Element properties of XLTRC^2 rotor model

Rotor Model Data Entry								
Shaft #	**Element #**	**Sub-Element#**	**Layer #**	**Length (m)**	**Left**		**Right**	
					OD(m)	**ID(m)**	**OD(m)**	**ID(m)**
1	1	1	1	0.250	0.200	0	0.200	0
1	2	1	1	0.150	0.200	0	0.200	0
1	3	1	1	0.350	0.300	0	0.300	0
1	4	1	1	0.100	0.250	0	0.250	0
1	5	1	1	0.100	0.250	0	0.250	0
1	6	1	1	0.100	0.300	0	0.300	0
1	7	1	1	0.050	0.300	0	0.300	0
1	8	1	1	0.400	0.400	0	0.400	0
1	9	1	1	0.200	0.400	0	0.400	0
1	10	1	1	0.250	0.400	0	0.400	0
1	11	1	1	0.125	0.400	0	0.400	0
1	12	1	1	0.125	0.400	0	0.400	0
1	13	1	1	0.250	0.400	0	0.400	0
1	14	1	1	0.250	0.400	0	0.400	0
1	15	1	1	0.150	0.400	0	0.400	0
1	16	1	1	0.400	0.400	0	0.400	0
1	17	1	1	0.100	0.300	0	0.300	0
1	18	1	1	0.100	0.300	0	0.300	0
1	19	1	1	0.100	0.250	0	0.250	0
1	20	1	1	0.100	0.250	0	0.250	0
1	21	1	1	0.350	0.300	0	0.300	0

Table 4 Lumped masses used to represent impellers in XLTRC2 rotor model

Added Mass & Inertia			
STN #	**Added Mass (Kg)**	**Added Ip (Kg-m²)**	**Added It (Kg-m²)**
2	120	5	5
10	100	20	10
11	100	20	10
13	1000	175	100
14	1000	175	100
15	1000	175	100
16	100	20	10

Table 5 Summary of individual element properties in XLTRC^2 rotor model

Elm #	Lft STN #	Rgt STN #	Beam Length (m)	Beam C.G. (m)	Axial CG (m)	Mass (Kg)	Inertia It (Kg-m²)	Inertia Ip (Kg-m²)
1	1	2	0.250	0.125	0.125	61.523	0.474	0.308
2	2	3	0.150	0.075	0.325	36.914	0.161	0.185
3	3	4	0.350	0.175	0.575	193.799	3.068	2.180
4	4	5	0.100	0.050	0.800	38.452	0.182	0.300
5	5	6	0.100	0.050	0.900	38.452	0.182	0.300
6	6	7	0.100	0.050	1.000	55.371	0.358	0.623
7	7	8	0.050	0.025	1.075	27.686	0.161	0.311
8	8	9	0.400	0.200	1.300	393.750	9.188	7.875
9	9	10	0.200	0.100	1.600	196.875	2.625	3.938
10	10	11	0.250	0.125	1.825	246.094	3.743	4.922
11	11	12	0.125	0.063	2.013	123.047	1.391	2.461
12	12	13	0.125	0.063	2.138	123.047	1.391	2.461
13	13	14	0.250	0.125	2.325	246.094	3.743	4.922
14	14	15	0.250	0.125	2.575	246.094	3.743	4.922
15	15	16	0.150	0.075	2.775	147.656	1.753	2.953
16	16	17	0.400	0.200	3.050	393.750	9.188	7.875
17	17	18	0.100	0.050	3.300	55.371	0.358	0.623
…	…	…	…	…	…	…	…	…
21	21	22	0.350	0.175	3.825	193.799	3.068	2.180
AW[9] 1		2			0.250	120.000	5.000	5.000
AW 2		10			1.700	100.000	10.000	20.000
AW 3		11			1.950	100.000	10.000	20.000
AW 4		13			2.200	1000.000	100.000	175.000
AW 5		14			2.450	1000.000	100.000	175.000
AW 6		15			2.700	1000.000	100.000	175.000
AW 7		16			2.850	100.000	10.000	20.000

[9] AW – Added Weight

Table 6 Summary of the complete XLTRC^2 rotor model

1st STN #	Nth STN #	Total Length (m)	Total Mass (Kg)	C.G. location (m)	Total It at C.G. (Kg-m²)	Total Ip about C.G. (Kg-m²)
1	21	4.00	6370.05	2.245	3971.324	640.56

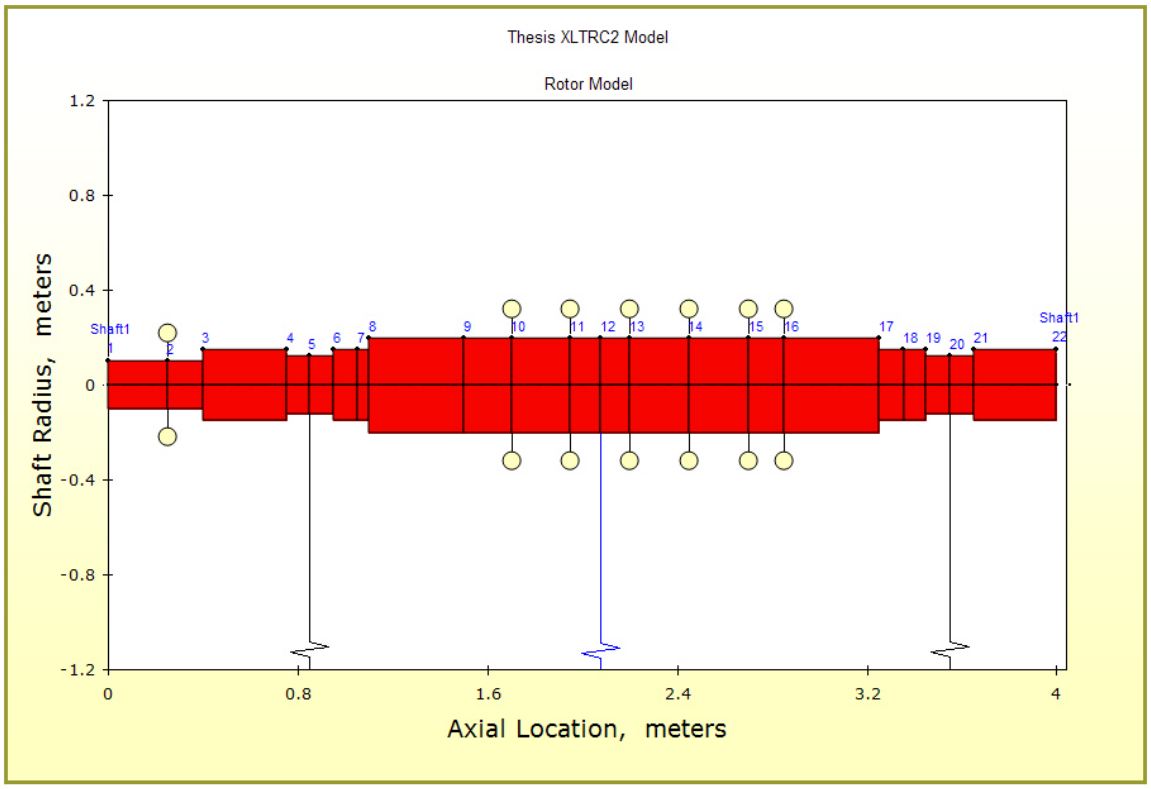

Figure 63 Geometric plot of XLTRC^2 rotor model

A model validation step is performed for the XLTRC^2 rotor model to ensure that it has been built correctly. It also provides a means to verify that the differences in parameters, such as coordinate systems, are accounted for correctly. This step is not essential to the process of incorporating the casing structure from ANSYS into XLTRC^2. Nevertheless, it is recommended. The validation step is documented in 0.

3.3 Bearing Model

Two 2-lobe sleeve journal bearings support the rotor. The bearings have a length of 0.16 m (6.30 in), diameter of 0.25 m (9.84 in), and pad clearance of 0.004 m (0.0157 in). The bearing use a lubricant with viscosity of 21.99e-03 Pa-s (21.99 cp) and density of 853.49 kg/m^3 (specific weight = 0.0308 lb/in^3). With a bearing span of 2.70 m (106.30 in) they connect to the rotor model at stations 5 and 20, as shown in Figure 63[10]. Bearing locations and rotor center of gravity are shown in Figure 64. These bearings will later be used to connect the rotor to the casing structure.

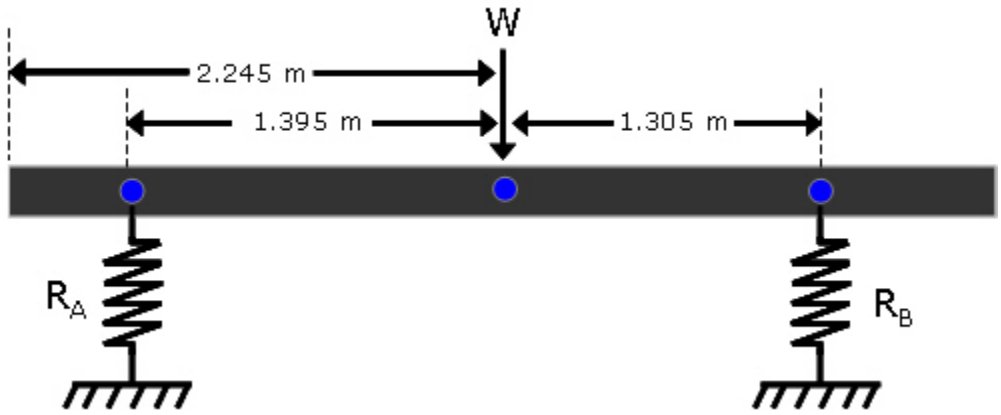

Figure 64 Bearing load calculation

The following force balance equation provides the reaction forces (R_A and R_B).

Total mass of rotor = 6370.05 kg (436.48 slug)

Weight of rotor, W = 62490.19 N (14048.40 lbf)

Center of gravity location = 2.245 m (88.385 in) from left end of rotor

$$R_A + R_B = 62490.19 \tag{74}$$

$$\text{Moment about A} \Rightarrow 2.7R_B - 6370.05 \times 1.395 = 0 \tag{75}$$

This results in

[10] The bearing stations use different numbering in the combined rotor-casing model

$$\therefore \; R_A = 30203.59N \qquad R_B = 32286.59N \tag{76}$$

XLJrnl™ Spreadsheet for Journal Bearing Coefficients

Title: Bearing 1

Bearing Type: 2 Lobe Sleeve

Bearing Length	0.16	meters
Bearing Diameter	0.25	meters
Pad Clr, Cp	0.0004	meters
Bearing Load, F	30203.59	Newtons
Bearing Preload, m	0.0001	--

Lubricant Viscosity	21.99953	cp
Lubricant Density	853.49	kg/m3

Speed	Kxx	Kxy	Kyx	Kyy	Cxx	Cxy	Cyx	Cyy
rpm	N/m	N/m	N/m	N/m	N-s/m	N-s/m	N-s/m	N-s/m
400	2.7E+08	-6.2E+07	-6.5E+08	1.02E+09	4809581	-7467756	-7467744	28654746
800	2.8E+08	13720457	-5.8E+08	6.95E+08	3229085	-3856346	-3856337	12963474
1200	2.91E+08	68087258	-5.5E+08	5.46E+08	2506482	-2500004	-2499999	8184931
1600	3E+08	1.11E+08	-5.4E+08	4.8E+08	2157678	-1885056	-1885048	6139058
1800	3.05E+08	1.32E+08	-5.4E+08	4.48E+08	2041411	-1680074	-1680065	5457101
2000	3.09E+08	1.52E+08	-5.4E+08	4.27E+08	1959460	-1526460	-1526450	4959466
2400	3.18E+08	1.91E+08	-5.5E+08	3.97E+08	1846033	-1304944	-1304933	4254169
2600	3.22E+08	2.1E+08	-5.6E+08	3.82E+08	1802408	-1219746	-1219734	3982901
3000	3.3E+08	2.48E+08	-5.7E+08	3.58E+08	1726101	-1078503	-1078489	3562145

Figure 65 Calculated rotordynamic coefficients of bearing 1

The stiffness and damping bearing coefficients for bearing 1 and bearing 2 are calculated as shown in Figure 65 and Figure 66, respectively. A third-order polynomial fit is used to obtain expressions for speed dependent stiffness and damping bearing coefficients. *N* represents the running speed in RPM. The equations for bearing 1 are shown in Eq.(77) and bearing 2 in Eq.(78).

$$
\begin{aligned}
K_{xx} &= 1066393315\times N^{-1} + 255286980.2\times N^{0} + 31095.3652\times N^{1} - 2.172088328\times N^{2}\\
K_{xy} &= -30104742824\times N^{-1} - 27798078.92\times N^{0} + 102487.8616\times N^{1} - 2.4442301\times N^{2}\\
K_{yx} &= -59619636440\times N^{-1} - 510140831.9\times N^{0} + 24557.04362\times N^{1} - 13.0524594\times N^{2}\\
K_{yy} &= 2.31531\text{E+}11\times N^{-1} + 487023684.1\times N^{0} - 128187.9399\times N^{1} + 20.20956004\times N^{2}\\
C_{xx} &= 1126279319\times N^{-1} + 2268914.8\times N^{0} - 725.3190345\times N^{1} + 0.142588357\times N^{2}\\
C_{xy} &= -2842395798\times N^{-1} - 508206.302\times N^{0} + 381.4519148\times N^{1} - 0.087678631\times N^{2}\\
C_{yx} &= -2842391408\times N^{-1} - 508206.8736\times N^{0} + 381.454552\times N^{1} - 0.087677984\times N^{2}\\
C_{yy} &= 13263960051\times N^{-1} - 5519587.151\times N^{0} + 2683.710808\times N^{1} - 0.378480913\times N^{2}
\end{aligned}
\tag{77}
$$

XLJrnl™ Spreadsheet for Journal Bearing Coefficients

Title: Bearing 2

Bearing Type: 2 Lobe Sleeve

Bearing Length	0.16	meters
Bearing Diameter	0.25	meters
Pad Clr, Cp	0.0004	meters
Bearing Load, F	32286.6	Newtons
Bearing Preload, m	0.0001	--

Lubricant Viscosity	21.99953	cp
Lubricant Density	853.49	kg/m3

Speed	Kxx	Kxy	Kyx	Kyy	Cxx	Cxy	Cyx	Cyy
rpm	N/m	N/m	N/m	N/m	N-s/m	N-s/m	N-s/m	N-s/m
400	2.88E+08	-7.4E+07	-7.1E+08	1.13E+09	4998424	-7950433	-7950420	30968583
800	2.98E+08	7025245	-6.2E+08	7.64E+08	3378899	-4138534	-4138525	13960643
1200	3.09E+08	62425760	-5.9E+08	6.08E+08	2604861	-2680561	-2680556	8808604
1600	3.18E+08	1.07E+08	-5.8E+08	5.32E+08	2229845	-2012287	-2012279	6562342
1800	3.23E+08	1.28E+08	-5.8E+08	4.99E+08	2105558	-1793168	-1793159	5833353
2000	3.28E+08	1.5E+08	-5.8E+08	4.66E+08	2006395	-1618121	-1618112	5251313
2400	3.36E+08	1.88E+08	-5.9E+08	4.37E+08	1885146	-1381329	-1381318	4497375
2600	3.4E+08	2.07E+08	-5.9E+08	4.22E+08	1838512	-1290255	-1290243	4207399
3000	3.49E+08	2.46E+08	-6E+08	3.92E+08	1763897	-1144537	-1144524	3743437

Figure 66 Calculated rotordynamic coefficients of bearing 2

The polynomial fit equations for bearing 2 are shown in Eq. (78).

$$
\begin{aligned}
K_{xx} &= \ 1453070445\times N^{-1} + 272186237.9\times N^{0} + 31603.41526\times N^{1} - 2.132270135\times N^{2} \\
K_{xy} &= -33145936257\times N^{-1} - 32508425.09\times N^{0} + 104532.0399\times N^{1} - 2.756220705\times N^{2} \\
K_{yx} &= -66023587471\times N^{-1} - 549617088.4\times N^{0} + 27529.90062\times N^{1} - 12.87745021\times N^{2} \\
K_{yy} &= \ 2.59554\text{E+}11\times N^{-1} + 527609699.1\times N^{0} - 131963.5864\times N^{1} + 19.72913164\times N^{2} \\
C_{xx} &= \ 1116961207\times N^{-1} + 2547929.708\times N^{0} - 904.1695253\times N^{1} + 0.17587026\times N^{2} \\
C_{xy} &= -2966327354\times N^{-1} - 742905.3155\times N^{0} + 546.9707955\times N^{1} - 0.119750611\times N^{2} \\
C_{yx} &= -2966321753\times N^{-1} - 742906.8109\times N^{0} + 546.9735545\times N^{1} - 0.119750085\times N^{2} \\
C_{yy} &= \ 14345445250\times N^{-1} - 5972848.052\times N^{0} + 2845.020331\times N^{1} - 0.402189446\times N^{2}
\end{aligned}
\tag{78}
$$

The stiffness and damping curve fits for bearing 1 are graphically represented by Figure 67 and Figure 68, respectively. Bearing 2 curve fits are represented by Figure 69 and Figure 70.

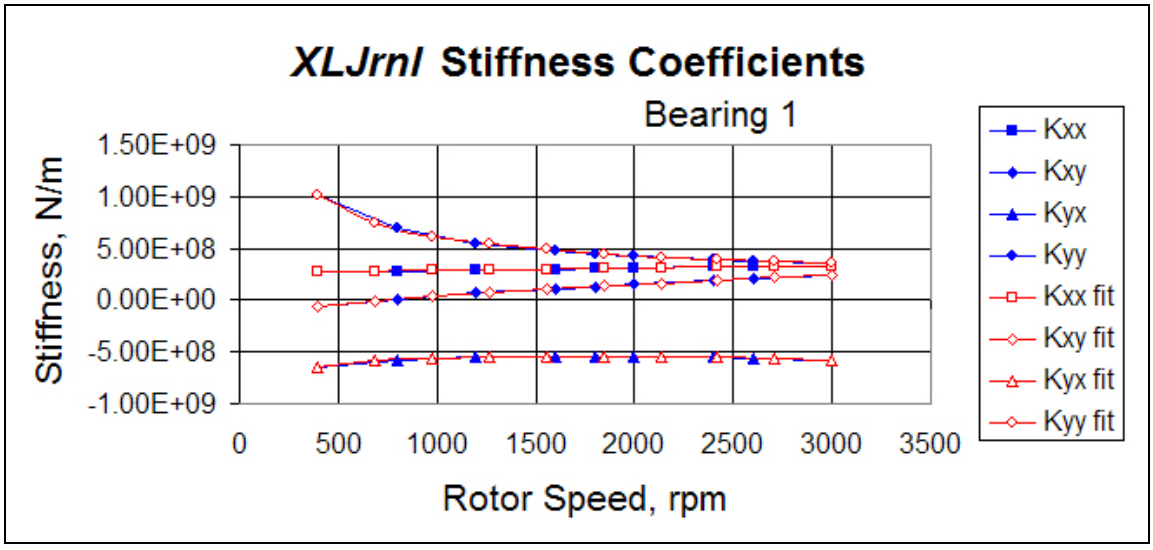

Figure 67 Stiffness coefficients curve fit plot for bearing 1

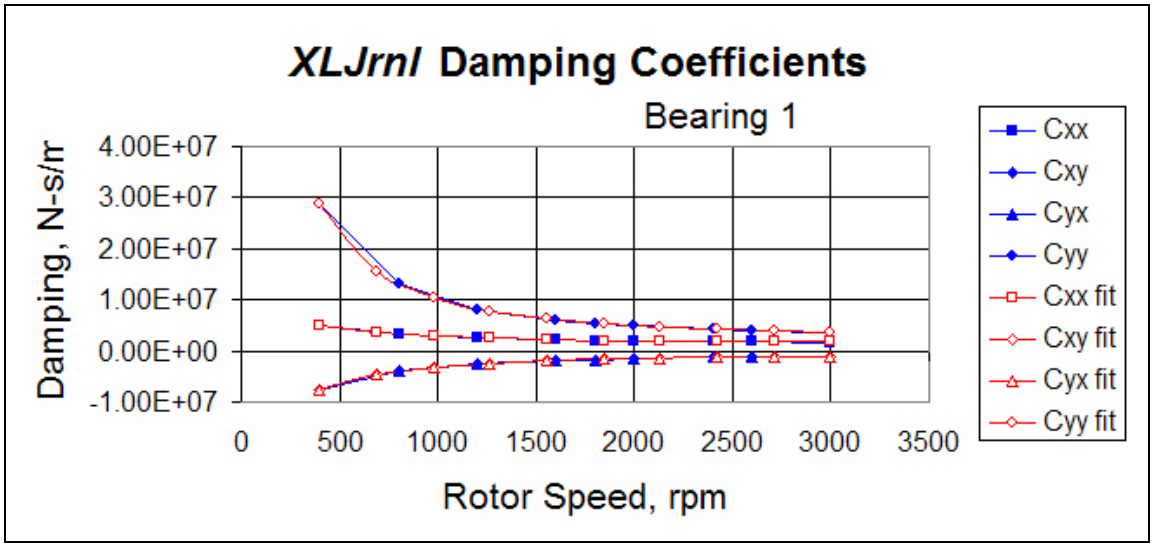

Figure 68 Damping coefficients curve fit plot for bearing 1

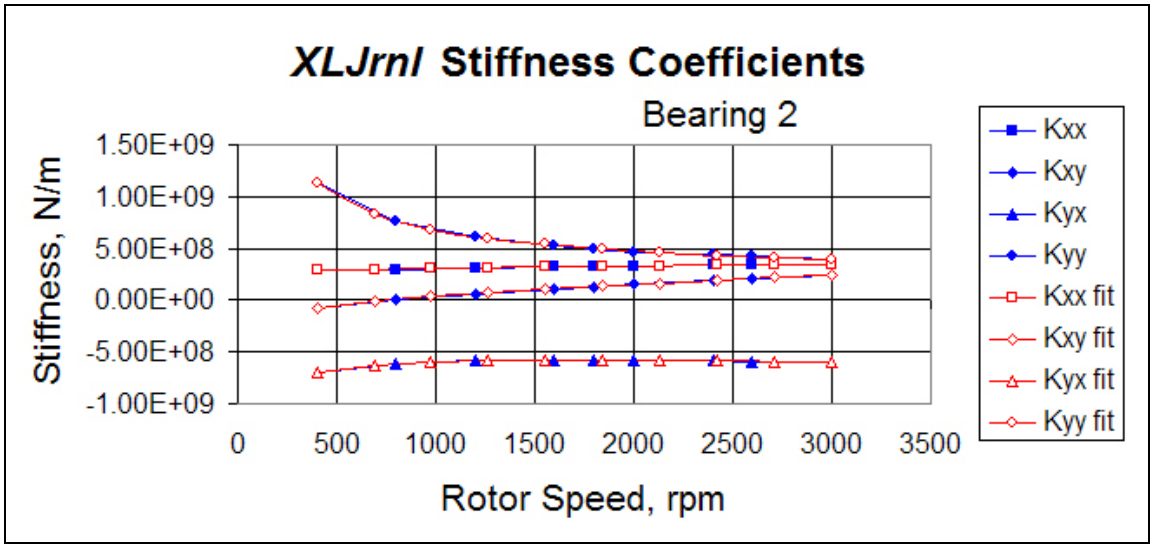

Figure 69 Stiffness coefficients curve fit plot for bearing 2

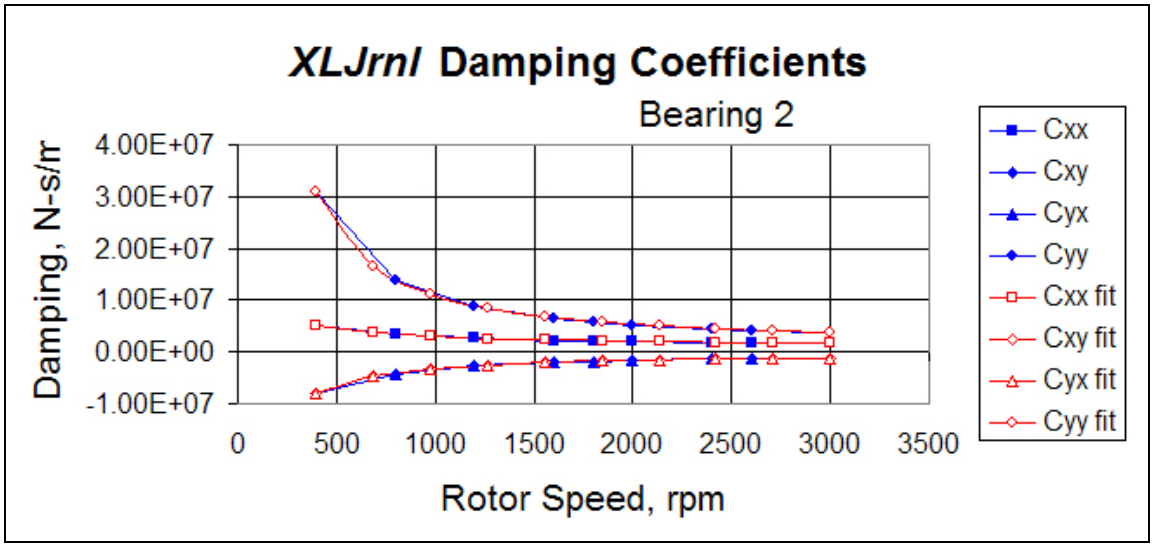

Figure 70 Damping coefficients curve fit plot for bearing 2

3.4 Seal Model

The rotor used in the analyses represents a straight-through compressor. The use of a seal in such an application prevents leakage losses that can occur across the various stages of a compressor. A simple made-up gas seal is used to include the effect of this rotordynamic element in the analysis, and it connects to the rotor at station 12, as shown in Figure 63. Note that this seal does not represent any actual data set and is used only as a representative model. Constant seal coefficients are used as illustrated in Figure 71.

Seal rotordynamic stiffness, damping and mass coefficients curve fits are represented in Figure 72, Figure 73, and Figure 74, respectively. Note that the direct coefficients have the same value, i.e. $K_{XX} = K_{YY}, C_{XX} = C_{YY}$, and $M_{XX} = M_{YY}$. Hence these plots appear to overlay each other on the figures.

XLUseKCM™ User Defined Support Stiffness, Damping, and Mass Rotordynamic Coefficients

Title: Seal

Speed	Kxx	Kxy	Kyx	Kyy	Cxx	Cxy	Cyx	Cyy	Mxx	Mxy	Myx	Myy
rpm	N/m	N/m	N/m	N/m	N-s/m	N-s/m	N-s/m	N-s/m	kg	kg	kg	kg
300	1.50E+08	0	0	1.50E+08	5.00E+05	0	0	5.00E+05	1.50E+01	0	0	1.50E+01
600	1.50E+08	0	0	1.50E+08	5.00E+05	0	0	5.00E+05	1.50E+01	0	0	1.50E+01
900	1.50E+08	0	0	1.50E+08	5.00E+05	0	0	5.00E+05	1.50E+01	0	0	1.50E+01
1200	1.50E+08	0	0	1.50E+08	5.00E+05	0	0	5.00E+05	1.50E+01	0	0	1.50E+01
1500	1.50E+08	0	0	1.50E+08	5.00E+05	0	0	5.00E+05	1.50E+01	0	0	1.50E+01
1800	1.50E+08	0	0	1.50E+08	5.00E+05	0	0	5.00E+05	1.50E+01	0	0	1.50E+01
2100	1.50E+08	0	0	1.50E+08	5.00E+05	0	0	5.00E+05	1.50E+01	0	0	1.50E+01
2400	1.50E+08	0	0	1.50E+08	5.00E+05	0	0	5.00E+05	1.50E+01	0	0	1.50E+01
2700	1.50E+08	0	0	1.50E+08	5.00E+05	0	0	5.00E+05	1.50E+01	0	0	1.50E+01
3000	1.50E+08	0	0	1.50E+08	5.00E+05	0	0	5.00E+05	1.50E+01	0	0	1.50E+01

Figure 71 Seal rotordynamic coefficients

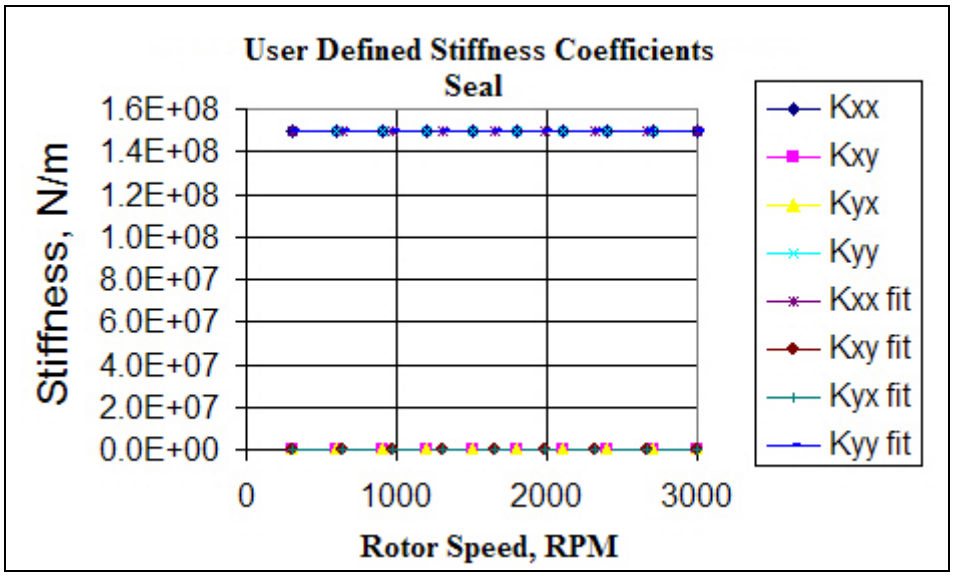

Figure 72 Stiffness coefficients curve fit plot for seal

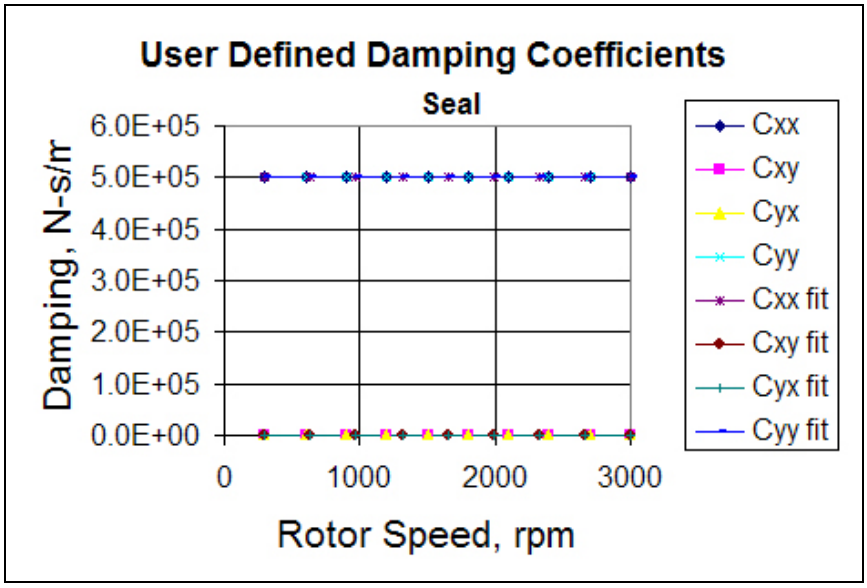

Figure 73 Damping coefficients curve fit plot for seal

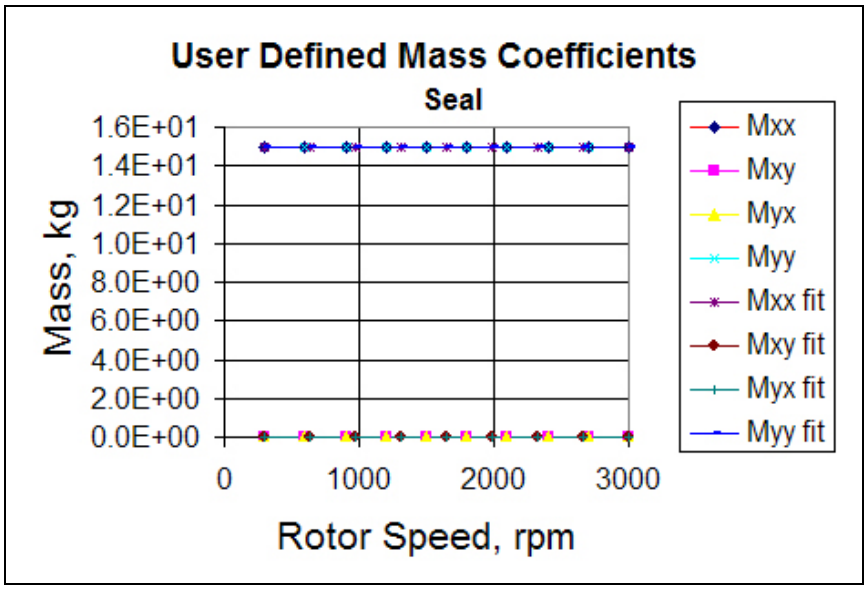

Figure 74 Mass coefficients curve fit plot for seal

3.5 Coupled Rotor–Casing Model

This section shows the models used for symmetrical and non-symmetrical coupled rotor-casing model. The rotor is connected to the casing at bearing locations, and the seal used at about midway of the rotor length. The casing is connected to ground using foundation supports. These supports are modeled as isotropic supports with no damping and stiffness of $5x10^8$ N/m ($2.86x10^6$ lb/in).

3.5.1 Axisymmetric Coupled XLTRC^2 Rotor–Casing Model

Figure 75 shows the XLTRC^2 model for coupled rotor-casing consisting of 181 elements and 183 stations (nodes). Table 7 describes the connecting elements.

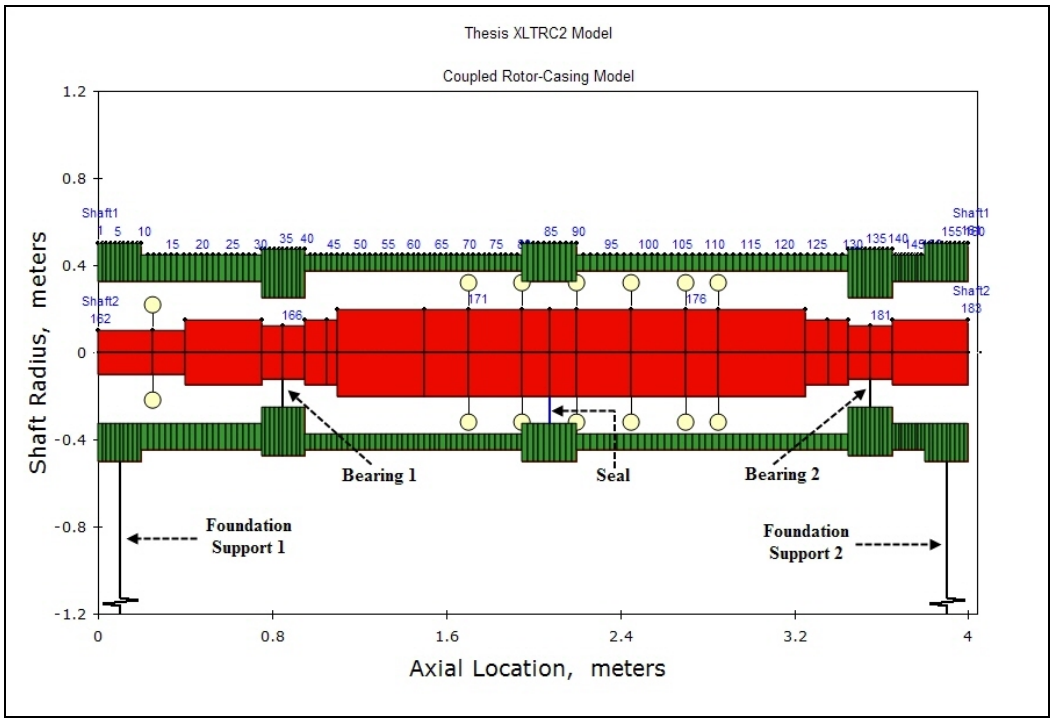

Figure 75 XLTRC^2 coupled rotor-casing model for symmetrical case

Table 7 Connecting elements between rotor and casing

Rotor Station #	Casing Station #	Connecting Element
166	36	Bearing 1
181	136	Bearing 2
173	86	Seal
-	6	Foundation Support 1
-	156	Foundation Support 2

3.5.2 Axisymmetric Coupled ANSYS Rotor–Casing Model

The ANSYS coupled rotor-casing model for the axisymmetric case is shown in Figure 76 and Figure 77.

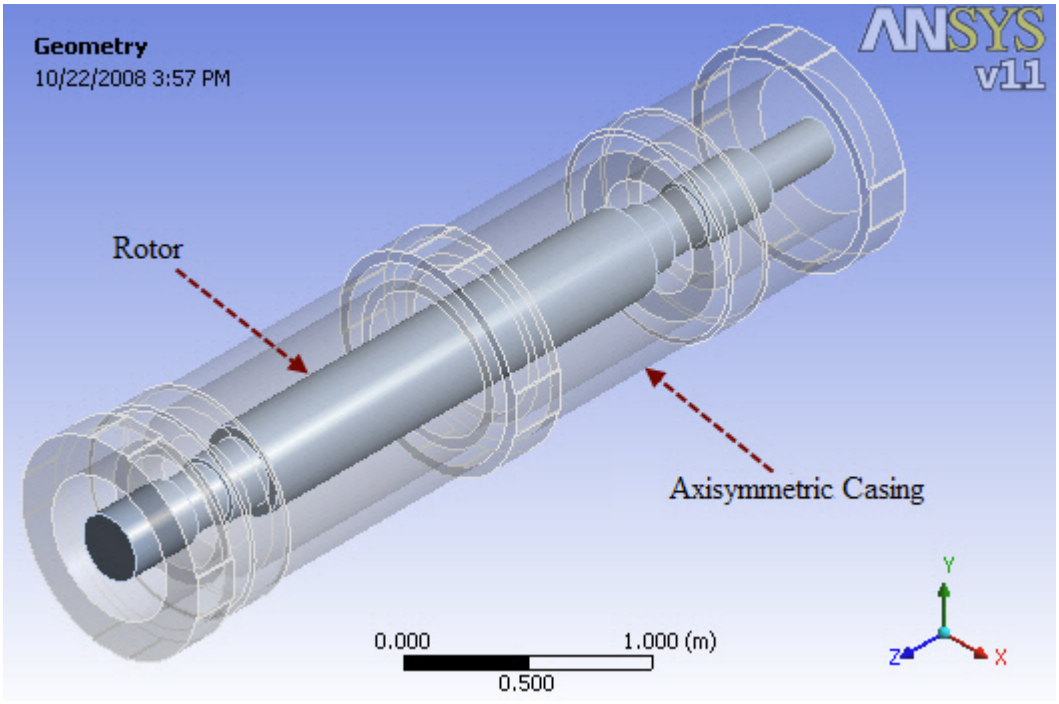

Figure 76 ANSYS coupled rotor-casing model for axisymmetric case

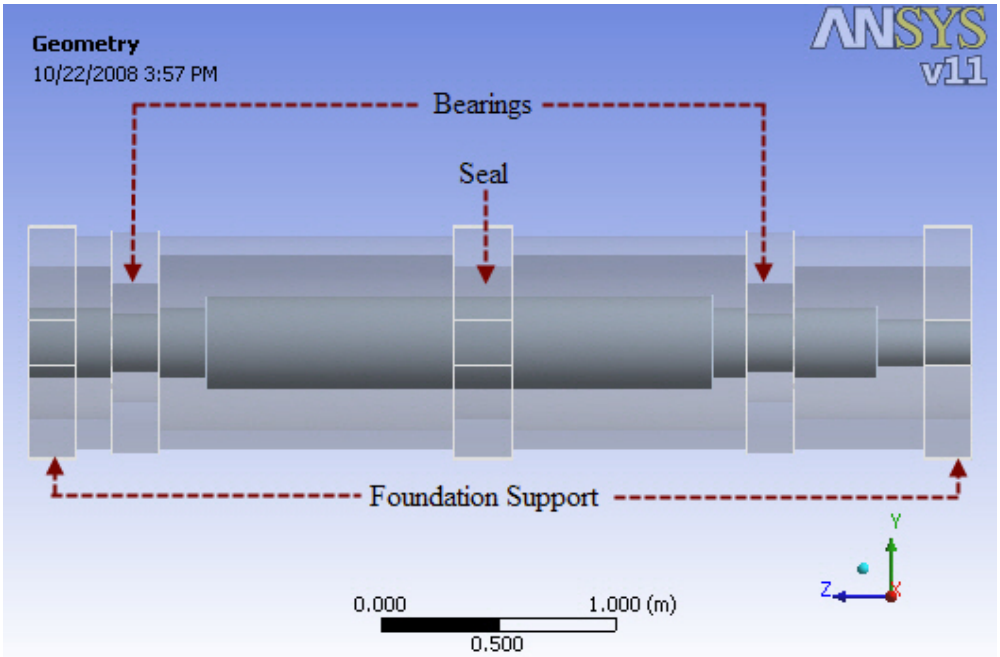

Figure 77 Axisymmetric coupled model with locations of connecting elements

3.5.3 Non–Axisymmetric Coupled ANSYS Rotor–Casing Model

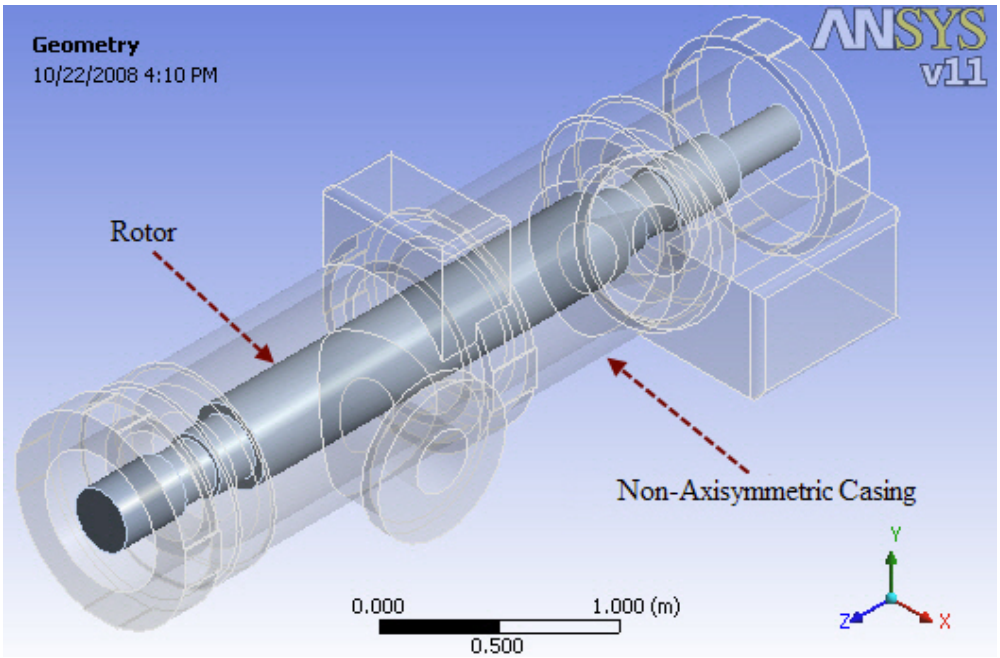

Figure 78 ANSYS coupled rotor-casing model for non-axisymmetric case

The ANSYS coupled rotor-casing model for the non-axisymmetric case is shown in Figure 78 and Figure 79.

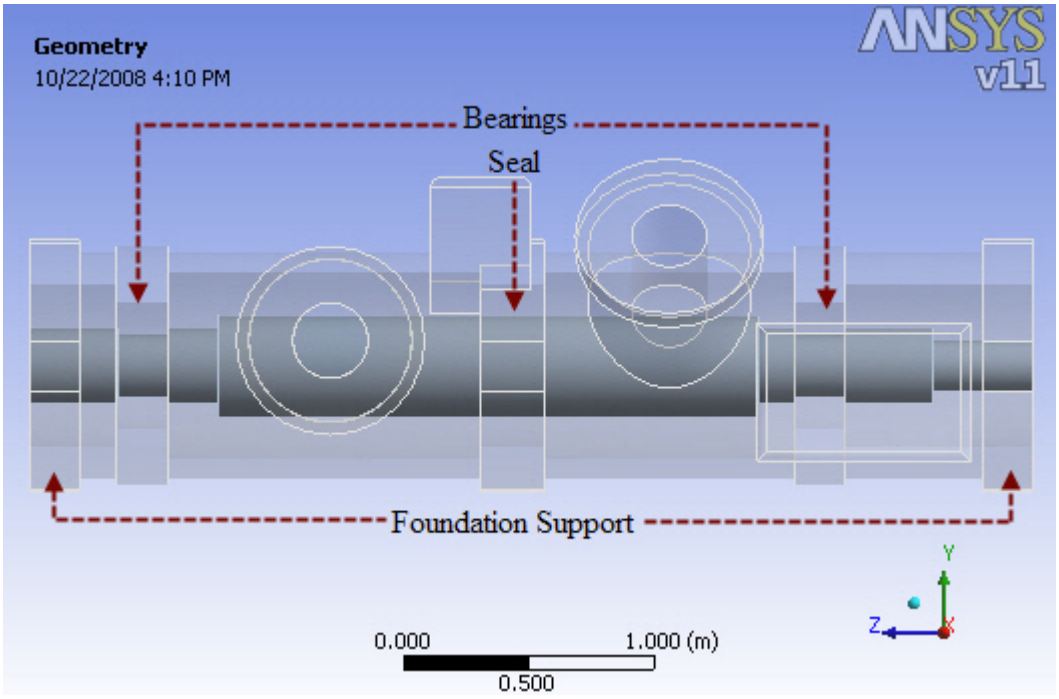

Figure 79 Non-axisymmetric coupled model showing connecting elements

3.6 Setting up Component Mode Synthesis in ANSYS

Depending on the level of accuracy desired, the type of component mode synthesis (CMS) method can be specified. The analyses used here employ the *Fixed-interface* method. In this method, interface nodes are specified and constrained while creating the superelement. This method is recommended in the ANSYS help manual for casings and structural materials where the accuracy of the lower modes is important. CMS analysis in ANSYS involves three distinct steps called passes. The passes are version-specific, so it is important to have them performed using the same version of ANSYS in which the database file is created. As of version 11 SP1, the CMS option in ANSYS generates only the reduced mass and stiffness matrices.

The first CMS pass is called *Generation Pass* and can be considered an extension of the substructuring procedure, described in section 2.3. It involves condensing a group of finite elements into a single superelement. Once a finite element model is built, a set of master degrees of freedom (MDOF) are identified. This will define the interface of the newly created superelement with other superelements or elements. The master DOF are essential to capture the dynamic characteristics for analyses. The CMS method and the frequency range of interest are specified. Applicable loads are defined, and the solution is initiated. The output of the generation pass is the superelement matrix file, identified by the default *.SUB* extension

The second CMS pass is called *Use Pass* and it makes use of the generated superelement file by making it part of the model. The entire model may eventually consist of only a single superelement or may be a combination of superelements and other non-superelements. The CMS use pass can be used for analysis types such as modal, static, force response, transient, etc. While a generation pass needs to be done for each component of the entire structure, the use pass is done only once because it uses all the superelements together in one full model.

The third pass, called the *Expansion Pass*, is optional. As the name suggests, it is used to expand results from the reduced model to the full-scale model. Figure 80 shows details of the commands used in an algorithm for CMS generation and use pass in ANSYS.

```
! **GENERATION PASS**
! Enter the solution processor
/SOLU
! Specify the substructure analysis type
ANTYPE, SUBSTR
! Set component mode synthesis options
CMSOPT, FIX, 5, , ,
! Set substructure options
SEOPT, brgpdstl, 2, 1, 0, resolve
! Specify solver and perform solution
EQSLV, SPARSE
! Start the solution phase
SOLVE
! Create substructure file listing
SELIST, brgpdstl, 0

FINISH

! **USE PASS**
! Enter the preprocessor
/PREP7
! Define superelement and reduced model as a superelement
ET, 3000, MATRIX50
! Create material type and real constant set
TYPE, 3000
REAL, 3000
! Load the CMS reduced substructure file
SE, brgpdstl, , , 0.1

FINISH
```

Figure 80 CMS generation and use pass

3.7 Coupled Rotor-Reduced Casing Model

Having described the substructuring and component mode synthesis algorithms in the previous section, the next step involves performing the reduction steps. The details of the steps are described in the following sub-sections.

3.7.1 Axisymmetric Coupled ANSYS Rotor–Reduced Casing Model

The integration of ANSYS into XLTRC^2 begins with the ANSYS database file. The ANSYS Workbench model is first imported into ANSYS Classic using the available

database conversion tools. Workbench is designed as a user-friendly application that encapsulates most of the powerful features of Classic through graphical user interface elements. However, many advanced features are unavailable such as flexibility and control over the use of elements and nodes. Figure 81 shows the casing model after it has been imported into ANSYS Classic.

Next the node matching step is performed. The theory behind this step is described in detail in section 2.7.3, and explained the creation of a new node at the center and then connecting them with rigid elements in the radial direction. Figure 82 shows the newly created nodes for the bearings and seals. These nodes, along with nodes at the foundation supports, are then included in the master degree of freedom (DOF) set.

Once the master DOFs are selected and necessary constraints applied, substructuring is performed. This reduces the casing model while retaining all essential dynamic characteristics.

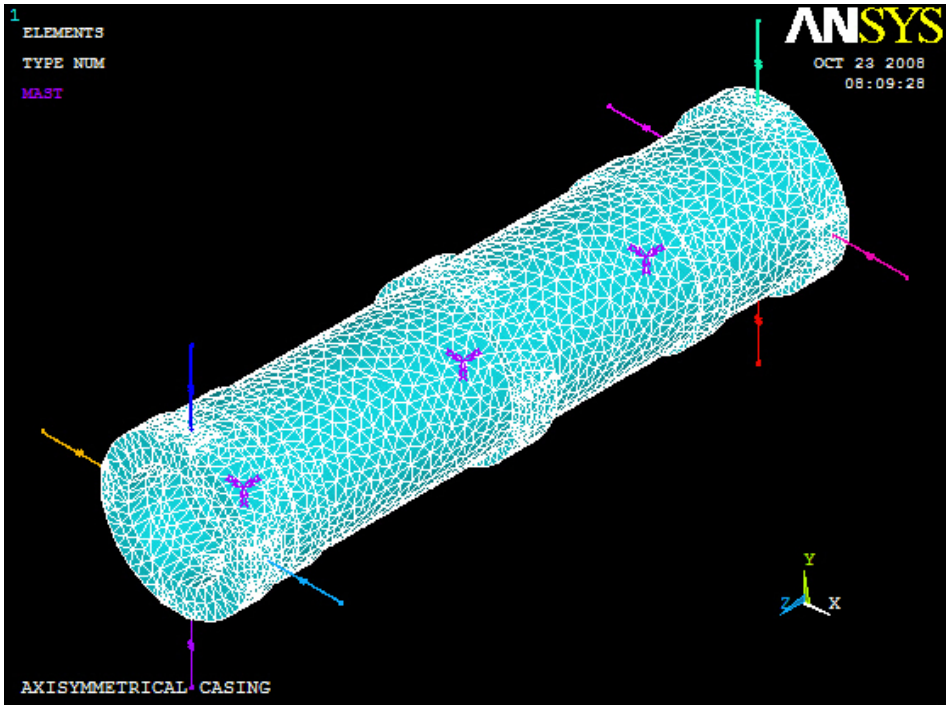

Figure 81 Axisymmetric casing model in ANSYS classic format

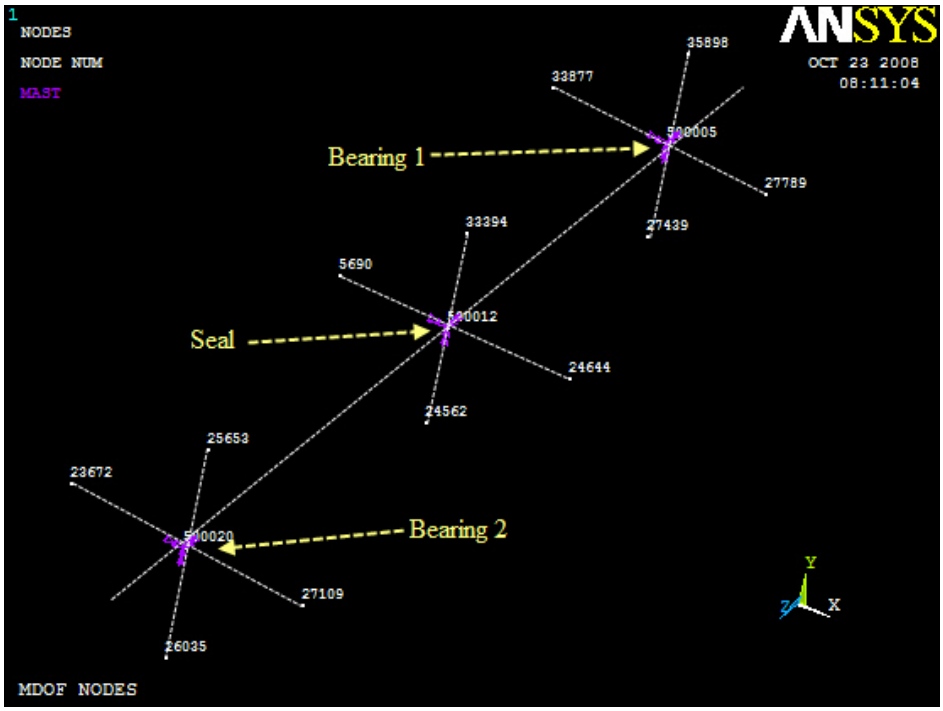

Figure 82 Nodes at bearing and seal locations that form MDOF set

Figure 83 shows the reduced casing model. Note that the missing graphical features do not indicate that those elements have been removed. The reduced casing model is then integrated with the rotor model, described in section 3.2, to form the coupled axisymmetric rotor-reduced casing model. Figure 84 shows the placement of the rotor within the axisymmetric casing structure. Figure 85 can be compared with Figure 77 for graphical validation. The APDL source code for axisymmetric casing substructuring has been included in APPENDIX E.

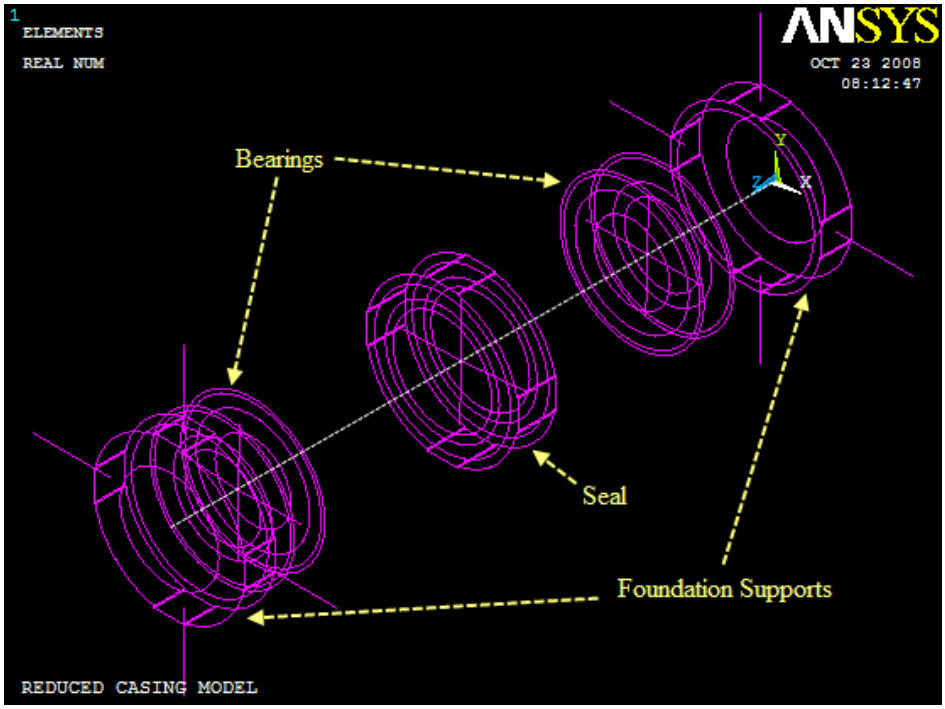

Figure 83 Reduced model of axisymmetric casing structure

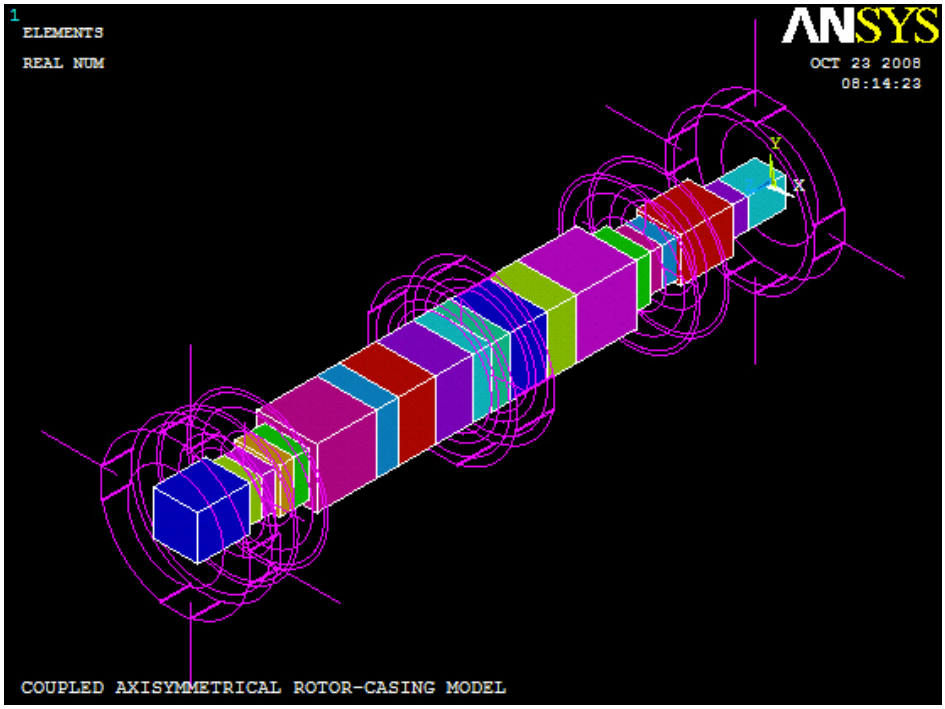

Figure 84 Isometric view showing combined rotor –reduced casing model

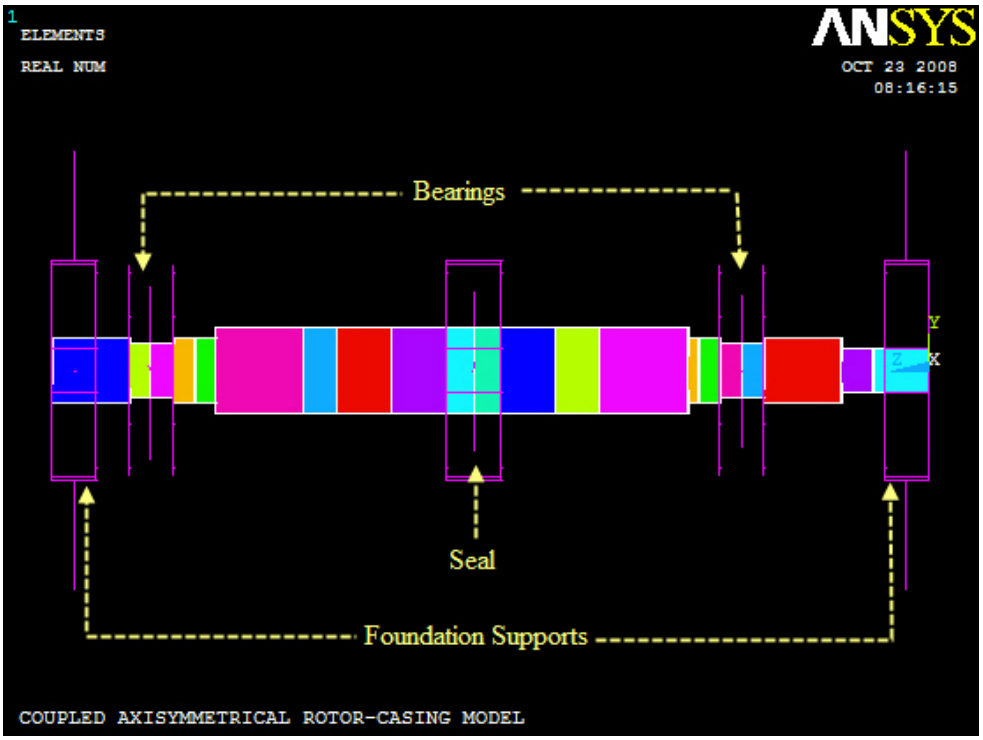

Figure 85 Side view of coupled axisymmetric model showing relative placement

3.7.2 Non–Axisymmetric Coupled ANSYS Rotor–Reduced Casing Model

Similar reduction steps are performed for the non-axisymmetric casing structure. Figure 86 shows the casing model when imported into ANSYS Classic. The node matching step is performed, and the selected master degree of freedom set is shown in Figure 87. Substructuring is performed and results in the reduced model, shown in Figure 88. The non-axisymmetric components can be seen clearly. The reduced casing model is then integrated with the rotor model. Figure 89 shows the placement of the rotor within the non-axisymmetric casing structure.

The APDL source code for axisymmetric casing substructuring has been included in APPENDIX E.

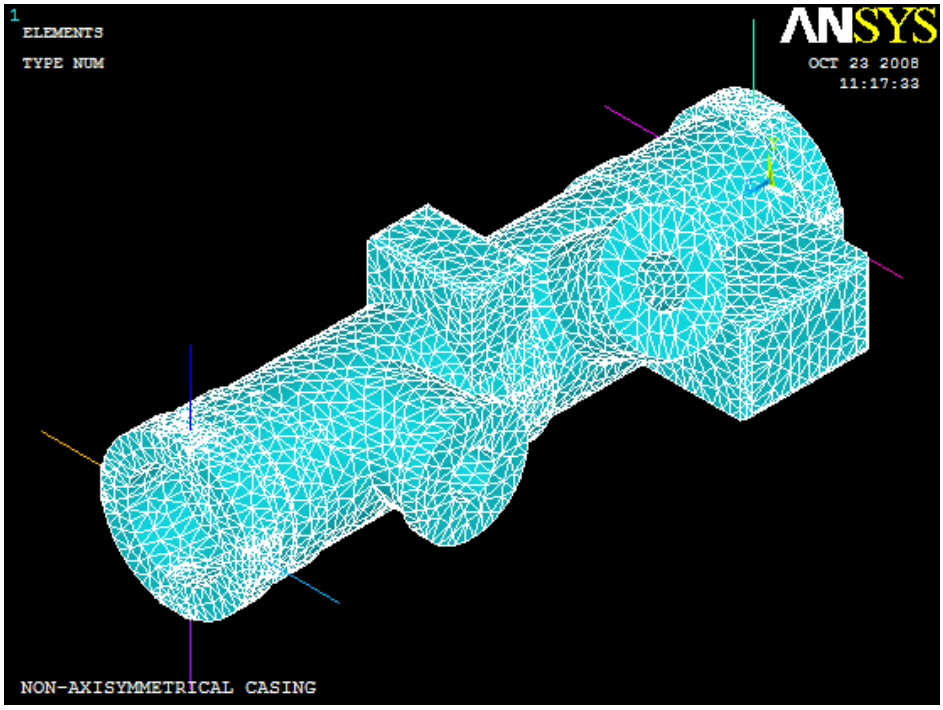

Figure 86 Non-axisymmetric casing model in ANSYS classic format

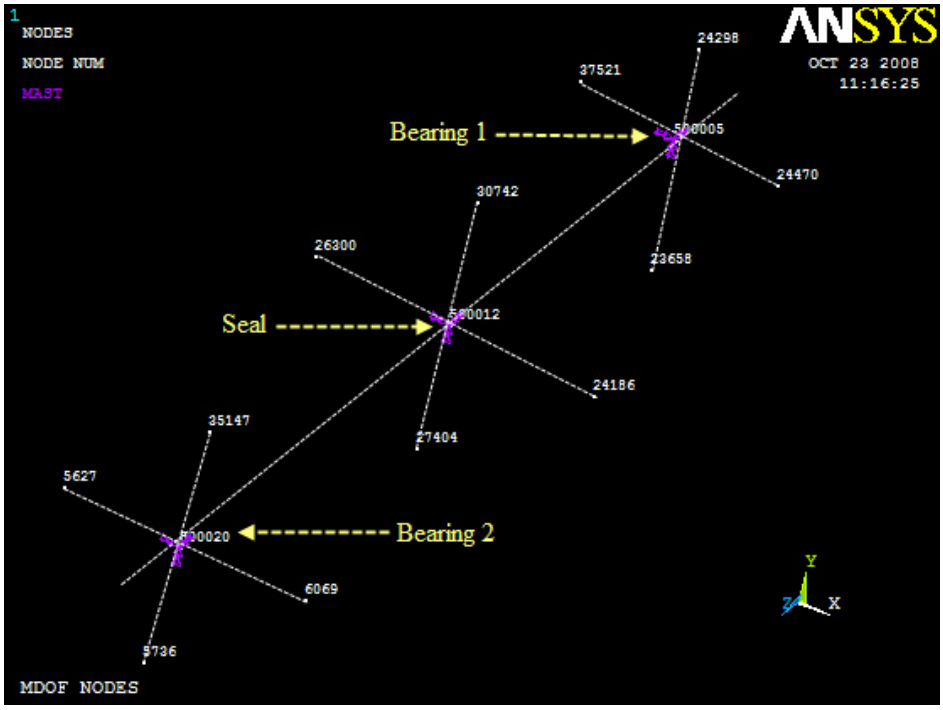

Figure 87 Nodes at bearing and seal locations that form MDOF set

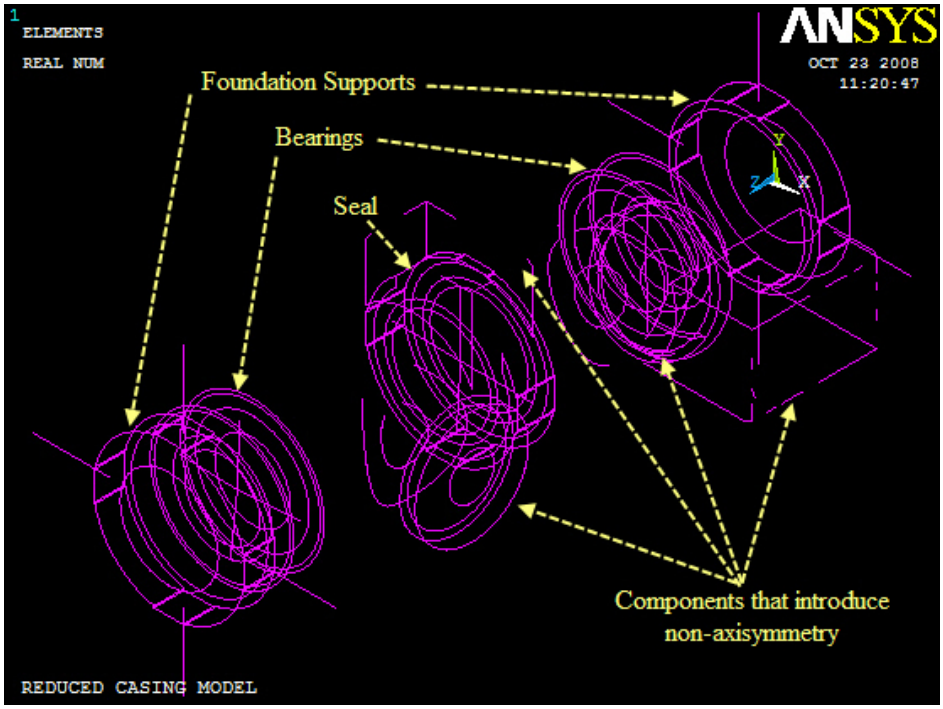

Figure 88 Reduced model of non-axisymmetric casing structure

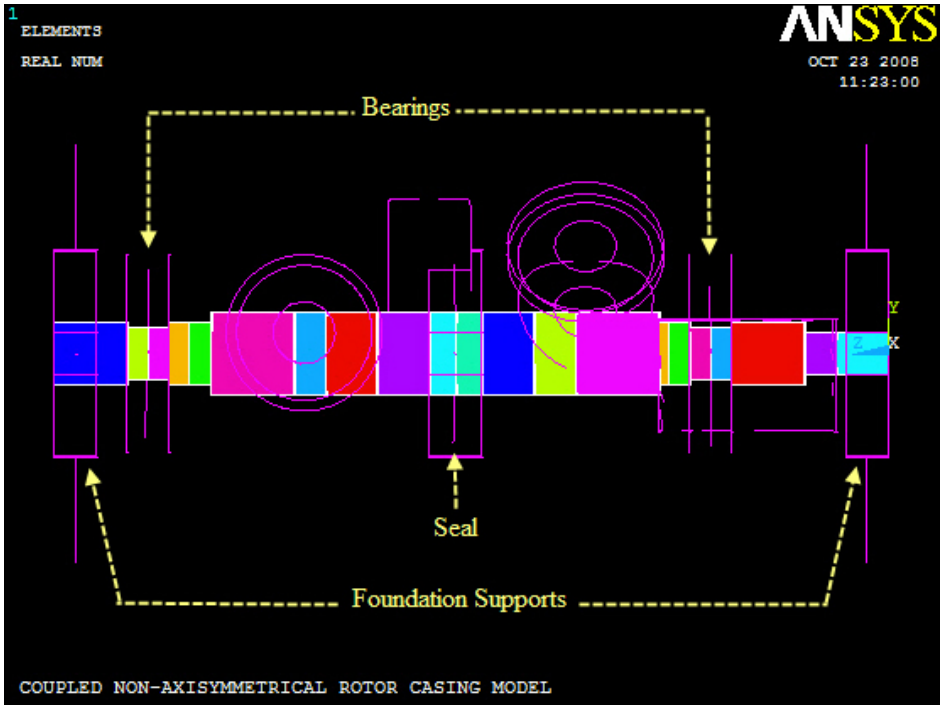

Figure 89 Coupled non-axisymmetric model showing relative placement

4 RESULTS AND DISCUSSION

Having described the casing, rotor, bearing and seal models in the previous section, the next step is to run the various analyses and calculate the results.

The analyses are first done for the rotor-only model. This provides a base for comparison, as the objective of this thesis is to adapt the beam-based XLTRC^2 rotordynamic model to accept a general three dimensional finite element casing model. Section 4.1 describes the details of the analysis. The unbalance magnitude specifications and configurations, mentioned in section 4.1.4, are also used in the casing structure analyses that follow. An unbalance response is performed with the axisymmetric model built in XLTRC^2 and this is compared with the axisymmetric model from ANSYS. This comparison serves to provide a direct measure of the accuracy of the existing XLTRC^2 suite.

Once the rotor model results are generated, the casing structure is included for the coupled rotor-casing model analyses, illustrated in section 4.2. With the casing structure, the first set of analysis uses the axisymmetric casing structure. Both the XLTRC^2 axisymmetric casing and the ANSYS axisymmetric casing are employed. The second set of analysis uses the non-axisymmetric casing structure model from ANSYS. This is compared with the axisymmetric model for changes in the rotordynamic behavior. The mode shapes and unbalance response are investigated.

A study is also conducted into the connection used for the interstage seal. The results obtained by connecting the seal between rotor and ground are compared with those obtained in the case where the seal connection is made between the rotor and the casing. These predictions are discussed in section 4.2.4.

4.1 Rotor-Only Model

This section describes the undamped critical speed, damped critical speed and unbalance response analysis done on the rotor and the results inferred.

4.1.1 Rotor Undamped Critical Speed Map

The undamped critical speed (UCS) analysis is performed on the rotor model to get a preliminary assessment of critical speeds and mode shapes of the rotor. This analysis does not include the effects of any damping on the system, and thus does not represent the actual dynamics of the rotor. However it gives insight into the general behavior of the rotor. UCS analysis is performed by applying varying amounts of stiffness at the support locations, which are the bearings in this case. The critical speeds and mode shapes are then calculated for each value of direct support stiffness. A UCS map is generated by plotting the support stiffness (abscissa axis) versus critical speed frequency (ordinate axis), as shown in Figure 90.

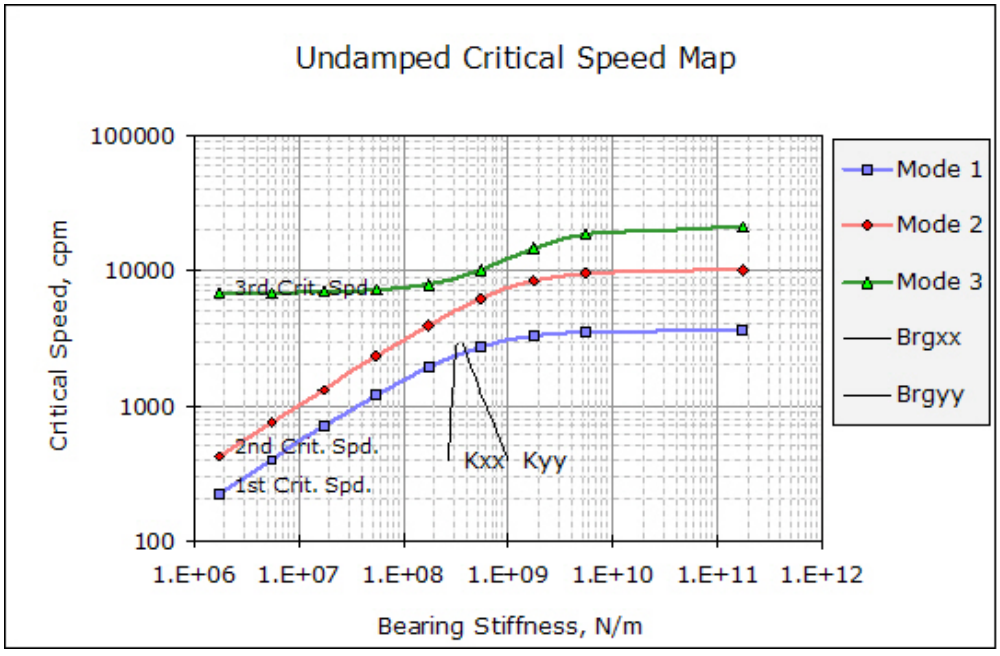

Figure 90 Rotor undamped critical speed map with bearing stiffness cross-plotted

The highlighting characteristic in the UCS map is the relationship between the rotor stiffness and the support stiffness. The controlling element in a system is the one with the lowest stiffness. Hence at lower support bearing stiffness, the frequencies of the system are influenced by the bearing stiffness and rotor mass. The left area of the UCS map is therefore called the stiff rotor part because the rotor does not undergo much bending. At higher bearing stiffness, as seen in the right area of the UCS map, the critical speeds are no longer influenced by the support stiffness and are influenced by the rotor stiffness and rotor mass. The support locations becomes node points and the rotor experiences higher degree of bending.

Once the UCS map is defined, the actual support characteristics are taken into account to assess the critical speeds. Speed-dependent direct bearing stiffness values for both the bearings, earlier calculated in section 3.3, are cross-plotted on the UCS map. The speeds where the coefficient curves corresponding to the support stiffness coincide with the critical-speed curves are estimated to be potential critical speeds of the system.

Based on Figure 90, the first critical speed lies roughly between 2000 rpm and 2750 rpm. The rotor is designed to run at 3600 rpm. Figure 91(a) through Figure 91(c) show the bending modes of the first critical under the effect of varying bearing support stiffness. The locations of the bearings are indicated by the dotted lines. As seen in Figure 91(a), at low bearing stiffness the rotor is stiff and does not have much bending. When the bearing stiffness increases, the locations of the bearings become node points and the rotor bends about these nodes. This is evident in Figure 91(c). American Petroleum Institute (API) specification [26] states that critical speeds up to twice the running speed should be accounted for. Figure 92(a) through Figure 92(b) show the bending modes of the second critical under varying bearing support stiffness. Similar to the first critical bending modes, under low bearing stiffness, the rotor shows rigid body modes. At high bearing stiffness, the stiffness of the rotor becomes the controlling element thereby showing rotor bending modes.

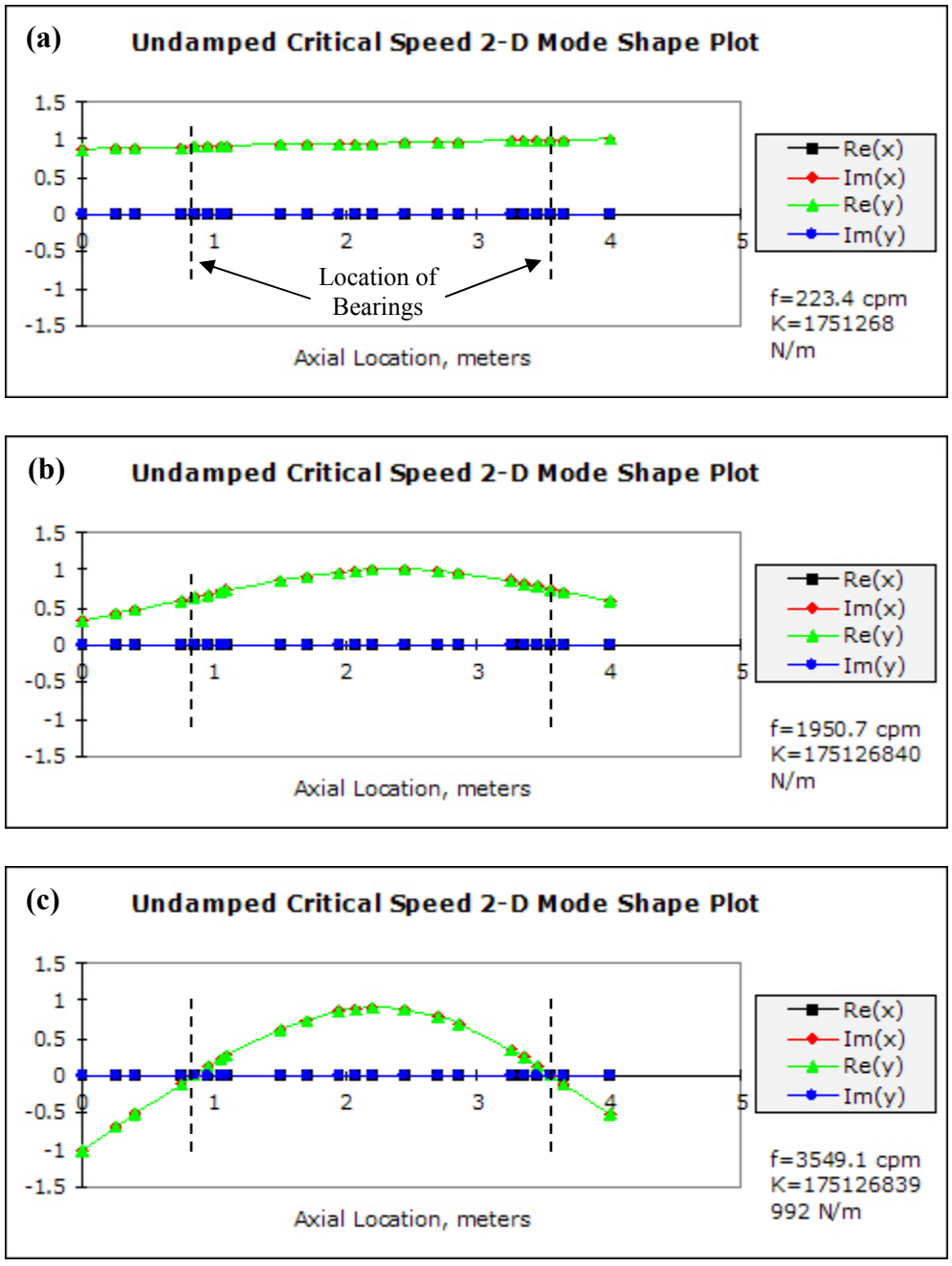

Figure 91 First undamped critical speed mode shape.
(a) at 223.40 rpm (3.72 Hz) with bearing stiffness of $1.751Ex10^{6}$ N/m
(b) at 1950.70 rpm (32.51 Hz) with bearing stiffness of $1.751x10^{7}$ N/m
(c) at 3549.10 rpm (59.15 Hz) with bearing stiffness of $1.751x10^{11}$ N/m

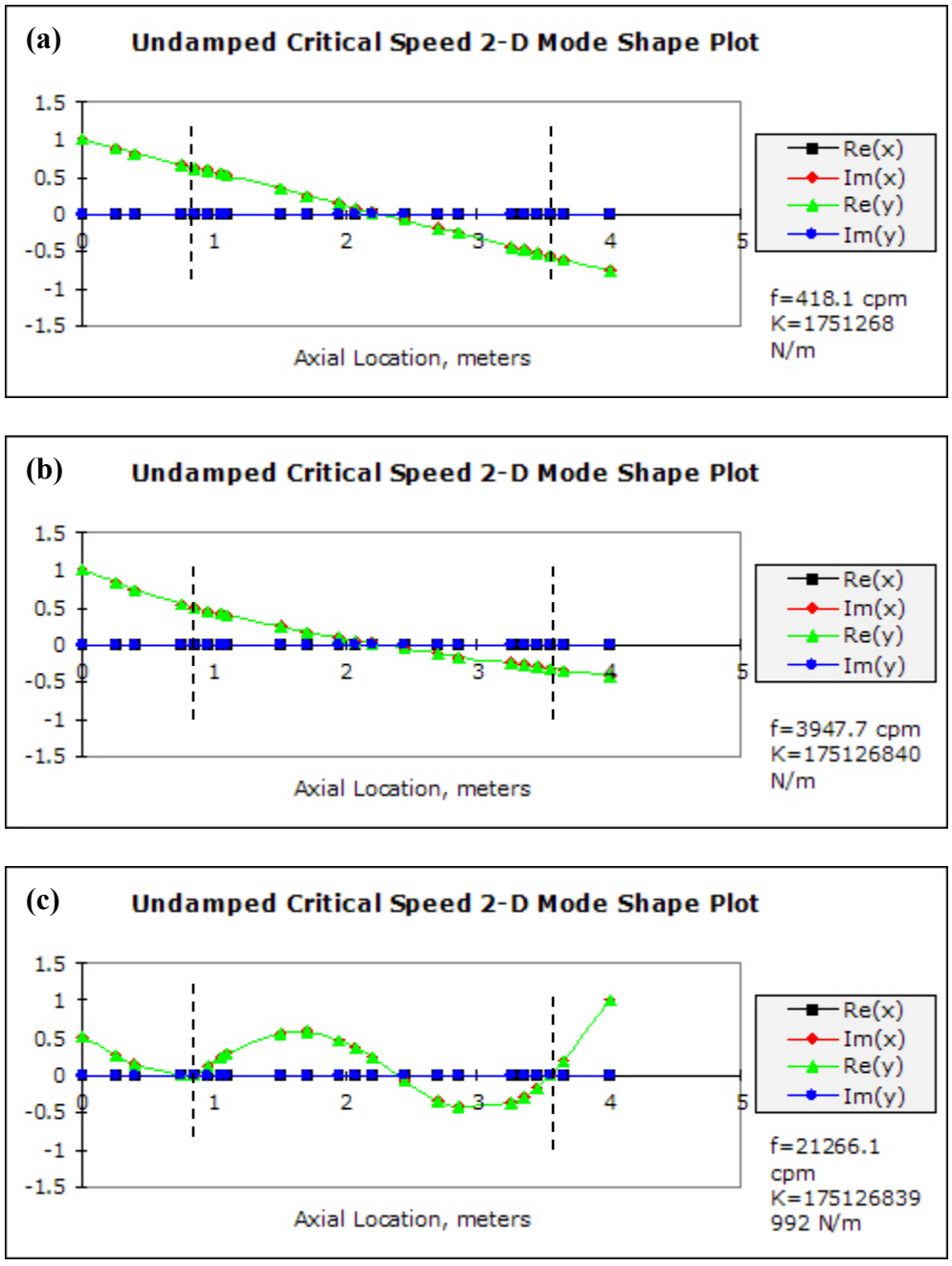

Figure 92 Second undamped critical speed mode shape.
(a) at 418.10 rpm (6.96 Hz) with bearing stiffness of 1.751×10^{6} N/m
(b) at 3947.70 rpm (65.79 Hz) with bearing stiffness of 1.751×10^{7} N/m
(c) at 21266.10 rpm (354.44 Hz) with bearing stiffness of 1.751×10^{11} N/m

4.1.2 Rotor-Only Damped Critical Speed Map

The damped critical speed analysis measures the stability index of the rotor. A damped eigenvalue is a complex number expressed in the form $s = p \pm i\omega_d$, where p is called damping exponent and is the measure of the stability of the system. A system is stable when p is negative and unstable when p is positive. As a measure of system stability, API specification [27] uses a derived quantity called log decrement given by $\delta = -2\pi p \div |\omega_d|$. A system is stable when δ is positive and unstable when it is negative.

The damped natural frequencies are calculated for the rotor model without and with the addition of the interstage seal (at station 12 in the rotor model). Figure 93 shows the natural frequency map for the rotor model without the effect of the seal. The synchronous excitation intersects the first and fourth modes. The addition of the seal at station 12 influences the rotordynamic system by slightly improving the stability, as will be seen in the next section. Figure 94 shows the natural frequency map for the rotor model with the addition of the seal. The synchronous excitation line moves slightly away from the first critical speed and tends to excite the third critical speed.

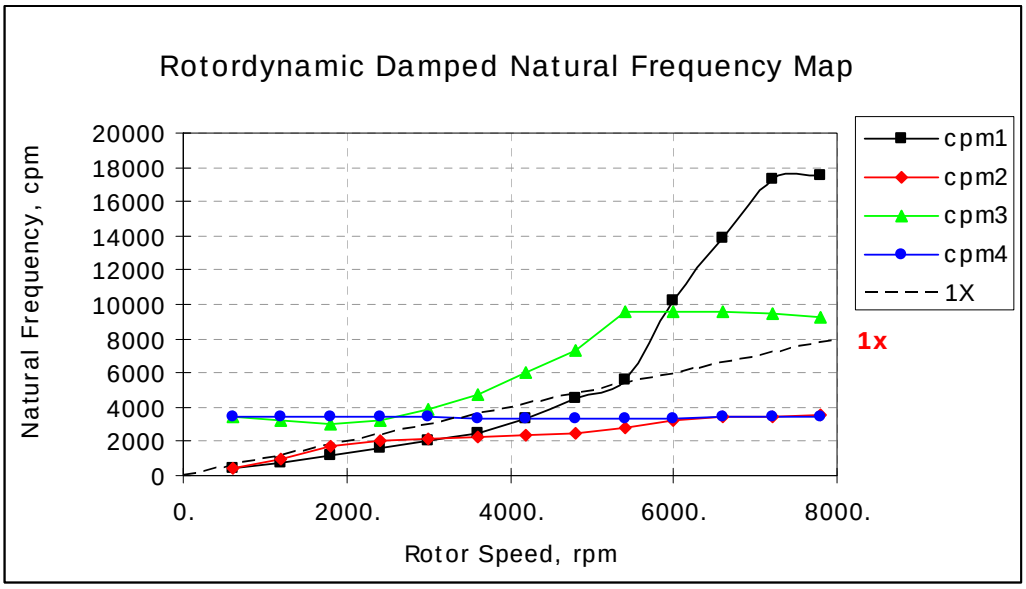

Figure 93 Damped natural frequency map without the effect of the seal

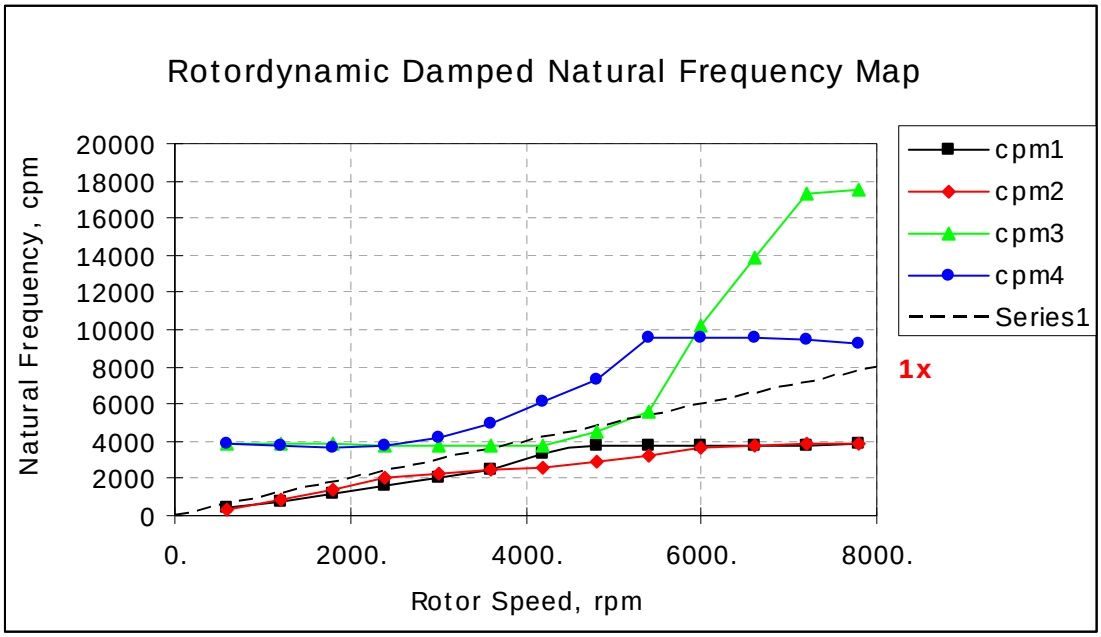

Figure 94 Damped natural frequency map with the addition of the seal

4.1.3 Rotor Damped Modes

The first four rotor damped mode shapes of the rotor, with and without the addition of the seal, are described in this section. Gyroscopic effects are included to obtain the modes and their corresponding mode shapes.

Table 8 shows a listing of log decrement and respective frequencies of the first four damped modes at various running speeds of the rotor without the addition of the seal. The modes are in forward whirl.

Table 8 First four damped modes without the effect of the seal

Speed	logd1	cpm1	logd2	cpm2	logd3	cpm3	logd4	cpm4
600	8.4	430.4	8.7	402.8	0.1	3488.7	1.3	3412.3
1200	5.9	952.9	7.1	782.3	0.3	3466.6	2.2	3244.8
1800	3.4	1680.3	6.0	1180.9	0.4	3438.8	3.7	2988.3
2400	1.7	2029.1	5.1	1586.8	0.5	3412.3	5.0	3275.3
3000	0.9	2152.4	4.2	2015.6	0.5	3387.6	4.7	3922.2
3600	0.3	2243.8	3.3	2519.1	0.6	3364.0	3.9	4708.2
4200	-0.2	2349.2	2.2	3301.8	0.6	3345.4	2.7	6029.6
4800	-0.8	2506.6	0.2	4510.1	0.6	3340.1	0.6	7319.9
5400	-1.3	2795.2	-2.2	5628.0	0.5	3350.6	0.4	9560.0
6000	-1.1	3242.9	-1.0	10228.4	0.5	3370.0	0.3	9539.1
6600	-0.7	3429.0	0.0	13817.6	0.4	3389.7	0.2	9520.2
7200	-0.4	3483.5	-0.1	17298.3	0.3	3405.1	0.1	9423.1
7800	-0.3	3507.5	0.0	17543.2	0.3	3414.1	0.0	9259.2

For the operational speed of 3600 rpm, Figure 95 (a) shows the first mode shape at 2243.8 rpm. This mode is in forward whirl with large deflection at the center of the rotor. The second mode at 2519.1 rpm is also in forward whirl, as seen in Figure 95 (b). A node is observed at the center of the rotor where the deflection produced is the least.

Figure 95 (c) shows the third mode shape at 3364.0 rpm. This mode shows pronounced elliptical orbits with large deflection at the center of the rotor. The fourth mode at 4708.2 rpm, as seen in Figure 95 (d), is above the running speed of the rotor and shows maximum deflection at the rotor ends.

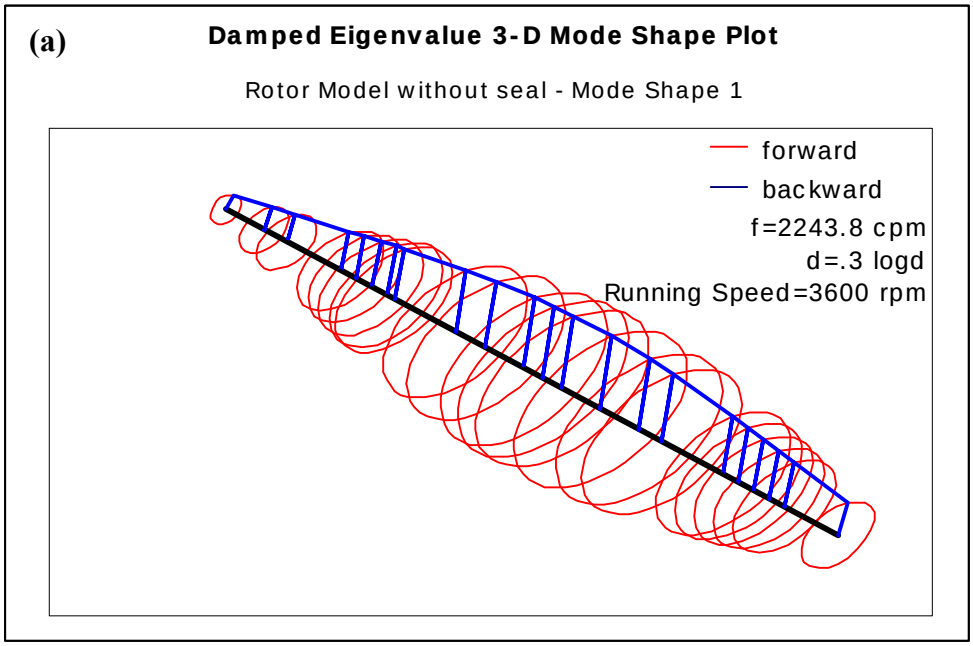

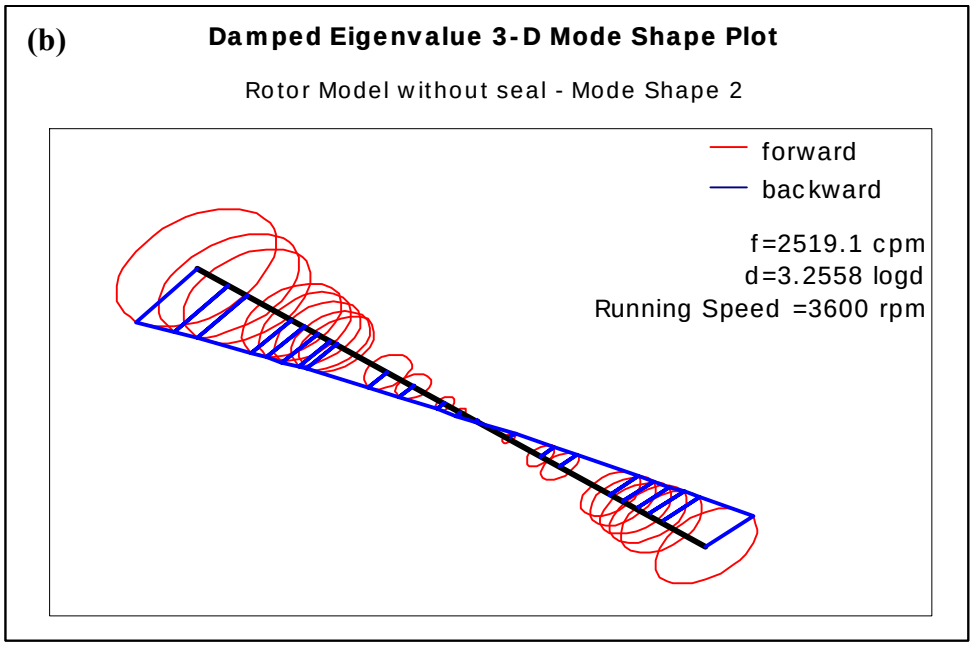

Figure 95 Damped mode shape for rotor model without seal.
(a) First mode at frequency of 2243.8 rpm
(b) Second mode at frequency of 2519.1 rpm

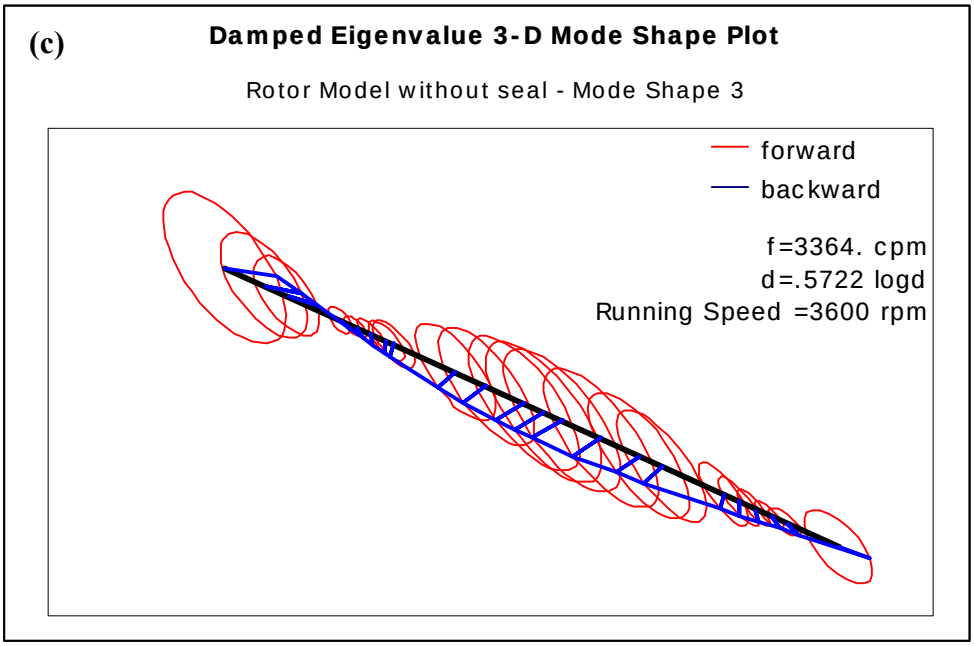

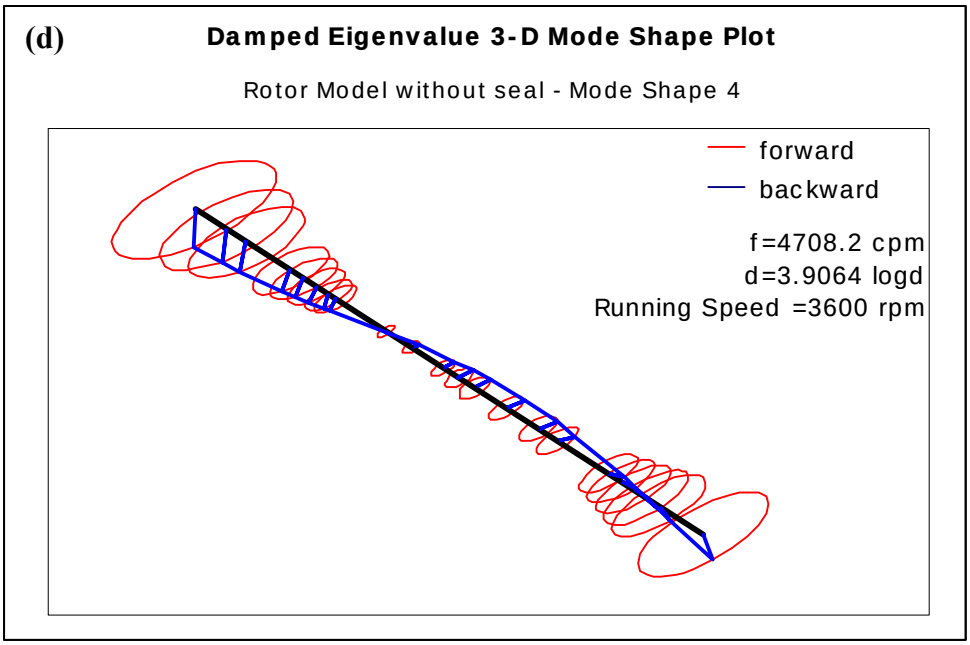

Figure 95 Continued
(c) Third mode at frequency of 3364.0 rpm
(d) Fourth mode at frequency of 4708.2 rpm

Table 9 shows a listing of the log decrements and frequencies of the first four damped modes at various running speeds of the rotor with the seal added to the model. Comparing the log decs of the rotor model without and with the seal indicate that at the rotor running speed there is improvement in stability once the seal is added, due to the increase in log dec.

Table 9 First four damped modes with the addition of the seal

Speed	logd1	cpm1	logd2	cpm2	logd3	cpm3	logd4	cpm4
600	12.2	362.4	8.8	402.7	0.9	3860.1	1.8	3868.0
1200	8.5	812.5	7.1	782.1	1.0	3850.2	2.4	3805.3
1800	5.9	1406.2	6.0	1177.1	1.1	3833.6	3.2	3704.1
2400	3.7	1989.9	5.1	1577.8	1.2	3815.1	4.1	3756.9
3000	2.5	2267.4	4.2	2005.0	1.3	3795.3	4.2	4224.1
3600	1.6	2430.5	3.3	2508.3	1.3	3774.1	3.7	4908.7
4200	1.0	2608.5	2.2	3288.5	1.3	3756.6	2.7	6129.5
4800	0.3	2865.4	1.3	3751.9	0.3	4498.0	0.7	7349.1
5400	-0.1	3277.2	1.3	3762.9	-2.2	5623.6	0.4	9561.8
6000	0.1	3663.3	1.2	3781.5	-1.0	10225.9	0.3	9537.2
6600	0.4	3786.3	1.2	3799.4	0.1	13841.4	0.2	9517.7
7200	0.5	3826.4	1.1	3813.3	0.1	17317.5	0.1	9421.7
7800	0.7	3843.0	1.0	3823.4	0.1	17560.9	0.0	9259.0

For the operational speed of 3600 rpm, Figure 96(a) shows the first mode shape at 2430.5 rpm. This mode is in forward whirl and produces large deflection at the center of the rotor, as seen in the case of the rotor without the seal. The second mode at 2508.3 rpm, seen in Figure 96 (b), is also in forward whirl. A node is observed at the center of the rotor where the deflection produced is the least.

Figure 96 (c) shows the third mode shape at 3774.1 rpm. This mode is in forward whirl. This mode has a pronounced elliptical orbit with large deflection at the center of the rotor. The fourth mode at 4908.7 rpm, as seen in Figure 96 (d), is above the running speed of the rotor and shows maximum deflection at the rotor ends.

Overall, the damped mode analysis of the rotor shows a change in critical speed with the addition of the seal. The critical speeds of the first, third and fourth modes show an increase while the second mode has a small decrease in the critical speed. Note that the mode shapes illustrated in this section pertain to the rotor and do not consider the

effect of the casing. These mode shapes will be compared later on with the coupled rotor-casing model.

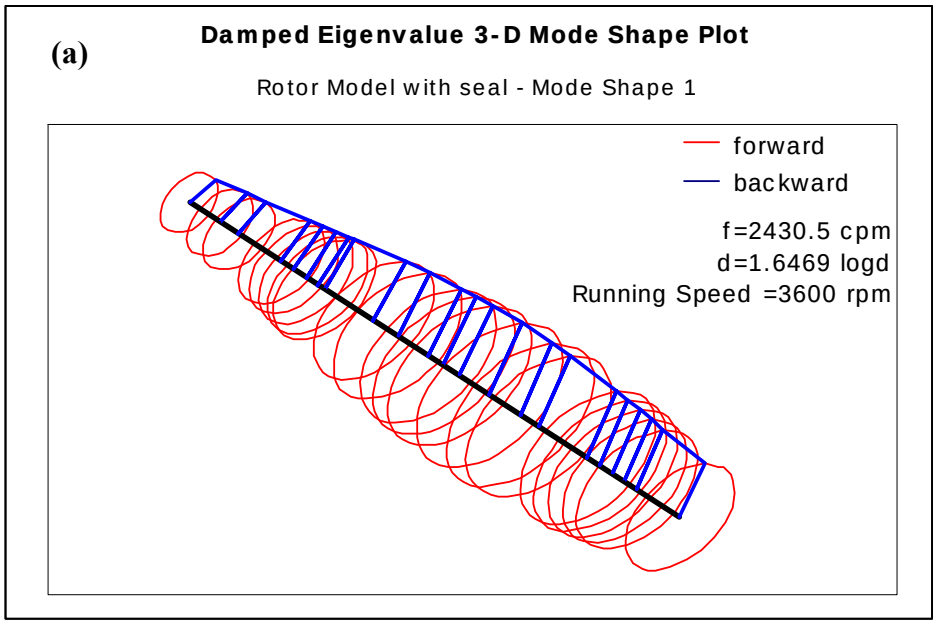

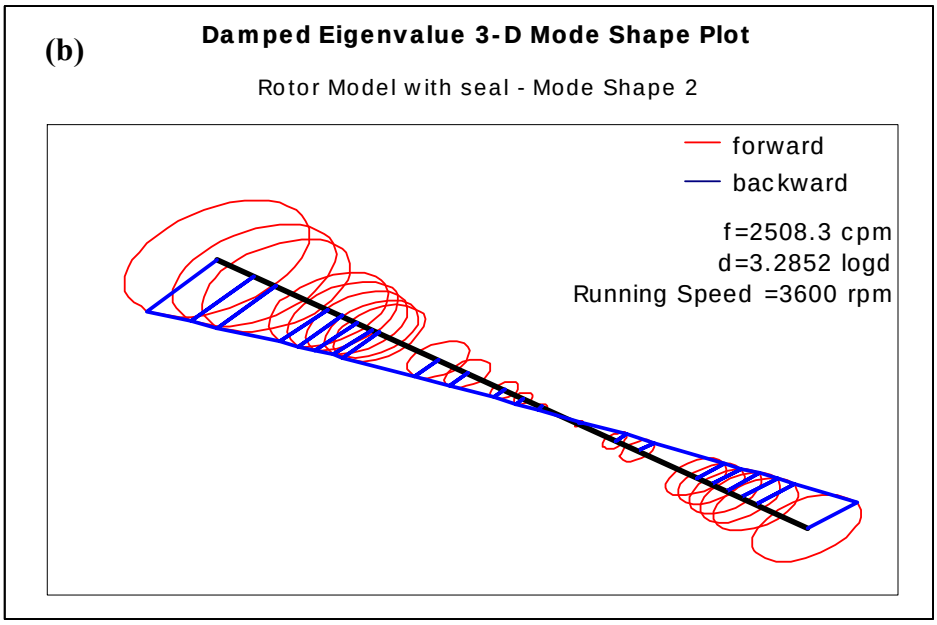

Figure 96 Damped mode shape for rotor model with seal.
(a) First mode at frequency of 2430.5 rpm
(b) Second mode at frequency of 2508.3 rpm

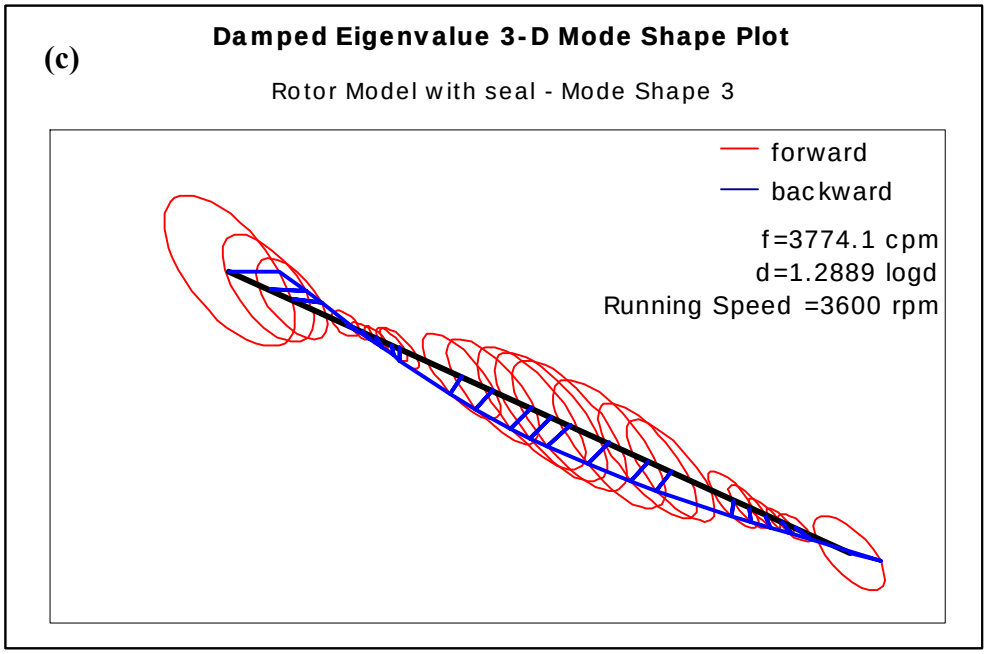

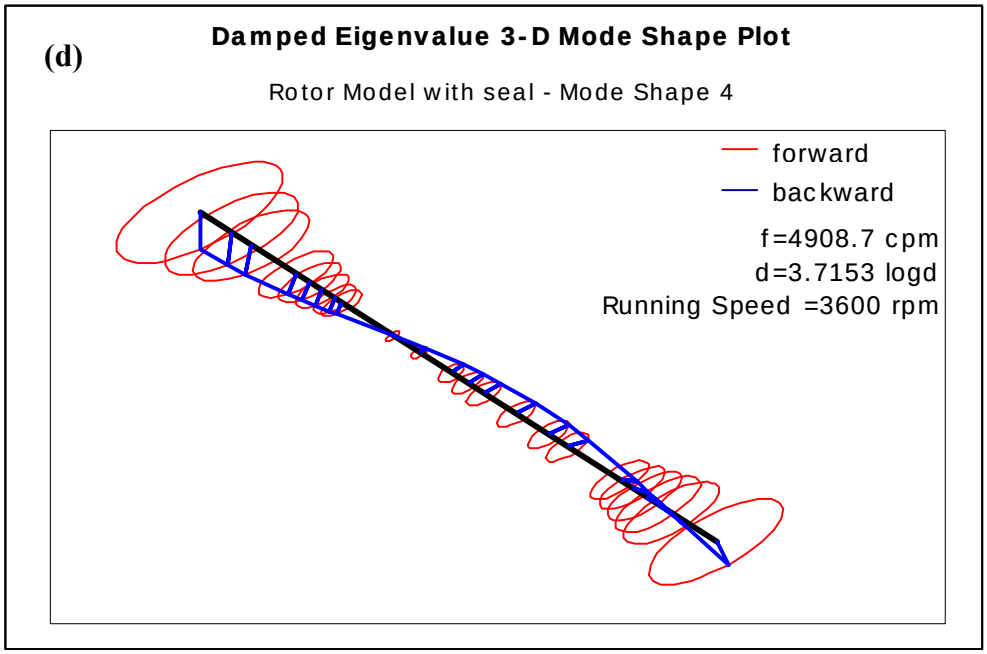

Figure 96 Continued
(c) Third mode at frequency of 3774.1 rpm
(d) Fourth mode at frequency of 4908.7 rpm

4.1.4 Rotor Unbalance Response

This section shows the unbalance response of the XLTRC^2 rotor-only model. These results will later be compared with the coupled rotor-casing models in section 4.2.3. The unbalance amount is calculated from the API unbalance equation shown in section 2.9.

$$\begin{aligned} W &= 6370.05 \text{ kg} \\ N &= 1800 \text{ rpm} \\ U &= 6350 \times \frac{W}{N} \quad [\text{SI Units}] \\ &= 22472.12 \text{ g-mm} \end{aligned} \tag{79}$$

A multiplier is sometimes used with the calculated unbalance magnitude and this serves as a factor of safety. A multiplier of approximately 3.75x is used here. The resulting total unbalance magnitude is rounded to 85,000 g-mm. The rotor model is a between-bearings design. An unbalance applied to the rotor mid-span typically tends to excite the first bending mode. When proportional unbalance amounts are applied close to the shaft end locations they are likely to excite the second bending mode, as seen earlier in Figure 54. Based on this, two cases of unbalance responses are performed.

The first unbalance response case uses an unbalance of 85,000 g-mm at the rotor mid span node. This corresponds to station 12 on the rotor. The unbalance response is obtained for a speed range of 600 rpm to 7800 rpm, with the maximum speed being little more than twice the design running speed. The analysis with the mid span unbalance amount is done for the cases without and with the addition of the interstage seal. Gyroscopic effects are included in the analysis. Figure 97(a), Figure 97 (b), and Figure 97 (c) show the unbalance response obtained at bearing 1, mid span and bearing 2 probe locations, respectively. The influence of the damping provided by the seal is evident in the smaller unbalance responses amplitudes. The second case of unbalance response analysis applies a distributed unbalance of 40,000 g-mm and 45,000 g-mm to rotor end locations at stations 8 and 17, respectively. Figure 98(a), Figure 98 (b), and Figure 98 (c) show the unbalance response obtained at the three probe locations, respectively. The effect of damping, by the seal, is also evident in this unbalance configuration.

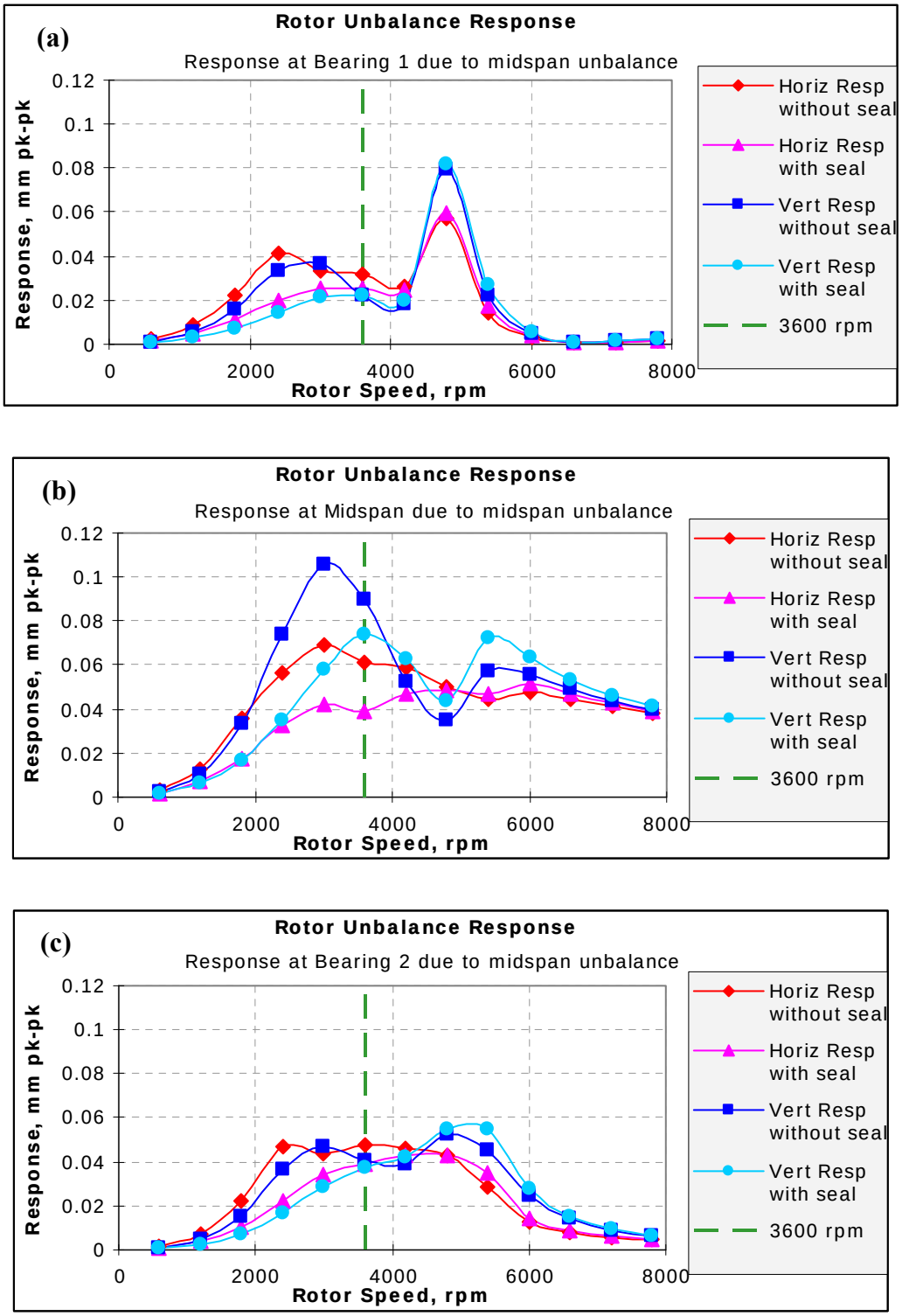

Figure 97 Unbalance response for mid span unbalance.
(a) at bearing 1 location, (b) at rotor mid span location, (c) at bearing 2 location

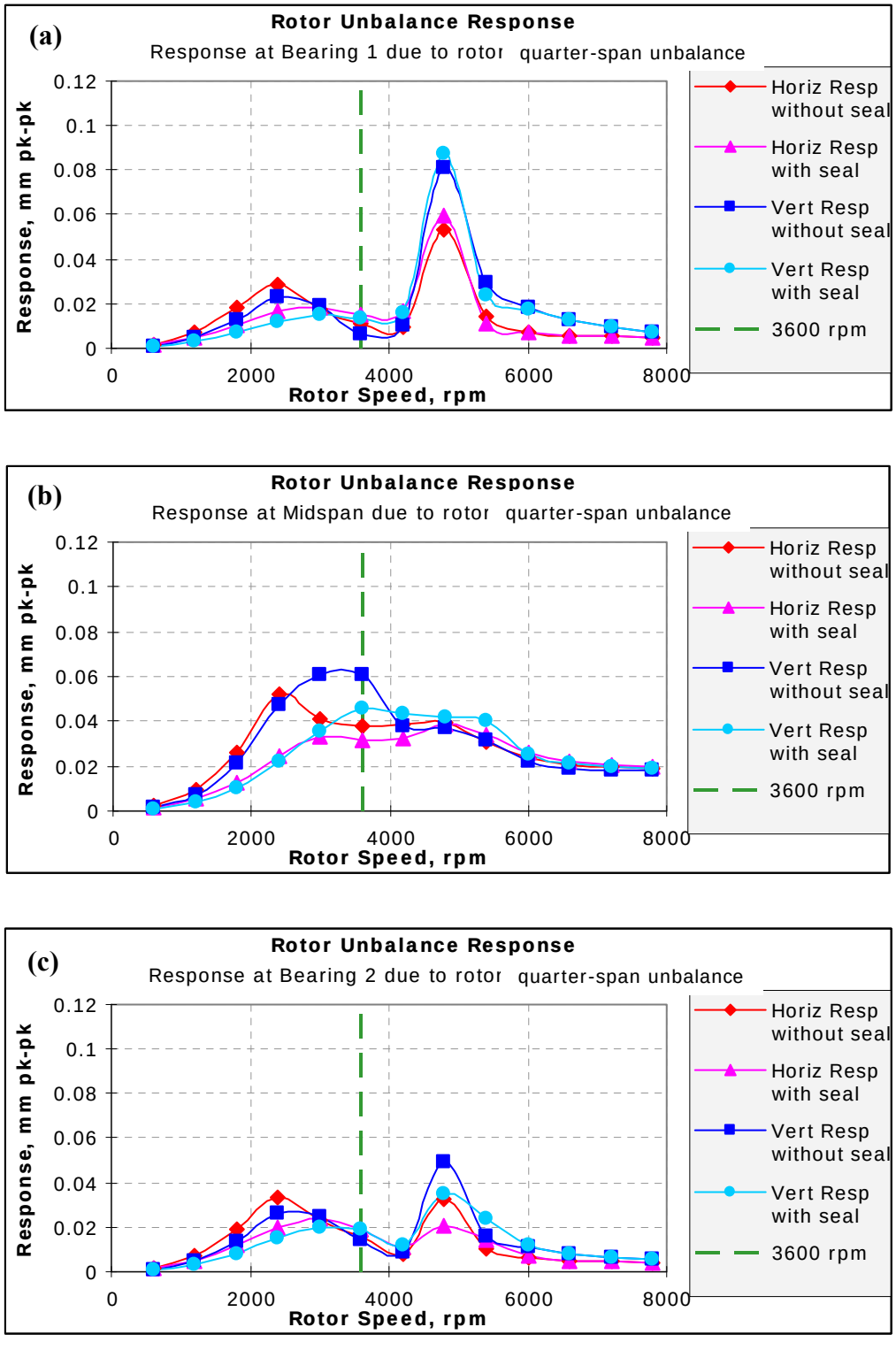

Figure 98 Unbalance response for rotor quarter-span unbalance. (a) at bearing 1 location, (b) at rotor mid span location, (c) at bearing 2 location

4.1.5 Rotor Unbalance Response Validation with ANSYS Data

In this section, an ANSYS generated rotor-only model is compared with an XLTRC^2 rotor-only model. This ensures the validity of the ANSYS data. Since this is only for validation, the unbalance response is compared only at bearing 1 and bearing 2 locations for the configuration with seals and the case where unbalance is applied to rotor quarter-span locations. Figure 99(a) and Figure 99 (b) show excellent agreement between XLTRC^2 rotor-only model results and those obtained with the ANSYS rotor-only model. The XLTRC^2 and ANSYS results in each direction overlap each other. Note that similar to the XLTRC^2 model, the ANSYS model also includes gyroscopic effects.

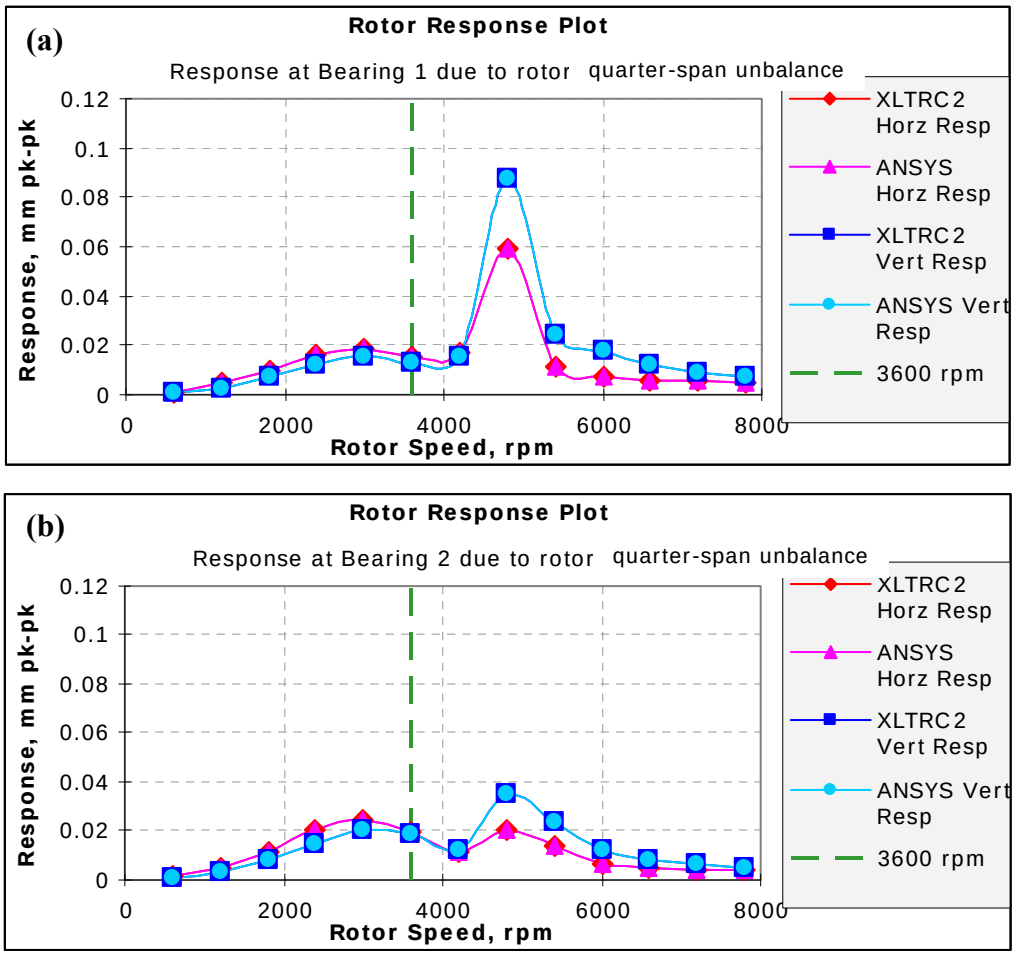

Figure 99 Comparison of XLTRC^2 and ANSYS unbalance responses. (a) at bearing 1 and (b) at bearing 2

4.2 Coupled Rotor–Casing Model

This section describes results of the analyses done on the coupled rotor-casing model, for axisymmetric and non-axisymmetric cases. The casing is connected to ground using foundation supports. These supports are modeled as isotropic supports with no damping and direct stiffness of $5x10^8$ N/m ($2.86x10^6$ lb/in).

4.2.1 Coupled Rotor–Axisymmetric Casing Models Damped Modes

The damped critical speed analysis is performed on the coupled rotor–axisymmetric casing model. Two sets of models are used. The first set has a XLTRC^2 rotor coupled with a XLTRC^2 axisymmetric casing, as shown in Figure 100. The second set has a XLTRC^2 rotor coupled with an ANSYS axisymmetric casing, seen in Figure 101. For the second set, the casing data from ANSYS is incorporated with the XLTRC^2 rotor model. This section only describes the configuration with the seal as similar results are obtained for the coupled model that does not include the seal.

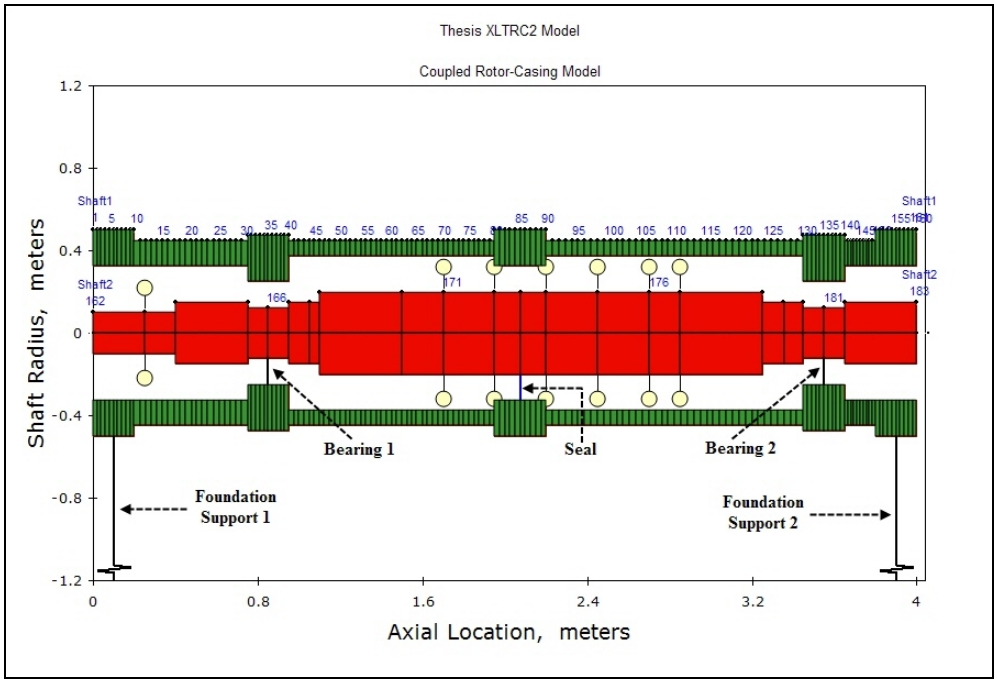

Figure 100 Coupled XLTRC^2 rotor- XLTRC^2 axisymmetric casing model

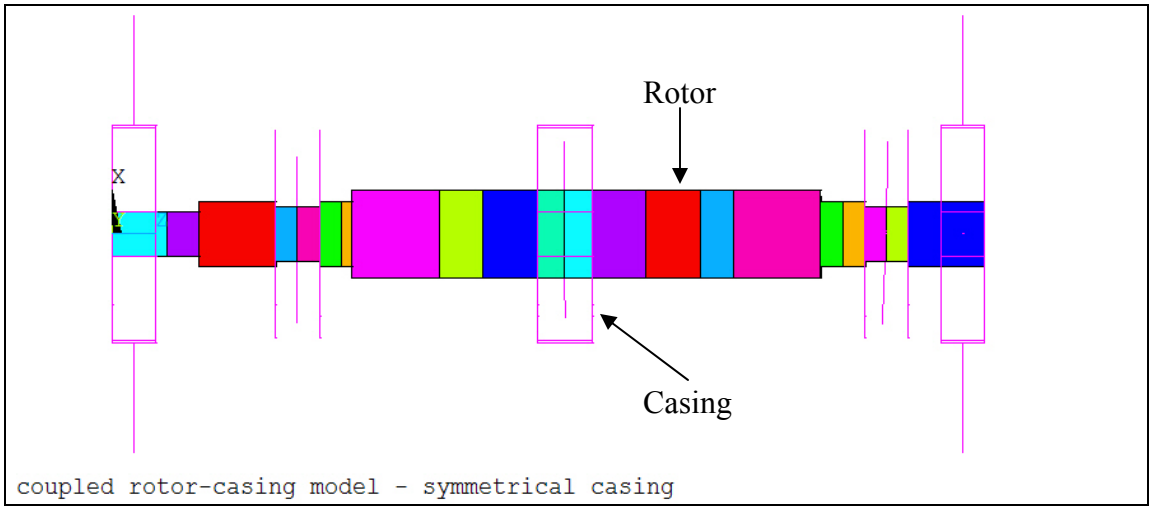

Figure 101 Coupled XLTRC^2 rotor- ANSYS axisymmetric casing model

Table 10 shows the natural frequencies of the first three modes in the coupled rotor–axisymmetric casing models compared with XLTRC^2 rotor-only model, seen in Table 9. XLTRC^2 can currently model axisymmetric casings. For reference, the first four natural frequencies of the casing-only model are shown in APPENDIX B. The comparison between the model that uses the XLTRC^2 axisymmetric casing and the one that uses the ANSYS axisymmetric casing is to ensure the validity of the existing modeling method in XLTRC^2. The eigenvalues observed in the both the symmetrical coupled models are the same in the $X-Z$ plane and $Y-Z$ plane. The modes calculated are at a rotor running speed of 3600 rpm.

Table 10 Natural frequency of first three modes in coupled rotor–axisymmetric casing model compared with XLTRC^2 rotor-only model

Mode	Coupled XLTRC^2 rotor–XLTRC^2 axisymmetric casing model		Coupled XLTRC^2 rotor–ANSYS axisymmetric casing model		XLTRC^2 rotor-only model	
	Log Dec	Frequency (rpm)	Log Dec	Frequency (rpm)	Log Dec	Frequency (rpm)
1	0.95	1811.3	0.98	1804.3	1.65	2430.5
2	2.20	2167.9	2.21	2139.1	3.29	2508.3
3	3.50	3435.2	3.57	3429.7	1.29	3774.1

The results of the coupled XLTRC^2 rotor-XLTRC^2 axisymmetric casing model and the XLTRC^2 rotor-ANSYS axisymmetric casing show that they are very close to each other. Both these models use the same rotor and the casings are built with the same dimensions. Hence it is expected that the results be similar. This establishes that the use of the ANSYS data with the XLTRC^2 model is valid and correct. For the remainder of this thesis the XLTRC^2 rotor-ANSYS axisymmetric casing model will be referenced and mentioned as *coupled rotor-axisymmetric casing model*.

Now on comparing the coupled rotor-axisymmetric casing models with the rotor-only model, it can be seen that the first three modes show a decrease in critical speeds which can be attributed to the following. The stiffness of the bearings connecting the rotor to the casing and the stiffness of the foundation supports are similar to each other in the order of 10^8 N/m. The two stiffness models act as springs in series which results in lower combined stiffness. This causes the critical frequency of the rotor in the coupled model to drop. The change in critical speeds is an indication that the casing influences the rotordynamic performance of the rotor. Log decs associated with the first two critical speeds of the coupled model show a decrease when compared with the XLTRC^2 rotor-only model and this indicates that the effective damping is less. However for the third critical speed, the log dec is observed to the higher for the coupled model. As seen in Figure 96(c), the rotor shows high deflection near the seals at the third critical speed. Figure 102(c) shows the same characteristic with the casing included. There is a higher relative motion between the rotor and the casing and the effective damping that is present in the model increases when the relative motion increases. This is the reason for the higher log dec observed.

Figure 102 (a) through Figure 102 (c) show the rotor mode shapes for the first three modes. The casing structure can also be seen in these figures. Comparing these to the mode shapes observed in the rotor-only model, seen in Figure 96 (a) through Figure 96 (c), indicates that they are similar. While the overall stiffness supporting the rotor has reduced, the deflected shape of the rotor for a particular mode does not differ by a large extent due to the symmetry of the casing.

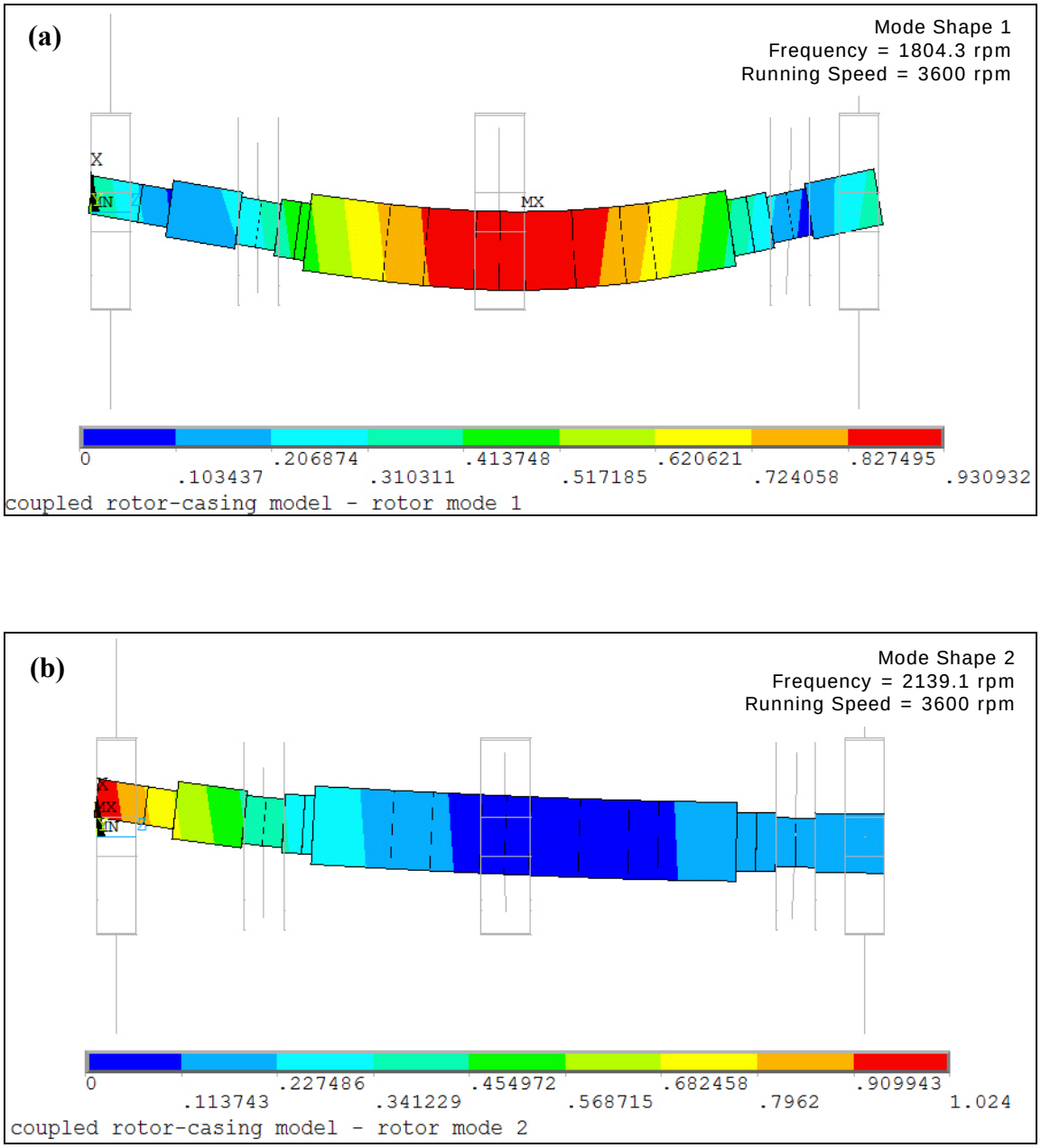

Figure 102 Damped critical speed mode shape.
(a) First mode at 1804.3 rpm (30.07 Hz)
(b) Second mode at 2139.1 rpm (35.65 Hz)

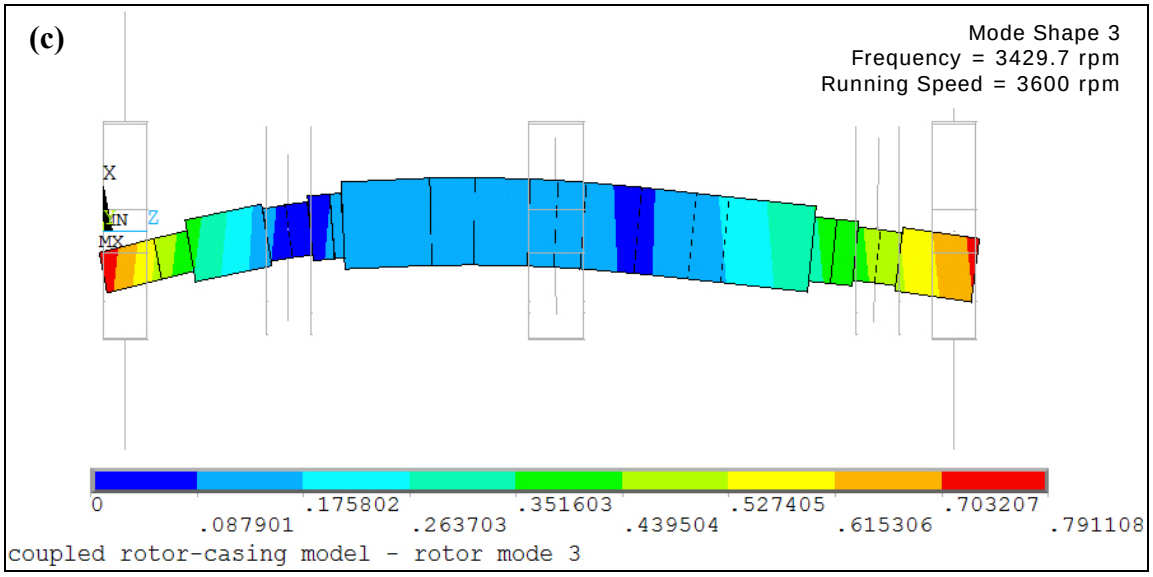

Figure 102 Continued
(c) Third mode at 3429.7 rpm (57.16 Hz)

4.2.2 Coupled Rotor–Non-Axisymmetric Casing Model Damped Modes

The casing data of the ANSYS non-axisymmetric casing is incorporated with the XLTRC^2 rotor model and a damped critical speed analysis is performed. This section describes the configuration with the seal. Similar results are observed for the coupled rotor-non-axisymmetric casing model configuration that does not include the seal. However these results are not presented in this thesis for brevity. Additionally, the previous section 4.2.1 showed that the coupled XLTRC^2 rotor-XLTRC^2 axisymmetric casing model and the XLTRC^2 rotor-ANSYS axisymmetric casing model have similar results. Therefore only results of the coupled XLTRC^2 rotor-ANSYS axisymmetric casing are used here for comparison.

Natural frequencies of the first three modes are shown in Table 11. In the coupled rotor-non-axisymmetric model, one set of eigenvalues are generated. The modes observed are at the rotor running speed of 3600 rpm. Table 11 also shows the frequencies seen in the coupled rotor-axisymmetric casing model and XLTRC^2 rotor-only model. These values are presented for comparison.

Table 11 Natural frequency data of first three modes in coupled rotor–non-axisymmetric casing model compared with earlier models

Mode	Coupled rotor–non-axisymmetric casing model		Coupled rotor–axisymmetric casing model		XLTRC^2 rotor-only model	
	Log Dec	Frequency (rpm)	Log Dec	Frequency (rpm)	Log Dec	Frequency (rpm)
1	0.87	1785.7	0.98	1804.3	1.65	2430.5
2	2.01	2100.8	2.21	2139.1	3.29	2508.3
3	3.43	3368.1	3.57	3429.7	1.29	3774.1

The rotor mode shapes for the first three modes with a non-axisymmetric casing can be seen in Figure 103 through Figure 105. The casing structure can also be seen in these figures. The eigenvectors shown in these figures have components in the $X-Z$ and $Y-Z$ planes, and the eigenvectors in each of these planes are different. In other words, the rotor has a slightly different mode shape in each of these planes.

When compared to the XLTRC^2 rotor-only model, the first three modes show a decrease in critical speeds. This is similar to the behavior shown by the coupled rotor-axisymmetric casing model, described in section 4.2.1 The lower combined stiffness. leads to lower critical frequency of the rotor in the coupled model. Log decs associated with the modes also show the same behavior. The first two critical speeds of the coupled model show a decrease in log decs when compared with the XLTRC^2 rotor-only model which indicates lower effective damping. The third critical speed shows a higher log dec when compared with the XLTRC^2 rotor-only model. This is because the higher relative motion between the rotor and the casing, as seen in Figure 105, results in more effective damping. Table 11 also indicates a small change in frequencies of the coupled rotor-non-axisymmetric model when compared to the coupled rotor-axisymmetric model. This shows that using a non-axisymmetric casing model, where necessary, will produce different results.

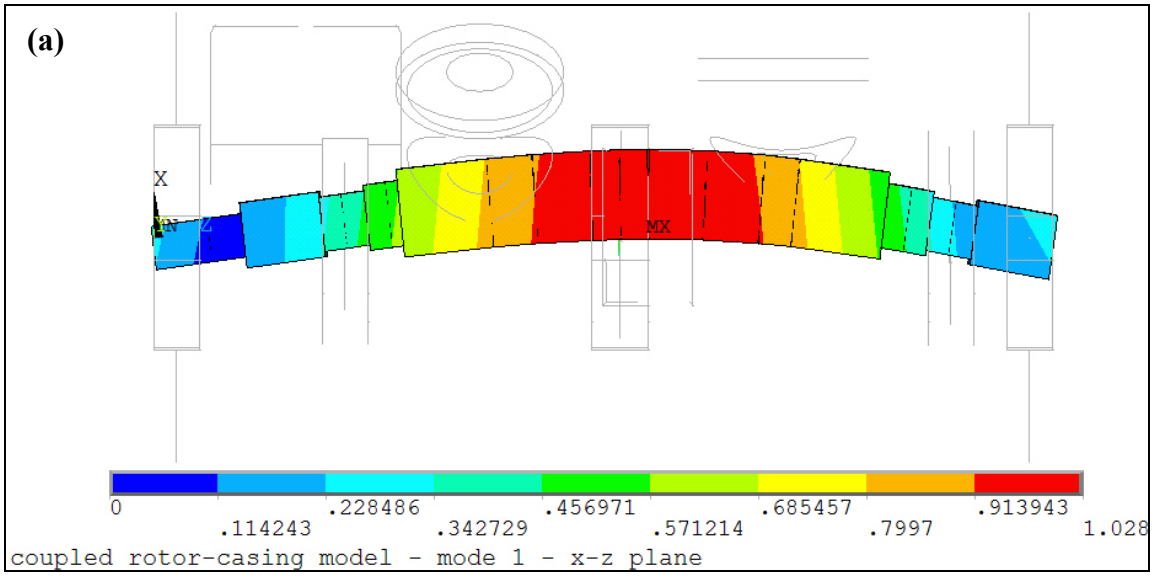

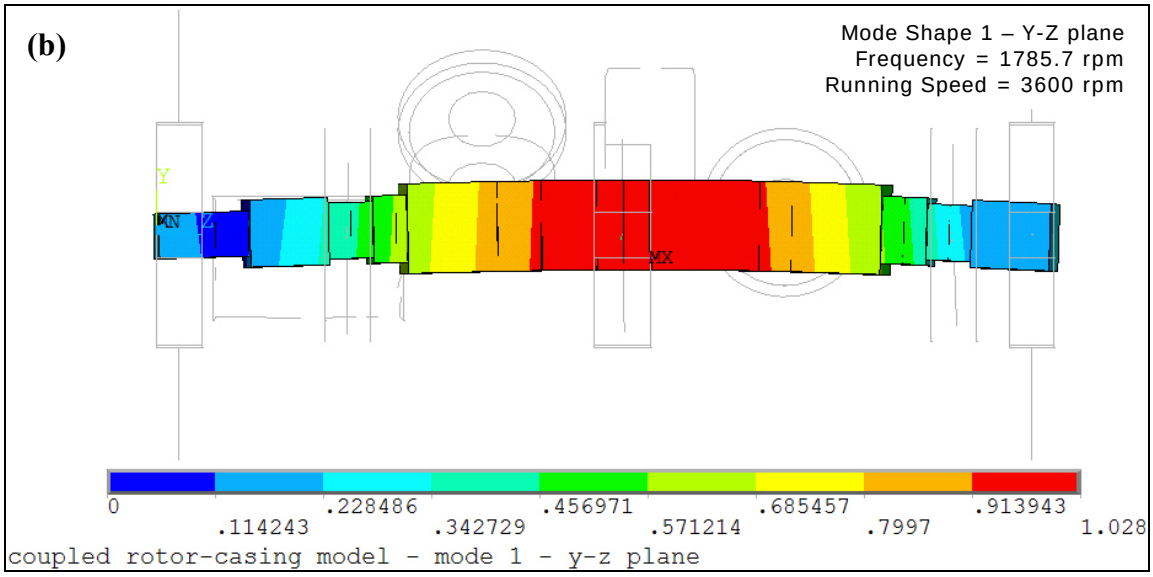

Figure 103 First damped critical speed mode shape for the coupled rotor-non-axisymmetric casing model.
(a) 1785.7 rpm (29.76 Hz) as observed in the X-Z plane
(b) 1785.7 rpm (29.76 Hz) as observed in the Y-Z plane

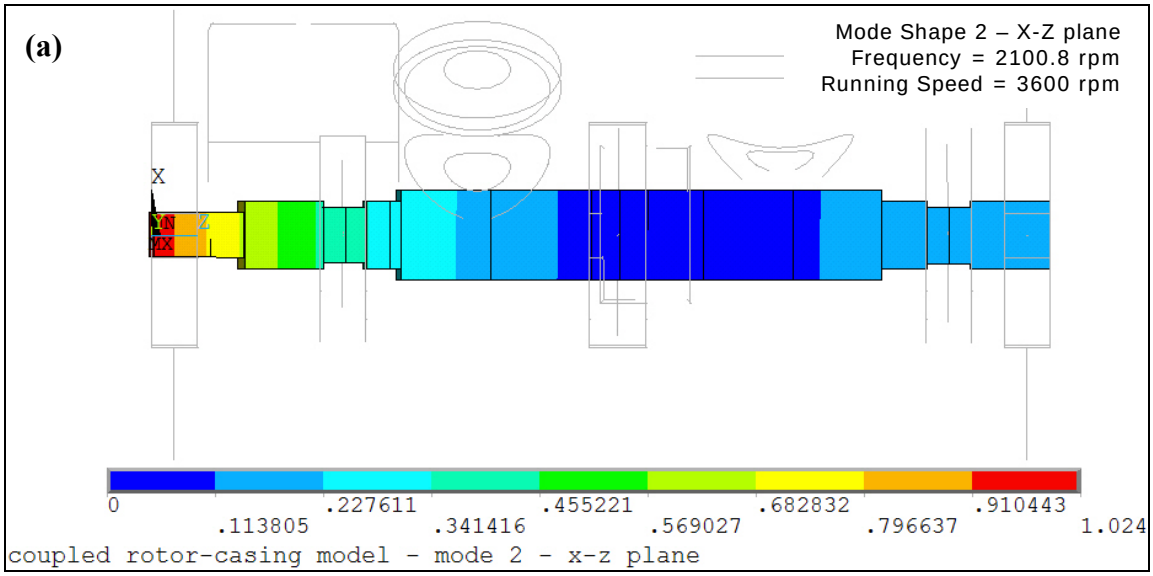

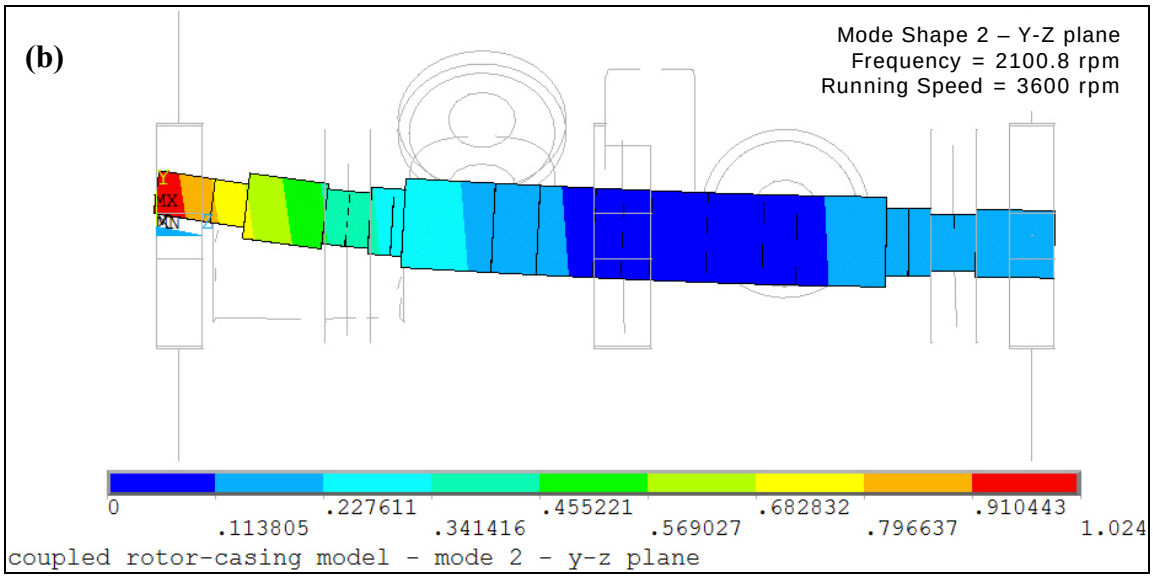

Figure 104 Second damped critical speed mode shape for the coupled rotor-non-axisymmetric casing model.
(a) 2100.8 rpm (35.01Hz) as observed in the X-Z plane
(b) 2100.8 rpm (35.01Hz) as observed in the Y-Z plane

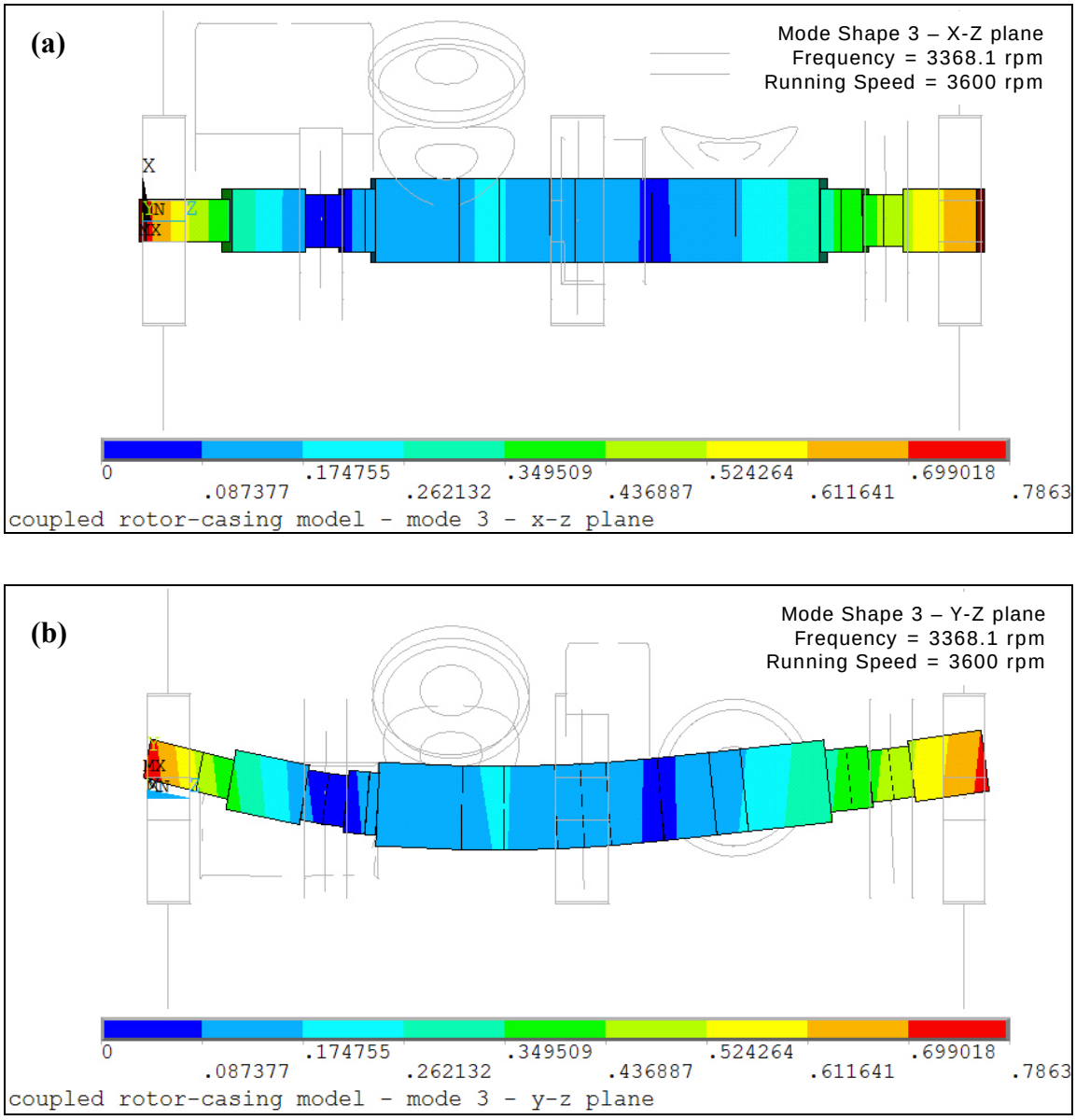

Figure 105 Third damped critical speed mode shape for the coupled rotor-non-axisymmetric casing model.
(a) 3368.1 rpm (56.14 Hz) as observed in the X-Z plane
(b) 3368.1 rpm (56.14 Hz) as observed in the Y-Z plane

4.2.3 Coupled Rotor–Casing Model Unbalance Response

This section describes the unbalance response analysis performed with the coupled XLTRC^2-rotor and ANSYS axisymmetric casing model as well as the coupled XLTRC^2-rotor and ANSYS non-axisymmetric casing model. In order to evaluate any change in unbalance response observed, the results obtained from these two models are compared with the XLTRC^2 rotor-only model which does not include the effect of the casing. Two separate configurations are used. In the first configuration there is no seal connection to the rotor. In other words, the rotor is supported only by the two bearings. In the second configuration, the seal is used. For the XLTRC^2 rotor-only model, the seal connection is to ground whereas in the other two models, the seal connects the rotor to the casing. Note that only one unbalance case is presented here – mid-span unbalance applied to the rotor. The unbalance response measured at the rotor mid-span location is shown for all the three models. The other cases that involved rotor-ends unbalance and response at the bearing 1 and bearing 2 locations are found to be similar in nature and are hence not presented. The unbalance amount and configurations used are the same as described in section 4.1.4.

Figure 106(a) and Figure 106(b) shows the rotor unbalance response at the midspan location along the horizontal and vertical directions, respectively, for the configuration that does not use the seal connection. These responses are in absolute rotor coordinates and not relative to the casing. The XLTRC^2 rotor-only model shows a resonance at about 3000 rpm. The rotor unbalance response in the axisymmetric and non- axisymmetric casing models show a peak at a frequency of 1900 rpm. There is a drop in the resonant frequency and can be attributed to the following. The stiffness of the bearings connecting the rotor to the casing and the stiffness of the foundation supports are similar to each other in the order of 10^8 N/m. The two stiffness models act as springs in series which results in lower combined stiffness. This causes the critical frequency of the rotor to drop. A similar behavior is observed at the second resonance. The XLTRC^2 rotor-only model shows a resonance at about 5100 rpm, whereas the models which have the casing have a lower resonant frequency.

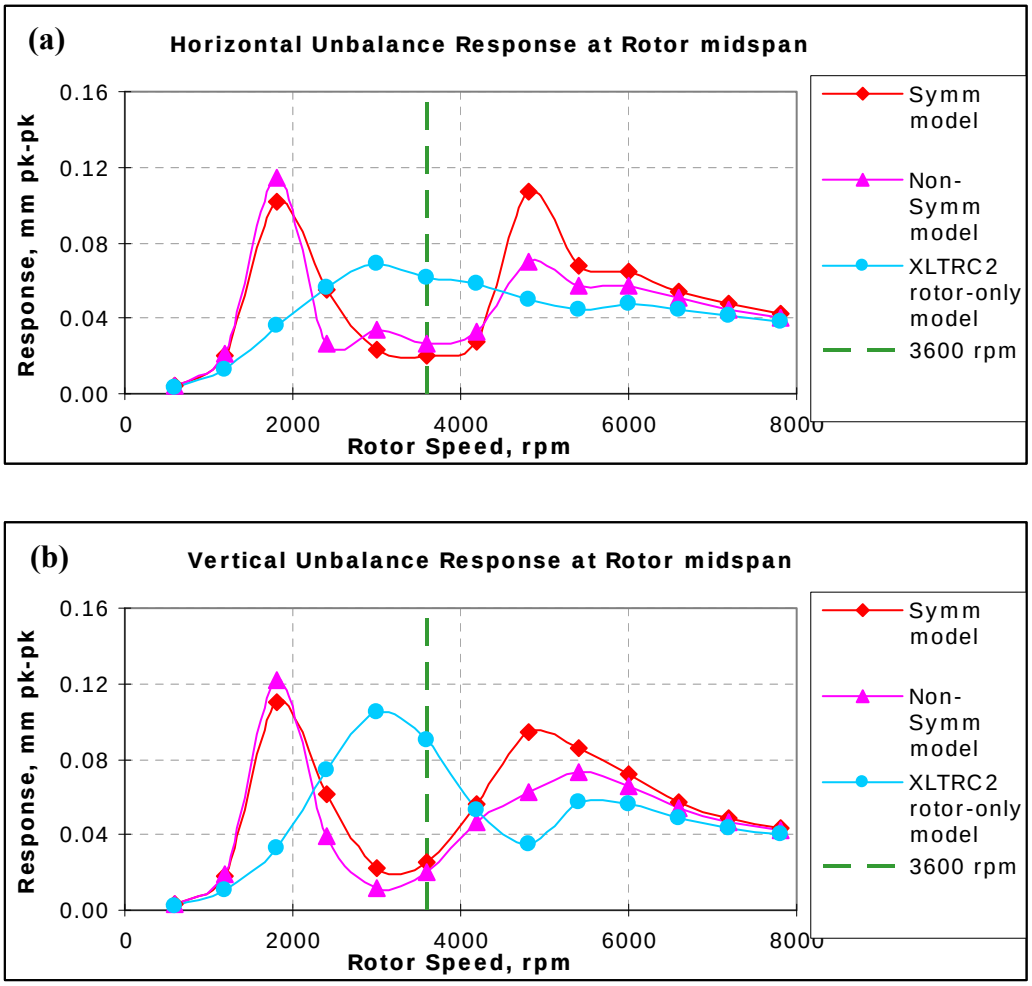

Figure 106 Rotor response at mid span location (without seal configuration) (a) Horizontal response (b) Vertical response

Figure 107(a) and Figure 107(b) shows the rotor unbalance response at the midspan location along the horizontal and vertical directions, respectively, for the configuration that uses the seal connection. These responses are in absolute rotor coordinates and not relative to the casing. The resonances follow the similar trend as those seen in the above case. The frequency is slightly higher than that seen in the case that does not use the seal and the reason is the damping provided by the seal. Also note that while the damping raised the critical frequency, it also brought the resonance of the XLTRC^2 rotor-only model closer to the running speed of 3600 rpm thus reducing the

separation margin. A decrease is seen in the rotor unbalance response amplitude in the axisymmetric and non- axisymmetric casing models, when compared to the configuration that does not use the seal. For both the horizontal and vertical responses, the resonant frequency of the coupled model is less than that seen in the XLTRC^2 rotor-only model.

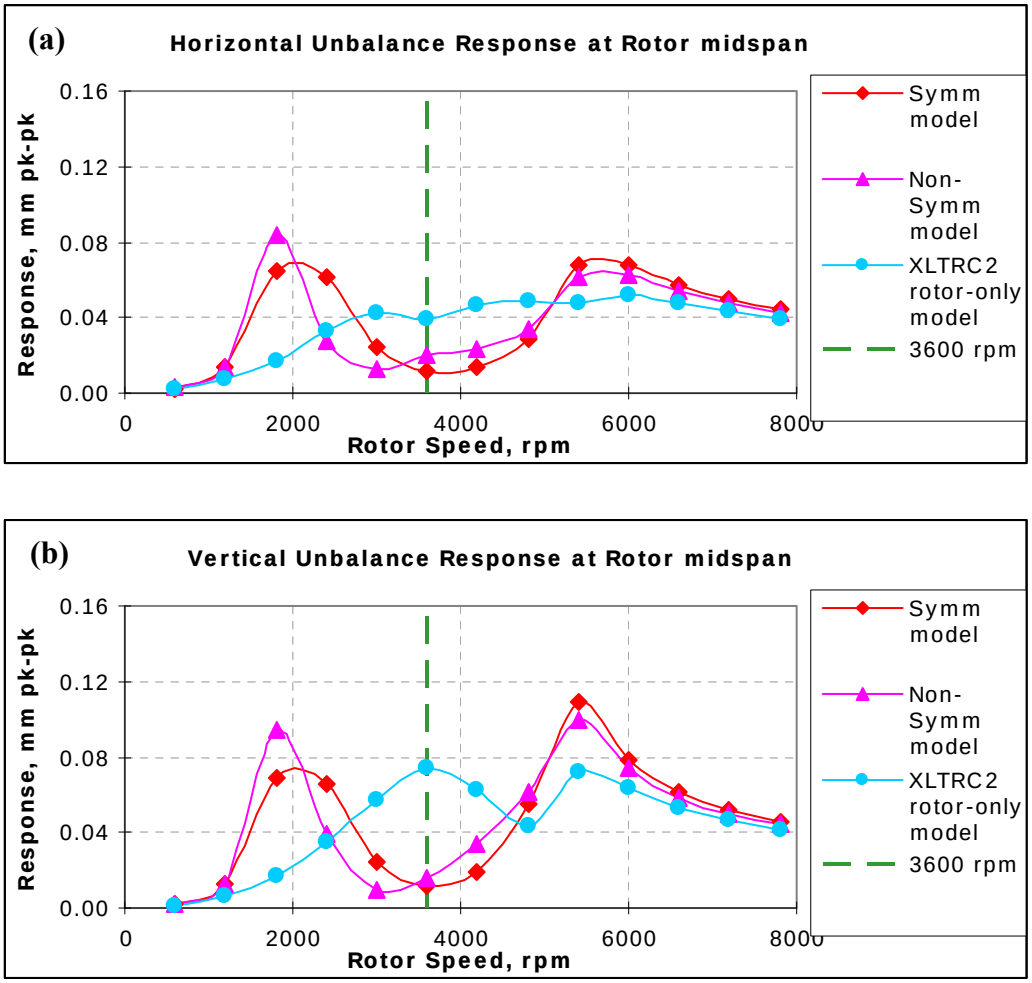

Figure 107 Rotor response at mid span location (without seal configuration) (a) Horizontal response (b) Vertical response

A comparison is also made for the rotor relative to casing amplitudes. This comparison is important because high relative amplitude could indicate that the rotor and casing are moving in opposing directions. Such a condition can lead to rubs. Small relative response amplitude can mean that the rotor and casing are moving in phase with each other. The relative response in horizontal and vertical directions for the configuration without the seal is shown in Figure 108(a) and Figure 108 (b), respectively. Likewise, responses for the configuration with the seal are shown in Figure 109(a) and Figure 109(b). These figures show that in both the axisymmetric and non-axisymmetric models, there is a higher relative response at the resonant frequencies. As the running speed increases, the relative response is higher.

The impact of using a coupled rotor-casing model, in particular the non-axisymmetric casing model, is evident in the results presented in this section. This shows that including a full-scale non-axisymmetric model can produce significantly different predictions than an approximated symmetric model.

The results obtained in XLTRC^2 by incorporating the reduced non-axisymmetric casing structure are verified in ANSYS. The ANSYS source code used for verification is included in APPENDIX E.

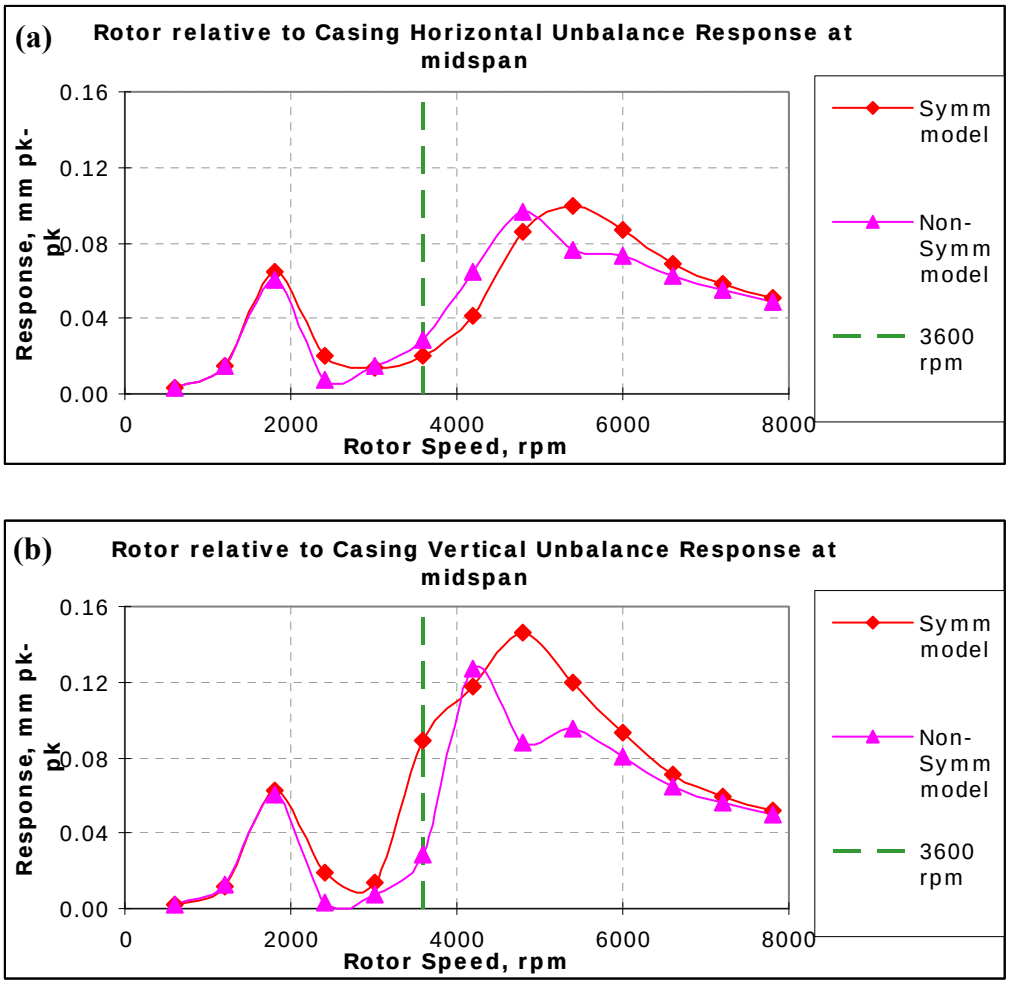

Figure 108 Rotor relative to casing response (without seal)
(a) Horizontal response (b) Vertical response

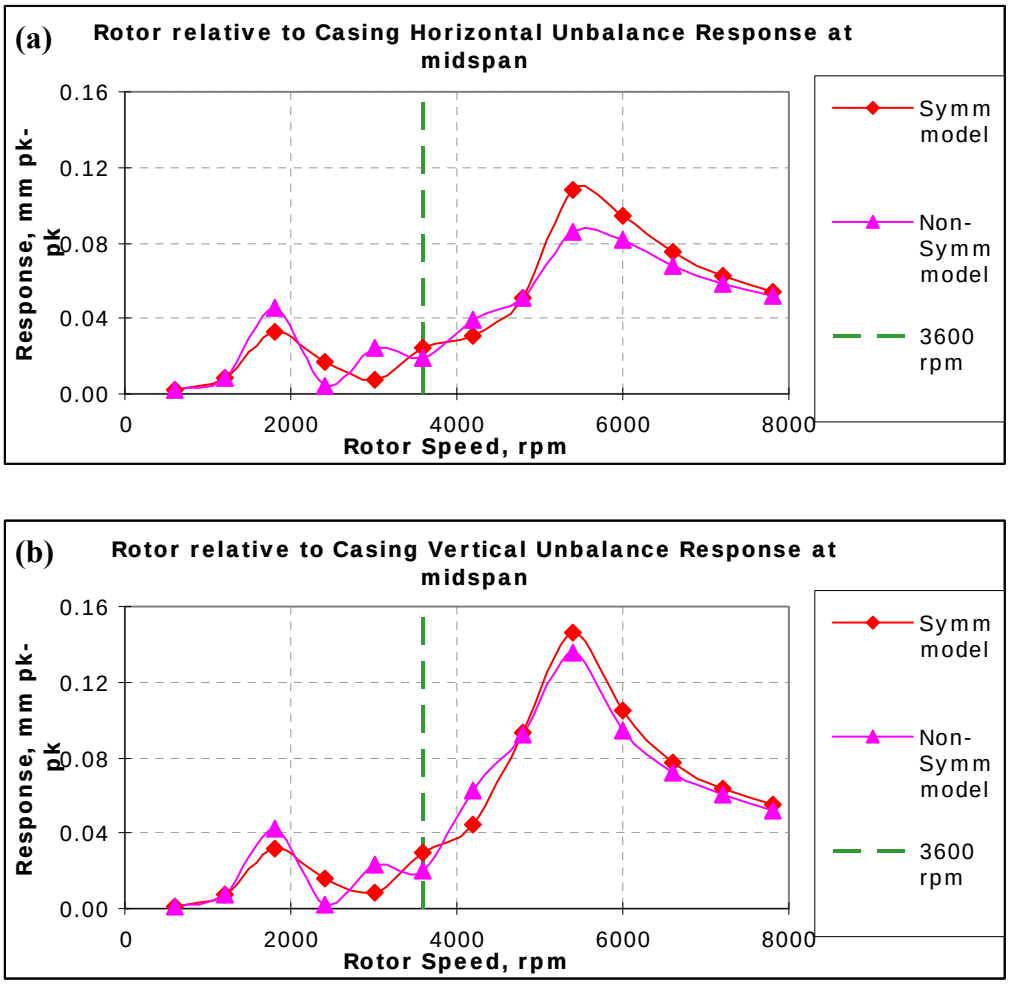

Figure 109 Rotor relative to casing response (with seal)
(a) Horizontal response (b) Vertical response

4.2.4 Seal Connected to Casing versus Seal Connected to Ground

Moore, et al. [18] uses a high-order polynomial in numerator-denominator transfer function format to model the connection between the rotor and ground for a large industrial turbo-compressor. Although this approach models the connections between the rotor and casing at the bearings, it erroneously leaves the connections at seals from rotor to ground, not rotor to casing.

In order to answer the question about the validity of connecting the seal from rotor to casing (Figure 110) versus rotor to ground (Figure 111), this section studies the

two cases in which the seal can be connected. For the remaining of this section, the case with seal connection from rotor to casing will be referred as Case I and the case with seal connection from rotor to ground will be referred as Case II.

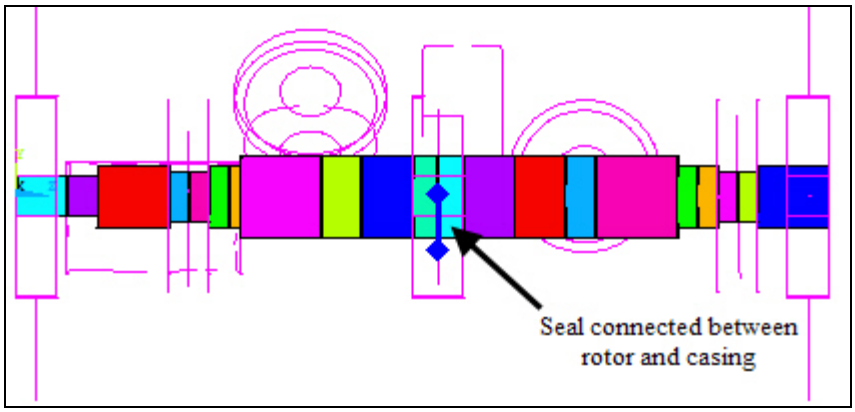

Figure 110 Representation of seal connected between rotor and casing

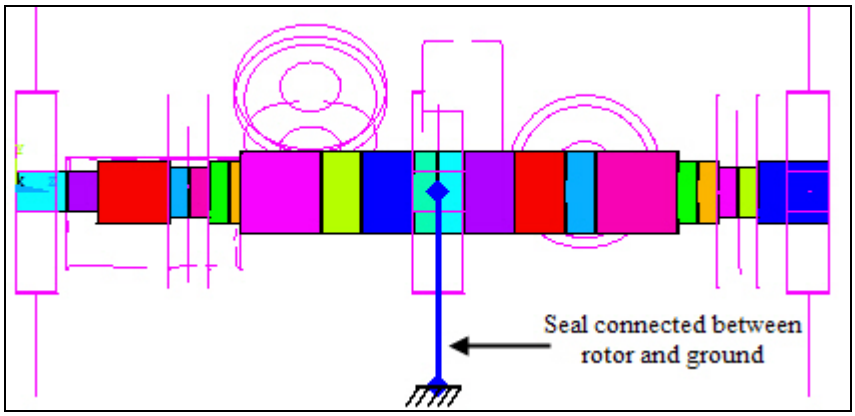

Figure 111 Representation of seal connected between rotor and ground

The results presented in this section pertain to the mid-span unbalance configuration and uses the non-axisymmetric casing. Rotor-end unbalance configurations and the axisymmetric casing show similar results but are not presented. Figure 112 through Figure 114 shows the horizontal and vertical responses of the rotor at the bearing 1, mid span, and bearing 2 locations, respectively. For case I, the first critical

response is predicted at a lower speed and its amplitude is higher when compared to Case II. Since the relative rotor to casing response is smaller at the first critical, as seen earlier in section 4.2.3, the effective damping provided by the seal is less. This explains the higher amplitude. As the speed increases, there is higher relative rotor to casing motion. The damping provided by the seal is now more effective and hence the response seen in case I is lower. The response of case II follows the similar profile as case I, with the exception that it over predicts the first critical response speed. At all other running speeds case II nearly coincides with the location of the critical responses reported by case I, but has higher response amplitudes. Similar trends can be seen in all the figures.

From the two cases presented in this section, it is clear that having the seal connection from rotor to ground shows different predictions in the first critical response location and response amplitudes. It is evident that making the seal connection from rotor to casing versus rotor to ground has a difference on the dynamic response of the system. This is because the dynamics of the casing structure now comes into effect. This has a potential significance in injection compressors with hole-patter-stator seals where the balance-piston or division-wall seals can be as stiff as the bearings.

As seen in the section 4.2.3, the first mode has less relative rotor-casing amplitude and hence the connection of seal to ground does not make a difference. At the second critical speed, there is large relative rotor-casing amplitude and hence the seal connected to ground shows more difference in amplitude. This is important in labyrinth seals where having large relative motion at the seals can produce large destabilizing forces on the rotor. The general effect of including the casing structure was also observed by Moore, et al, as seen in Figure 17.

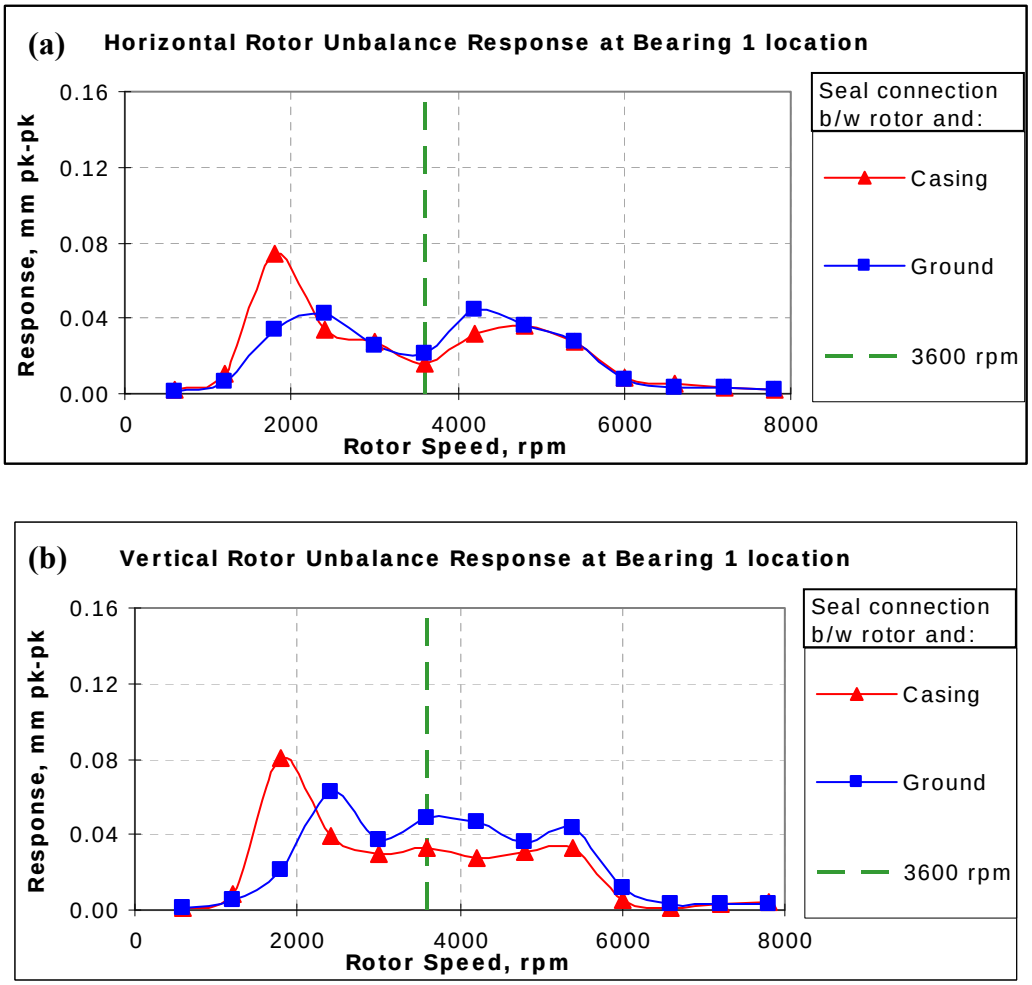

Figure 112 Unbalance response at bearing 1 location
(a) Horizontal response (b) Vertical response

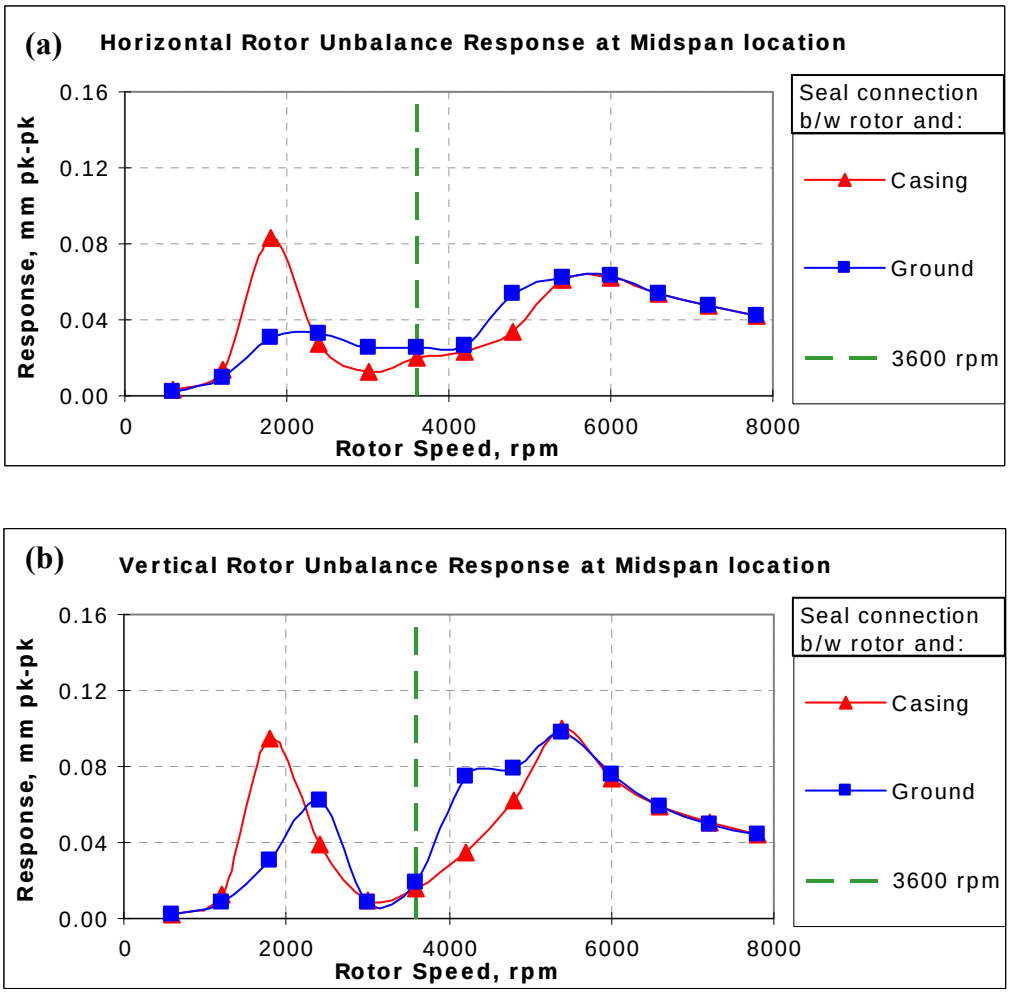

Figure 113 Unbalance response at mid span location
(a) Horizontal response (b) Vertical response

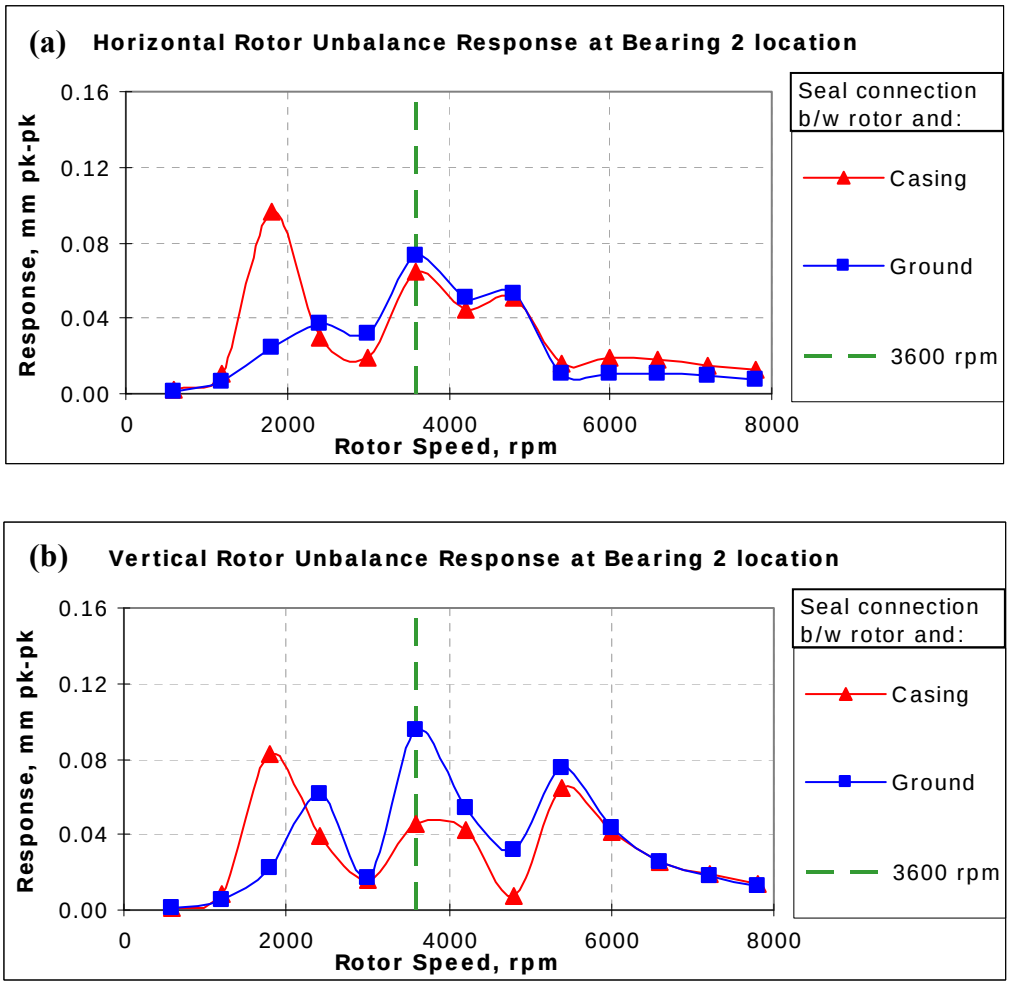

Figure 114 Unbalance response at bearing 2 location
(a) Horizontal response (b) Vertical response

5 CONCLUSION

Research is conducted to extend the capabilities of the beam-element based XLTRC^2 rotordynamic software suite to accept a general 3D finite-element casing model. This study broadens the work done by Clark and Jurjevic [17]. ANSYS serves as a powerful tool to model complex axisymmetric and non-axisymmetric casing structures. Using component mode synthesis reduction technique, reduced casing structure modal information is generated. Algorithms are developed that provided the necessary interface for the data to be incorporated with XLTRC^2.

Various validation steps are conducted to certify the techniques and algorithms used. The existing beam–element based modeling is verified for rotor and casing structure by comparing critical speeds and mode shapes. The current use of axisymmetric casing structures is verified by direct comparison of results obtained from XLTRC^2 and ANSYS. The impact of the non-axisymmetric casing is evident in the results presented. When the relative response amplitude between a rotor and casing is low, including the casing in the analysis may not have a significant benefit. However, cases in which there is high relative amplitude between the rotor and casing are common in industrial applications and not including the casing can produce erroneous predictions.

The work presented by Moore, et al. [18] posed the question of validity of analysis when a seal connection is involved. The comparison of connecting a seal between rotor and casing versus connecting the seal between rotor and ground, presented in this thesis, shows that the relevance of seal connection between rotor and casing depends on the relative amplitudes between the rotor and casing. If it is significant and the seal forces are large, then leaving a seal connection to ground will not produce accurate results.

Overall, this work has opened a new area of analysis in XLTRC^2. Casing models can now be modeled more accurately. Combined with the speed and user-friendliness of XLTRC^2, this will be an effective tool for future analyses.

REFERENCES

[1] Nelson, H., and McVaugh, J., 1976, "The Dynamics of Rotor-Bearing Systems Using Finite Elements," Journal of Engineering for Industry, **99**, pp. 593-600.

[2] Nelson, H., 1980, "A Finite Rotating Shaft Element Using Timoshenko Beam Theory," Journal of Mechanical Design, **2**(4), pp. 793-803.

[3] XLTRC^2 ™ Rotordynamic Software Suite, Version 2.4, Turbomachinery Laboratory, Texas A&M University, College Station, Texas, 2007.

[4] Turbo Exchange & Performance TEP Turbocharger Troubleshooting guide (http://www.tepturbos.com/troubleshooting.htm), accessed on March 2010.

[5] Childs, D. W., 1976, "A Modal Transient Rotordynamic Model for Dual Rotor Jet Engine Systems," Journal of Engineering for Industry, pp 876-882.

[6] Childs, D. W., 1978, "The Space Shuttle Main Engine High Pressure Fuel Turbopump Rotordynamic Instability Problem," ASME Trans., Journal of Engineering for Power, January 1978, **100**, pp 48-57.

[7] Childs, D.W., 1975, "SSME Turbopump Technology Improvements via Transient Rotordynamic Analysis," Contract Report NAS8-31233, The University of Louisville/Speed Scientific School, Louisville, Kentucky, December 1975.

[8] Darlow, M. S., Smalley, A. J. and Ogg, J., 1978, "Critical Speeds and Response of a Large Vertical Pump," ASME Paper 78-PVP-34, San Antonio, Texas.

[9] Lund, J.W., "User's Manual, MTI Computer Program CAD-26", Mechanical Technology Inc.

[10] Lund, J.W., "User's Manual, MTI Computer Program CAD-27", Mechanical Technology Inc.

[11] Memmott, E., 2003, "Usage of the Lund Rotordynamic Programs in the Analysis of centrifugal Compressors," Journal of Vibration and Acoustics, **125**(4), pp 500-506.

[12] Bellamy, R.A., Jonson, C.P., Gaffney, R., 1985, "Developing Concepts in the Rotordynamic Analysis of Aero Gas Turbines," Paper 85-GT-230, ASME Gas Turbine Conference and Exhibit, Houston, Texas.

[13] Gerardin, M. and Kill, N., 1986, “A 3-Dimensional Approach To Dynamic Analysis of Rotating Shaft-Disk Flexible Systems,” Proceedings, IFToMM International Conference on Rotordynamics, Tokyo, Japan, pp. 87-93.

[14] Gerardin, M. and Kill, N., 1990, “Dynamic Analysis of Aircraft Engines Subjected to Maneuvers,” Proceedings, IFToMM International Conference on Rotordynamics, Lyon, France, pp. 397-402.

[15] Hylton, P. and Burns, D., 1994, “Turbofan Blade Loss Tools,” Proceedings, IFToMM International Conference on Rotordynamics, Chicago, USA, pp. 81-83.

[16] Corbo, M. A., Stefanko, D. B. and Leishear, R. A., 2002, “Practical Use of Rotordynamic Analysis to Correct a Vertical Long Shaft Pump’s Whirl Problem,” Proceedings of the 19th International Pump Users Symposium, Turbomachinery Laboratory, Texas A&M University, College Station, Texas.

[17] Clark, A., and Jurjevic, Z., 2007, “Fast Simulation Of Dynamic Behaviour Of Heavy Duty Gas Turbines For Quality Improvement And Reduced Design Cycle Time,” GT2007-27382, Proceedings of ASME Turbo Expo 2007 : Power for Land, Sea and Air.

[18] Moore, J., Vannini, G., Camatti, M., and Bianchi, P., 2006, “Rotordynamic Analysis of a Large Industrial Turbo-Compressor including Finite Element Substructure Modeling,” GT2006-90481, Proceedings of GT2006: ASME Turbo Expo 2006: Power for Land, Sea and Air.

[19] Guyan, R. J., 1965, "Reduction of Stiffness and Mass Matrices," AIAA Journal, **3**(2), pp. 380.

[20] Rouch, K., and Kao, J., 1980, “Dynamic Reduction in Rotor Dynamics by the Finite-Element Method,” Journal of Mechanical Design, **102**, pp. 360-368.

[21] Glasgow, D.A., and Nelson, H.D., 1979, “Stability Analysis of Rotor-Bearing Systems Using Component Mode Synthesis,” Journal of Mechanical Engineering Design, **102**(2), pp. 352-359.

[22] Childs, D. W., 1993, “Turbomachinery Rotordynamics Phenomena, Modeling, & Analysis,” John Wiley and Sons, Inc., Hoboken, New Jersey

[23] Childs, D. W., 2005, “MEEN 363 Dynamics and Vibration: Dynamics in Engineering Practice,” Sixth Edition, John Wiley and Sons, Inc., Hoboken, New Jersey

[24] Baruh, H., 1999, “Analytical Dynamics,” McGraw-Hill International Editions, New York City, New York.

[25] Release 11.0 Documentation for ANSYS, ANSYS Inc., 2007.

[26] API Standard 617, Axial and Centrifugal Compressors and Expander-compressors for Petroleum, Chemical and Gas Industry Services, American Petroleum Institute, Seventh Edition, July 2002.

[27] API Recommended Practice 684, API Standard Paragraphs Rotordynamic Tutorial: Lateral Critical Speeds, Unbalance Response Stability, Train Torsionals, and Rotor Balancing, American Petroleum Institute, Second Edition, August 2005.

[28] Guide to Interfacing with ANSYS, ANSYS Release 10.0 documentation, ANSYS Inc., 2005.

[29] User’s Manual, Intel Visual FORTRAN, Intel Corp, 2007.

APPENDIX A

VALIDATION OF SIMULATION TOOLS

A verification test is required to make sure that the results obtained by the different simulation tools agree with each other. A solid cylindrical model is tested in XLTRC^2, ANSYS Classic using APDL and ANSYS Workbench and the results are compared. The beam is 2.25 m (88.58 in) in length, has a diameter of 0.3 m (11.81 in) and uses the following material properties.

Density (ρ) = 7833.412 kg/m^3 (0.283 lbm/in^3)

Elastic Modulus (E) = 206.842E+9 N/m^2 (30.0E+6 lbf/in^2)

Shear Modulus (G) = 82.737E+9 N/m^2 (12.0E+6 lbf/in^2)

XLTRC^2 and ANSYS Classic models are divided into 200 beam elements, as shown in Figure 115 and Figure 116 respectively, whereas ANSYS Workbench used solid elements as shown in Figure 117. Figure 116 shows the graphical representation as a series of cube-shaped elements. Table 12 shows the first 5 bending modes[11] which show excellent agreement with each other. Figure 118 through Figure 132 shows the mode shapes of the first 5 bending modes.

Table 12 First five bending mode frequencies compared to XLTRC^2 results

Mode	XLTRC^2	ANSYS Classic (Hz)	Percentage Change (%)	ANSYS Workbench (Hz)	Percentage change
1	259.42	260.97	0.59	259.54	0.05
2	666.78	666.12	-0.09	667.73	0.14
3	1201.87	1203.70	0.15	1204.90	0.25
4	1814.37	1814.50	0.01	1821.00	0.37
5	2472.83	2470.00	-0.11	2484.30	0.46

[11] XLTRC^2 uses 2D beam elements and does not have degrees of freedom along the axial direction. Hence axial bending modes from the ANSYS Classic and ANSYS Workbench results are ignored. Note that any comparisons between XLTRC^2 and ANSYS mentioned in this thesis does not account for axial modes.

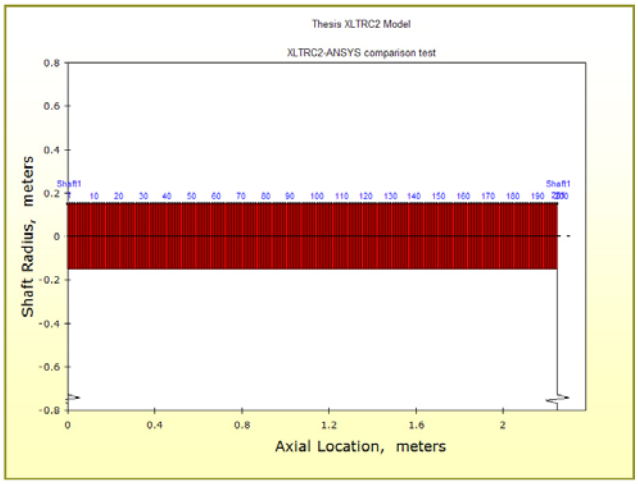

Figure 115 XLTRC2 model constructed with 2D beam elements

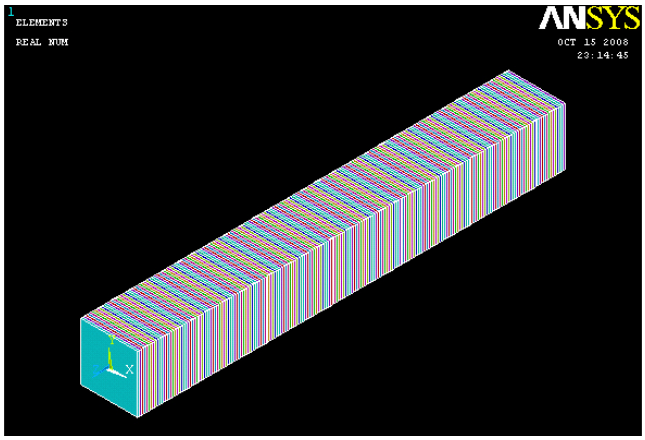

Figure 116 ANSYS Classic APDL model constructed with 3D beam elements

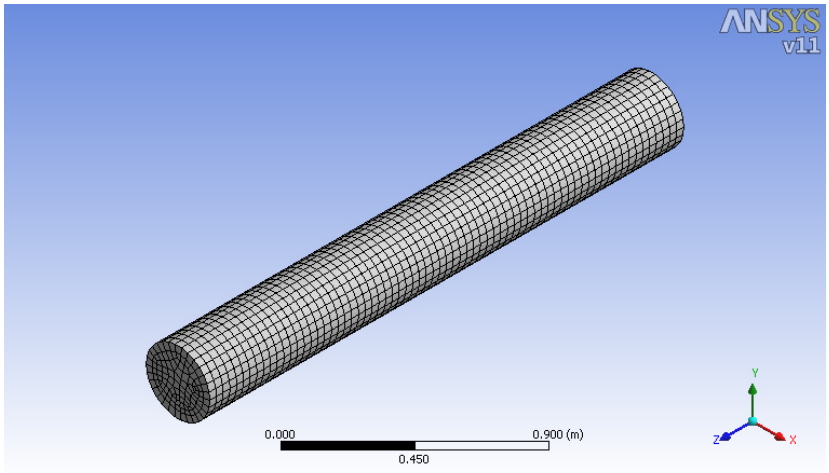

Figure 117 ANSYS Workbench model constructed with solid elements

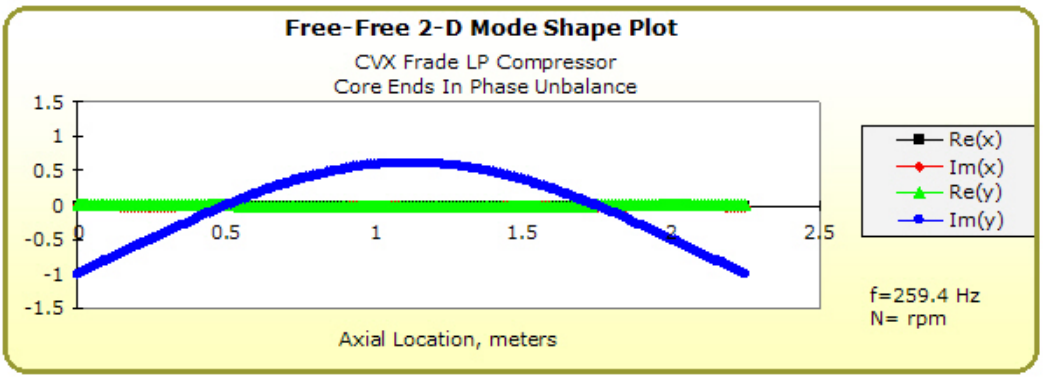

Figure 118 First bending mode of XLTRC^2 model (259.42 Hz)

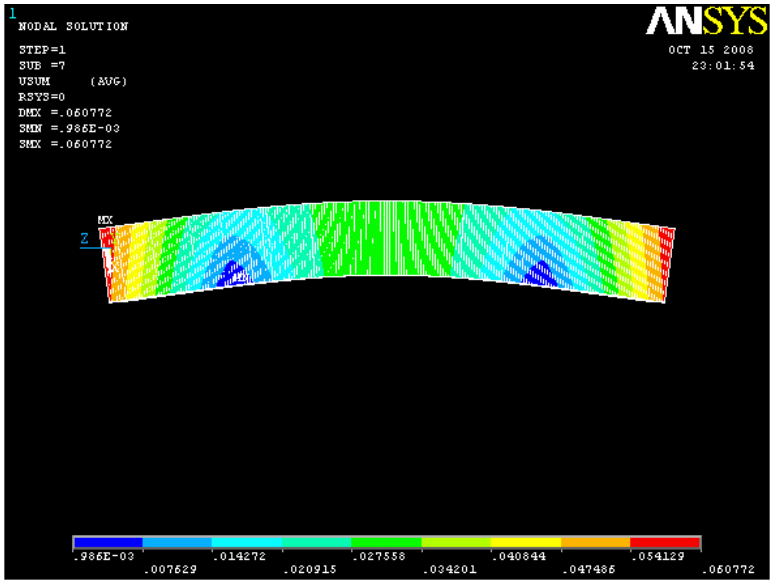

Figure 119 First bending mode of ANSYS Classic model (260.97 Hz)

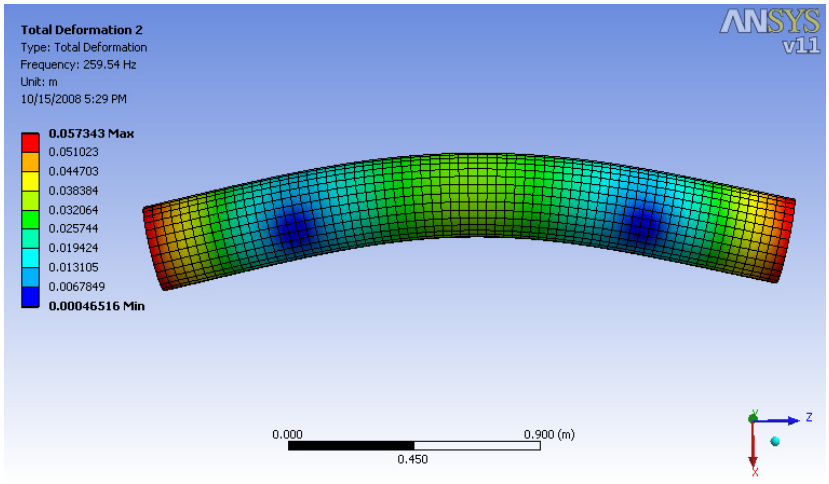

Figure 120 First bending mode of ANSYS Workbench model (259.54 Hz)

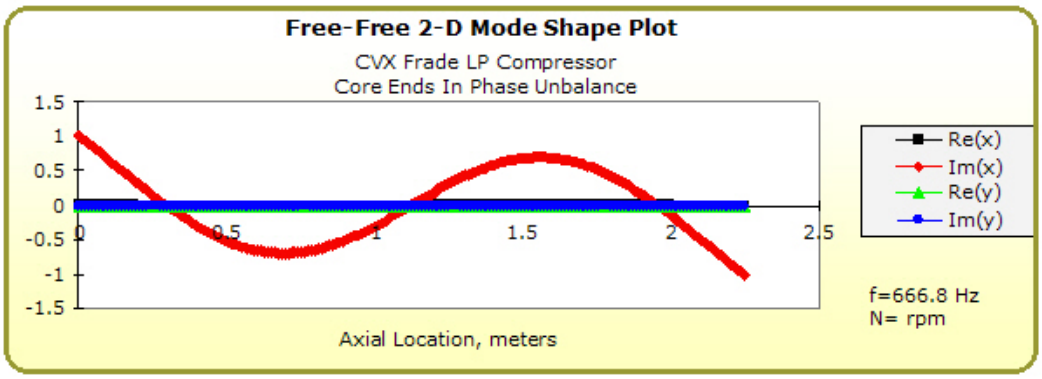

Figure 121 Second bending mode of XLTRC^2 model (666.78 Hz)

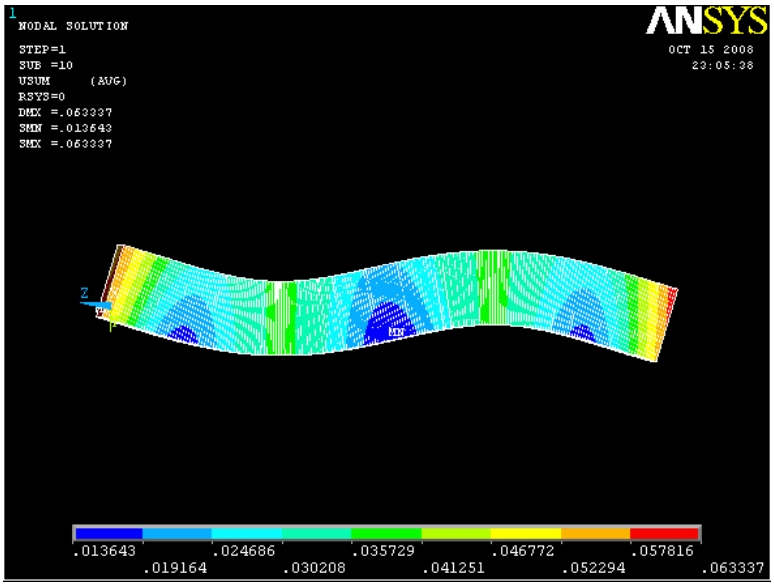

Figure 122 Second bending mode of ANSYS Classic model (666.12 Hz)

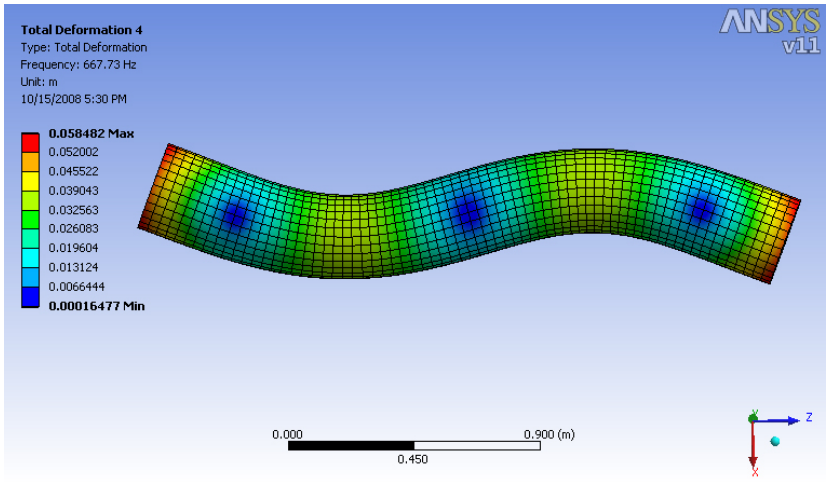

Figure 123 Second bending mode of ANSYS Workbench model (667.73 Hz)

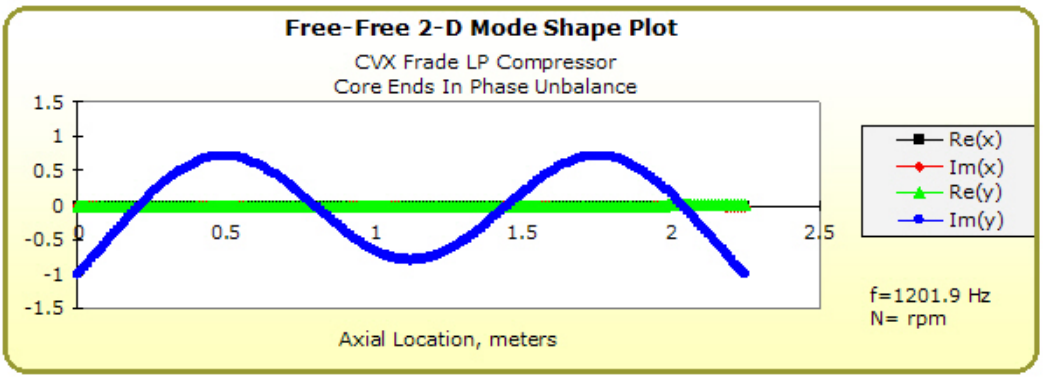

Figure 124 Third bending mode of XLTRC^2 model (1201.87 Hz)

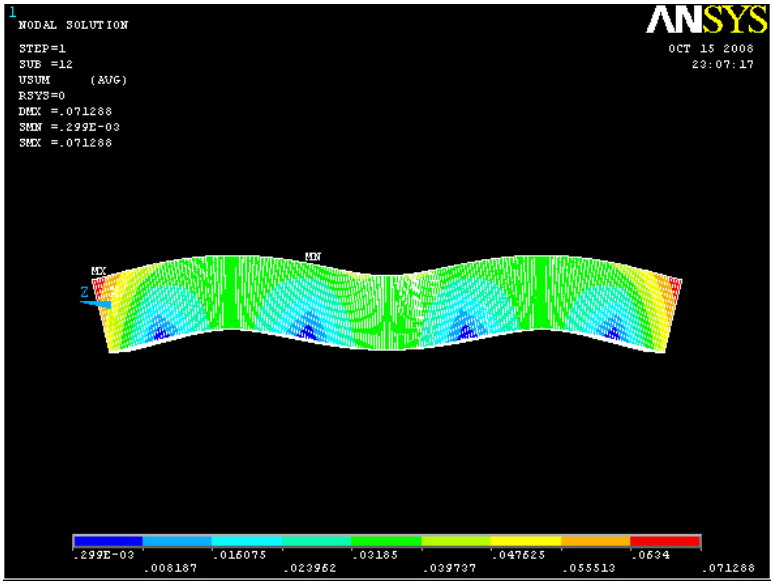

Figure 125 Third bending mode of ANSYS Classic model (1203.70 Hz)

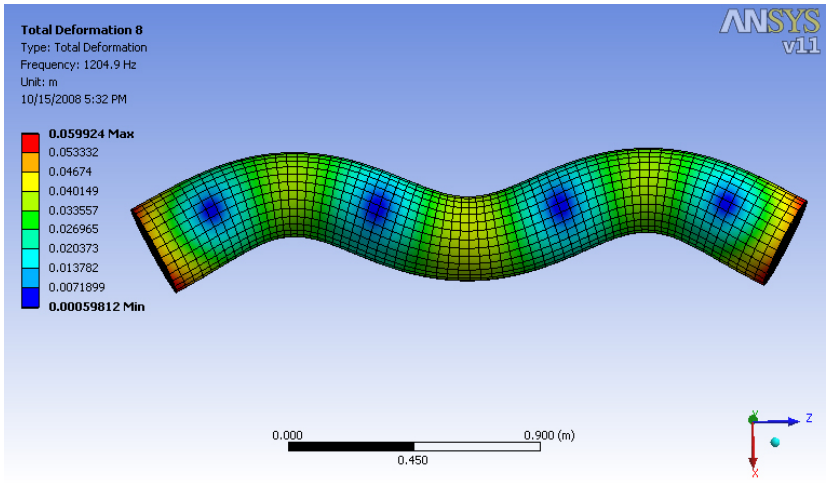

Figure 126 Third bending mode of ANSYS Workbench model (1204.90 Hz)

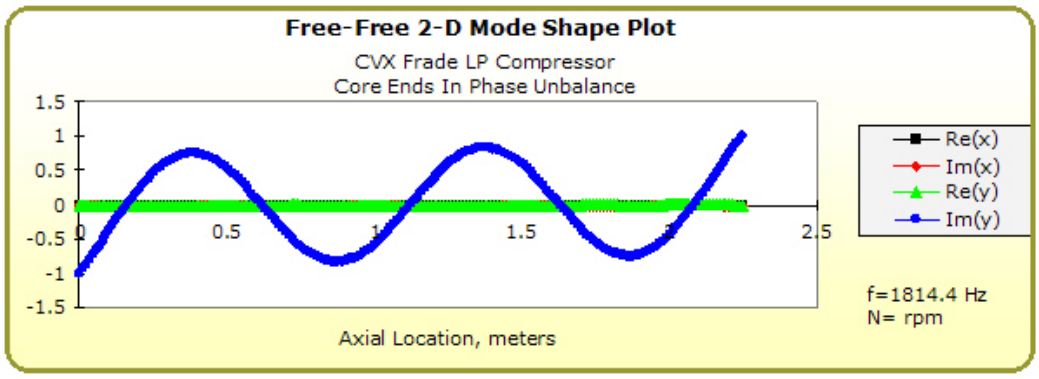

Figure 127 Fourth bending mode of XLTRC^2 model (1814.37 Hz)

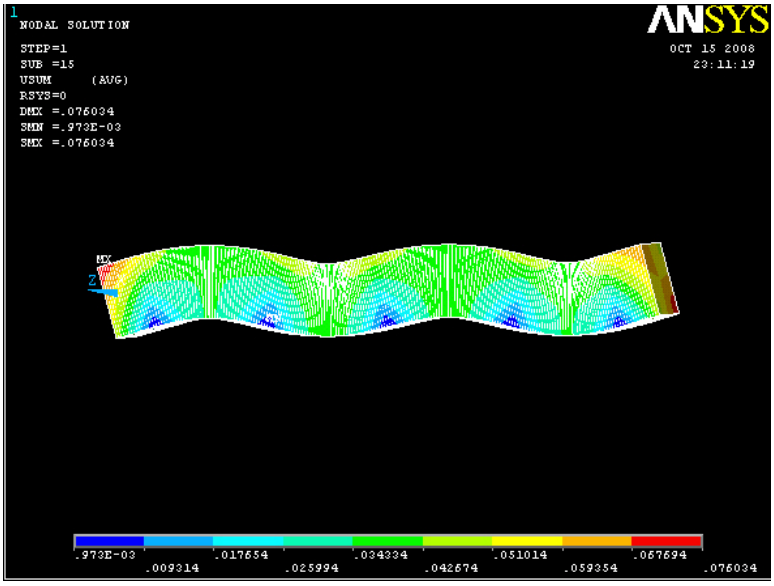

Figure 128 Fourth bending mode of ANSYS Classic model (1814.50 Hz)

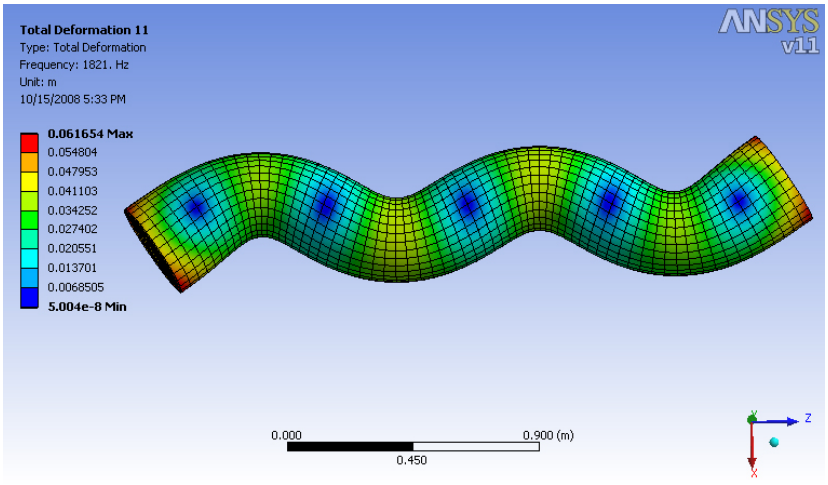

Figure 129 Fourth bending mode of ANSYS Workbench model (1821.00 Hz)

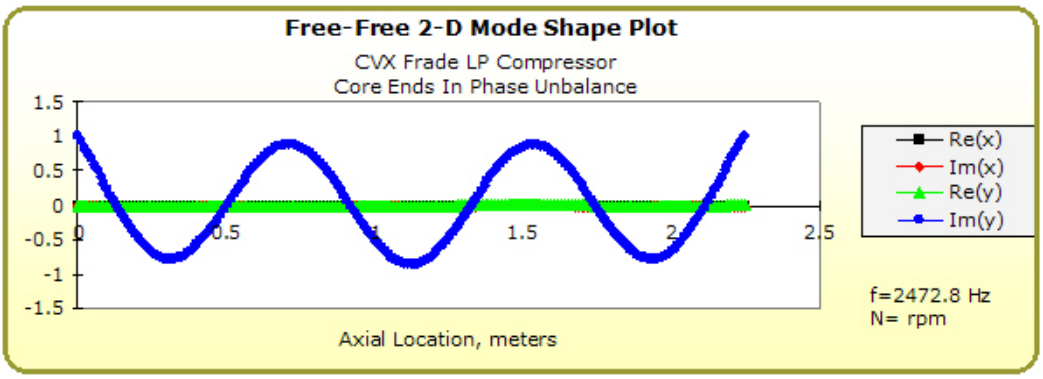

Figure 130 Fifth bending mode of XLTRC^2 model (2472.83 Hz)

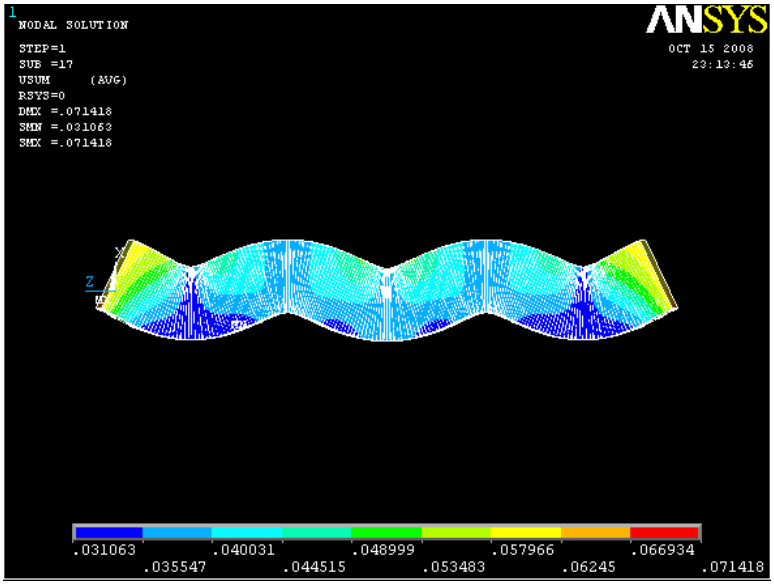

Figure 131 Fifth bending mode of ANSYS Classic model (2470.00 Hz)

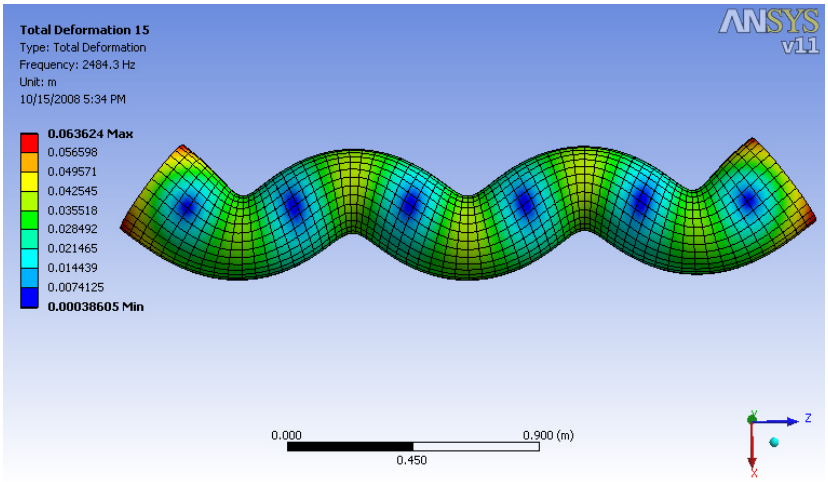

Figure 132 Fifth bending mode of ANSYS Workbench model (2484.30 Hz)

APPENDIX B

MESH DENSITY VALIDATION FOR CASING MODEL

To determine an acceptable mesh density in the XLTRC^2 casing model, three test casing models are made. The first case uses ANSYS solid elements, as illustrated in Figure 133, and has 19,225 elements. The second case, made of XLTRC^2 beam elements, uses low mesh density of 14 elements, seen in Figure 134. The third case, also made with XLTRC^2 beam elements, has a higher mesh density of 160 elements, shown in Figure 135.

Table 13 shows comparison of the first four bending modes. It shows that the higher mesh density XLTRC^2 model is closer in agreement with the ANSYS results than the one with lower mesh density. The high mesh density XLTRC^2 model is therefore used. Figure 136 through Figure 147 show the similar mode shapes.

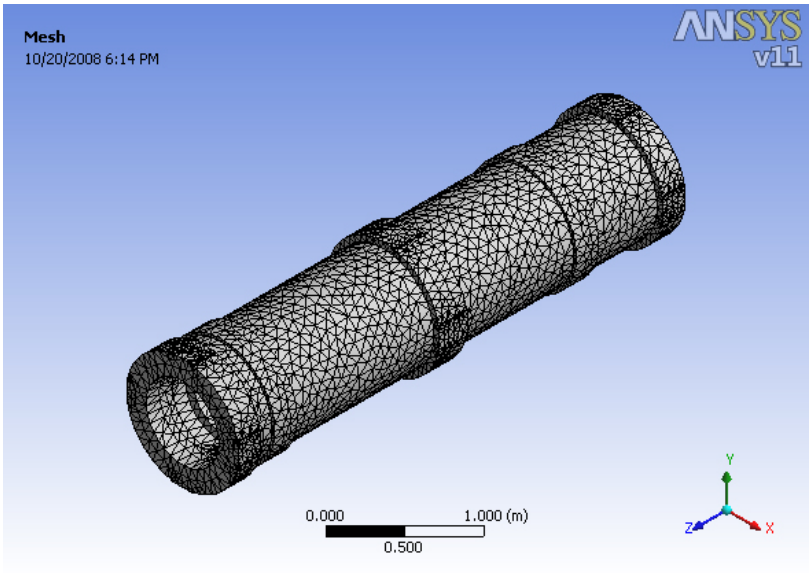

Figure 133 ANSYS solid element casing model

Table 13 Comparison of first four bending mode frequencies (in Hertz)

Mode	ANSYS	XLTRC^2 Low Mesh	Percentage Change (%)	XLTRC^2 High Mesh	Percentage Change (%)
1	224.37	227.96	1.60	226.82	1.09
2	515.99	549.05	6.41	522.15	1.19
3	732.80	784.03	6.99	755.73	3.12
4	978.87	1190.39	21.61	1031.64	5.39

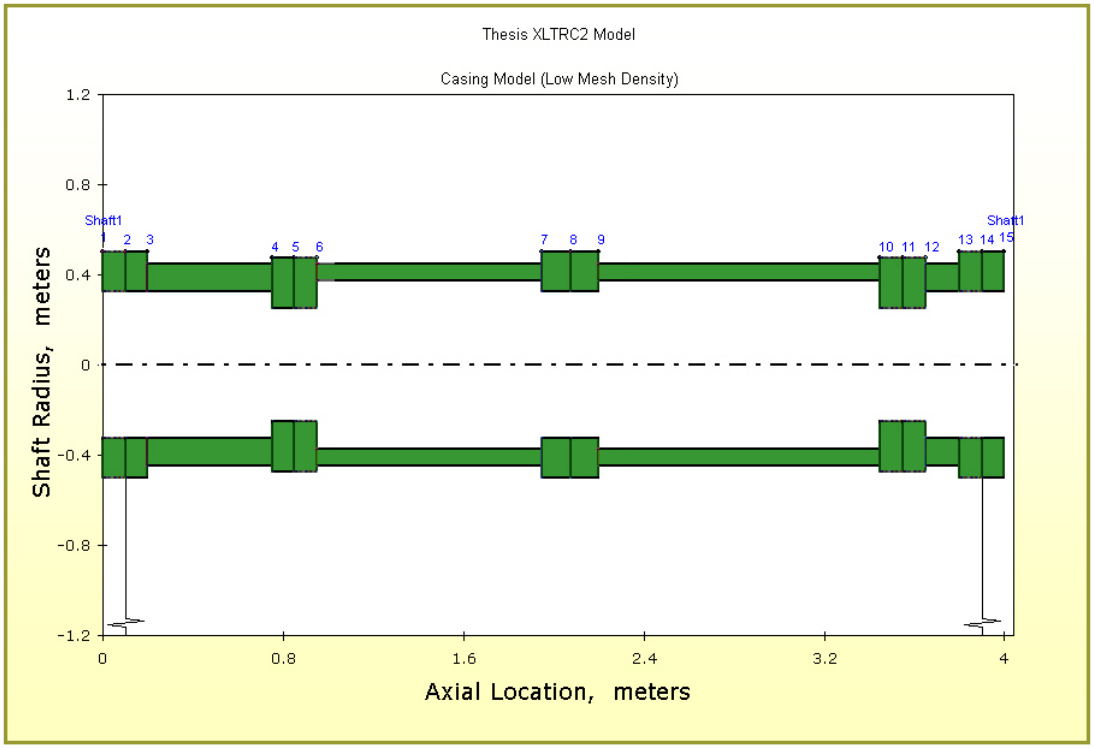

Figure 134 Low mesh density XLTRC^2 beam element casing model

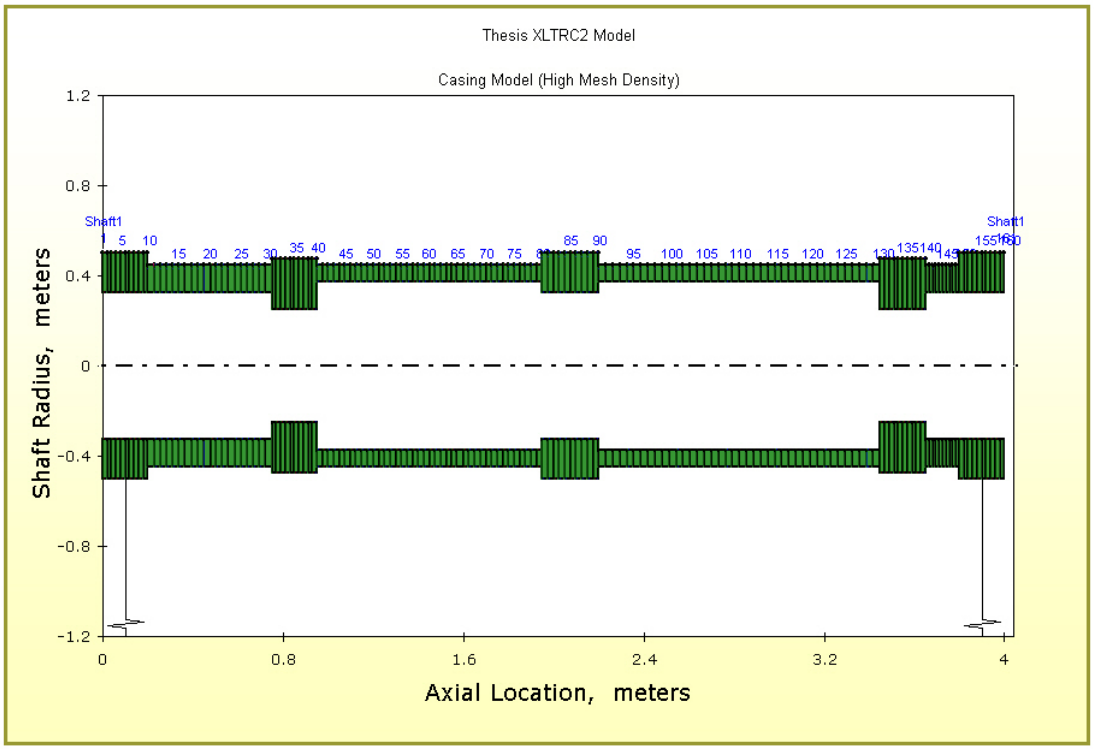

Figure 135 High mesh density XLTRC^2 beam element casing model

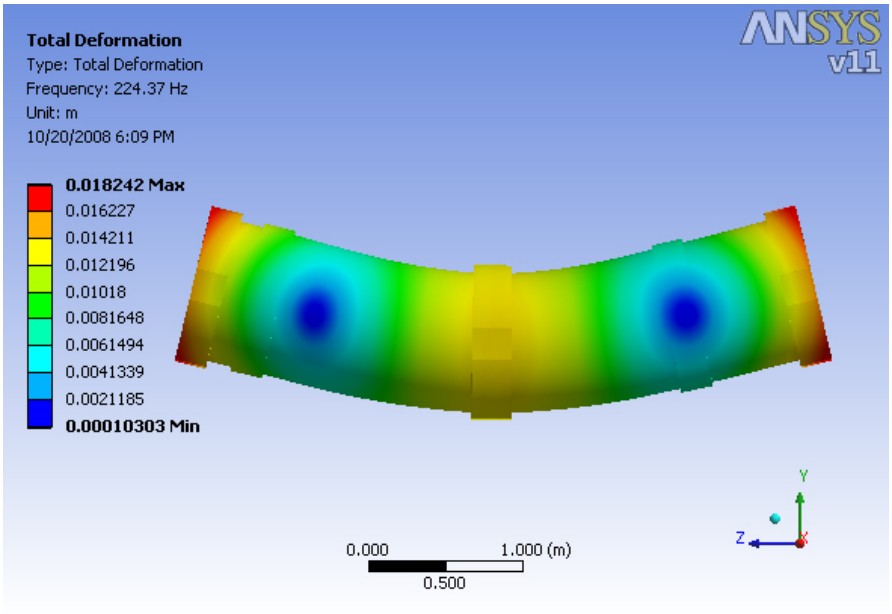

Figure 136 ANSYS model first bending mode at 224.37 Hz

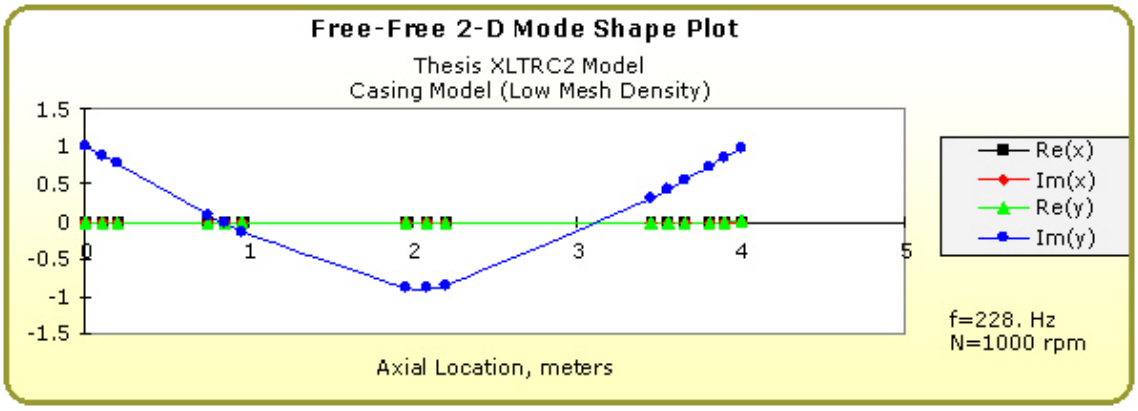

Figure 137 XLTRC^2 low mesh density first bending mode at 227.96 Hz

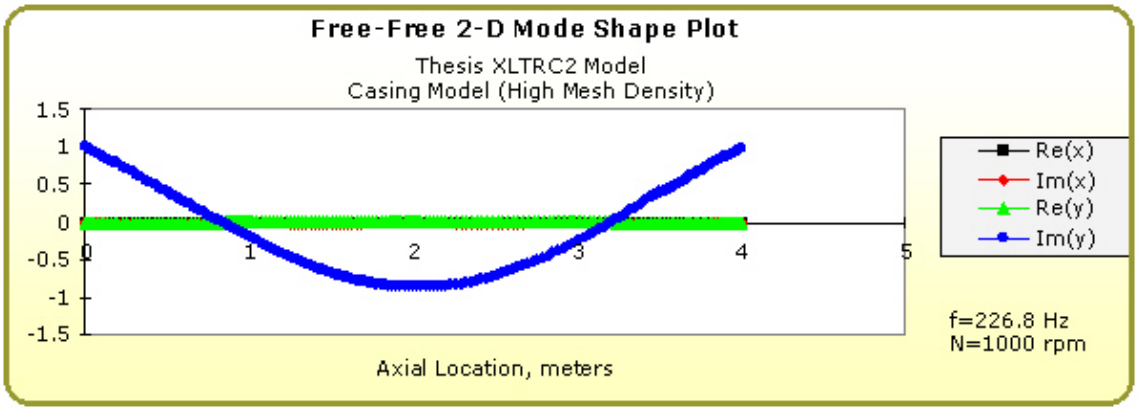

Figure 138 XLTRC^2 high mesh density first bending mode at 226.82 Hz

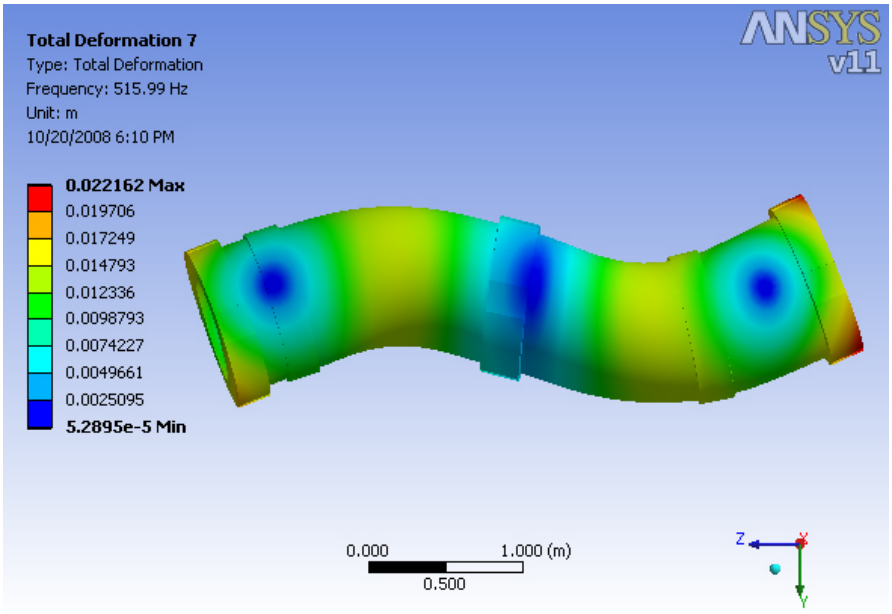

Figure 139 ANSYS model second bending mode at 515.99 Hz

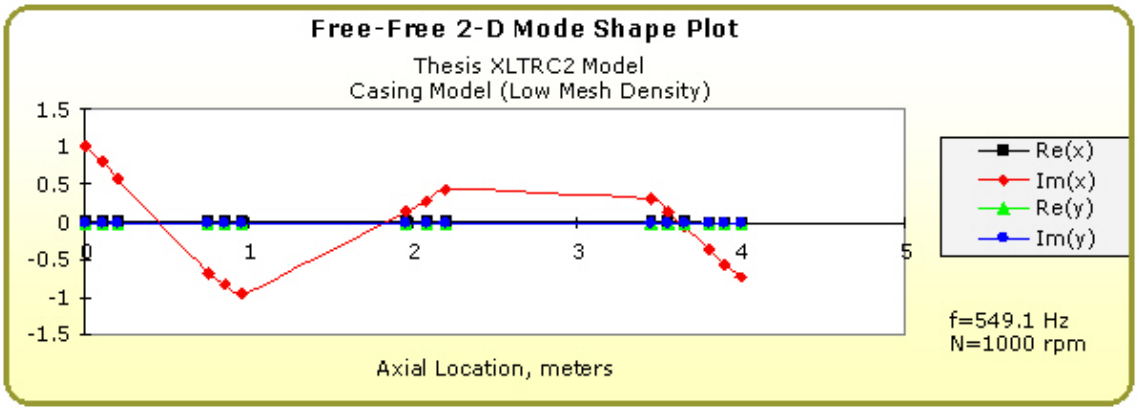

Figure 140 XLTRC^2 low mesh density second bending mode at 549.05 Hz

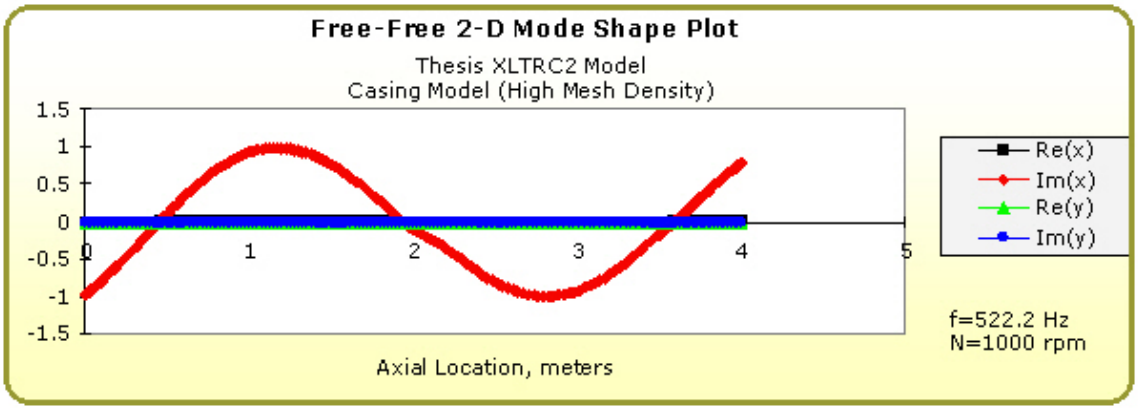

Figure 141 XLTRC^2 high mesh density second bending mode at 522.15 Hz

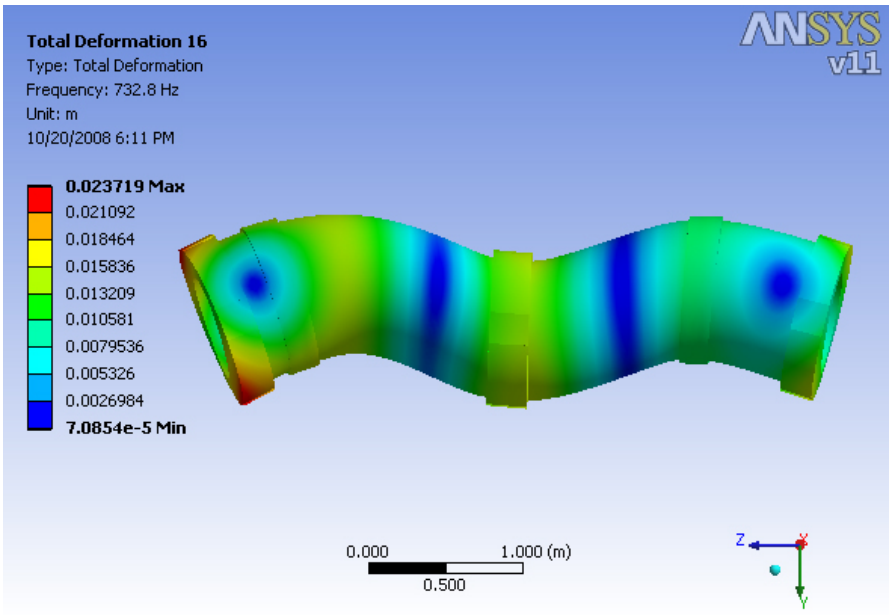

Figure 142 ANSYS model third bending mode at 732.80 Hz

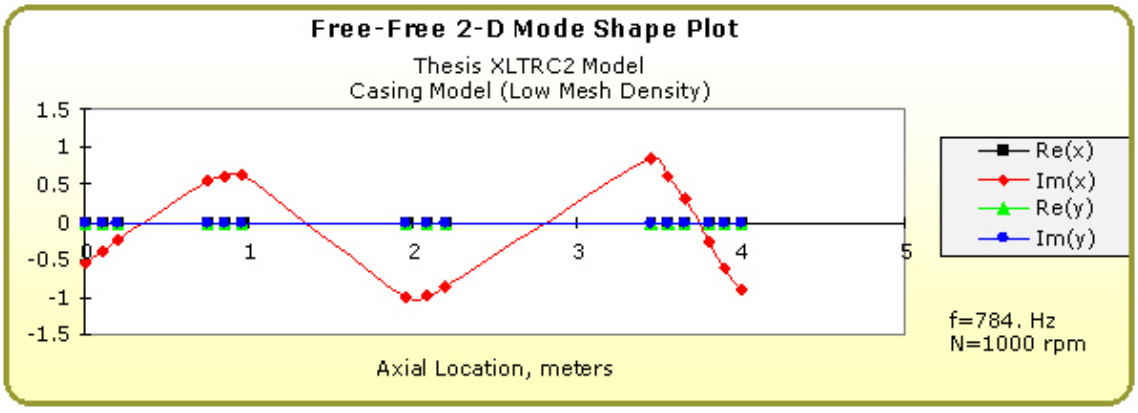

Figure 143 XLTRC^2 low mesh density third bending mode at 784.03 Hz

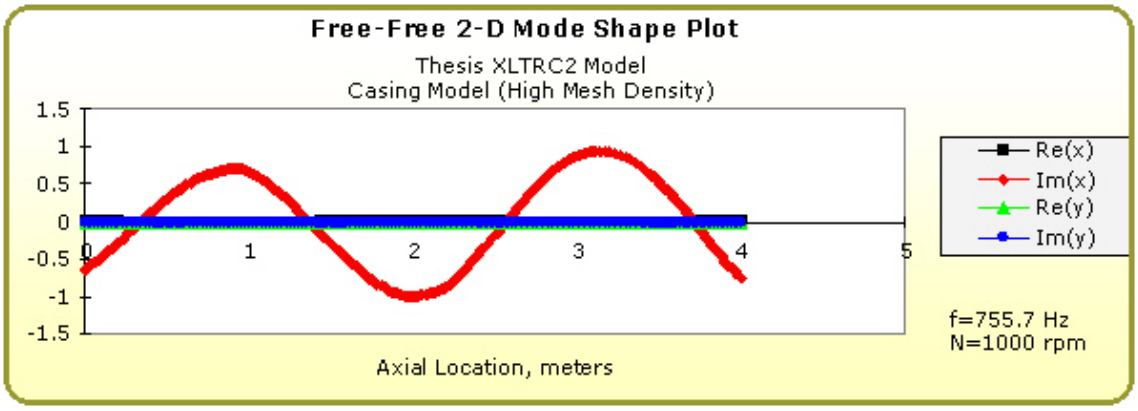

Figure 144 XLTRC^2 high mesh density third bending mode at 755.73 Hz

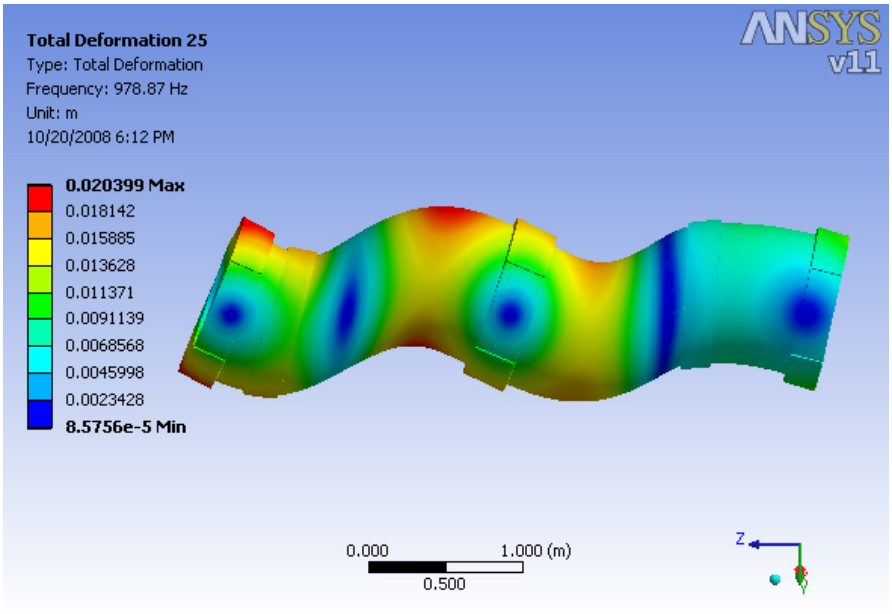

Figure 145 ANSYS model fourth bending mode at 978.87 Hz

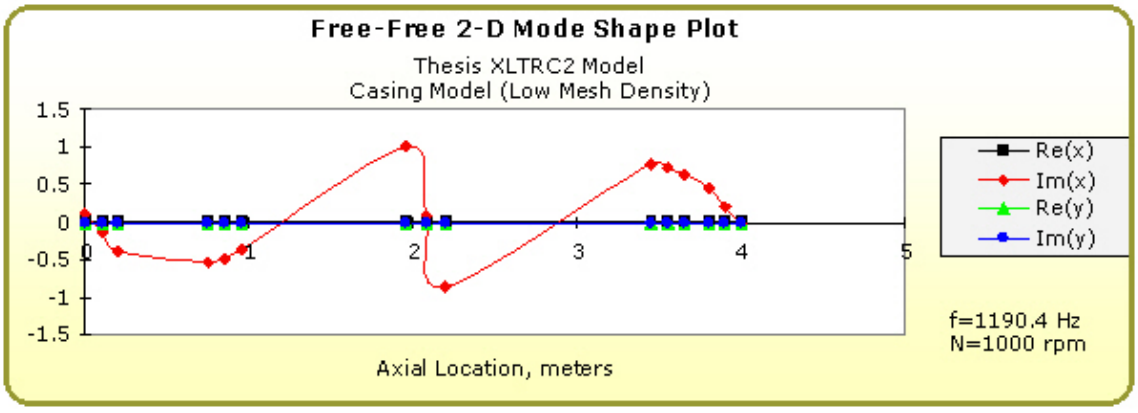

Figure 146 XLTRC^2 low mesh density fourth bending mode at 1190.39 Hz

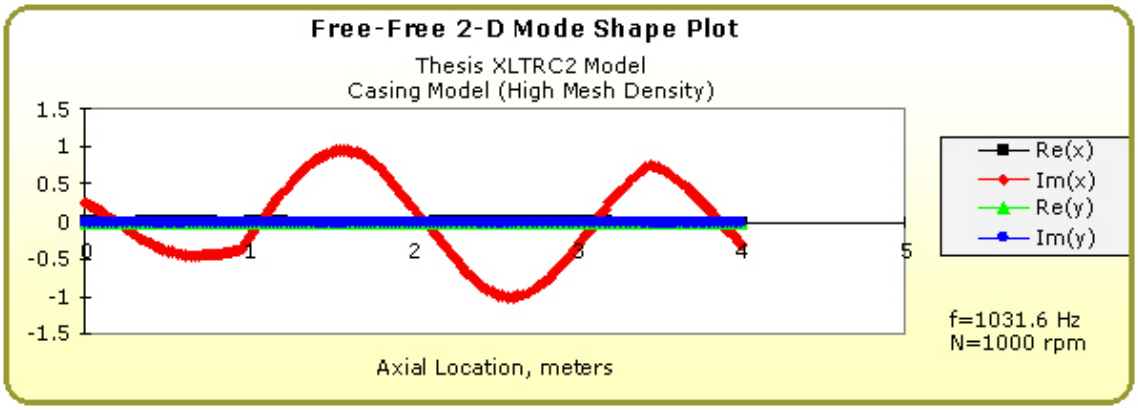

Figure 147 XLTRC^2 high mesh density fourth bending mode at 1031.64 Hz

APPENDIX C

CASING MODEL VALIDATION FOR END SUPPORT

Figure 148 shows the original ANSYS axisymmetric geometry for the casing model. Figure 149 shows the model after additional surface have been created to provide the interface to connect foundation supports to ground. Table 14 shows comparison of the first seven free-free mode frequencies.

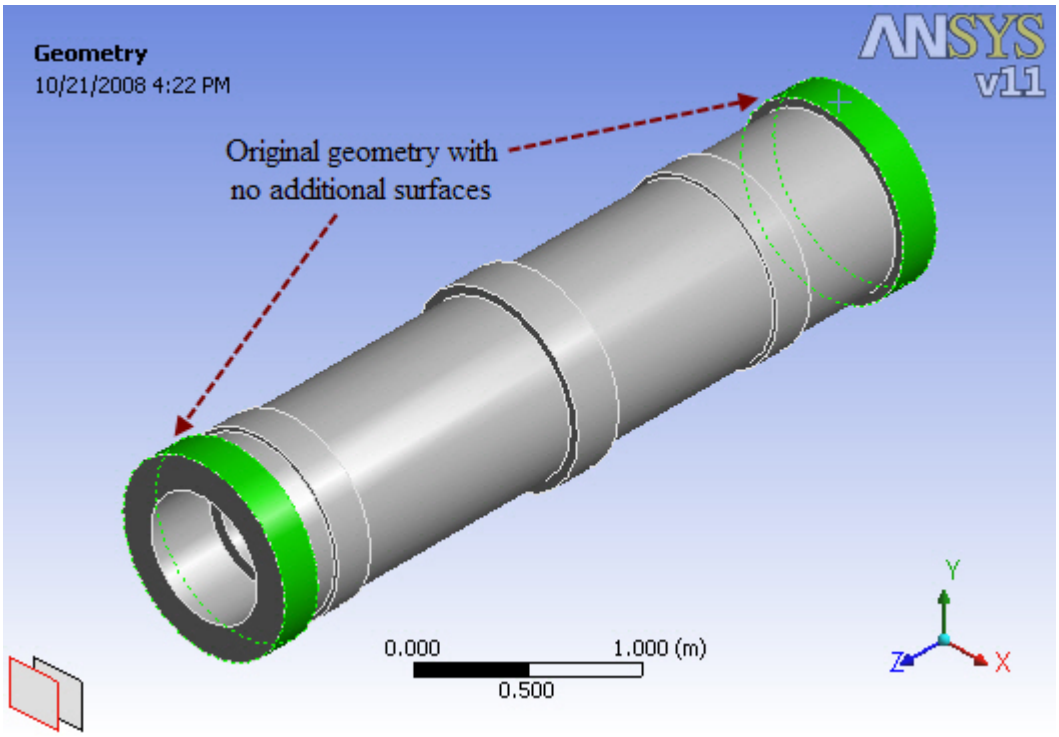

Figure 148 ANSYS axisymmetric casing model with original geometry

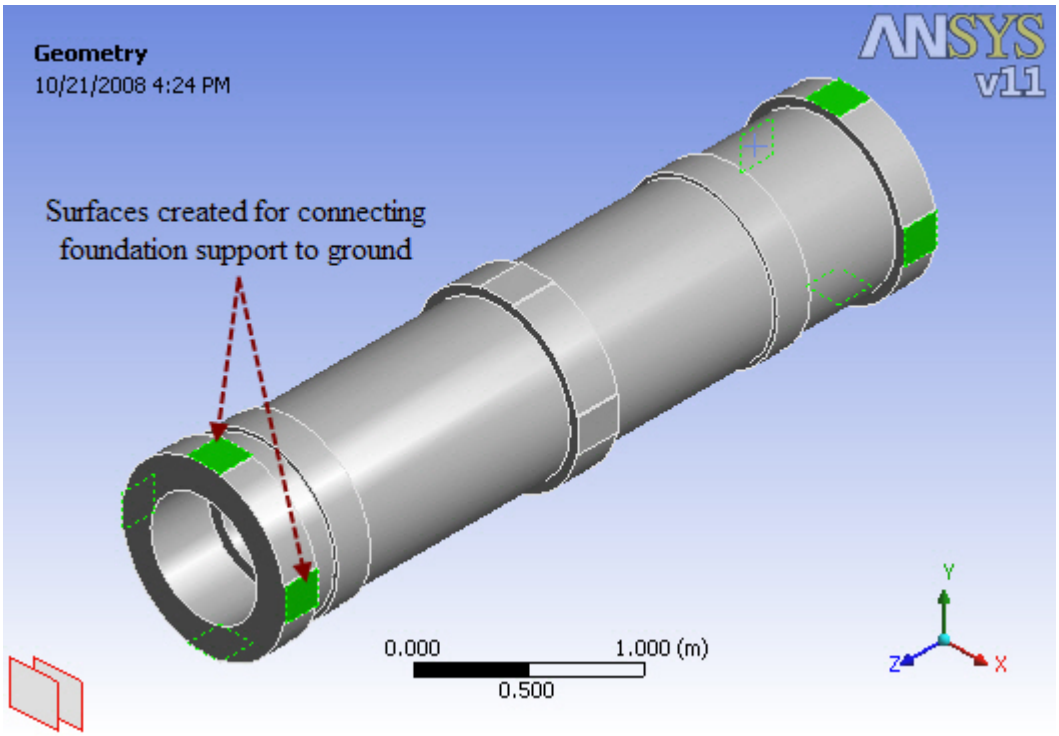

Figure 149 Above model with additional surfaces on end supports

Table 14 Comparison of first seven Free-Free mode frequencies

Mode	Original Model	Model with additional surfaces	Percentage Change (%)
1	224.80	224.37	0.19
2	224.83	224.38	0.20
3	332.55	332.05	0.15
4	437.34	437.04	0.07
5	437.38	437.21	0.04
6	515.61	514.98	0.12
7	516.63	515.99	0.12

APPENDIX D

ROTOR MODEL VALIDATION

The simplest method to validate the rotor model is to perform a Free-Free modal analysis. Free-Free modes are the resonant frequencies obtained when an object is subjected to a strike. The resonant frequencies obtained from such a test are also called fundamental frequencies. The effect of all bearings and seals are excluded in such an analysis. If rotor gyroscopic effects are included, then the Free-Free modes are a function of the rotor speed. Field hammer test data are usually done on freely suspended rotors and hence do not include gyroscopic effects. XLTRC^2 and ANSYS have the capability of including or excluding these gyroscopic effects. For the purpose of this validation, gyroscopic effects are not included.

Table 15 shows a comparison of the frequencies (in Hertz) corresponding the first five bending modes of the rotor. The values show excellent agreement between XLTRC^2 and ANSYS codes. Figure 150 through Figure 159 show the mode shapes obtained in ANSYS and XLTRC^2 which also show excellent agreement. This completes the validation step for the rotor.

Table 15 Free-Free bending modes frequencies compared between ANSYS and XLTRC^2

Mode	ANSYS (Hz)	XLTRC^2 (Hz)	Percentage Difference (%)
1	102.57	102.59	0.02
2	211.31	211.41	0.05
3	335.66	335.88	0.07
4	502.00	502.34	0.07
5	659.77	660.43	0.01

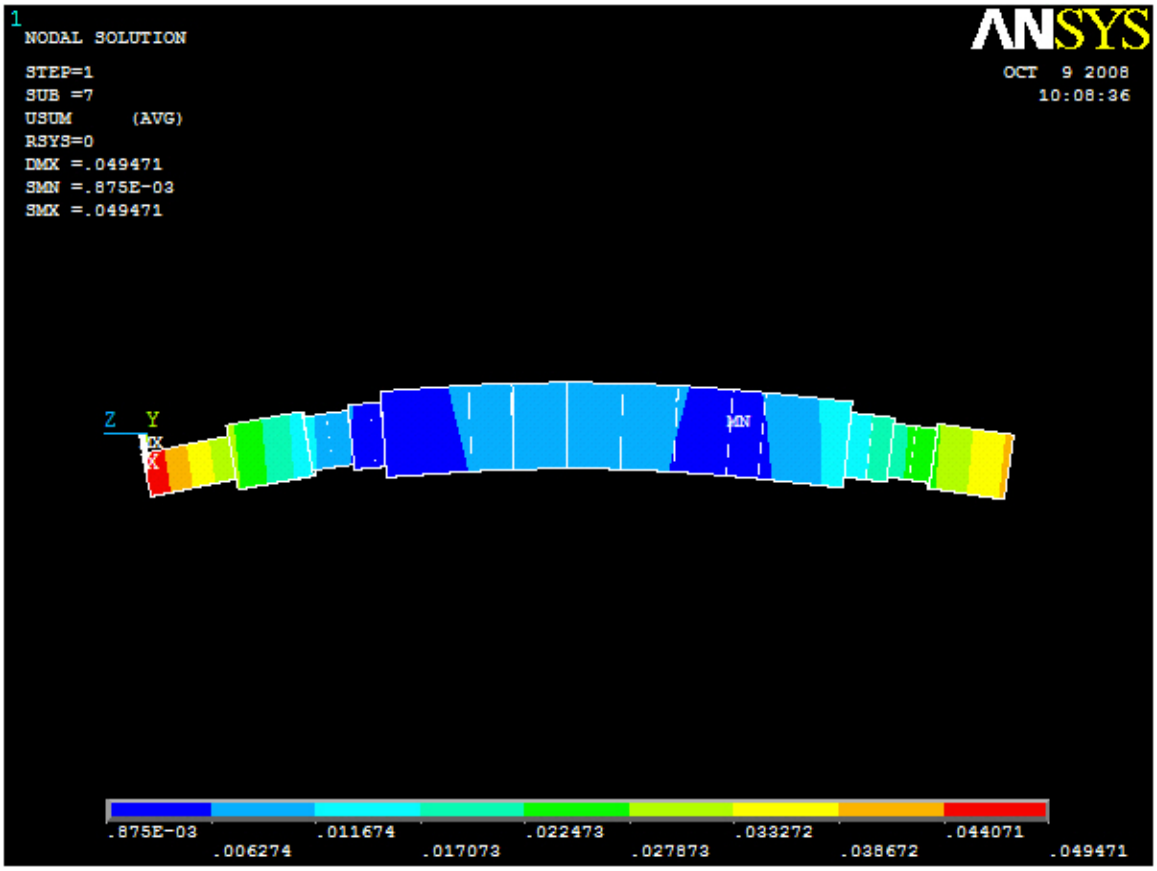

Figure 150 ANSYS first bending mode at 102.57 Hz

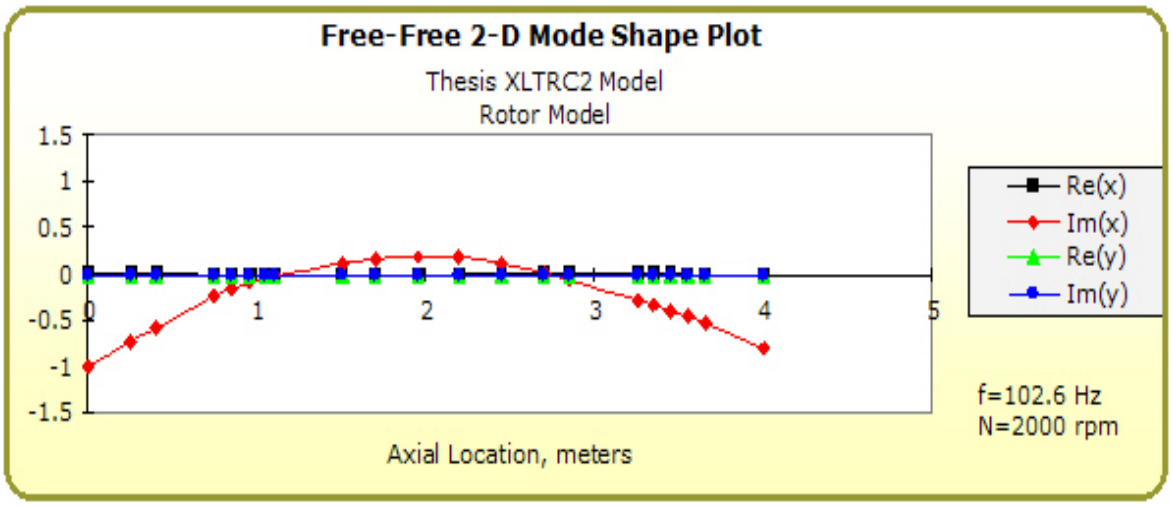

Figure 151 XLTRC^2 first bending mode at 102.59 Hz

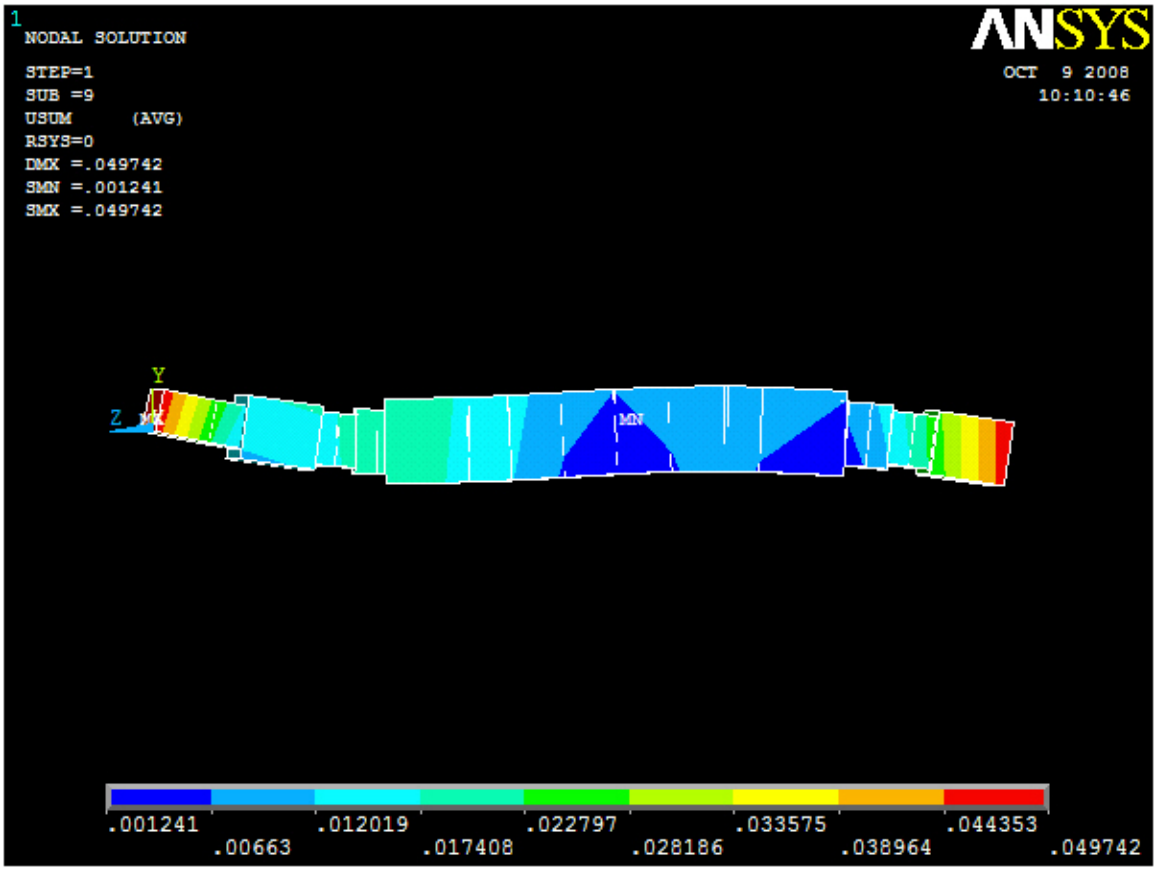

Figure 152 ANSYS second bending mode at 211.31 Hz

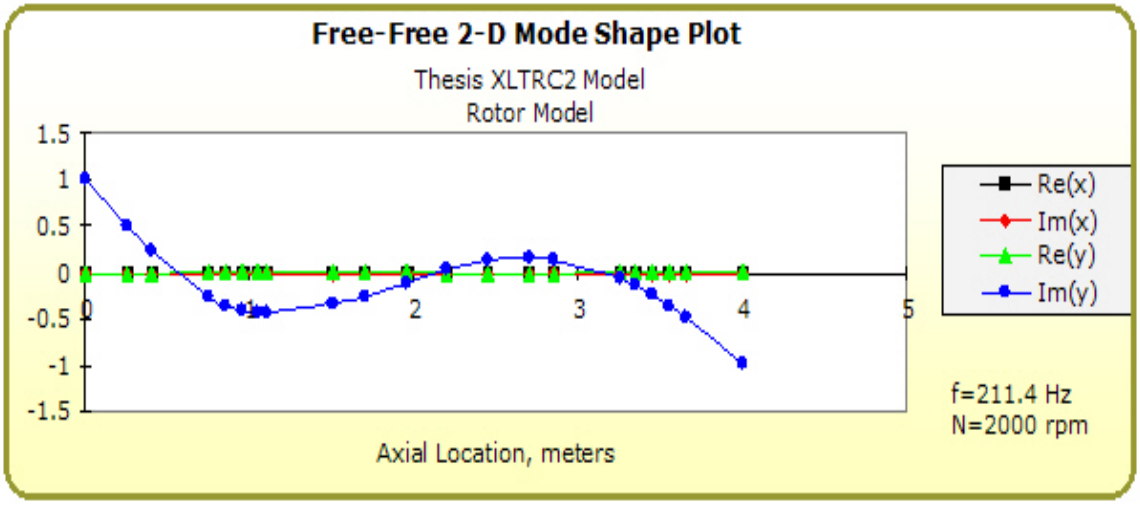

Figure 153 XLTRC^2 second bending mode at 211.41 Hz

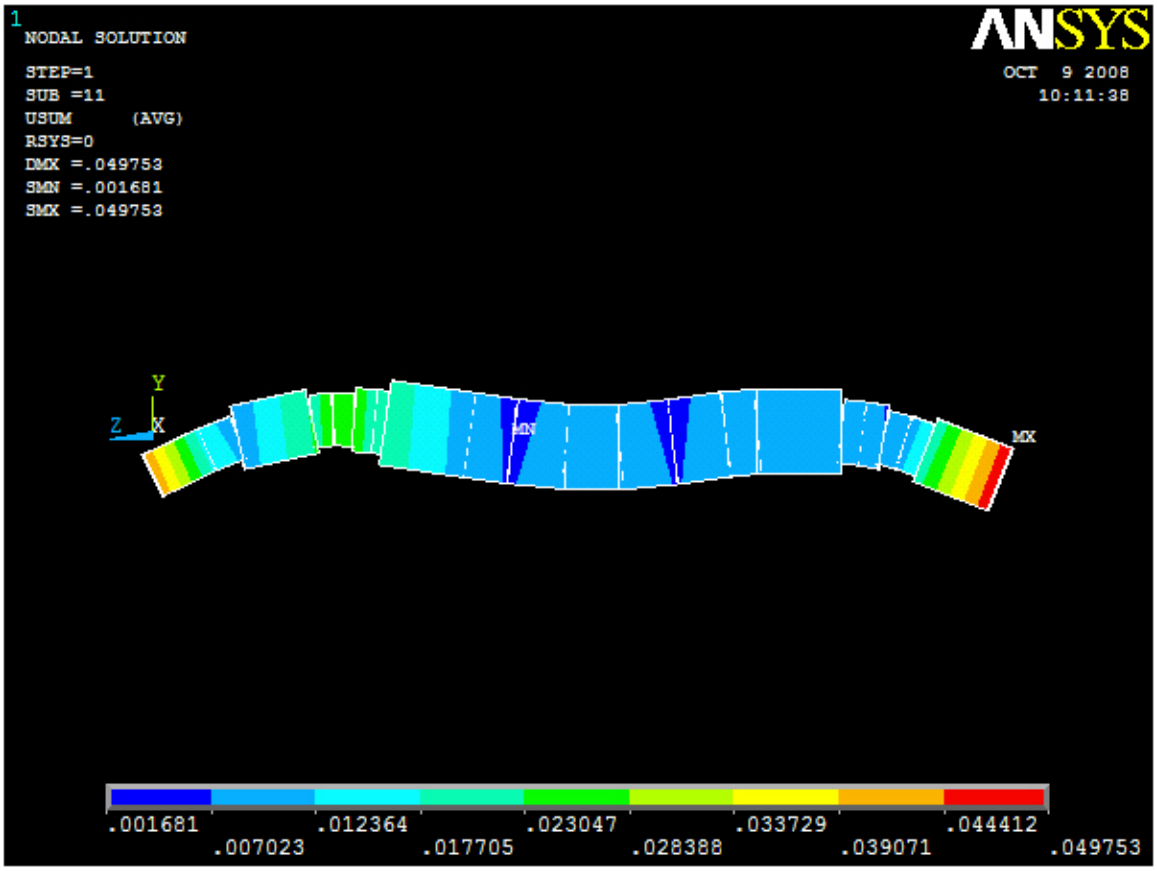

Figure 154 ANSYS third bending mode at 335.66 Hz

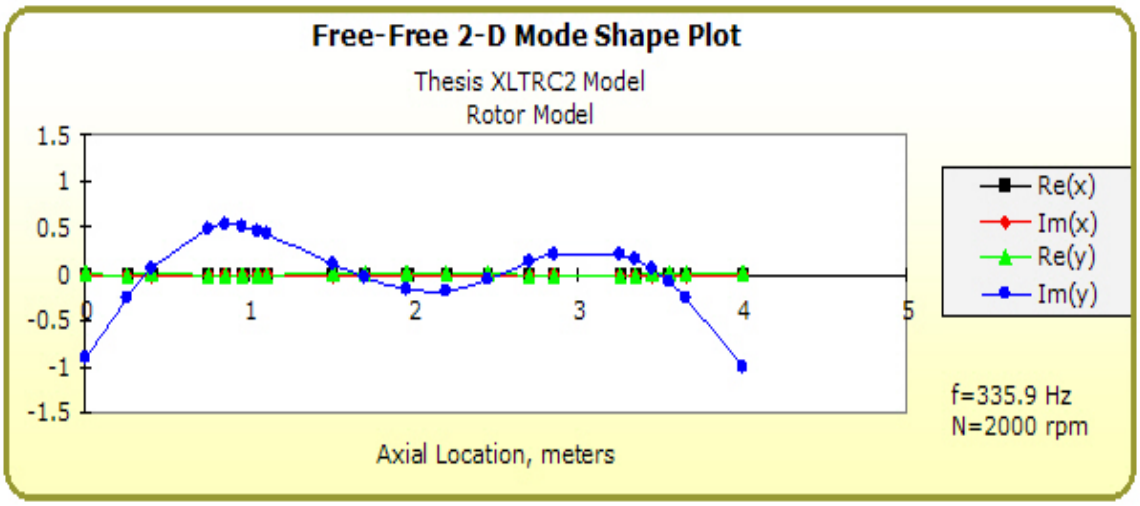

Figure 155 XLTRC^2 third bending mode at 335.88 Hz

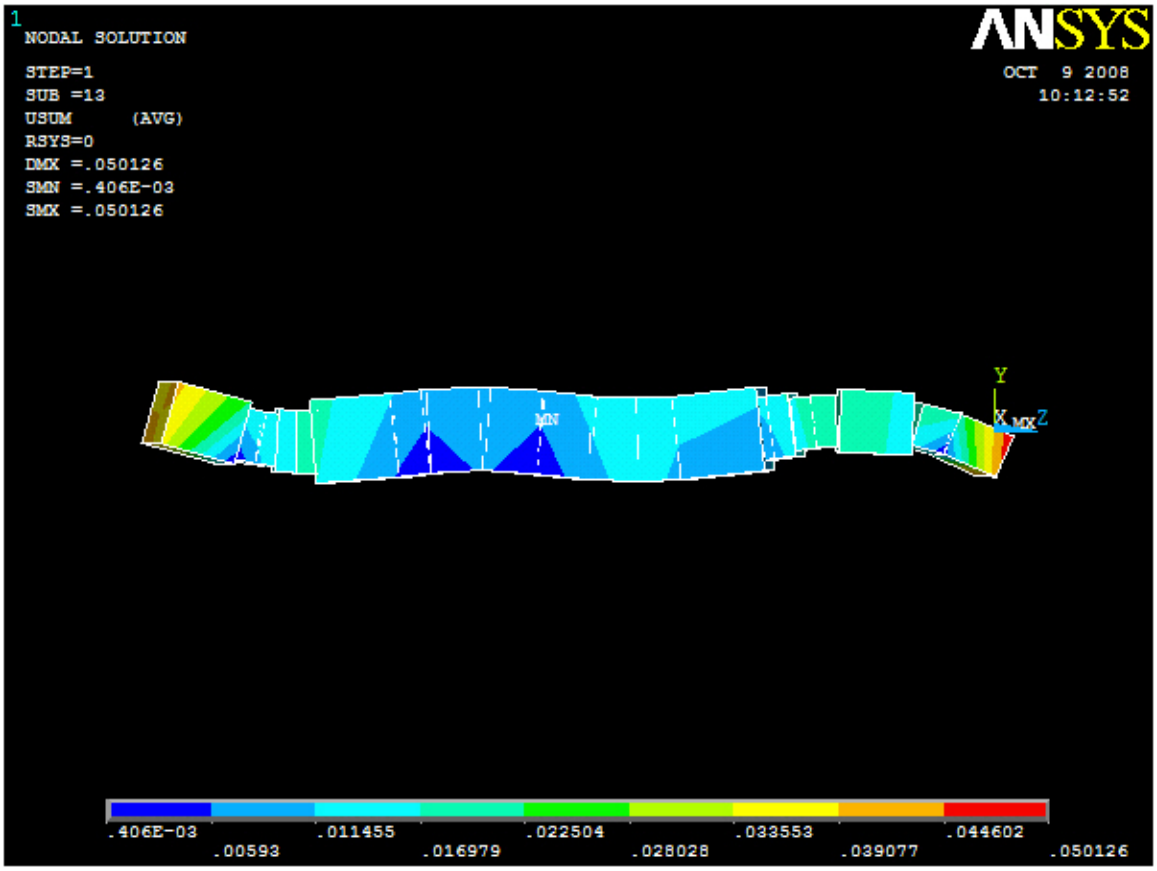

Figure 156 ANSYS fourth bending mode at 502.00 Hz

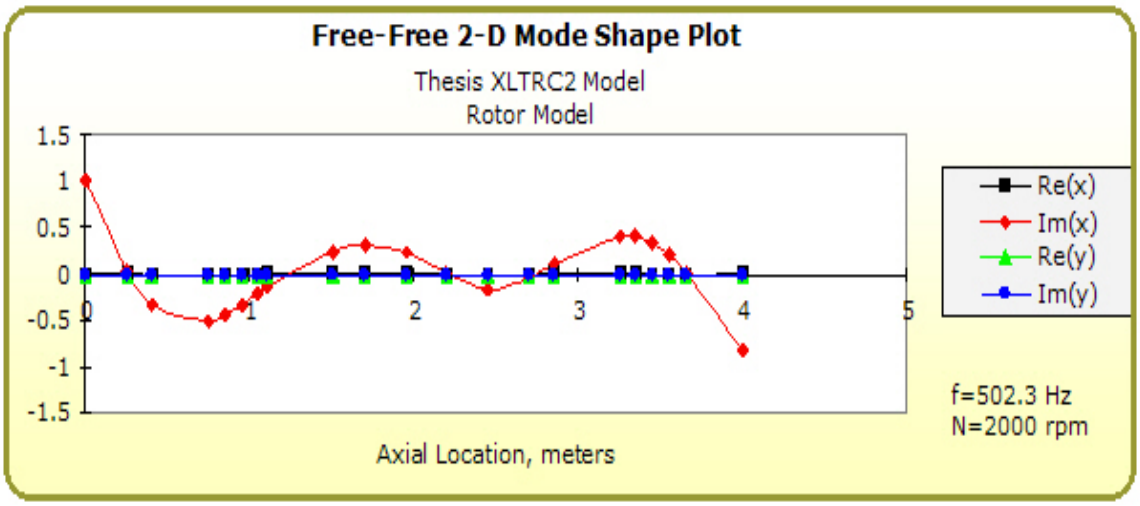

Figure 157 XLTRC^2 fourth bending mode at 502.34 Hz

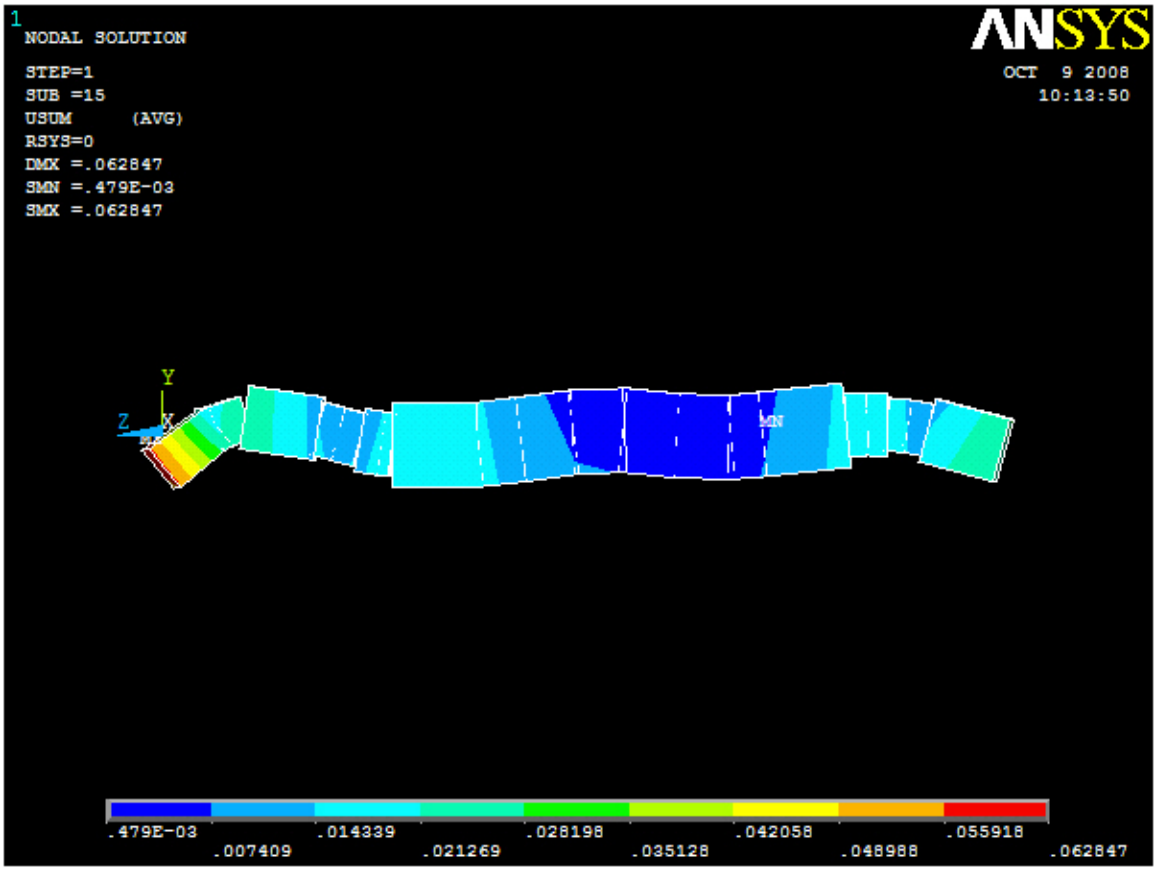

Figure 158 ANSYS fifth bending mode at 659.77 Hz

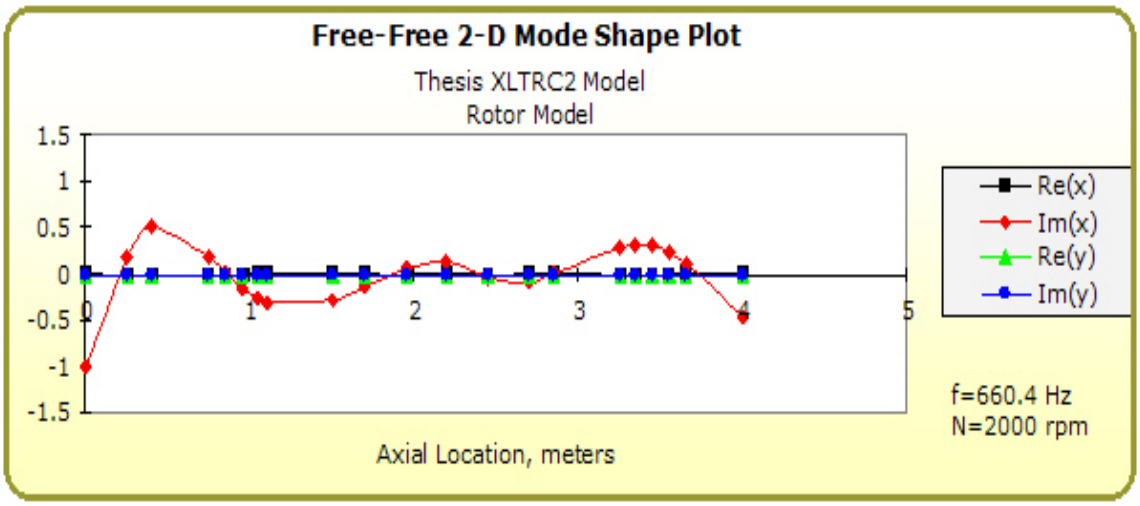

Figure 159 XLTRC^2 fifth bending mode at 660.43 Hz

APPENDIX E

APDL SOURCE CODE

E.1 Rotor Model

```
!*****************************************************************************
!*
!* PROJECT           : Thesis
!* PROJECT TITLE     : Rotor Analysis
!*
!* AUTHOR            : Stephen James
!*
!* OBJECTIVE         : 1) Build rotor model of XLTRC2 Rotor and save database
!*                     2) Compare Free-Free modes to ensure model validity
!*****************************************************************************

FINISH
/CLEAR,START
/input,start110,ans,'C:\Program Files\Ansys Inc\v110\ANSYS\apdl\',,,,,,,,,,,,,,,1
/TITLE,Thesis Rotor Model
/FILNAME,rotor_pz,1
/UNITS, SI
/GRAPHICS, POWER
/OUT,,OUT

/PREP7
/ESHAPE,1
/VIEW,1,1,1,1
/ANG,1
/REP,FAST
/PBC,ALL,,1

G=9.81               !Gravity
RPM = 2000
W=(RPM)*3.14159/30   !Change to Omega for Gyroscopics

!!!!!!!!!!!!!!!!!!!!!!!!!!!!!!!!
! MATERIAL PROPERTIES START HERE
!!!!!!!!!!!!!!!!!!!!!!!!!!!!!!!!
!Material 1 Properties
MP,EX,1,206.8423E+09
MP,PRXY,1,0.3
MP,DENS,1,7833.412
!!!!!!!!!!!!!!!!!!!!!!!!!!!!!!!!
! MATERIAL PROPERTIES END HERE
!!!!!!!!!!!!!!!!!!!!!!!!!!!!!!!!

! Beam Model
ET,101,BEAM4
KEYOPT,101,2,0
KEYOPT,101,6,0
KEYOPT,101,7,1
KEYOPT,101,9,0
KEYOPT,101,10,0

! Added Mass
ET,102,MASS21
KEYOPT,102,1,0
KEYOPT,102,2,0
KEYOPT,102,3,0
```

```
!!!!!!!!!!!!!!!!!!!!!!!!!!!!!!!
! REAL CONSTANTS FOR ENTIRE MODEL START HERE
!!!!!!!!!!!!!!!!!!!!!!!!!!!!!!!
! *** SHAFT REAL CONSTANTS ***
R,1,3.1416E-02,7.8540E-05,7.8540E-05,2.0000E-01,2.0000E-01,0.0000E+00
RMORE,0.0000E+00,3.0762E-01,1.1100E+00,1.1100E+00,2.0944E+02,0.0000E+00
R,2,3.1416E-02,7.8540E-05,7.8540E-05,2.0000E-01,2.0000E-01,0.0000E+00
RMORE,0.0000E+00,1.8457E-01,1.1100E+00,1.1100E+00,2.0944E+02,0.0000E+00
R,3,7.0686E-02,3.9761E-04,3.9761E-04,3.0000E-01,3.0000E-01,0.0000E+00
RMORE,0.0000E+00,2.1802E+00,1.1100E+00,1.1100E+00,2.0944E+02,0.0000E+00
R,4,4.9087E-02,1.9175E-04,1.9175E-04,2.5000E-01,2.5000E-01,0.0000E+00
RMORE,0.0000E+00,3.0041E-01,1.1100E+00,1.1100E+00,2.0944E+02,0.0000E+00
R,5,4.9087E-02,1.9175E-04,1.9175E-04,2.5000E-01,2.5000E-01,0.0000E+00
RMORE,0.0000E+00,3.0041E-01,1.1100E+00,1.1100E+00,2.0944E+02,0.0000E+00
R,6,7.0686E-02,3.9761E-04,3.9761E-04,3.0000E-01,3.0000E-01,0.0000E+00
RMORE,0.0000E+00,6.2293E-01,1.1100E+00,1.1100E+00,2.0944E+02,0.0000E+00
R,7,7.0686E-02,3.9761E-04,3.9761E-04,3.0000E-01,3.0000E-01,0.0000E+00
RMORE,0.0000E+00,3.1146E-01,1.1100E+00,1.1100E+00,2.0944E+02,0.0000E+00
R,8,1.2566E-01,1.2566E-03,1.2566E-03,4.0000E-01,4.0000E-01,0.0000E+00
RMORE,0.0000E+00,7.8750E+00,1.1100E+00,1.1100E+00,2.0944E+02,0.0000E+00
R,9,1.2566E-01,1.2566E-03,1.2566E-03,4.0000E-01,4.0000E-01,0.0000E+00
RMORE,0.0000E+00,3.9375E+00,1.1100E+00,1.1100E+00,2.0944E+02,0.0000E+00
R,10,1.2566E-01,1.2566E-03,1.2566E-03,4.0000E-01,4.0000E-01,0.0000E+00
RMORE,0.0000E+00,4.9219E+00,1.1100E+00,1.1100E+00,2.0944E+02,0.0000E+00
R,11,1.2566E-01,1.2566E-03,1.2566E-03,4.0000E-01,4.0000E-01,0.0000E+00
RMORE,0.0000E+00,2.4609E+00,1.1100E+00,1.1100E+00,2.0944E+02,0.0000E+00
R,12,1.2566E-01,1.2566E-03,1.2566E-03,4.0000E-01,4.0000E-01,0.0000E+00
RMORE,0.0000E+00,2.4609E+00,1.1100E+00,1.1100E+00,2.0944E+02,0.0000E+00
R,13,1.2566E-01,1.2566E-03,1.2566E-03,4.0000E-01,4.0000E-01,0.0000E+00
RMORE,0.0000E+00,4.9219E+00,1.1100E+00,1.1100E+00,2.0944E+02,0.0000E+00
R,14,1.2566E-01,1.2566E-03,1.2566E-03,4.0000E-01,4.0000E-01,0.0000E+00
RMORE,0.0000E+00,4.9219E+00,1.1100E+00,1.1100E+00,2.0944E+02,0.0000E+00
R,15,1.2566E-01,1.2566E-03,1.2566E-03,4.0000E-01,4.0000E-01,0.0000E+00
RMORE,0.0000E+00,2.9531E+00,1.1100E+00,1.1100E+00,2.0944E+02,0.0000E+00
R,16,1.2566E-01,1.2566E-03,1.2566E-03,4.0000E-01,4.0000E-01,0.0000E+00
RMORE,0.0000E+00,7.8750E+00,1.1100E+00,1.1100E+00,2.0944E+02,0.0000E+00
R,17,7.0686E-02,3.9761E-04,3.9761E-04,3.0000E-01,3.0000E-01,0.0000E+00
RMORE,0.0000E+00,6.2293E-01,1.1100E+00,1.1100E+00,2.0944E+02,0.0000E+00
R,18,7.0686E-02,3.9761E-04,3.9761E-04,3.0000E-01,3.0000E-01,0.0000E+00
RMORE,0.0000E+00,6.2293E-01,1.1100E+00,1.1100E+00,2.0944E+02,0.0000E+00
R,19,4.9087E-02,1.9175E-04,1.9175E-04,2.5000E-01,2.5000E-01,0.0000E+00
RMORE,0.0000E+00,3.0041E-01,1.1100E+00,1.1100E+00,2.0944E+02,0.0000E+00
R,20,4.9087E-02,1.9175E-04,1.9175E-04,2.5000E-01,2.5000E-01,0.0000E+00
RMORE,0.0000E+00,3.0041E-01,1.1100E+00,1.1100E+00,2.0944E+02,0.0000E+00
R,21,7.0686E-02,3.9761E-04,3.9761E-04,3.0000E-01,3.0000E-01,0.0000E+00
RMORE,0.0000E+00,2.1802E+00,1.1100E+00,1.1100E+00,2.0944E+02,0.0000E+00

! *** ADDED MASS REAL CONSTANTS ***
R,230,120,120,120,5,5,5
R,231,100,100,100,10,10,20
R,232,100,100,100,10,10,20
R,233,1000,1000,1000,100,100,175
R,234,1000,1000,1000,100,100,175
R,235,1000,1000,1000,100,100,175
R,236,100,100,100,10,10,20
!!!!!!!!!!!!!!!!!!!!!!!!!!!!!!!
! REAL CONSTANTS FOR ENTIRE MODEL END HERE
!!!!!!!!!!!!!!!!!!!!!!!!!!!!!!!

!!!!!!!!!!!!!!!!!!!!!!!!!!!!!!!
! NODE DEFINITIONS START HERE
!!!!!!!!!!!!!!!!!!!!!!!!!!!!!!!
N,1,0,0,0.00000
N,2,0,0,0.25000
N,3,0,0,0.40000
N,4,0,0,0.75000
N,5,0,0,0.85000
N,6,0,0,0.95000
N,7,0,0,1.05000
N,8,0,0,1.10000
N,9,0,0,1.50000
N,10,0,0,1.70000
```

```
N,11,0,0,1.95000
N,12,0,0,2.07500
N,13,0,0,2.20000
N,14,0,0,2.45000
N,15,0,0,2.70000
N,16,0,0,2.85000
N,17,0,0,3.25000
N,18,0,0,3.35000
N,19,0,0,3.45000
N,20,0,0,3.55000
N,21,0,0,3.65000
N,22,0,0,4.00000
!!!!!!!!!!!!!!!!!!!!!!!!!!!!!!!!
! NODE DEFINITIONS END HERE
!!!!!!!!!!!!!!!!!!!!!!!!!!!!!!!!

!!!!!!!!!!!!!!!!!!!!!!!!!!!!!!!!
! ELEMENT DEFINITIONS START HERE
!!!!!!!!!!!!!!!!!!!!!!!!!!!!!!!!
TYPE,101

! *** SHAFT ELEMENTS ***
MAT,1
REAL,1
E,1,2
MAT,1
REAL,2
E,2,3
MAT,1
REAL,3
E,3,4
MAT,1
REAL,4
E,4,5
MAT,1
REAL,5
E,5,6
MAT,1
REAL,6
E,6,7
MAT,1
REAL,7
E,7,8
MAT,1
REAL,8
E,8,9
MAT,1
REAL,9
E,9,10
MAT,1
REAL,10
E,10,11
MAT,1
REAL,11
E,11,12
MAT,1
REAL,12
E,12,13
MAT,1
REAL,13
E,13,14
MAT,1
REAL,14
E,14,15
MAT,1
REAL,15
E,15,16
MAT,1
REAL,16
E,16,17
MAT,1
REAL,17
```

```
E,17,18
MAT,1
REAL,18
E,18,19
MAT,1
REAL,19
E,19,20
MAT,1
REAL,20
E,20,21
MAT,1
REAL,21
E,21,22

TYPE,102
MAT,1

! *** ADDED MASS ELEMENTS ***
REAL,230
E,2
REAL,231
E,10
REAL,232
E,11
REAL,233
E,13
REAL,234
E,14
REAL,235
E,15
REAL,236
E,16

!!!!!!!!!!!!!!!!!!!!!!!!!!!!!!!!
! ELEMENT DEFINITIONS END HERE
!!!!!!!!!!!!!!!!!!!!!!!!!!!!!!!!

CSYS, 0
/NUMBER,1
/PNUM,REAL,1
/REPLOT
EPLOT

ALLSEL,ALL
CM,ROTOR,ELEM

/PREP7
!LIST ALL NODES TO OUTPUT FILE FOR REFERENCE
NLIST,ALL, , , ,NODE,NODE,NODE

! Enter solution processor for static analysis to include pre-stress effects
/SOLU
ANTYPE,STATIC,NEW
PSTRES,ON
CORIOLIS,ON,,,ON
CMOMEGA,ROTOR, , , W
SOLVE
FINISH

! Enter solution processor for modal analysis
/SOLU
ANTYPE,MODAL
MODOPT,QRDAMP,60
MXPAND,60
DMPRAT,0.0
PSTRES,ON
CORIOLIS,ON,,,ON
CMOMEGA,ROTOR, , , W
SOLVE

FINISH
/EOF
```

E.2 Substructure Algorithm for Axisymmetric Casing Model

```
!*****************************************************************************
!*
!*
!* PROJECT           : Thesis
!* PROJECT TITLE     : Axisymmetric Casing Substructuring Analysis
!*
!* AUTHOR            : Stephen James
!*
!* OBJECTIVE         : 1) Define bearing center nodes and constrained locations
!*                     2) Create substructure of axisymmetric casing model
!*
!*****************************************************************************
*


FINISH

! Header
/TITLE,Axisymmetric Casing
/CLEAR,START
/input,start110,ans,'C:\Program Files\Ansys Inc\v110\ANSYS\apdl\',,,,,,,,,,,,,,,1
/FILNAME,symmcas,1
/UNITS, SI
/GRAPHICS, POWER
/OUT,,OUT

! Resume casing model
RESUME
/PREP7
/ESHAPE,1
/VIEW,1,1,1,1
/ANG,1
/REP,FAST
/PBC,ALL,,1

EPLOT

!define matl props for rigid beams
MP,DENS,2000,0.01

!define beam element type
ET,2000,MPC184
KEYOPT,2000,1,1             ! Rigid Beam Behavior
KEYOPT,2000,2,0             ! Direct elimination reduction method

!switch to global coor system first
CSYS,0

! Create center nodes
! Bearing 1
N,500005,0.0,0.0,0.850
! Seal location
N,500012,0.0,0.0,2.075
! Bearing 2
N,500020,0.0,0.0,3.550

!mesh rigid connections
TYPE,2000
MAT,2000

! Bearing 1
E,500005,35898
E,500005,27789
E,500005,27439
E,500005,33877

! Seal
E,500012,33394
E,500012,24644
```

```
E,500012,24562
E,500012,5690

! Bearing 2
E,500020,25653
E,500020,27109
E,500020,26035
E,500020,23672

! Delete the existing constraints on the casing model so that
! CMS includes these coordinates in the substructure.
DDELE,36724,ALL,36738,2

! Select center nodes as master dof
M,500005,ALL
M,500012,ALL
M,500020,ALL

! Select constraint locations as master dof
M,36724,ALL
M,36726,ALL
M,36728,ALL
M,36730,ALL
M,36732,ALL
M,36734,ALL
M,36736,ALL
M,36738,ALL

EPLOT
/AUTO,1
/REP,FAST
/TRIAD,RBOT

! Show coordinate system on display
/PSYMB,CS,1

! Enter solution processor for substructure analysis
/SOLU
ANTYPE,SUBSTR
! Specify CMS reduction option
CMSOPT,FIX,15,,,
SEOPT,SYMMCAS,2,1,0, RESOLVE
EQSLV,SPARSE

! Create substructure file listing
SOLVE
SELIST,,0

FINISH
/OUT
/EOF
```

E.3 Substructure Algorithm for Non–Axisymmetric Casing Model

```
!*****************************************************************************
!*
!* PROJECT           : Thesis
!* PROJECT TITLE     : Non-axisymmetric Casing Substructuring Analysis
!*
!* AUTHOR            : Stephen James
!*
!* OBJECTIVE         : 1) Define bearing center nodes and constrained locations
!*                     2) Create substructure of non-axisymmetric casing model
!*
!*****************************************************************************

FINISH
! Header
/TITLE,Non-axisymmetric Casing
/CLEAR,START
/input,start110,ans,'C:\Program Files\Ansys Inc\v110\ANSYS\apdl\',,,,,,,,,,,,,,,1
/FILNAME,nsymmcas,1
/UNITS, SI
/GRAPHICS, POWER
/OUT,,OUT

! Resume casing model
RESUME
/PREP7
/ESHAPE,1
/VIEW,1,1,1,1
/ANG,1
/REP,FAST
/PBC,ALL,,1

EPLOT

!define matl props for rigid beams
MP,DENS,2000,0.01

!define beam element type
ET,2000,MPC184
KEYOPT,2000,1,1             ! Rigid beam behavior
KEYOPT,2000,2,0             ! Direct elimination reduction method

!switch to global coor system first
CSYS,0

! Create center nodes
! Drive End (DE) Bearing 1
N,500005,0.0,0.0,0.850
! Seal location
N,500012,0.0,0.0,2.075
! Non-Drive End (NDE) Bearing 2
N,500020,0.0,0.0,3.550

!mesh rigid connections
TYPE,2000
MAT,2000

! Bearing 1
E,500005,24298
E,500005,24470
E,500005,23658
E,500005,37521

! Seal
E,500012,30742
E,500012,24186
E,500012,27404
E,500012,26300
```

```
! Bearing 2
E,500020,35147
E,500020,6069
E,500020,5736
E,500020,5627

! Delete the existing constraints on the casing model so that
! CMS includes these coordinates in the substructure.
DDELE,39392,ALL,39406,2

! Select center nodes as master dof
M,500005,ALL
M,500012,ALL
M,500020,ALL

! Select constraint locations as master dof
M,39392,ALL
M,39394,ALL
M,39396,ALL
M,39398,ALL
M,39400,ALL
M,39402,ALL
M,39404,ALL
M,39406,ALL

EPLOT
/AUTO,1
/REP,FAST
/TRIAD,RBOT

! Show coordinate system on display
/PSYMB,CS,1

! Enter solution processor for substructure analysis
/SOLU
ANTYPE,SUBSTR
! Specify CMS reduction option
CMSOPT,fix,15,,,
SEOPT,NSYMMCAS,2,1,0, RESOLVE
EQSLV,SPARSE

/EOF

! Create substructure file listing
SOLVE
SELIST,,0
FINISH

/OUT

/EOF
```

E.4 Unbalance Response Algorithm for Coupled Rotor and Non–Axisymmetric Casing Model

```
!*************************************************************************
!*
!* PROJECT           : Thesis
!* PROJECT TITLE     : Coupled Non-Axisymmetric Rotor-Casing Analysis
!*
!* AUTHOR            : Stephen James
!*
!* OBJECTIVE         : 1) Import rotor and non-axisymmetric databases
!*                     2) Use bearing and seal coefficients
!*                     3) Calculate forced unbalance response of combined  model
!*
!*************************************************************************

FINISH
! ** HEADER INFORMATION **
/CLEAR,START
/input,start110,ans,'C:\Program Files\Ansys Inc\v110\ANSYS\apdl\',,,,,,,,,,,,,,,1
/TITLE, COUPLED NON-AXISYMM ROTOR-CASING UNBAL RESP

! ** RESUME ROTOR MODEL **
RESUME,rotor_pz,DB

! Define rotor component as group of all existing elements in resumed rotor model
CM, ROTOR, ELEM

/FILNAME,nsymm_rc_unbal,1

! ** GRAPHIC SETTINGS **
/UNITS, SI
/GRAPHICS, POWER
/OUT,,OUT

/PREP7
/ESHAPE,1
/VIEW,1,1,1,1
/ANG,1
/PBC,ALL,,1
CSYS, 0
/NUMBER,1
/PNUM,NODE,1
/PNUM,REAL,1

! Define superelement and import casing model as a superelement
ET,3000,MATRIX50
TYPE,3000
REAL,3000
SE,nsymmcas,,,0.1

/REPLOT
EPLOT

! ** INPUT FOR UNBALANCE RESPONSE **
 minrpm=    50              ! minimum response speed in rpm
 maxrpm=  4200              ! maximum response speed in rpm
 incrpm=    10              ! speed increment in rpm
    MR8= 40000.00    ! Unbalance from XLTRC2 Model at station 8
   MR17= 45000.00    ! Unbalance from XLTRC2 Model at station 17


! ** UNBALANCE LOAD AND RESPONSE STATIONS **
  ucase =       2    ! 1 = Unbalance at mid-span station 12
                     ! 2 = Unbalance at stations 8 and 17
inc_seal=       1    ! 0 = DO NOT include seal  model, 1 = include seal
     ua =       8    ! bearing 1 unbalance node number
     ub =      12    ! mid-span unbalance node number
     uc =      17    ! bearing 2 unbalance node number
    pra =       5    ! bearing 1 probe node number on rotor - output station
```

```
    pca=   500005    ! bearing 1 probe node number on casing - output station
    prb =      12    ! seal probe node number on rotor - output station
    pcb =  500012    ! seal probe node number on rotor - output station
    prc =      20    ! bearing 2 probe node number on rotor - output station
    pcc=   500020    ! bearing 2 probe node number on casing - output station

/PREP7

! ** REAL CONSTANT DEFINITIONS **
  rbrg1 =   1000     ! real consant set number for bearing 1
  rbrg2 =   rbrg1+2  ! real consant set number for bearing 2

 rtrnd1 =      5     ! rotor brg1 node
 casnd1 = 500005     ! casing brg1 node

 rtrnd2 =     20     ! rotor brg2 node
 casnd2 = 500020     ! casing brg2 node

*IF,inc_seal,EQ,1,THEN
       rtrnd3 =     12      ! rotor seal node
       casnd3 = 500012      ! casing seal node

       rsealK = 2000
       rsealC = 2001
       rsealM = 2002

       ! Call to seal macro
       seal,rsealK,rsealC,rsealM
*ENDIF

! ** GET STATION COORDINATES **
*GET,BRG1X,NODE,rtrnd1,LOC,X
*GET,BRG1Y,NODE,rtrnd1,LOC,Y
*GET,BRG1Z,NODE,rtrnd1,LOC,Z
*GET,BRG2Z,NODE,rtrnd2,LOC,Z
*IF,inc_seal,EQ,1,THEN
       *GET,BRG3Z,NODE,rtrnd3,LOC,Z
*ENDIF

! ** ROTATION DIRECTION **
! Check for +Z rotation vector - this insures that the shaft rotation
! is always about the +Z axis
*IF,BRG1Z,GT,BRG2Z,THEN
       RTR1Z=BRG2Z
       RTR2Z=BRG1Z
*ELSE
       RTR1Z=BRG1Z
       RTR2Z=BRG2Z
*ENDIF

! Show local coordinate system (CS) and nodal CS symbols on display
/PSYMB,CS,1
/PSYMB,NDIR,1

! ** OUTPUT ARRAY DEFINITIONS **
*AFUN,DEG                          ! output phase angle in degrees
*dim,UOUT,array,1,2                ! output array to hold real and imaginary part
ncol=(maxrpm-minrpm)/incrpm+1
*dim,rs,array,24,ncol              ! main array
*dim,rsr,array,12,ncol             ! array to store rotor info
*dim,rsc,array,12,ncol             ! array to store casing info

col=0

/PREP7
ET,105,COMBI214,,0,1        ! 2-D Spring-Damper element used to represent bearing

! Add constraints to all DOFs at baseplate nodes
D,39392,ALL,,,39406,2

! Create a status bar to show progress
*ABSET, 'Unbalance Response Solution Progress',BAR
```

```
! Scales the progress bar to (0 to 100%) scale
pncol=ncol/100

! Refresh the display screen
/AUTO,1
/REP,FAST


! ** UNBALANCE RESPONSE LOOP STARTS **
*DO,RPM,minrpm,maxrpm,incrpm
       col=col+1

       ! Update the progress bar
       REMAINDER = MOD(col,pncol)
       *IF,REMAINDER,EQ,0,THEN
              *abcheck,col/pncol
       *ENDIF

       /PREP7
       *MSG,NOTE,RPM
       Calc Response for %I rpm

       HZ=RPM/60                          !Change to Hz for Harmic
       W=(RPM)*3.14159/30          !Change to Omega for Gyroscopics
       W2=W**2

       ! Select unbalance case
       *IF,ucase,EQ,1,THEN
              FUNBAL0= (MR8+MR17)*W2*.001*.001
       *ELSEIF,ucase,EQ,2,THEN
              FUNBAL1= MR8*W2*.001*.001
              FUNBAL2=MR17*W2*.001*.001
       *ENDIF

       ! Call to bearing macros
       brg1,rpm,rbrg1,1
       brg2,rpm,rbrg2,2

       !ONLY MESH ON FIRST LOOP
       *IF,RPM,EQ,minrpm,THEN
              *IF,inc_seal,EQ,1,THEN
                     TYPE,106
                     !Stiffness at seal location
                     REAL,rsealK
                     E,rtrnd3,casnd3

                     TYPE,107
                     !Damping at seal location
                     REAL,rsealC
                     E,rtrnd3,casnd3

                     TYPE,108
                     !Inertia  at seal location
                     REAL,rsealM
                     E,rtrnd3,casnd3
              *ENDIF

              TYPE,105

              !Bearing 1
              REAL,rbrg1
              E,rtrnd1,casnd1

              !Bearing 2
              REAL,rbrg2
              E,rtrnd2,casnd2
       *ENDIF

       ! ** SOLUTION PROCESSOR **
       /SOLU
       ANTYPE,HARMIC
       DMPRAT,strdamp
```

```
        coriolis,on,,,on
        CMOMEGA, rotor, W, , , BRG1X, BRG1Y, RTR1Z, BRG1X, BRG1Y, RTR2Z, 0
        HROPT,FULL
        HROUT,OFF
        OUTPR,ALL,NONE
        NSUBST,1
        HARFRQ,HZ,HZ
        KBC,1

        *IF,ucase,EQ,1,THEN                ! Unbalance at rotor midspan
               F,ub,FX, 0, FUNBAL0
               F,ub,FY, FUNBAL0, 0
        *ELSEIF,ucase,EQ,2,THEN            ! Unbalances at outer stations
               !UNBALANCE COUPLE AT STATION 8
               F,ua,FX, 0, FUNBAL1
               F,ua,FY, FUNBAL1, 0

               !UNBALANCE COUPLE AT STATION 17
               F,uc,FX, 0, FUNBAL2
               F,uc,FY, FUNBAL2, 0
        *ENDIF

        SOLVE
        FINISH

        ! ** POST-PROCESSOR **
        /POST26
        PRCPLX,1

        ! Overide default 10 variables allowed in POST26
        NUMVAR, 13

         NSOL,  2, pra,U,X
         NSOL,  3, pra,U,Y
         NSOL,  4, prb,U,X
         NSOL,  5, prb,U,Y
         NSOL,  6, prc,U,X
         NSOL,  7, prc,U,Y
         NSOL,  8, pca,U,X
         NSOL,  9, pca,U,Y
         NSOL, 10, pcb,U,X
         NSOL, 11, pcb,U,Y
         NSOL, 12, pcc,U,X
         NSOL, 13, pcc,U,Y

        STORE,MERGE

        *DO,parm,1,12,1
               row=(parm-1)*2+1

               VGET,UOUT(1,1),parm+1,,0
               VGET,UOUT(1,2),parm+1,,1

               rs(row,col)=SQRT((UOUT(1,1))**2+(UOUT(1,2))**2)
               ! Use ATAN2 because it correctly takes care of the signs in the phase
               rs(row+1,col)=ATAN2(UOUT(1,2),UOUT(1,1))
        *ENDDO
        FINISH
*ENDDO

! Close the progress bar
*abfinish
FINISH

! Split into two arrays for two reasons:
! (1) *VWRITE can only output 19 parms at a time.
! (2) Even with two files, the array outputs more values to file than array index
*DO,row,1,12,1
        *DO,col,1,ncol,1
               rsr(row,col)=rs(row,col)
        *ENDDO
*ENDDO
```

```
*DO,row,1,12,1
       *DO,col,1,ncol,1
              rsc(row,col)=rs(row+12,col)
       *ENDDO
*ENDDO


! Reset message status boxes
/UIS, MSGPOP, 2
/UIS, ABORT, ON

! Refresh the display screen
/AUTO,1
/REP,FAST

PRINT_PHASE = 1             ! 0=Do not print phase, 1=Print phase in output file

! ** CREATE TWO OUTPUT FILES (ROTOR AND CASING) BECASUSE *VWRITE SUPPORTS MAX 19
PARMS OUTPUT

! ** ROTOR ABSOLUTE FILE
! Open formatted text file for output of response at required locations
*CFOPEN,UNBAL_UR%ucase%,OUT,,

! Ouput file header info
*IF,PRINT_PHASE,EQ,1,THEN
*VWRITE,'RPM','MX_R%pra%','PX_R%pra%','MY_R%pra%','PY_R%pra%','MX_R%prb%','PX_R%prb
%','MY_R%prb%','PY_R%prb%','MX_R%prc%','PX_R%prc%','MY_R%prc%','PY_R%prc%'
(4X,A8,6X,A8,6X,A8,6X,A8,6X,A8,6X,A8,6X,A8,6X,A8,6X,A8,6X,A8,6X,A8,6X,A8)
*ELSE
*VWRITE,'RPM','MX_R%pra%','MY_R%pra%','MX_R%prb%','MY_R%prb%','MX_R%prc%','MY_R%prc
%'
(4X,A8,6X,A8,6X,A8,6X,A8,6X,A8,6X,A8,6X,A8)
*ENDIF

rw=0
*DO,rpm,minrpm,maxrpm,incrpm
  rw=rw+1

! Amplitude in ANSYS is 0-pk. To compare to XLTRC2 multiply by 2.
! Here 2000 is for conversion of 0-pk to pk-pk and m to mm.

*IF,PRINT_PHASE,EQ,1,THEN
*VWRITE,rpm,rsr(1,rw)*2000,rsr(2,rw),rsr(3,rw)*2000,rsr(4,rw),rsr(5,rw)*2000,rsr(6,
rw),rsr(7,rw)*2000,rsr(8,rw),rsr(9,rw)*2000,rsr(10,rw),rsr(11,rw)*2000,rsr(12,rw)
(E12.4,2X,E12.4,2X,E12.4,2X,E12.4,2X,E12.4,2X,E12.4,2X,E12.4,2X,E12.4,2X,E12.4,2X,E
12.4,2X,E12.4,2X,E12.4,2X,E12.4)
*ELSE
*VWRITE,rpm,rsr(1,rw)*2000,rsr(3,rw)*2000,rsr(5,rw)*2000,rsr(7,rw)*2000,rsr(9,rw)*2
000,rsr(11,rw)*2000
(E12.4,2X,E12.4,2X,E12.4,2X,E12.4,2X,E12.4,2X,E12.4,2X,E12.4)
*ENDIF

*ENDDO
*CFCLOSE

! ** CASING ABSOLUTE FILE
! Open formatted text file for output of response at required locations
*CFOPEN,UNBAL_UC%ucase%,OUT,,

! Ouput file header info
*IF,PRINT_PHASE,EQ,1,THEN
*VWRITE,'RPM','MX_C%pra%','PX_C%pra%','MY_C%pra%','PY_C%pra%','MX_C%prb%','PX_C%prb
%','MY_C%prb%','PY_C%prb%','MX_C%prc%','PX_C%prc%','MY_C%prc%','PY_C%prc%'
(4X,A8,6X,A8,6X,A8,6X,A8,6X,A8,6X,A8,6X,A8,6X,A8,6X,A8,6X,A8,6X,A8,6X,A8)
*ELSE
*VWRITE,'RPM','MX_C%pra%','MY_C%pra%','MX_C%prb%','MY_C%prb%','MX_C%prc%','MY_C%prc
%'
(4X,A8,6X,A8,6X,A8,6X,A8,6X,A8,6X,A8,6X,A8)
*ENDIF
```

```
rw=0
*DO,rpm,minrpm,maxrpm,incrpm
  rw=rw+1

! Amplitude in ANSYS is 0-pk. To compare to XLTRC2 multiply by 2.
! Here 2000 is for conversion of 0-pk to pk-pk and m to mm.

*IF,PRINT_PHASE,EQ,1,THEN
*VWRITE,rpm,rsc(1,rw)*2000,rsc(2,rw),rsc(3,rw)*2000,rsc(4,rw),rsc(5,rw)*2000,rsc(6,
rw),rsc(7,rw)*2000,rsc(8,rw),rsc(9,rw)*2000,rsc(10,rw),rsc(11,rw)*2000,rsc(12,rw)
(E12.4,2X,E12.4,2X,E12.4,2X,E12.4,2X,E12.4,2X,E12.4,2X,E12.4,2X,E12.4,2X,E12.4,2X,E
12.4,2X,E12.4,2X,E12.4,2X,E12.4)
*ELSE
*VWRITE,rpm,rsc(1,rw)*2000,rsc(3,rw)*2000,rsc(5,rw)*2000,rsc(7,rw)*2000,rsc(9,rw)*2
000,rsc(11,rw)*2000
(E12.4,2X,E12.4,2X,E12.4,2X,E12.4,2X,E12.4,2X,E12.4,2X,E12.4)
*ENDIF

*ENDDO
*CFCLOSE

/EOF


!*************************************************************************
!* PROJECT           : Thesis
!* PROJECT TITLE     : Bearing 1 macro[12]
!*
!* AUTHOR            : Stephen James
!*
!* OBJECTIVE         : 1) Calculate speed dependent bearing coefficients
!*************************************************************************

! Input parameters from main file
   rpm= arg1
  rbrg= arg2
brgnum= arg3

*MSG, NOTE, brgnum, rpm
Setting Bearing Location %I Coefficients for %I rpm

! Create real constant set
R,rbrg

! The curve fit coefficients are taken from the XLTRC2 bearing sheet
! Stiffness coefficients
KXX=    1066393315*(RPM**(-1))        +    255286980.2    +    31095.3652*RPM    -
2.172088328*(RPM**(2))
KXY=-30104742824*(RPM**(-1))    -    27798078.92        +    102487.8616*RPM    -
2.4442301*(RPM**(2))
KYX=-59619636440*(RPM**(-1))     -     510140831.9     +     24557.04362*RPM     -
13.0524594*(RPM**(2))
KYY=2.31531E+11*(RPM**(-1))     +     487023684.1     -     128187.9399*RPM     +
20.20956004*(RPM**(2))

! Damping coefficients
CXX=       1126279319*(RPM**(-1))        +    2268914.8    -    725.3190345*RPM    +
0.142588357*(RPM**(2))
CXY=-2842395798*(RPM**(-1))    -    508206.302         +    381.4519148*RPM    -
0.087678631*(RPM**(2))
CYX=    -2842391408*(RPM**(-1))    -    508206.8736    +    381.454552*RPM    -
0.087677984*(RPM**(2))
CYY=13263960051*(RPM**(-1))     -     5519587.151     +     2683.710808*RPM     -
0.378480913*(RPM**(2))

!  Real Constants order in ANSYS for COMBI214 element:
!  K11, K22, K12, K21 , C11, C22, C12, C21
```

[12] Bearing 2 macro has not been included because it differs only in the curve fit data

```
! Assign calculated values to real constant set
RMODIF,rbrg, 1, KXX
RMODIF,rbrg, 2, KYY
RMODIF,rbrg, 3, KXY
RMODIF,rbrg, 4, KYX
RMODIF,rbrg, 5, CXX
RMODIF,rbrg, 6, CYY
RMODIF,rbrg, 7, CXY
RMODIF,rbrg, 8, CYX


!*************************************************************************
!* PROJECT           : Thesis
!* PROJECT TITLE     : Seal macro
!* AUTHOR            : Stephen James
!* OBJECTIVE         : 1) Use seal coefficients. Speed independent coefficients
!*                       are used here, however the macro file can be easily
!*                       adapted for speed-dep coeff.
!*************************************************************************
rsealK = arg1
rsealC = arg2
rsealM = arg3

KXX    =      150000000
KXY    =      0
KYX    =      0
KYY    =      150000000

CXX    =      500000
CXY    =      0
CYX    =      0
CYY    =      500000

MXX    =      15
MXY    =      0
MYX    =      0
MYY    =      15

! The indices of the RMODIF statement are very important and have changed between
ANSYS versions 10 and 11.
!
! Unsymmetric Stiffness Matrix
!
ET,106, MATRIX27,,2,4,0
R,rsealK
RMODIF,rsealK,  1, KXX  ! KXX
RMODIF,rsealK, 79, KXX
RMODIF,rsealK,  7,-KXX  !-KXX
RMODIF,rsealK, 73,-KXX  !
RMODIF,rsealK, 14, KYY  ! KYY
RMODIF,rsealK, 92, KYY
RMODIF,rsealK, 20,-KYY  !-KYY
RMODIF,rsealK, 86,-KYY  !
RMODIF,rsealK,  2, KXY  ! KXY
RMODIF,rsealK, 80, KXY
RMODIF,rsealK,  8,-KXY  !-KXY
RMODIF,rsealK, 74,-KXY  !
RMODIF,rsealK, 13, KYX  ! KYX
RMODIF,rsealK, 91, KYX
RMODIF,rsealK, 19,-KYX  !-KYX
RMODIF,rsealK, 85,-KYX

!
! Unsymmetric Damping Matrix
!
ET, 107, MATRIX27,,2,5,0
R,rsealC
RMODIF,rsealC,  1, CXX  ! CXX
RMODIF,rsealC, 79, CXX
RMODIF,rsealC,  7,-CXX  !-CXX
RMODIF,rsealC, 73,-CXX  !
RMODIF,rsealC, 14, CYY  ! CYY
```

```
RMODIF,rsealC, 92, CYY
RMODIF,rsealC, 20,-CYY  !-CYY
RMODIF,rsealC, 86,-CYY  !
RMODIF,rsealC,  2, CXY  ! CXY
RMODIF,rsealC, 80, CXY
RMODIF,rsealC,  8,-CXY  !-CXY
RMODIF,rsealC, 74,-CXY  !
RMODIF,rsealC, 13, CYX  ! CYX
RMODIF,rsealC, 91, CYX
RMODIF,rsealC, 19,-CYX  !-CYX
RMODIF,rsealC, 85,-CYX

!
! Unsymmetric Mass Matrix
!
ET, 108, MATRIX27,,2,2,0
R,rsealM
RMODIF,rsealM,  1, MXX  ! MXX
RMODIF,rsealM, 79, MXX
RMODIF,rsealM,  7,-MXX  !-MXX
RMODIF,rsealM, 73,-MXX  !
RMODIF,rsealM, 14, MYY  ! MYY
RMODIF,rsealM, 92, MYY
RMODIF,rsealM, 20,-MYY  !-MYY
RMODIF,rsealM, 86,-MYY  !
RMODIF,rsealM,  2, MXY  ! MXY
RMODIF,rsealM, 80, MXY
RMODIF,rsealM,  8,-MXY  !-MXY
RMODIF,rsealM, 74,-MXY  !
RMODIF,rsealM, 13, MYX  ! MYX
RMODIF,rsealM, 91, MYX
RMODIF,rsealM, 19,-MYX  !-MYX
RMODIF,rsealM, 85,-MYX
```

VITA

Stephen Mathew James was born in Al-Ahmadi, Kuwait. After completing high school at The Indian School Kuwait, he moved to India in 1998 to pursue a degree in engineering. He graduated from the University of Kerala, India, in 2002 with a B.Tech. in mechanical engineering. For the next three years, he worked at COMPRO Technologies Pvt. Ltd., New Delhi, India as a mechanical design and software engineer, developing system configurators and analysis utilities for motion control applications.

In 2005, he enrolled at Texas A&M University, College Station. He worked as a research assistant in the Turbomachinery Laboratory under the guidance of Dr. Dara Childs. A large part of his work involved development of the XLTRC^2 rotordynamics software, as well as technical support to the Turbo Research Consortium (TRC).

In 2008, Stephen joined the Rotating Machinery section in the Fluids & Machinery Engineering Department at Southwest Research Institute. His research interests are in the areas of rotating machinery rotordynamics, structural dynamics, finite element analysis, machinery design, tools and simulation systems, plant systems, software programming, and instrumentation. He also spends time researching software development, compilers, hardware, and memory-and-time-saving algorithms.

Stephen received his Master of Science degree in mechanical engineering from Texas A&M University in May 2010.

Stephen may be reached at Southwest Research Institute, 6220 Culebra Road, San Antonio, TX 78238. His email is stephen.james@swri.org.